

## Comprehensive review on high entropy alloy-based coating

Santosh Kumar

*Department of Mechanical Engineering, Chandigarh Group of Colleges, Landran, Mohali, Punjab, India*



### ARTICLE INFO

**Keywords:**

Traditional alloys  
High entropy alloys  
High entropy alloy coatings  
Applications  
3D printing  
Mechanical & tribological properties  
Challenges

### ABSTRACT

High-entropy alloys (HEAs) based coatings have great potential in distinct sectors owing to their attractive properties. These alloys offered high specific strength, superior mechanical properties, superconductivity, superparamagnetism, high fracture toughness at cryogenic temperatures, etc. These alloys contain multiple principal elements, with the possible number of high entropy alloy compositions extending significantly more than conventional alloys. Hence, the use of HEAs as feedstock material for coating processes has increased, especially for surface protection of various materials in distinct environments. Therefore this manuscript aims to provide an overview of HEA coatings, types, fabrication methods, post-processing of HEAs coatings and their diverse applications. Then, the mechanical and tribological properties of the HEAs-based coating developed by various researchers are summarized. In addition, this paper discusses the properties of HEAs and compares HEAs with traditional alloys. Finally, this paper presents the recent advances in HEAs for 3D printing, including research lapses, prospects and future opportunities.

### 1. Introduction

The durability and performance of any material or part in a different environment mainly depend upon the part's surface quality, functional and mechanical properties. Thus, to achieve excellent surface properties, various surface modifications are used. However, surface coating is an effective technique to increase the functional and mechanical properties of different machine parts or components. However, high entropy alloys (HEAs) based coatings are gaining more importance than traditional coatings due to their outstanding properties in distinct environments [1]. These attractive properties include: "high hardness, high fracture toughness, high strength, high-temperature oxidation resistance, hot corrosion resistance, unique magnetic and electrical properties which are potentially appropriate for applications as functional and structural materials" [2–9]. However, these alloys still have some drawbacks, such as the cost of high entropy alloys being more than traditional alloys. This higher cost may be owing to the inclusion of more costly elements such as niobium (Nb), chromium (Cr), vanadium (V), tungsten (W), nickel (Ni), titanium (Ti), and cobalt (Co) etc. [10]. These HEAs coatings are widely used in various engineering and industrial applications to resist erosion, corrosion, stress, etc. [1].

Moreover, numerous factors affect the performance, quality and durability of coatings. These factors include the type of base material, residual stresses, composition, adhesion, working temperature, toughness, humidity, & wear etc. [11]. In addition, to these factors, various

techniques are used to fabricate HEA coatings, such as: "laser cladding, thermal spraying, magnetron sputtering, electro-deposition, plasma-transferred arc cladding and others" [12–18]. Among these techniques, thermal spray coating is widely used as a surface modification technique. In these processes, the feedstock material (wire, rod or powder form) is fed into a spray torch and heated (near or up to a molten state) and then accelerated toward the substrate [19–23]. These processes are further divided into three categories, as shown in Fig. 1.

However, the flexibility offered by thermal spray in terms of the broad spectrum of thermal spray processes w.r.t. flame temperature and particle velocity is shown in Fig. 2.

In addition, the potential of HEAs-based coating deposited using a thermal spray is increasing rapidly, as shown in Fig. 3.

At present, the binary or ternary film has been extensively explored. But, owing to the drawbacks of alloy entropy, the conventional carbide, metal nitride, and oxide film or layer (low entropy films) could not fulfil the rising requirements criteria. The continuous research on high-entropy alloys (HEAs) has evolved the development of high-entropy films (HEFs) [25]. These high entropy films have shown better performances than HEAs and find wide applications in different sectors. These include: "solar thermal conversion systems, corrosion resistant coating, high hardness coating, diffusion barriers in the integrated circuit (IC) systems etc." [26].

E-mail address: [santoshdgc@gmail.com](mailto:santoshdgc@gmail.com).

### 1.1. Historical development

Over the era, metals (alloys) have played an essential role in almost all aspects of human lives, including agriculture equipment and hunting tools. Subsequently, metals and alloys were utilized in energy, transportation, aerospace and defence sectors etc. [27–30]. The periodic evolution of metals and alloys is shown in Fig. 4.

The historical evolution of high entropy alloys goes back to 2004 when the concept of HEAs was 1st published. Further, with the continuous research on HEAs, has developed high entropy film (HEF) in 2005 by Chang et al. [28]. Various researchers termed high entropy alloys multi-principal elements and compositionally complex alloys [29]. The historical evolution of HEAs is represented in Fig. 5.

Chang et al. [28] have successfully deposited nano-structured nitride films of multi-element high-entropy alloys (Fe-Co-Ni-Cr-Cu-Al-Mn & Fe-Co-Ni-Cr-Cu-Al<sub>0.5</sub>) by utilizing reactive DC sputtering techniques. The results showed that the film deposition rate reduced with the gas flow (nitrogen) rise. In addition, the maximum deposited film thickness was in surplus of 2.5-micron meters. The resistivity of Fe-Co-Ni-Cr-Cu-Al-Mn and Fe-Co-Ni-Cr-Cu-Al<sub>0.5</sub> alloy was found to be 108 and 135  $\mu\Omega \text{ cm}$ , respectively. In addition, the surface roughness of the nitride films decreased from (9 to 13 nm) to (1 to 3 nm). However, the hardness of HEF was increased (for alloy films: 4 GPa, and for nitride films: 11 GPa). Huang et al. [31] studied “the microstructure, resistivity, hardness, and thermal stability of sputtered oxide films of AlCoCrCu<sub>0.5</sub>NiFe HEA. The film was successfully deposited on a silicon wafer radio frequency sputter system.

Further, the samples were annealed at different temperatures (500 °C, 700 °C and 900 °C, respectively. With the increase in annealing temperature, the crystal grains tend to grow up & the micro-hole size among grains is enhanced along with the resistivity of the oxide film steps up. In addition, a slight variation in oxide-film thickness was observed during annealing”[31]. Later on, Tsai et al. [32] “studied the diffusion barrier characteristics of AlMoNbSiTaTiVZr alloy b/w silicon and copper wafer. The AlMoNbSiTaTiVZr & Cu layers were deposited successively, without breaking vacuum, onto Si substrates using DC magnetron sputtering. The AlMoNbSiTaTiVZr films were observed to have a stable amorphous structure owing to their limited diffusion kinetics and high entropy. The AlMoNbSiTaTiVZr HEA film is determined to avoid copper-silicide development up to 700 °C for half an hour. Overall, HEAs have great potential to be used as efficient diffusion barriers for copper metallization [32]. Ye et al. [33] “fabricated high-entropy alloy (FeCoNiCuCr) by using the laser cladding technique. The microstructure, constituent phases and chemical composition of the synthesized alloy were characterized by XRD, SEM, EDS and TEM, respectively. The result revealed that FeCoNiCuCr clad layers contain FCC and BCC phases. However, the clad layers demonstrate higher

hardness at higher aluminium atomic content and offer higher hardness between 400 °C to 700 °C. Although the high entropy film typically includes oxide and nitride films, its composition design is similar to that of high entropy alloys. HEAs are generally categorized into two elements, as depicted in Fig. 6.

Recently, HEAs have more potential in many industries than typical alloys. High entropy alloys (HEAs) are hard, strong, and have many properties, including thermostability and corrosion resistance. HEAs also had exceptional chemical and mechanical characteristics. As a result, these alloys offer enormous development potential [34].

Till Jan. 2022, more than 300 high entropy alloys have been processed along with more than 35 principal elements. The concept of HEAs is different from traditional alloys because HEAs are not made up of just one or two components. HEAs have been defined in two ways by researchers: the first is based on composition, while the second is based on entropy [35].

So, based on composition, high entropy alloys contain a minimum of 5 main elements in the equimolar or near equimolar ratios, as depicted in Fig. 7.

The atomic % of each element for these alloys lies between 5 % to 35 %. Although several additional elements were included in the high entropy alloys, the overall percentage of these elements are <5% [36]. However, based on entropy, the HEAs are defined as the random blending of distinct features that yields configurational entropy ( $\Delta S_{\text{conf}}$ ). Further, these alloys are categorized into three types of alloys, as shown in Fig. 8.

These materials are termed as high entropy alloys owing to the fact that their random solid & liquid state has basically higher entropies as compared to those in conventional alloys. The evolution of HEAs from conventional alloys is shown in Fig. 9.

The main properties of HEAs are as given below:

a) High hardness and strength.

In the case of HEAs, the uneven atomic radius of distinct elements causes an intensive lattice distortion effect. These types of effects obstruct the dislocation movement, leading to very high hardness and strength [34]. The lattice distortion of HEA containing chromium is shown in Fig. 10.

Li et al. [35] also reported that severe lattice distortion could occur in the high entropy alloy, and each element has its unique and specific atomic size. Fig. 11 represents the schematic representation of a dislocation motion by overcoming a periodic Peierls-Nabarro energy field in HEAs.

The lattice distortion effect disrupts the ideal crystal structure, affecting the mechanical properties of high entropy alloys [36]. In addition, the distinct size of atoms leads to the distortion of sites which provides their excess entropy. This impact is small in dilute solid solutions when the surrounding main atoms strain a tiny number of atoms,

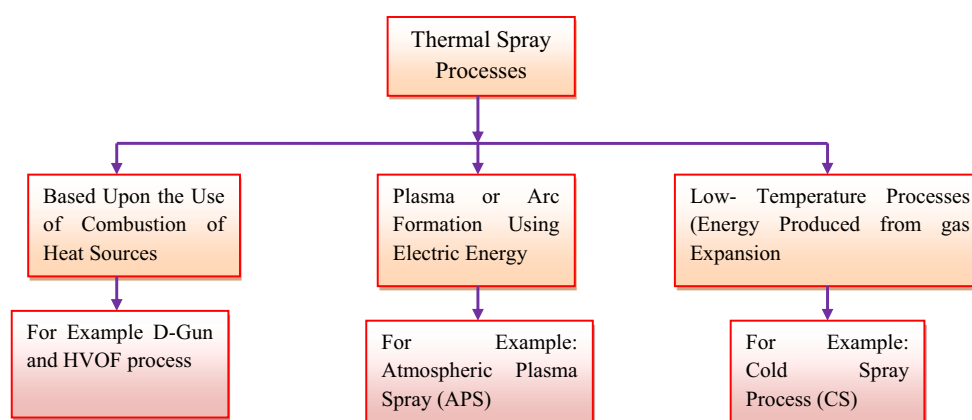


Fig. 1. General classification of thermal spray processes.

as seen in Fig. 11. (a). This lattice-distortion effect can also be used to modify the mechanical properties (such as solid solution strengthening) of a complicated, concentrated solid solution, as shown in Fig. 11. (b). On the other hand, Ranganathan S. [37] developed the notion of “cocktail alloys,” in which single-phase crystalline alloys or bulk metallic glasses can be created by mixing metals in a multi-element mixture. However, in the case of metallic materials, the cocktail effect is not primarily scientific. Still, it merely indicates that unexpected features can be obtained by combining several elements, which cannot be done in a material composed of a single independent element. Further, Gludovatz et al. [38] investigated the fracture resistance behaviour of HEA (cantor alloy) for cryogenic applications. Fig. 12 depicts the fracture toughness vs. yield strength of the most commonly utilized structural materials.

In Fig. 12, the top right portion of high entropy alloy indicates an outstanding combination of damage-tolerant mechanical characteristics compared to other materials. Similarly, a graph between fracture toughness and yield strength of HEAs and some traditional materials is plotted by Li et al. [40], as shown in Fig. 13.

Fig. 13 shows that face-centred cubic high entropy alloy has a better resistance against fracture than the face-centred cubic + body-centred cubic mixture and body-centred cubic high entropy alloys. In addition, the high entropy alloy offered superior fracture resistance compared with polymers, foams, elastomers, ceramics, glasses, and some traditional metals and alloys (such as Mg alloys, Pd alloys, Zn alloys, Cu alloys, Al alloys and Ni alloys). However, the high entropy alloys exhibited comparable fracture resistance to low alloy steels, stainless steels, Ni-based superalloys, cryogenic steels, bulk metallic glasses, tungsten alloys, titanium alloys, carbon steels and cast irons. From this, it is clear that high entropy alloys have great potential to be utilized as structural materials [40,41]. Raabe et al. [42] developed HEA steel that comprises b/w 20 to 50 at.% Fe. The developed steels offered an attractive combination of ductility and strength that exceeds that of the best twin-induced plasticity (TWIP) and transformation-induced plasticity (TRIP) steels. The behaviour of high entropy steels in the ultimate ductility-strength space is shown in Fig. 14 (a). To promote work

hardening, these steels exploit the shift from face-centred cubic to hexagonal close-packing martensite during plastic deformation, as seen in Fig. 14. (b).

Fig. 14 (b) indicates the peripheral micrographs of high entropy alloy that show the transformation from face-centred cubic (red colour) to close hexagonal packing (blue colour) is linked with the strong work hardening [41].

Further, Li et al. [43] reported that HEAs offered superior and comparable properties to traditional alloys. The authors compare the ductility and strength of high entropy alloys with conventional alloys. This comparison is made in Fig. 15 by overlapping the ductility-strength map of high entropy alloys in Fig. 16 on that of traditional alloy.

Overall, it is not clear that high entropy alloys outperform traditional alloys in ductility and strength. Furthermore, the latter's manufacturing cost is expected to be significantly lower. As a result, ongoing research and development in the development of high-strength yet ductile high-entropy alloys is still required.

#### (a) Corrosion resistance

Corrosion destroys >3 % of the world's gross domestic product. Hence, the design and development of materials which are highly resistant to corrosion are required. HEAs featured novel microstructures, which are solid solutions with random configurations of >5 elements, compared to traditional alloys [44]. The cost of corrosion in the US was \$1 trillion in 2013, which is approximately 6.2 % of the United States' gross domestic product [45]. Although, among various metallic materials, noble metals such as silver, gold, and platinum have good resistance against corrosion. However, their poor mechanical properties and high cost restrict their applications [46]. The resistance against corrosion of HEAs is better than plenty of widely utilized stainless steel. Numerous HEAs exhibited dendritic segregation structures, which are composed of body structure and simple surface structure. In addition, there are many nanometer particles and disordered structures in dendritic segregation structures. The presence of these structures has significantly enhanced the resistance against corrosion of HEAs [47].

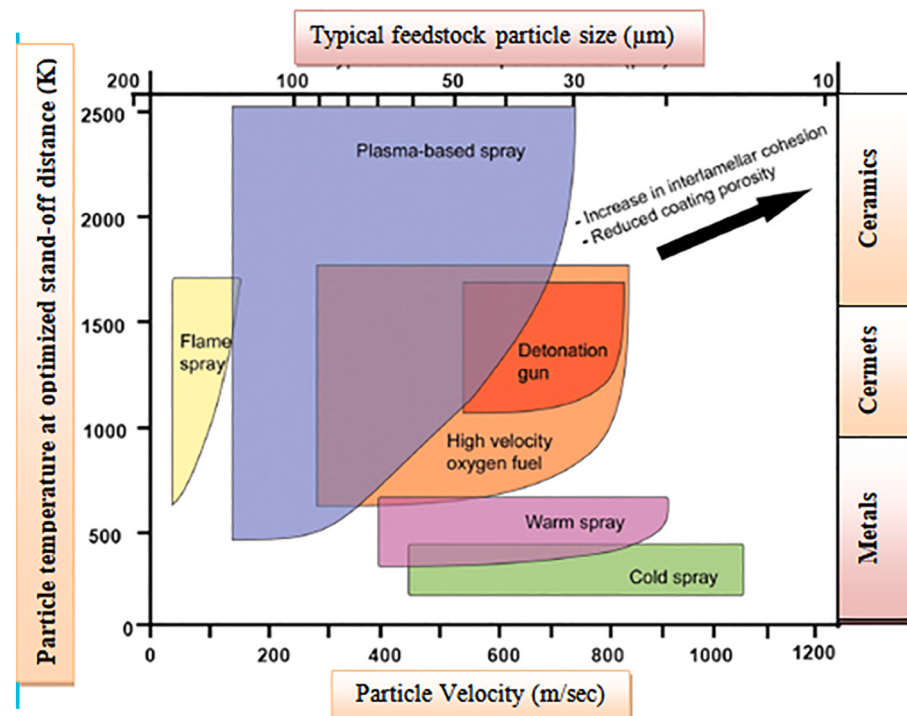


Fig. 2. Classification of TS technique based upon (a) velocity of particle, (b) temperature of particle, (c) size of feedstock [24].

Moreover, traditional alloys have insufficient high-temperature stability that weakens the resistance against corrosion and mechanical properties. Hence, the use of conventional alloys is restricting their applications in a very high-temperature environment [48]. HEAs, on the other hand, include five or more primary elements, resulting in a disordered solid solution with a body-centred cubic (BCC), face-centred cubic (FCC), or hexagonal closed-packed (HCP) structure rather than complex intermetallic compounds [49–57]. The random presence of various elements in a solid solution leads to a specific locally disordered chemical environment. This results in unique corrosion-resistant properties [38]. During the last decade, various researchers [58–62] have investigated the corrosion performance of high entropy alloys in distinct aqueous environments. The presence of different passivating elements such as nickel, molybdenum, and chromium in high entropy alloys offered better corrosion-resistant properties than traditional alloys [58,59]. In addition, due to the exceptional properties of HEAs make them suitable for extreme service environments (turbine, aerospace, nuclear power plant etc.). These properties include harsh service environments, high fracture toughness, improved fatigue resistance, high thermal stability, etc. [63,64,65–71]. The corrosion behaviour of different HEAs and traditional alloys in distinct environments is summarized in Table 1.

From Table 1, it is clear that with increasing copper and aluminium content, the corrosion current density is enhanced while the pitting potential reduces, indicating the degradation of the resistance corrosion. Further, the addition of molybdenum enhances and then reduces the resistance against corrosion owing to the development of a chromium-rich sigma phase. Overall, it is concluded that the addition of aluminium, molybdenum, copper, and boron to distinct high entropy alloy systems all impact the resistance against corrosion, which is reflected by the decrease of  $\Delta E_b$  and increase of  $i_{corr}$ .

However, Shi et al. [78] give a detailed comparison of corrosion performance b/w traditional and high entropy alloys in acid (0.5 M

$H_2SO_4$ ) and salt water (3.5 wt% NaCl), as shown in Figs. 17 and 18, respectively.

In Fig. 17, the higher value of corrosion potential ( $E_{corr}$ ) stands for a more noble state of the alloys. However, compared with steels, copper alloys, titanium alloys and nickel alloys, the lower right location of the high entropy alloys shows the novel corrosion performance of high entropy alloys in acid [39,79–91].

However, Fig. 18 indicates the comparison of pitting potential and current density, which is relevant to the corrosion rate. The results are compared to the traditional alloys (aluminium alloys, stainless steel, copper alloys, titanium alloys, and nickel alloys) with high entropy alloys [79–91]. The high entropy alloys lie in the lower right part, as indicated in Fig. 18. High entropy alloys have substantially higher pitting potentials than copper, aluminium, and titanium alloys. They are comparable to nickel alloys and stainless steels, showing superior resistance to localized corrosion, which is the most common failure mode of alloys in Cl-containing solutions. Compared to titanium and copper alloys, the corrosion current densities of high entropy alloys are substantially lower, indicating a lower corrosion rate. In brief, the general corrosion-resistant and localized characteristics of high entropy alloys are comparable to or even better than those of traditional corrosion-resistant alloys in the 3.5 wt% NaCl solution.

#### (b) Thermal stability

In thermodynamics, the term ‘entropy’ is the physical quantity of the system chaos. The higher entropy means the higher the degree of chaos. As per the function of “Gibbs free energy” the entropy of the system is given by the equation.

$$G = H - T \cdot S \quad (1)$$

Here, G = Gibbs free energy; S = entropy of the system; T = temperature; H = enthalpy.

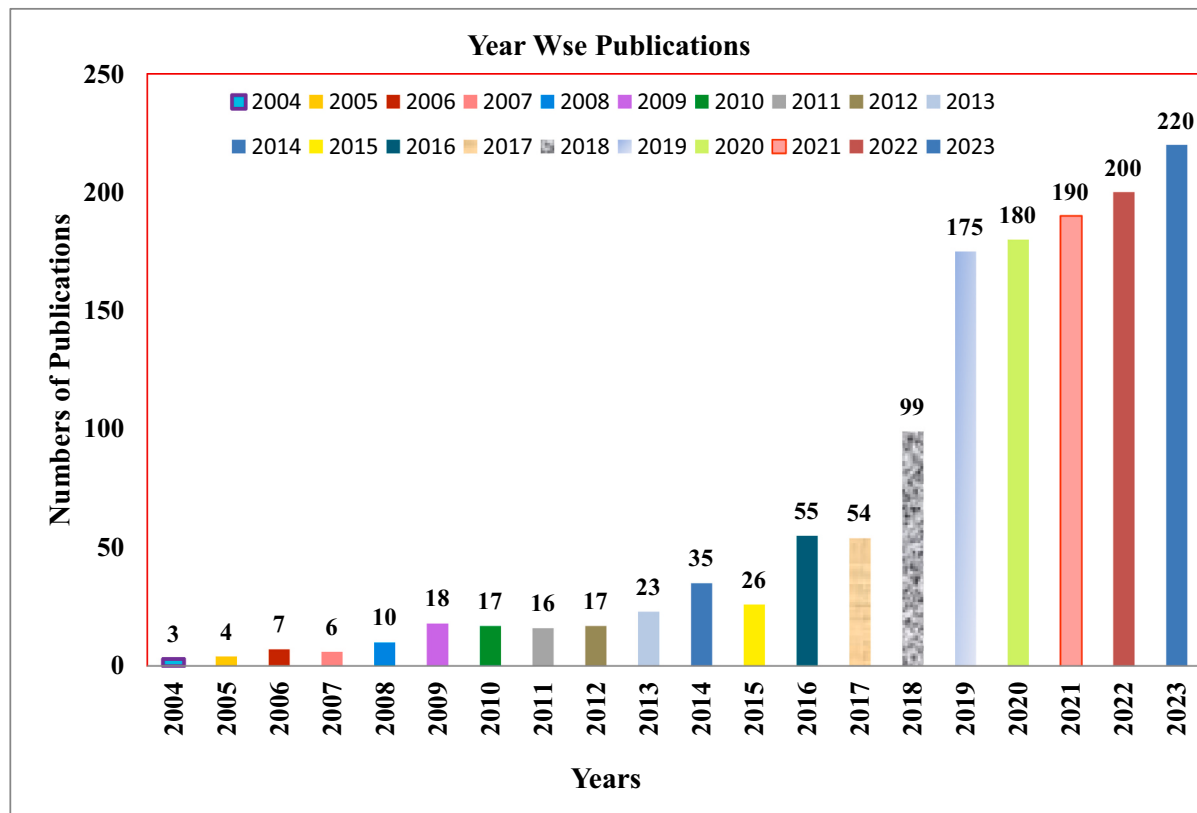


Fig. 3. Years-wise research articles published in peer-reviewed journals on high entropy alloy coating deposited by thermal spray [24].

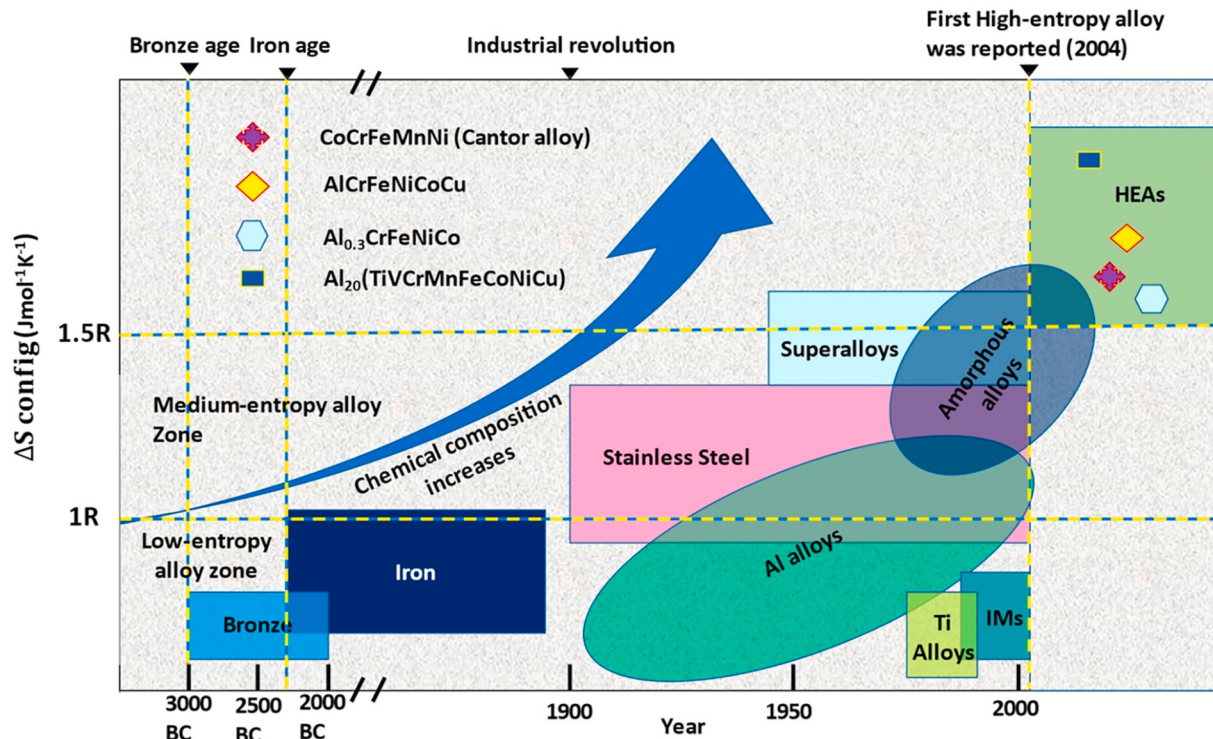


Fig. 4. Periodic evolution of metals and alloys [27,30].

It is well established that a higher value of entropy makes the system more stable. In addition, the higher temperature can also decrease the free energy of the system. Due to this, the HEAs offered superior thermal stability [47].

Several HEAs have recently been produced, providing a new technique for designing unique alloys [92]. The sluggish diffusion and high entropy effect in kinetic in high entropy alloys lead to face-centred structure or simple body structure, distinct from conventional alloys where many intermetallics appear. Apart from various mechanical and heat resistance properties of HEAs, the parts subjected to very high temperatures also need excellent thermal stability to avoid failures. Hence, the research and study of thermal stability are imperative to estimate the service safety for high entropy alloy parts [69,93–96]. At high temperatures, Liu et al. [97] investigated the thermal stability of FeCrNiTiAl HEA. According to the results, the as-cast alloy has dendritic, interdendritic, and eutectic microstructures.

The alloy retains its petal-like structure after exposure to high temperatures, with just minor grain coarsening. After 72 h of exposure, there is no change in micro-hardness. Furthermore, after ageing at 800 °C to 1100 °C for 144 h, no new phase is observed, although there is a modest shift in the phase composition of the laves phase. These findings demonstrate the FeCrNiTiAl alloy's high thermal stability. Because the hardness of a material is proportionate to its strength, it has high thermal stability.

Presently, some HEAs are effective and promising for high-temperature applications. These HEAs have the potential to replace the nickel-based traditional superalloys. Takeuchi et al. [98,99] also reported a new alloy system (Ir-Mo-Rh-Ru-W) having excellent thermal stability. He observed that annealing at 2373 K for 1 h, the Ir<sub>26</sub>Mo<sub>20</sub>Rh<sub>22.5</sub>Ru<sub>20</sub>W<sub>11.5</sub> and Ir<sub>25.5</sub>Mo<sub>20</sub>Rh<sub>20</sub>Ru<sub>25</sub>W<sub>9.5</sub> alloys exhibit single-phase hexagonal close-packed structures. However, another novel alloy (Ir<sub>29.0678</sub>Mo<sub>15</sub>Rh<sub>29.0678</sub>Ru<sub>11.8644</sub>) maintains the single hexagonal close-packed structure after annealing at 1273 K for 200 h. The comparison of distinct refractory HEAs is given in Table 2.

HEAs-based coatings (in the form of thin or thick layers) are widely used to protect the material/parts serving in extreme environmental

conditions. In addition, many high entropy alloys have also been produced, indicating lightweight, and resistance against oxidation, wear, erosion and corrosion. Due to these properties, HEAs find wide application in distinct sectors [102–104]. Hence, this paper aims to give an overview of the classification of HEA-based coating materials, fabrication techniques, post-processing coatings, properties, applications and future scope, as summarized in Fig. 19.

## 2. HEAs based coatings & its classification

The high entropy alloy coatings are classified into 3 categories as shown in Fig. 20.

### 2.1. Metallic HEA coatings

These coatings consist of FeCoNiMnCr series elements, commonly termed Cantor-based alloys [49]. It consists of transition and refractory metals. These refractory HEAs are used for high-temperature applications to reduce corrosion, wear, erosion and oxidation. Some examples of refractory HEAs are CrNbVZr, TaNbZrHf, TaMoNbW, TaNbCrMo series etc. [105,106]. However, AlLiMgScTi, Al<sub>20</sub>Be<sub>20</sub>Fe<sub>10</sub>Si<sub>15</sub>Ti<sub>35</sub>, AlCu-SiZnFe, AlCuFeMnMgTi etc., are some examples of metallic lightweight alloys [107–110].

### 2.2. Ceramic HEA coatings

These coatings consist of metal carbides and nitrides of transition elements and find wide applications in nuclear power plants owing to the coatings' high strength, anti-corrosion performance, and thermal stability [105,111]. Various researchers [112–114] have deposited distinct high entropy alloy nitrides, oxides, carbides and perovskite materials by magnetron sputtering in different environments such as oxygen, methane, nitrogen, hydrogen etc. However, in the case of hard ceramic high entropy alloy coatings, some impurities (oxygen, carbon, hydrogen and nitrogen) exist in the solid solution and indicate a high entropy effect. In addition, distinct ceramic forming elements

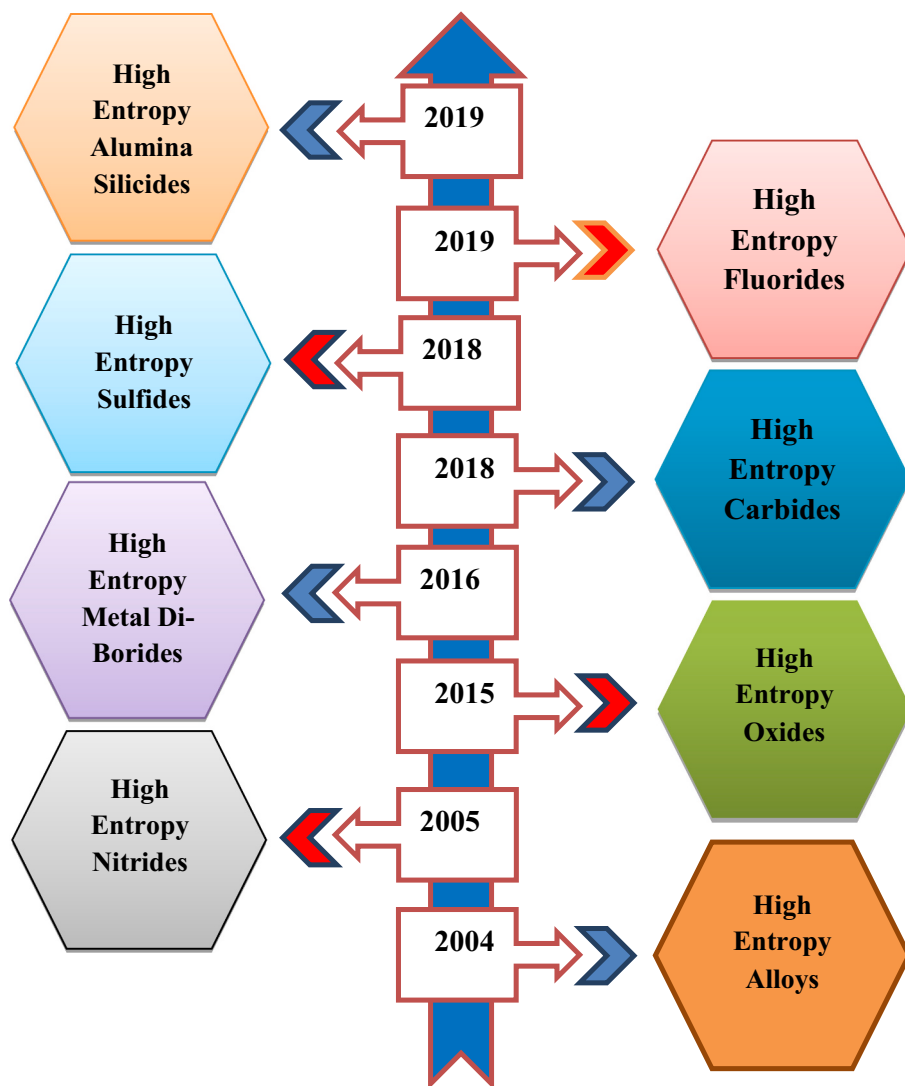


**Fig. 5.** Historical evolution of high entropy alloys [30].

(chromium, zirconium, titanium, aluminium, silicon, etc.) are utilized for hard ceramic high entropy alloy coatings [115,116].

### 2.3. Composite HEA coatings

These coatings can be synthesized by reinforcing the high entropy matrix with appropriate ceramic reinforcements. These coatings offered better resistance against corrosion and wear [117]. However, various researchers [47,118,119] have developed many ceramic reinforcements such as aluminium oxide, silicon carbide, titanium carbide, tungsten carbide, titanium nitride, titanium boride etc. These reinforcements are used to enhance hardness, resistance against wear, and bonding with HEA matrix coatings [28,120,121].

### 3. Fabrication methods of HEAs coatings

Presently, numerous methods are used for the fabrication of HEAs coatings. However, the general classifications of distinct fabrication methods of HEA coatings are shown in Fig. 21.

#### 3.1. Laser-based methods

These methods are widely used for the fabrication of HEAs coating due to high energy density, material/time-saving, flexibility and

environmentally friendly [123,124]. The main advantages of laser-based methods are uniform microstructure and high bond strength (strong bonding between the coating and substrate). However, there is a smaller thermal damage owing to the rapid cooling and heating rates involved in the laser-based method. In addition, this method involves high residual stresses, the development of a heat-affected zone & elemental dilution of the high entropy alloy coating and substrate [35,125].

##### 3.1.1. Laser cladding

This is one of the most widely used modern laser-based coating methods for surface repair and strengthening. During this method, the powder of cladding quickly melts & solidifies under laser irradiation. Thus, owing to the high-temperature gradient, this method develops a fine-grained and tough coating on the base material (substrate) with good metallurgical bonding [126]. The most widely utilized laser cladding methods are coaxial & preplaced powder systems, as depicted in Fig. 22.

In a coaxial powder system, “the laser beams irradiate the surface of base material and develop a liquid melt pool. Then, the powder to be melted is ejected from this nozzle into the liquid melt pool by the carrier gas (in the nozzle). The powder is also melted into a cladding layer by the laser beam. As a result, the laser beam moves synchronously with the powder feeding nozzle, scanning the base material line by line [126].

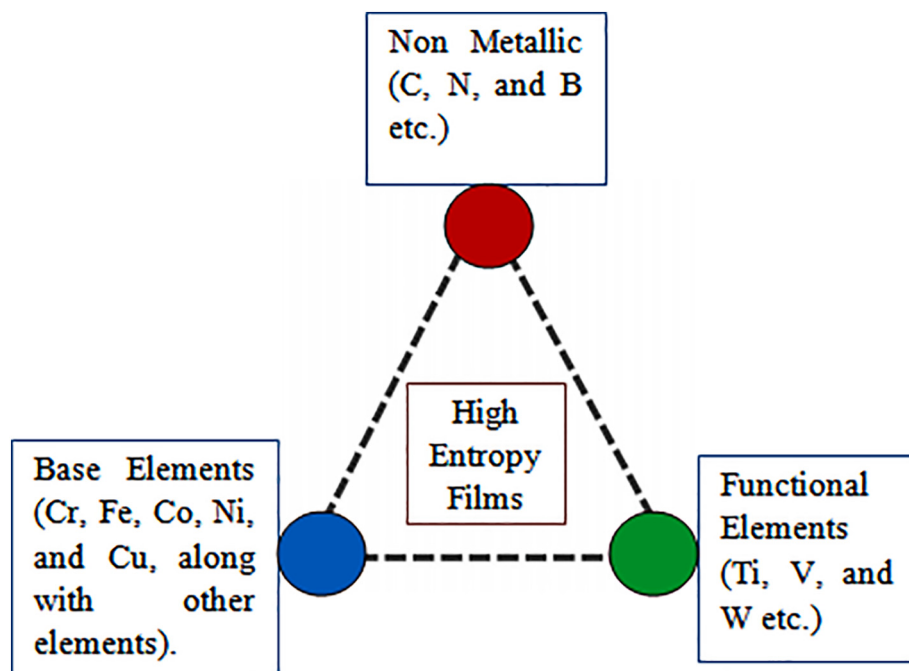


Fig. 6. Composition design of HEFs [25].

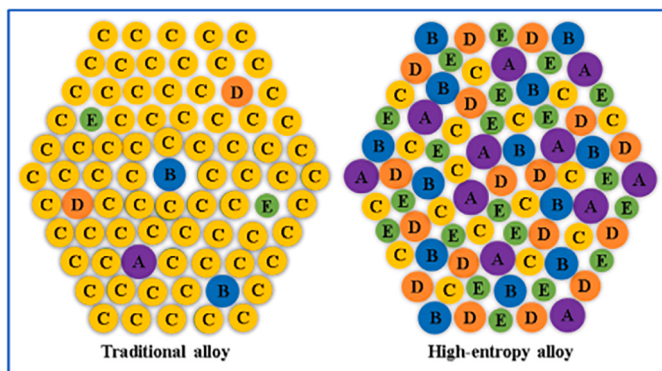


Fig. 7. The schematic illustration represents the atomic structure of traditional and high entropy alloy [35].

In the preplaced powder system, “the base material is already changed by cladding material. Then the laser beam scans the preplaced powder. Subsequently, it melts & cools down rapidly, thus developing a cladding zone” [126].

### 3.1.2. Plasma cladding

It is a high-energy coating cladding technique widely utilized for depositing high entropy alloy coating [128–130]. Plasma cladding offered a more considerable blowing force and higher heat input than laser surface alloying and cladding. As a result, molten coating components melt and mix to obtain a homogenous microstructure [1]. This technique has also attracted attention in developing HEAs coating rather than laser cladding owing to its attractive benefits. These benefits include tremendously high energy density, low thermal distortion, low dilution of substrate materials, low cost, good interfacial bonding strength etc. [131].

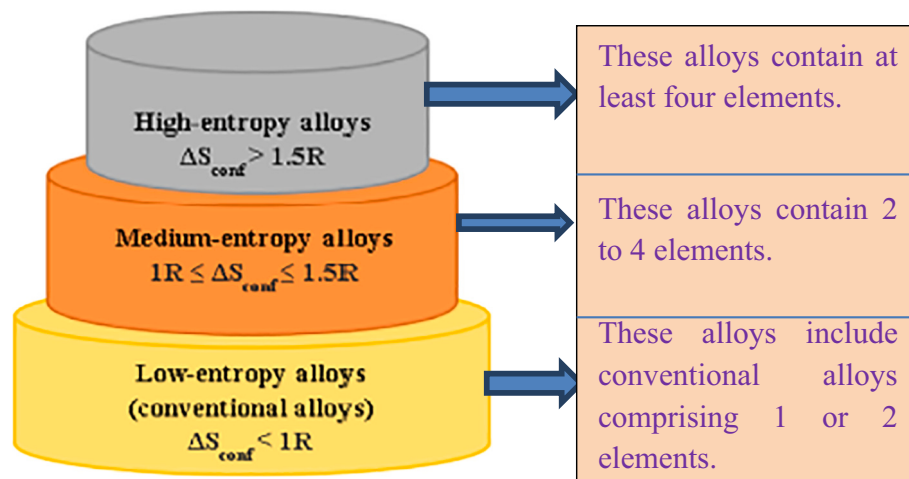


Fig. 8. Types of HEAs based on entropy [35,37].

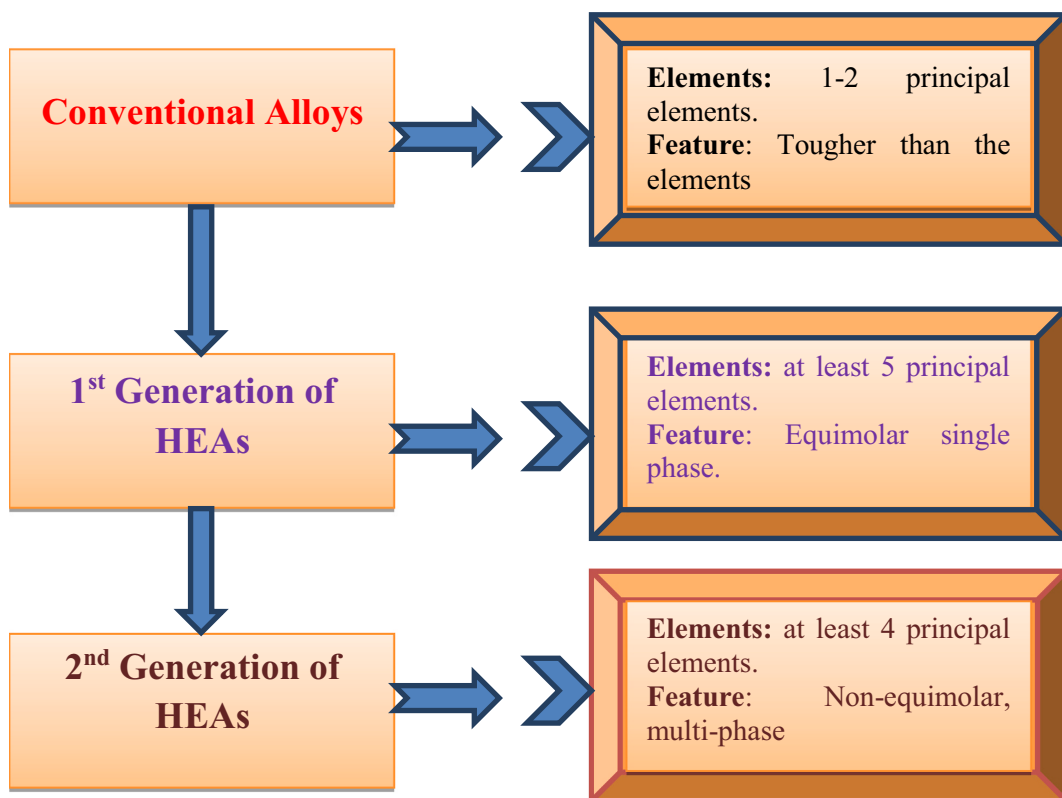


Fig. 9. Schematic diagram showing the evolution of HEAs from conventional alloys [35].

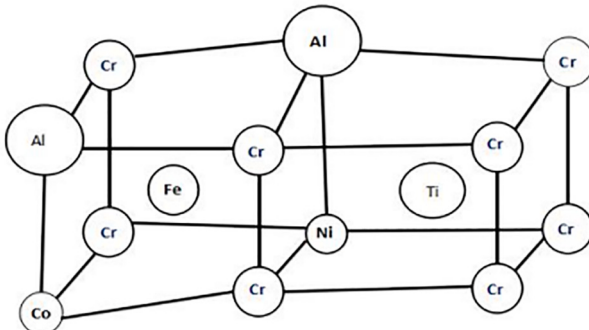


Fig. 10. Schematic representation of lattice distortion of HEA containing chromium [34].

### 3.1.3. Laser re-melting

Before laser re-melting, the substrate surface is cleaned with sandblast and acetone. Then, the HEAs powders are sprayed on substrate material at room temperature. For re-melting the coating, a laser generator (power = 2000 W, spot size = 5 mm × 1 mm and scanning speed = 7 mm/s) is used [132]. The schematic illustration of the laser re-melting technique is shown in Fig. 23.

In this technique, the coating material is irradiated by laser to develop an instantaneous molten pool. However, the depth of the molten pool is usually <1 mm. The front portion of the molten pool is the melting zone, the solid phase is continuously melted, and the back portion is the solidified zone.

The laser re-melting of coatings or bulk material surfaces can effectively enhance surface roughness, resistance against corrosion and wear, the adhesion strength of the substrate-coating and the amount of porosity [133]. In addition, this method is very effective in developing and keeping non-equilibrium phases owing to its high cooling rate

and high temperatures [134]. This method is also utilized to enhance the microstructural characteristics of thermal sprayed coating [135].

#### 3.1.4. Laser surface alloying

This process is commonly used for high entropy alloy coatings and is similar to laser cladding in many ways. The degree of dilution of the coating is the main distinction between this approach and laser cladding. During this method, the dilution rate is much higher than the laser cladding technique. The coating developed by this method is equiaxed or dendrite, FCC or BCC solid solution intermetallic compounds & a thickness of 100 µm [1]. This technique offered a unique feature, such as a fast-melting solidification method, which contributed to the development of non-equilibrium phases, and a dense coating bonded metallurgy to the base material. In addition, this method provides homogeneity in microstructure with a thick coating (millimetre range) [136].

The summary of various HEA coatings fabricated by laser-based coating methods is given in Table 3.

**3.1.4.1. Summary of the relationship between laser-based methods and their features.** Laser-based fabrication methods, including laser cladding, plasma cladding, laser re-melting, and laser surface alloying, offer precise control over the deposition and modification of high-entropy alloy (HEA) coatings, resulting in a range of desirable features and enhanced properties.

**3.1.4.2. Laser cladding.** Laser cladding involves melting a focused laser beam onto the substrate surface, creating a localized heat source that melts the HEA powder or wire material to form the coating. This method allows for precise control over the coating thickness, composition, and microstructure, leading to:

- (a) Fine-grained microstructures: The rapid cooling rates associated with laser cladding promote the formation of fine grains, which

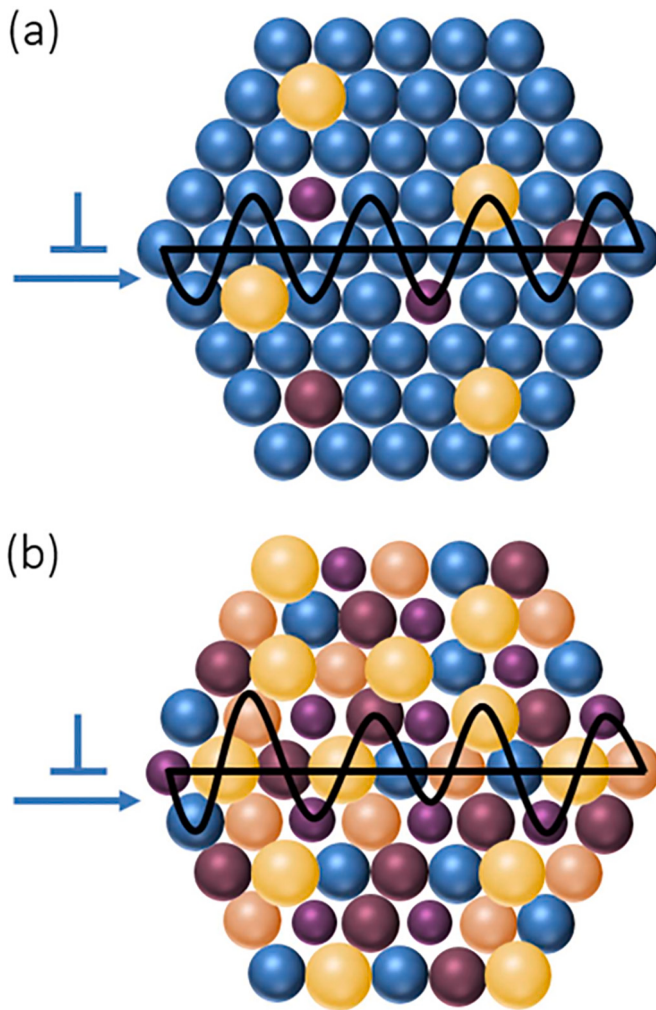


**Fig. 11.** Schematic representation of dislocation motion by overcoming periodic Peierls-Nabarro energy barrier field in (a) a dilute solid-solution, & (b) a complex, concentrated solid solution with 5 elements [35].

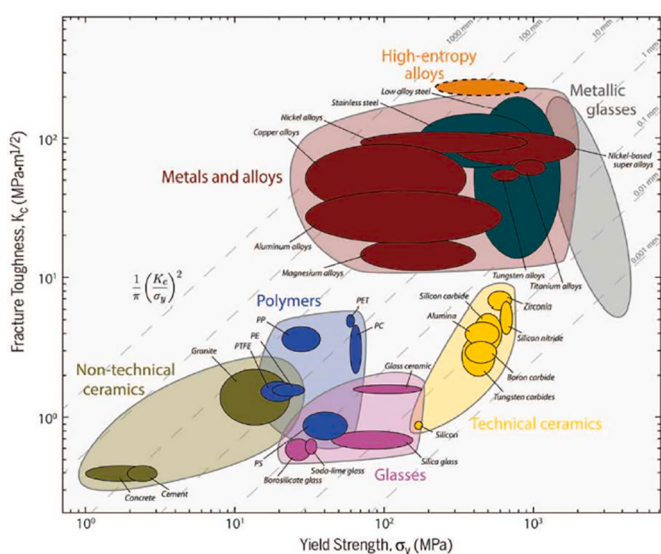


**Fig. 12.** Schematic graph of fracture toughness w.r.t. yield strength of structural materials [38,39].

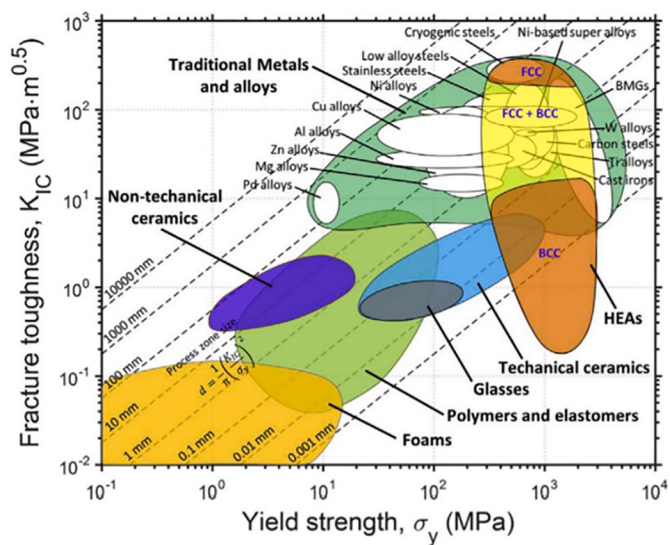


**Fig. 13.** Fracture toughness w.r.t. yield strength plot of high entropy alloy and some traditional materials [40].

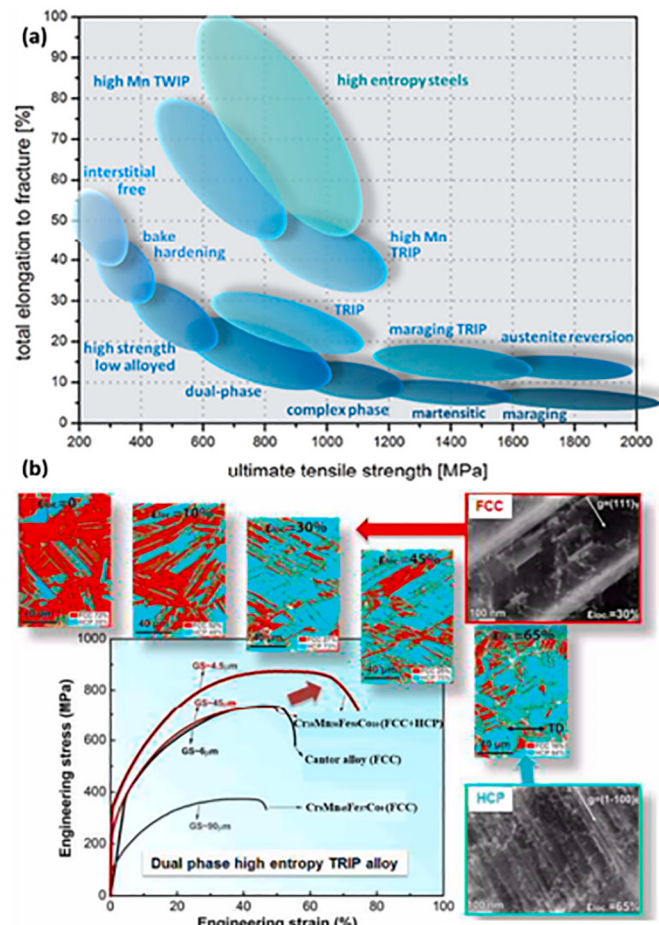


**Fig. 14.** (a) Plot between Ultimate strength and ductility for steels indicating high-entropy steel with superior performance [42]. (b) The graph between engineering tensile stress and engineering strain for distinct HEAs indicates the superior performance of the transformation-induced plasticity high entropy alloy [41].

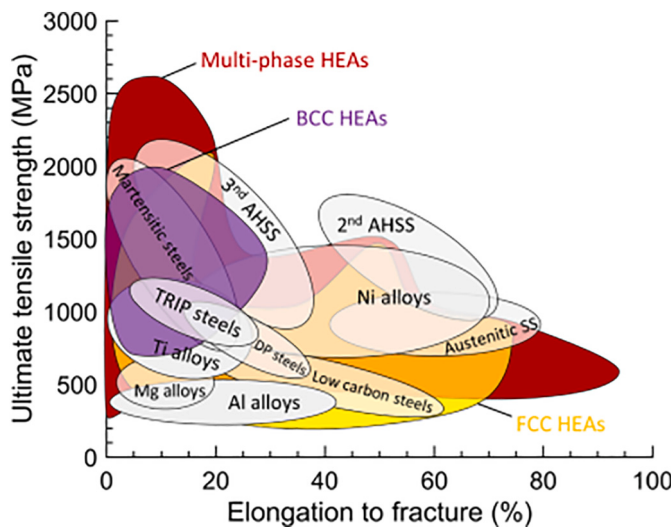


**Fig. 15.** Ultimate tensile strength-ductility map of high entropy alloys in the context of conventional alloys [43].

- enhance the strength, hardness, and wear resistance of the coating [145].
- (b) Reduced dilution: The localized heating minimizes the mixing of the HEA material with the substrate, resulting in a coating with minimal dilution and preserved HEA properties [146].
- (c) Strong adhesion: The laser beam creates a strong metallurgical bond between the coating and the substrate, ensuring excellent adhesion and durability [147].

**3.1.4.3. Plasma cladding.** Plasma cladding utilizes a high-energy plasma jet to accelerate and melt HEA powder particles, depositing them onto the substrate to form the coating. This method offers:

- (a) High deposition rates: Plasma cladding enables the deposition of thick coatings at relatively high speeds, making it suitable for large-scale applications [148].
- (b) Reduced porosity: The high-energy plasma stream promotes splattering and fusion of HEA particles, resulting in a coating with low porosity and improved wear resistance [149].

- (c) Versatility: Plasma cladding can accommodate a wide range of HEA compositions and substrate materials, making it a versatile coating technique [150].

**3.1.4.4. Laser re-melting.** Laser re-melting involves post-processing an initially deposited HEA coating using a laser beam to further refine its microstructure and enhance its properties.

This technique offers:

- (a) Grain refinement: The laser beam induces localized melting and rapid solidification, leading to the formation of finer grains and improved mechanical properties [151].
- (b) Homogenization: Laser re-melting can homogenize the microstructure and composition of the coating, reducing the segregation of elements and improving overall performance [152].
- (c) Enhanced wear resistance: The refined microstructure and reduced porosity resulting from laser re-melting contribute to improved wear resistance and extended coating life [153].

**3.1.4.5. Laser surface alloying.** Laser surface alloying involves melting a thin layer of the substrate surface along with a pre-deposited HEA powder or wire material to form an alloyed coating.

This method offers:

- (a) Tailored compositions: By controlling the laser parameters and HEA composition, a customized alloyed coating can be created with the desired properties [154].
- (b) Improved surface properties: The alloyed coating enhances the surface properties of the substrate, such as hardness, wear resistance, and corrosion resistance [155].
- (c) Minimal substrate distortion: The localized heating and rapid solidification minimize the thermal distortion of the substrate, making it suitable for sensitive components [156].

In summary, laser-based fabrication methods provide a range of advantages for producing HEA coatings with enhanced properties, including fine-grained microstructures, reduced dilution, strong adhesion, high deposition rates, low porosity, grain refinement, homogenization, enhanced wear resistance, tailored compositions, improved surface properties, and minimal substrate distortion. The choice of laser-based fabrication method depends on the specific coating requirements and the desired properties of the HEA coating.

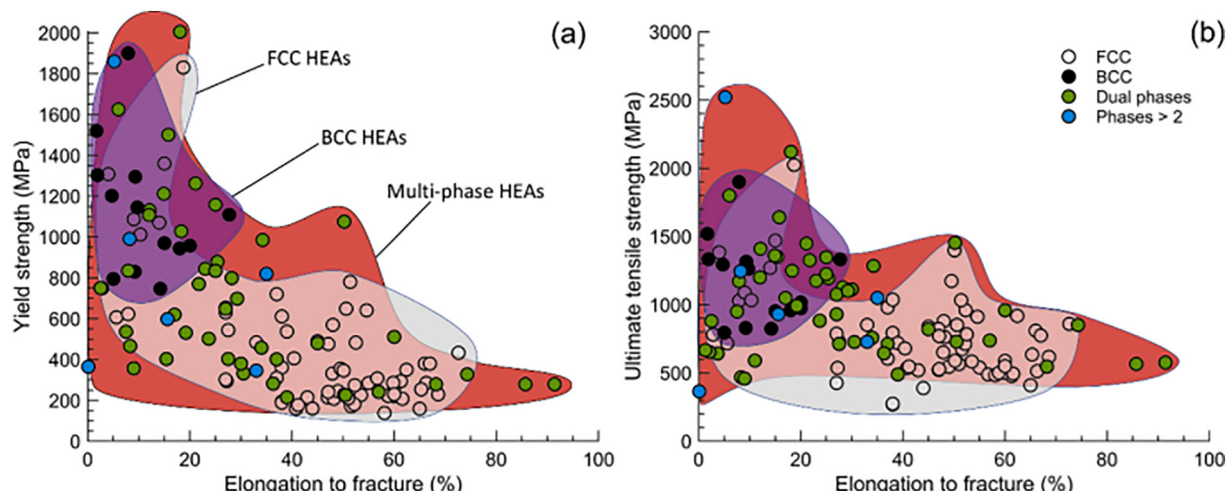


**Fig. 16.** Maps of (a) tensile yield strength w.r.t. % elongation to fracture (b) ultimate tensile strength w.r.t. % elongation to fracture of high entropy alloys, summarized by phase structures [43].

**Table 1**

Corrosion performance (electrochemical parameters) of distinct HEAs and traditional alloys in distinct solutions.

S-No.	Authors	Alloy	Solution	$E_{corr.}$ (mV <sub>SHE</sub> )	$i_{corr.}$ (A/cm <sup>2</sup> )	$i_{crit.}$ (A/cm <sup>2</sup> )	$E_{pp}$ (mV <sub>SHE</sub> )	$i_{pass}$ (A/cm <sup>2</sup> )	$\Delta E$ (mV <sub>SHE</sub> )
1	Lee et al. [72]	CrFe <sub>1.5</sub> MnNi <sub>0.5</sub>	0.5 M H <sub>2</sub> SO <sub>4</sub>	-229	$6.86 \times 10^{-4}$	$1.26 \times 10^{-2}$	-55	$3.14 \times 10^{-5}$	1227
		Al <sub>0.3</sub> CrFe <sub>1.5</sub> MnNi <sub>0.5</sub>	0.5 M H <sub>2</sub> SO <sub>4</sub>	-194	$2.39 \times 10^{-3}$	$2.36 \times 10^{-2}$	-12	$7.39 \times 10^{-5}$	1176
		Al <sub>0.5</sub> CrFe <sub>1.5</sub> MnNi <sub>0.5</sub>	0.5 M H <sub>2</sub> SO <sub>4</sub>	-206	$5.08 \times 10^{-3}$	$5.54 \times 10^{-2}$	47	$6.82 \times 10^{-5}$	1114
		304 stainless steel	0.5 M H <sub>2</sub> SO <sub>4</sub>	-186	$7.45 \times 10^{-5}$	$8.19 \times 10^{-4}$	-22	$8.05 \times 10^{-6}$	1178
		CrFe <sub>1.5</sub> MnNi <sub>0.5</sub>	0.5 M H <sub>2</sub> SO <sub>4</sub>	-221	$6.86 \times 10^{-4}$	NA	NA	$3.14 \times 10^{-5}$	1218
		CrFe <sub>1.5</sub> MnNi <sub>0.5</sub>	0.5 M H <sub>2</sub> SO <sub>4</sub> + 0.10 M NaCl	-242	$2.06 \times 10^{-3}$	NA	NA	$7.09 \times 10^{-5}$	1150
		CrFe <sub>1.5</sub> MnNi <sub>0.5</sub>	0.5 M H <sub>2</sub> SO <sub>4</sub> 0.25 M NaCl	-238	$4.60 \times 10^{-3}$	NA	NA	$4.75 \times 10^{-3}$	495
		CrFe <sub>1.5</sub> MnNi <sub>0.5</sub>	0.5 M H <sub>2</sub> SO <sub>4</sub> 0.50 M NaCl	-240	$9.75 \times 10^{-3}$	NA	NA	$5.78 \times 10^{-3}$	352
		Al <sub>0.3</sub> CrFe <sub>1.5</sub> MnNi <sub>0.5</sub>	0.5 M H <sub>2</sub> SO <sub>4</sub>	-194	$2.39 \times 10^{-3}$	NA	NA	$7.39 \times 10^{-5}$	1176
		Al <sub>0.3</sub> CrFe <sub>1.5</sub> MnNi <sub>0.5</sub>	0.5 M H <sub>2</sub> SO <sub>4</sub> + 0.10 M NaCl	-219	$2.48 \times 10^{-3}$	NA	NA	$1.21 \times 10^{-4}$	1127
2	Chou et al. [73]	Al <sub>0.3</sub> CrFe <sub>1.5</sub> MnNi <sub>0.5</sub>	0.5 M H <sub>2</sub> SO <sub>4</sub> 0.25 M NaCl	-231	$6.05 \times 10^{-3}$	NA	NA	$1.78 \times 10^{-3}$	*
		Al <sub>0.3</sub> CrFe <sub>1.5</sub> MnNi <sub>0.5</sub>	0.5 M H <sub>2</sub> SO <sub>4</sub> 0.50 M NaCl	-250	$1.04 \times 10^{-2}$	NA	NA	$3.95 \times 10^{-2}$	*
		Co <sub>1.5</sub> CrFeNi <sub>1.5</sub> Ti <sub>0.5</sub> Mo <sub>0</sub>	0.5 M H <sub>2</sub> SO <sub>4</sub>	-92	$30 \times 10^{-6}$	$46 \times 10^{-6}$	-41	$9 \times 10^{-6}$	1130
		Co <sub>1.5</sub> CrFeNi <sub>1.5</sub> Ti <sub>0.5</sub> Mo <sub>0.1</sub>	0.5 M H <sub>2</sub> SO <sub>4</sub>	-71	$78 \times 10^{-6}$	$45 \times 10^{-6}$	-23	$9 \times 10^{-6}$	1112
		Co <sub>1.5</sub> CrFeNi <sub>1.5</sub> Ti <sub>0.5</sub> Mo <sub>0.5</sub>	0.5 M H <sub>2</sub> SO <sub>4</sub>	-64	$72 \times 10^{-6}$	$41 \times 10^{-6}$	-20	$11 \times 10^{-6}$	1109
		Co <sub>1.5</sub> CrFeNi <sub>1.5</sub> Ti <sub>0.5</sub> Mo <sub>0.8</sub>	0.5 M H <sub>2</sub> SO <sub>4</sub>	-70	$69 \times 10^{-6}$	$44 \times 10^{-6}$	-20	$22 \times 10^{-6}$	1109
		Co <sub>1.5</sub> CrFeNi <sub>1.5</sub> Ti <sub>0.5</sub> Mo <sub>0</sub>	1 M NaOH	-546	$0.09 \times 10^{-6}$	$0.20 \times 10^{-6}$	-485	NA	NA
		Co <sub>1.5</sub> CrFeNi <sub>1.5</sub> Ti <sub>0.5</sub> Mo <sub>0.1</sub>	1 M NaOH	-379	$0.11 \times 10^{-6}$	$0.23 \times 10^{-6}$	-307	NA	NA
		Co <sub>1.5</sub> CrFeNi <sub>1.5</sub> Ti <sub>0.5</sub> Mo <sub>0.5</sub>	1 M NaOH	-657	$0.16 \times 10^{-6}$	$0.62 \times 10^{-6}$	-545	NA	NA
		Co <sub>1.5</sub> CrFeNi <sub>1.5</sub> Ti <sub>0.5</sub> Mo <sub>0.8</sub>	1 M NaOH	-589	$0.25 \times 10^{-6}$	$0.63 \times 10^{-6}$	-509	NA	NA
3	Hsu et al. [6]	FeCoNiCr	3.5 % NaCl	-260	$3.15 \times 10^{-8}$	NA	NA	NA	NA
		FeCoNiCrCu <sub>0.5</sub>	3.5 % NaCl	-290	$7.23 \times 10^{-7}$	NA	NA	NA	NA
		FeCoNiCrCu	3.5 % NaCl	-330	$1.32 \times 10^{-6}$	NA	NA	NA	NA
		304 L stainless steel	3.5 % NaCl	-250	$6.01 \times 10^{-7}$	NA	NA	NA	NA
4	Kao et al. [74]	Al <sub>0</sub> CoCrFeNi	0.5 M H <sub>2</sub> SO <sub>4</sub>	-81	$15.8 \times 10^{-6}$	$42.8 \times 10^{-6}$	2	$4.5 \times 10^{-6}$	NA
		Al <sub>0.25</sub> CoCrFeNi	0.5 M H <sub>2</sub> SO <sub>4</sub>	-95	$16.7 \times 10^{-6}$	$87.4 \times 10^{-6}$	8	$7.1 \times 10^{-6}$	NA
		Al <sub>0.50</sub> CoCrFeNi	0.5 M H <sub>2</sub> SO <sub>4</sub>	-84	$13.4 \times 10^{-6}$	$117.2 \times 10^{-6}$	17	$6.4 \times 10^{-6}$	NA
5	Lee et al. [75]	Al <sub>1.0</sub> CoCrFeNi	0.5 M H <sub>2</sub> SO <sub>4</sub>	-94	$13.1 \times 10^{-6}$	$198 \times 10^{-6}$	10	$13.9 \times 10^{-6}$	NA
		SS-304	0.5 M H <sub>2</sub> SO <sub>4</sub>	-185	$45.3 \times 10^{-6}$	$603 \times 10^{-6}$	-71	$19.1 \times 10^{-6}$	NA
		Al <sub>0.5</sub> CoCrCuFeNi	1 N H <sub>2</sub> SO <sub>4</sub>	-94	$3.188 \times 10^{-6}$	NA	NA	NA	NA
		Al <sub>0.5</sub> CoCrCuFeNiB <sub>0.2</sub>	1 N H <sub>2</sub> SO <sub>4</sub>	-128	$7.257 \times 10^{-6}$	NA	NA	NA	NA
		Al <sub>0.5</sub> CoCrCuFeNiB <sub>0.6</sub>	1 N H <sub>2</sub> SO <sub>4</sub>	-132	$1.290 \times 10^{-5}$	NA	NA	NA	NA
6	Ye et al. [76]	Al <sub>0.5</sub> CoCrCuFeNiB <sub>1.0</sub>	1 N H <sub>2</sub> SO <sub>4</sub>	-135	$2.259 \times 10^{-5}$	NA	NA	NA	NA
		304 stainless steel	1 N H <sub>2</sub> SO <sub>4</sub>	-165	$3.319 \times 10^{-5}$	NA	NA	NA	NA
		AlCoCrFeNi	0.05 M HCl	550	$29.2 \times 10^{-6}$	NA	NA	NA	NA
		Al <sub>1.3</sub> CoCrFeNi	0.05 M HCl	580	$47.9 \times 10^{-6}$	NA	NA	NA	NA
7	Qiu et al. [77]	Al <sub>1.5</sub> CoCrFeNi	0.05 M HCl	920	$31.4 \times 10^{-6}$	NA	NA	NA	NA
		Al <sub>1.8</sub> CoCrFeNi	0.05 M HCl	673	$7.6 \times 10^{-6}$	NA	NA	NA	NA
		Al <sub>2</sub> CoCrFeNi	0.05 M HCl	666	$31.7 \times 10^{-6}$	NA	NA	NA	NA
		314 L stainless steel	0.05 M HCl	-872	3231	NA	NA	NA	NA
		Al <sub>2</sub> CrFeCoCuTiNi <sub>0.0</sub>	3.5 % NaCl	510	$6.8 \times 10^{-5}$	NA	NA	NA	NA
		Al <sub>2</sub> CrFeCoCuTiNi <sub>0.5</sub>	3.5 % NaCl	-430	$3.2 \times 10^{-5}$	NA	NA	NA	NA
		Al <sub>2</sub> CrFeCoCuTiNi <sub>1.0</sub>	3.5 % NaCl	-220	$1.3 \times 10^{-5}$	NA	NA	NA	NA
8	Qiu et al. [63]	Al <sub>2</sub> CrFeCoCuTiNi <sub>1.5</sub>	3.5 % NaCl	-480	$6.4 \times 10^{-5}$	NA	NA	NA	NA
		Al <sub>2</sub> CrFeCoCuTiNi <sub>2.0</sub>	3.5 % NaCl	-500	$6.7 \times 10^{-5}$	NA	NA	NA	NA
		Q235 steel	3.5 % NaCl	-570	$7.1 \times 10^{-4}$	NA	NA	NA	NA
		Al <sub>2</sub> CrFeNiCoCu	0.5 M HNO <sub>3</sub>	-180	$38 \times 10^{-2}$	NA	NA	NA	NA
		Al <sub>2</sub> CrFeNiCoCuTi <sub>0.5</sub>	0.5 M HNO <sub>3</sub>	-300	$22 \times 10^{-2}$	NA	NA	NA	NA
		Al <sub>2</sub> CrFeNiCoCuTi <sub>1</sub>	0.5 M HNO <sub>3</sub>	-330	$7.3 \times 10^{-3}$	NA	NA	NA	NA
		Al <sub>2</sub> CrFeNiCoCuTi <sub>1.5</sub>	0.5 M HNO <sub>3</sub>	-300	$4.4 \times 10^{-3}$	NA	NA	NA	NA
		Al <sub>2</sub> CrFeNiCoCuTi <sub>2</sub>	0.5 M HNO <sub>3</sub>	-150	$2.7 \times 10^{-3}$	NA	NA	NA	NA
		Q235 steel	0.5 M HNO <sub>3</sub>	-350	$2.4 \times 10^{-1}$	NA	NA	NA	NA

Here \* means the passive region observed was so small that it can be neglected, NA = data not available.

E<sub>corr</sub>: Corrosion potential; i<sub>corr</sub>: corrosion current density; V<sub>SHE</sub>: potential versus standard hydrogen electrode (SHE); I<sub>crit</sub>: critical current density; i<sub>pass</sub>: passive current density; E<sub>pp</sub>: primary passivation potential; and ΔE: a potential difference between E<sub>b</sub> and E<sub>pp</sub>.

### 3.2. Vapour deposition

These coating fabrication methods generally consist of HEA carbide, nitride and metallic coatings. The high entropy-based nitride coatings tend to develop structures having nano-sized. This improves mechanical and physical properties (resistance against oxidation, wear, corrosion thermal stability, etc.) [157,158]. These methods include vacuum arc, magnetron sputtering, and reactive magnetron sputtering.

#### 3.2.1. Vacuum arc deposition

This method uses the heat energy of the arc to evaporate the target materials on the workpiece surface, commonly known as substrate. It has a dominant position in developing high entropy alloy-based ceramic films. The ceramic film exhibited nanocomposite, columnar, and amorphous structures along with good properties such as high resistance against oxidation/wear, low residual stress, excellent thermal stability etc.[159].

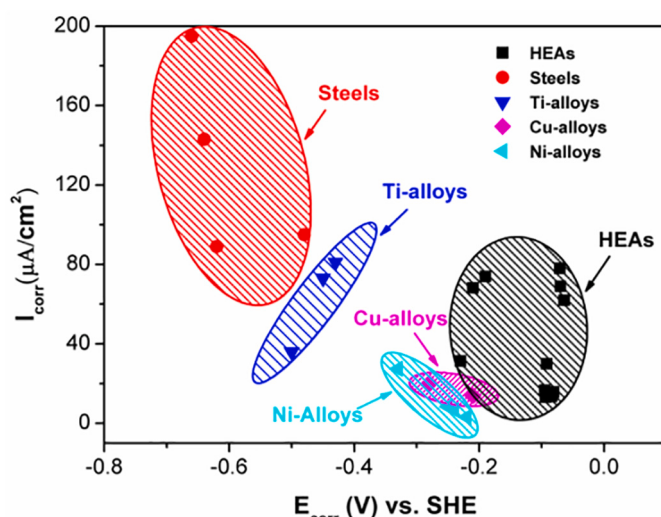


**Fig. 17.** Comparison of the corrosion potential ( $E_{corr}$ ) and corrosion current density ( $i_{corr}$ ) b/w traditional and high entropy alloy in a  $0.5\text{M}\text{H}_2\text{SO}_4$  solution at room temperature [78].

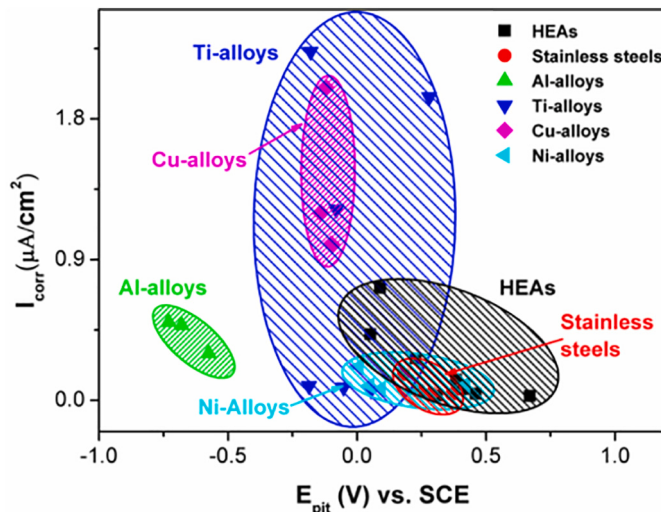


**Fig. 18.** Comparison of the pitting potential ( $E_{pit}$ ) and current density ( $i_{corr}$ ) b/w traditional materials and high entropy alloys in the  $3.5\text{ wt\% NaCl}$  solution at room temperature [78].

### 3.2.2. Magnetron sputtering/reactive magnetron sputtering

In this technique, “an electric field is developed b/w two electrodes within a vacuum chamber. Then, the inert gas (argon) is pumped into the chamber & is positively ionized owing to the electric field colloids with the electric field negatively charged plate. After that, the collision of  $\text{Ar}^+$  ions with the targeted material located on the negatively charged ion leads to the ejection of molecules/atoms of high entropy alloys from

the target area towards the base material (substrate)” [160,161]. Fig. 24 shows a schematic diagram of the magnetron sputtering process.

However, depending upon the configuration of the magnetic field b/w magnetic poles that develop magnetrons, this process can be either unbalanced or balanced.

If the magnets are organized in such a way that the magnetic field lines coming out of the outer pole at the target surface are close to the sputtering chamber at the target surface and inner pole, then the sputtering process is known as balanced sputtering. The schematic illustration of magnetic field lines in balanced magnetron sputtering is depicted in Fig. 25 (a).

On the other hand, if only a few magnetic field lines are closed b/w the outer and inner pole, then the system is known as unbalanced magnetron sputtering, as depicted in Fig. 25 (b).

The magnetron sputtering technique includes reactive deposition. This process is stable and fast. However, during sputtering, if oxygen, nitrogen or alkane is mixed into an argon (Ar) environment, then the reactive sputtering deposition technique will take place. This technique effectively develops nitride, carbide or oxide high entropy ceramic films [163].

The summaries of various HEA coating fabricated by vapour deposition coating methods are given in Table 4.

**3.2.2.1. Summary of the relationship between Vapour deposition-based methods and their features.** Vapour deposition fabrication methods, including vacuum arc deposition (VAD) and magnetron sputtering/reactive magnetron sputtering (MS/RMS), offer precise control over the deposition of high-entropy alloy (HEA) coatings, resulting in a range of desirable features and enhanced properties.

**3.2.2.2. Vacuum arc deposition (VAD).** VAD involves ionizing and accelerating metal atoms from a target material in a vacuum chamber, depositing them onto a substrate to form the coating.

This method offers:

- High-purity coatings: The vacuum environment minimizes contamination, resulting in high-purity HEA coatings with minimal impurities [171].
- Dense microstructures: The high-energy ion bombardment promotes the formation of dense, well-adhered coatings with low porosity [172].
- Versatile deposition: VAD can accommodate a wide range of HEA compositions and substrate materials [173].

**3.2.2.3. Magnetron sputtering (MS)/reactive magnetron sputtering (RMS).** MS involves sputtering HEA target material using magnetized plasma and depositing the sputtered atoms onto a substrate to form the coating. RMS introduces reactive gases into the plasma chamber to create compound HEA coatings, such as nitrides or oxides.

These methods offer:

- Controlled deposition: The precise control of plasma parameters allows for tailoring the coating thickness, composition, and microstructure [174].

**Table 2**  
Comparison of distinct refractory HEAs.

Authors	HEAs	Melting point (°C)	Structure	Density (g/cm <sup>3</sup> )	Phase stable condition (Annealing temperature/Time)
Takeuchi et al. [98]	$\text{Ir}_{26}\text{Mo}_{20}\text{Rh}_{22.5}\text{Ru}_{20}\text{W}_{11.5}$	2459	HCP	15.37	2373 K/1 h
Takeuchi et al. [99]	$\text{Ir}_{25.5}\text{Mo}_{20}\text{Rh}_{20}\text{Ru}_{25}\text{W}_{9.5}$	2444		15.18	1273 K/2000 h
Senkov et al. [50]	$\text{Ir}_{29.0678}\text{Mo}_{15}\text{Rh}_{29.0678}\text{Ru}_{11.8644}\text{W}_{15}$	2463	HCP	16.07	1673 K/19 h
Senkov et al. [100]	$\text{Nb}_{25}\text{Mo}_{25}\text{Ta}_{25}\text{W}_{25}$	2904	BCC	13.64	1473 K/3 h
Wu et al. [101]	$\text{Nb}_{20}\text{Mo}_{20}\text{Ta}_{20}\text{W}_{20}\text{V}_{20}$	2673	BCC	12.36	1573 K/6 h
	$\text{Ti}_{20}\text{Zr}_{20}\text{Hf}_{20}\text{Nb}_{20}\text{Ta}_{20}$	2231	BCC	9.94	
	$\text{Hf}_{25}\text{Nb}_{25}\text{Ti}_{25}\text{Zr}_{25}$	2039	BCC	8.4	

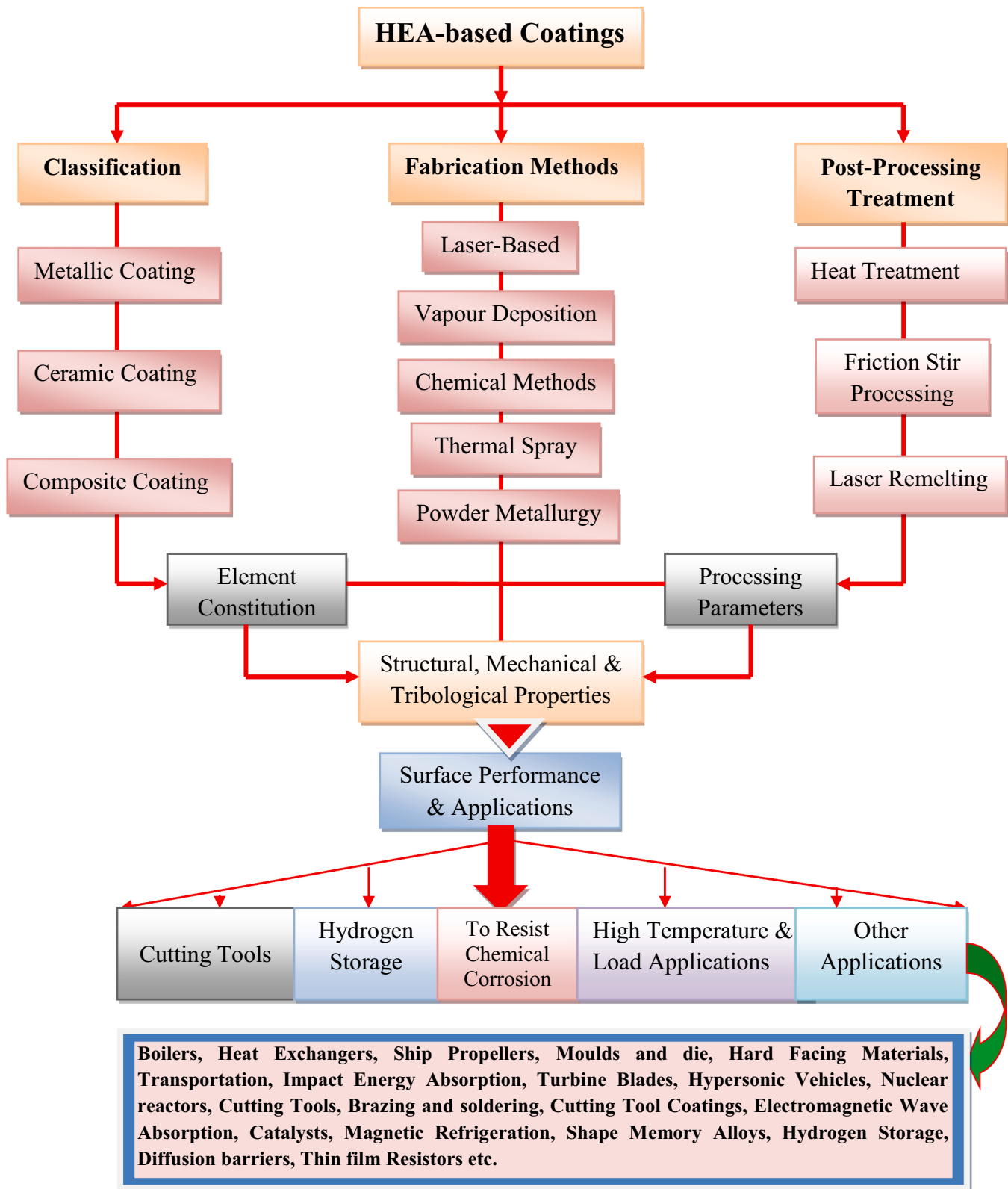


Fig. 19. Summary of the review paper: HEAs coating (coating materials, fabrication techniques, post-processing coatings, properties, applications and future scope).

- (b) Low-temperature deposition: MS and RMS can be performed at lower temperatures compared to VAD, making them suitable for temperature-sensitive substrates [175].
- (c) Large-area coatings: MS and RMS can be used to deposit uniform HEA coatings over large areas [176].

The features of HEA coatings produced by vapour deposition methods depend on the specific deposition parameters, the HEA composition, and the substrate material. However, general features include:

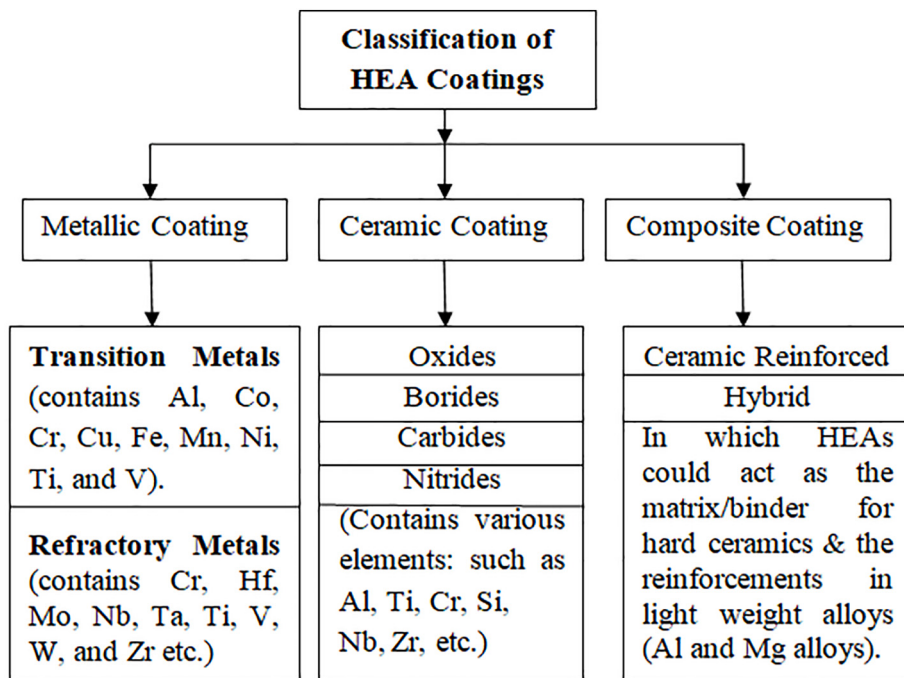


Fig. 20. Classifications of HEAs coatings [1].

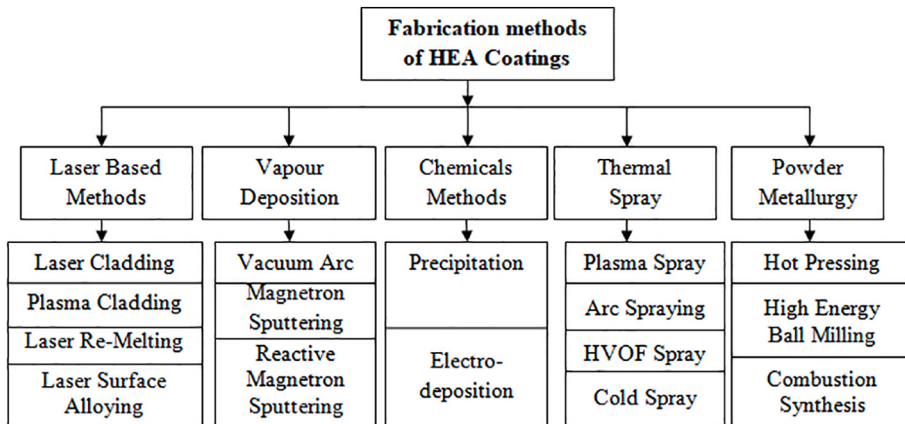


Fig. 21. General classification of fabrication methods of HEAs coating [122].

- (a) Fine-grained microstructures: The high energy input during deposition promotes the formation of fine grains, enhancing the strength, hardness, and wear resistance of the coating.
- (b) Strong adhesion: The physical impact of the deposited atoms during vapour deposition creates a strong metallurgical bond between the coating and the substrate, ensuring excellent adhesion and durability.
- (c) Tunable properties: The composition and microstructure of HEA coatings can be tailored to achieve specific properties, such as enhanced corrosion resistance, biocompatibility, or electrical conductivity [177].

In summary, vapour deposition methods provide a versatile and controlled approach to producing HEA coatings with enhanced properties, including high purity, dense microstructures, controlled deposition, low-temperature deposition, large-area coatings, fine-grained microstructures, strong adhesion, and tunable properties. The choice of vapour deposition method depends on the specific coating requirements and the desired properties of the HEA coating.

### 3.3. Chemical methods

In these methods, high entropy alloy coatings possess spherical-shaped grainy and granular structures. Among chemical methods, electro-deposition is most widely used to fabricate high entropy alloy coatings at low temperatures due to lower energy consumption and economical than laser and solid-state processes [178–180].

Electro-deposition or electroplating is widely used for the development of semiconductor thin films. In this method, the material is deposited onto a conductive substrate from a solution comprising ionic species. These methods help to enhance the external characteristics of materials such as corrosion resistance, abrasion resistance, and functional properties [181]. Fig. 26 shows a schematic representation of the electro-deposition process.

This method uses three electrodes (working, reference & counter). These electrodes are linked to a deposition-controlling instrument known as a potentiostat. In addition, these electrodes are kept within a container comprising a liquid with ionic species dissolved within it. For example, the Cu ion is dissolved in water [181].

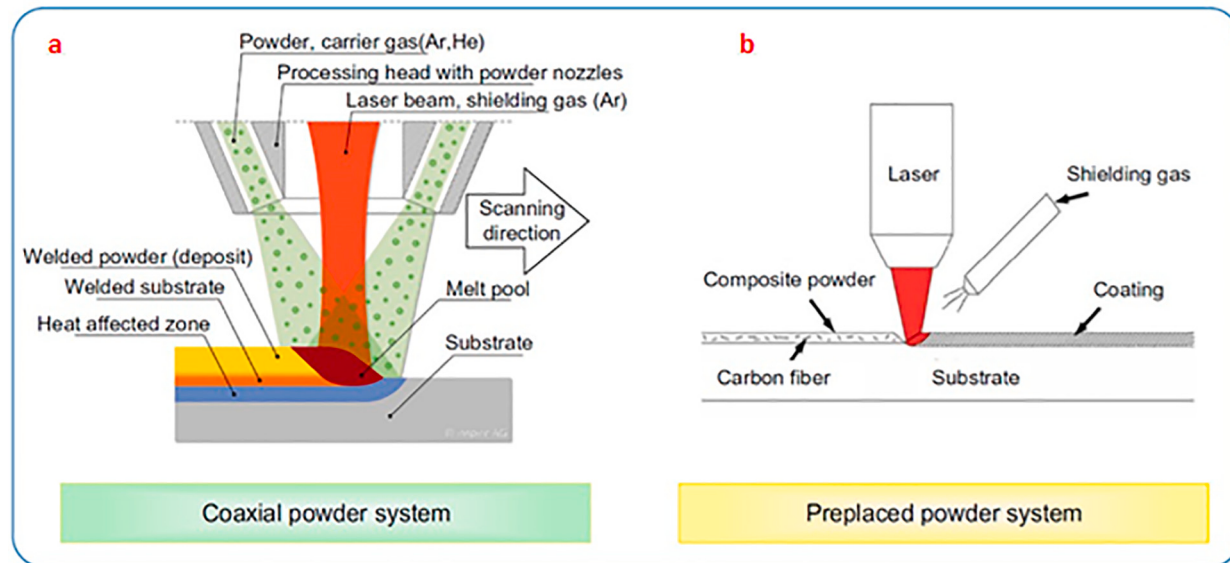


Fig. 22. Laser cladding system (a) coaxial powder system (b) preplaced powder system [126,127].

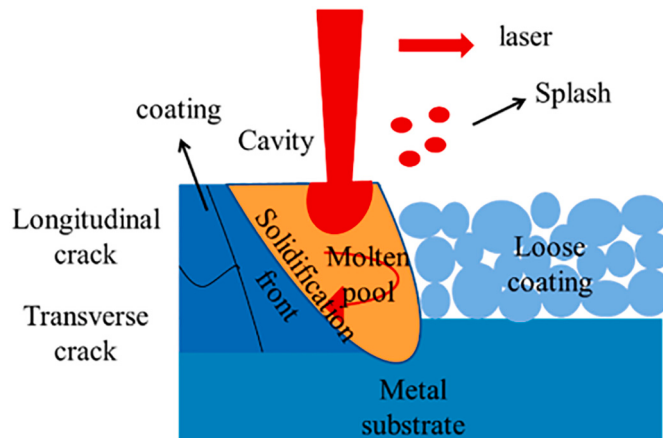


Fig. 23. Schematics illustration of laser re-melting principle [133].

The summaries of various HEA coating fabricated by chemical methods (electro-deposition) are given in Table 5.

**3.3.1.1. Summary of the relationship between chemical-based methods and their features.** Chemical-based fabrication methods, including precipitation and electrodeposition, offer a unique approach to producing high-entropy alloy (HEA) coatings with tailored compositions and microstructures. These methods result in a range of desirable features and enhanced properties.

**3.3.1.2. Precipitation.** Precipitation involves the formation of HEA nanoparticles from a solution of metallic salts. The nanoparticles are then deposited onto a substrate to form the coating. This method offers:

- (a) Low-temperature synthesis: Precipitation can be performed at relatively low temperatures, making it suitable for temperature-sensitive substrates [189].
- (b) Controlled particle size: The size of the HEA nanoparticles can be controlled by adjusting the precipitation parameters, influencing the coating microstructure and properties.

(c) Homogeneous composition: Precipitation ensures a uniform distribution of elements in the HEA nanoparticles, resulting in coatings with consistent properties [190].

**3.3.1.3. Electrodeposition.** Electrodeposition involves the reduction of metallic ions from a solution onto a conductive substrate to form the HEA coating. This method offers:

- (a) Precise control over coating thickness: The thickness of the HEA coating can be precisely controlled by adjusting the electrodeposition parameters, ensuring accurate tailoring of coating properties [191].
- (b) Complex geometries: Electrodeposition can be used to deposit HEA coatings onto complex geometries, such as intricate patterns or internal surfaces.
- (c) Compositional tailoring: The composition of the HEA coating can be tailored by adjusting the electrolyte composition, allowing for the creation of customized coatings with specific properties [192].

The features of HEA coatings produced by chemical-based methods depend on the specific deposition parameters, the HEA composition, and the substrate material. However, general features include:

- (a) Nanoscale microstructures: The chemical synthesis processes involved in precipitation and electrodeposition can result in the formation of HEA nanoparticles, leading to coatings with nanoscale microstructures [193].
- (b) Strong adhesion: The chemical bonding between the HEA coating and the substrate ensures strong adhesion and durability of the coating.
- (c) Tailored compositions: The composition of HEA coatings produced by chemical-based methods can be precisely controlled, allowing for the creation of customized coatings with specific properties, such as enhanced corrosion resistance, wear resistance, or biocompatibility [194].

In summary, chemical-based fabrication methods provide a versatile and controlled approach to producing HEA coatings with tailored compositions and nanoscale microstructures. These methods result in a range of desirable features and enhanced properties, including low-temperature synthesis, controlled particle size, homogeneous

**Table 3**

HEA coatings fabricated by laser-based coating techniques.

S. No.	Authors /reference	Substrate	Coating material	Processing parameters	Coating thickness	Microstructure	Hardness		Phase	Conclusions
							Bare	Coated		
1	Ni et al. [137]	5083 Aluminium	Al <sub>0.5</sub> FeCu <sub>0.7</sub> NiCoCr	Laser power = 1.1 kW, scanning speed = 270 mm/min., 360 mm/min, 450 mm/min and 630 mm/min., the flow rate of Ar gas = 10 l/min., laser wavelength = 1.06 μm, dia. of laser beam = 2 mm	0.8 mm	Equiaxed grains and columnar grains	93.7 HV <sub>0.2</sub>	750 HV <sub>0.2</sub>	FCC + BCC and Al phases	Crack- and porosity-free The crack and porosity-free coating were obtained by utilizing the optimized processing parameters.
2	Zhang et al. [138]	AZ31Mg	AlCoCrCuFeNiSi <sub>0.5</sub> /Y <sub>2</sub> O <sub>3</sub>	Laser power = 2 kW, scanning speed = 400 mm/min., dia. of laser beam = 4 mm.	1.5 mm	Core-shell microstructure	NA	NA	FCC + BCC	For the liquid phase separation, the addition of nano-sized Y <sub>2</sub> O <sub>3</sub> powder serves as the catalyst.
3	Qiu et al. [63]	Q235 steel	Al <sub>2</sub> CrFeNiCoCuTi <sub>x</sub>	Power = 2500 W, Dia. of spot = 4 mm, scanning speed = 3 mm/s.	1.0 mm	Equiaxed grains and columnar crystals	NA	NA	FCC + BCC	Improved resistance against wear and corrosion.
4	Ye et al. [139]	ISI 1045 steel	AlxFeCoNiCuCr	Power = 1200 W to 2000 W, scanning speed = 2 mm/s to 30 mm/s, Dia. of laser spot = 1 to 5 mm.	1.6 mm	Spherical shape precipitates	NA	At x = 1, 253.9 HV <sub>5.0</sub> At x = 1.3, 520.8 HV <sub>5.0</sub> At x = 1.5, 397.6 HV <sub>5.0</sub> At x = 1.8, 986.1 HV <sub>5.0</sub>	FCC + BCC	Higher abrasion resistance was observed at x = 2.0 than at x = 1.5.
5	Zhang et al. [140]	Q235 steel	6FeNiCoSiCrAlTi	Power = 2.0 kW, Dia. of beam = 4.5 mm, scanning speed = 400 mm/min.	1.2 mm	Equiaxed polygonal grains with interdendritic regions	280 HV	780HV <sub>0.5</sub>	BCC	Enhancement in hardness and soft magnetic property.
6	Zhang et al. [141]	Q235 steel	FeCoNiCrCu+Si, Mn, Mo	Power = 2.0 kW, Dia. of beam = 4.5 mm, scanning speed = 400 mm/min.	1.2 mm	Columnar and equiaxed grains	300 HV <sub>0.5</sub>	450 HV <sub>0.5</sub>	FCC	Enhancement in microhardness, resistance against corrosion and softening was observed in 5 % H <sub>2</sub> SO <sub>4</sub> solution
7	Zhang et al. [142]	AISI 304	AlCoCrFeNiSi	Power = 2.2 kW, Dia. of beam = 4.5 mm, scanning speed = 5 mm/s, powder feed rate = 3.3 g/min., Flow rate of Ar = 4 l/min.	NA	Dense and uniform microstructure	210 HV <sub>0.3</sub>	630.36 HV <sub>0.3</sub>	BCC	The coating offered excellent hardness and resistance against wear and corrosion. A significant improvement in hardness and resistance against wear was observed with the addition of NbC particles.
8	Li et al. [47]	Q235 steel	AlCoCrFeNi/NbC	Power = 2.5 kW, Dia. of beam = 4 mm, scanning speed = 3 mm/s	1.1 mm	Rod-like and blocky particles with equiaxed fine structure	160 HV	525 HV	FCC + BCC + NbC	The refinement in grain structure and latent heat of the coating was increased after the addition of CeO <sub>2</sub> . The coating developed with the lowest Fe-to-Co ratio of about 1:1 offered the highest amorphous content (66.7%).
9	Cui et al. [143]	TC 4 alloy	FeCoNiCrMo	Power = 2.2 kW, Dia. of beam = 3 mm, scanning speed = 400 mm/min, powder feed rate = 12 g/min.	NA	Bright white structure	350 HV <sub>0.3</sub>	850 HV <sub>0.3</sub> 950 HV <sub>0.3</sub>	BCC	
10	Shu et al. [144]	H13 steel	FeCoCrBNiSi	Power = 467, Dia. of laser spot = 2.5 mm, scanning speed = 100 mm/min, powder feed rate = 15 l/min.	200 μm	Equiaxed microstructure	850 HV <sub>0.2</sub>	350 HV <sub>0.2</sub>	FCC + Amorphous	

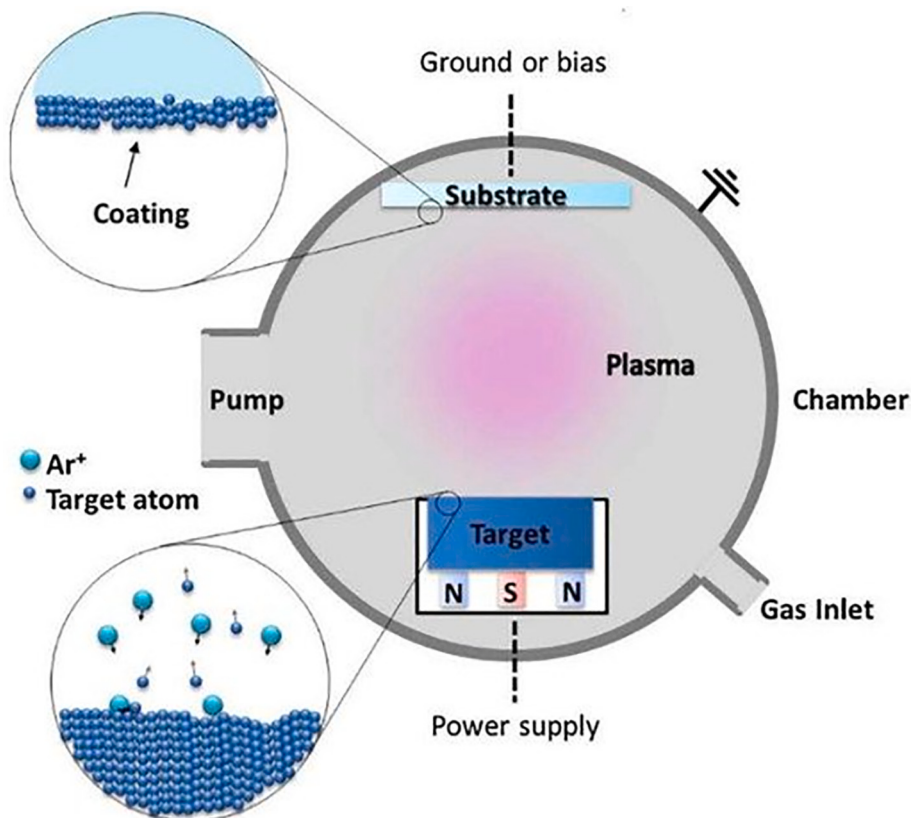


Fig. 24. Schematic illustration of magnetron sputtering [161].

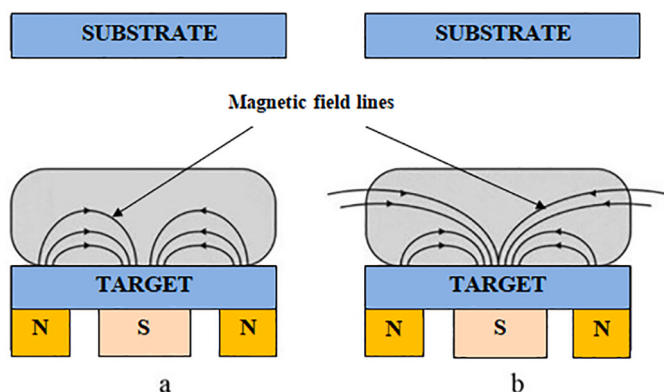


Fig. 25. Schematic illustration of magnetron sputtering system (a) Balanced (b) Unbalanced [162].

composition, precise control over coating thickness, ability to deposit coatings on complex geometries, compositional tailoring, nanoscale microstructures, strong adhesion, and tailored compositions. The choice of a chemical-based fabrication method depends on the specific coating requirements and the desired properties of the HEA coating.

### 3.4. Thermal spray

Thermal spray coating methods are widely utilized to fabricate HEA-based coatings because these coating processes are versatile to protect the base material or parts against oxidation, wear, erosion and corrosion in extreme and aggressive environments. In addition, these coating processes improved the functional and mechanical properties of the substrate [195]. Coating precursors (both semi-molten and molten) are

heated and accelerated to spray onto the substrate surface in these processes. As a result, it creates a tough, thick, and functional coating [196]. Fig. 27 depicts a schematic depiction of the thermal spray process.

In thermal spraying, the flexibility of jet configuration and thermal sources give rise to distinct categories of thermal spraying methods, such as flame spraying (wire/powder), arc spraying, high-velocity oxy-fuel spraying, plasma spraying, D-gun spraying, cold gas dynamic spraying, etc. Currently, High-velocity oxy-fuel (HVOF), plasma spraying and cold gas dynamic spraying are used by various researchers to fabricate high entropy alloy-based coating with enhanced functionality and mechanical performance.

The summaries of various HEA coating fabricated by thermal spray methods are given in Table 6.

**3.4.1.1. Summary of the relationship between thermal spray methods and their features.** Thermal spray fabrication methods, including plasma spray, arc spray, HVOF spray, and cold spray, offer a range of advantages for producing high-entropy alloy (HEA) coatings with tailored properties and enhanced performance.

**3.4.1.2. Plasma spray (PS).** Plasma spray utilizes a high-energy plasma jet to accelerate and melt HEA powder particles, depositing them onto the substrate to form the coating. This method offers:

- High deposition rates: Plasma spray enables the deposition of thick coatings at relatively high speeds, making it suitable for large-scale applications [211].
- Broad HEA compatibility: Plasma spray can accommodate a wide range of HEA compositions.

**Table 4**

HEA coatings fabricated by vapour deposition coating techniques.

S. No.	Authors /reference	Substrate	Coating material	Coating process	Processing parameters	Coating thickness	Microstructure	Hardness		Phase	Conclusions
								Bare	coated		
1	Baker et al. [164]	Si wafer	CrCu <sub>0.02</sub> N <sub>0.24</sub>	Magnetron co sputtering	Ar pressure = 3.5 mTorr, N <sub>2</sub> flow rate = 10 sccm, Substrate temperature = 300 °C to 350 °C	1–3 nm	Finer grain size	NA	25 GPa	Single phase α-Cr (N) structure	Results showed that nanocomposite structures help to enhance the resistance against fatigue.
			CrCu <sub>0.04</sub> N <sub>0.27</sub>						27 GPa	2 phase α –Cr	
			CrCu <sub>0.02</sub> N <sub>0.19</sub>						30 GPa	(N) + β -(Cr <sub>2</sub> ) N nanocrystalline structure	
		AISI 316 stainless- steel	CrCu <sub>0.12</sub> N <sub>0.30</sub>						22 GPa	2 phase Cr (N) + Cr <sub>2</sub> N structure	
			CrCu <sub>0.44</sub> N <sub>0.44</sub>						17 GPa	3-phase Cu/Cr (N)/Cr <sub>2</sub> N nanocrystalline structure	
			M2 tool-steel						15 GPa		
2	Shen et al. [165]	Silicon wafer	CrCu <sub>1.81</sub> N <sub>0.45</sub>								
			(Al 0.34								
			Cr 0.22								
			Nb 0.11								
			Si 0.11								
			Ti 0.22								
			) 50								
			N 50								
			(Al 0.34								
			Cr 0.22								
			Nb 0.11	Reactive magnetron sputtering	Pressure of 0.667 Pa Pressure = 0.667 Pa, gas flow rate = 20 (for Ar and N <sub>2</sub> ),	1.4 μm	Crystallographic structure	NA	36GPa	FCC	Coating offered high hardness, oxidation resistance and good thermal stability.
			Si 0.11								
			Ti 0.22								
			) 50								
			N 50								
			Al 0.34								
			Cr 0.22								
			Nb 0.11								
			Si 0.11								
			Ti 0.22								
			) 50								

(continued on next page)

**Table 4 (continued)**

S. No.	Authors /reference	Substrate	Coating material	Coating process	Processing parameters	Coating thickness	Microstructure	Hardness		Phase	Conclusions
								Bare	coated		
3	Khan et al. [166]	Silicon wafers Quartz Plate	50 N 50 (Al <sub>0.34</sub> Cr <sub>0.22</sub> Nb <sub>0.11</sub> Si <sub>0.11</sub> Ti <sub>0.22</sub> ) <sub>50</sub> N <sub>50</sub>	Reactive magnetron sputtering	Pressure = 0.275 Pa, gas flow rate = 20 (for Ar and N <sub>2</sub> ),	60–240 nm	Amorphous	NA	45 GPa to 80.2 GPa	NA	With the increase in Ar content, the H/E ratio increased. The coated sample offered higher resistance against corrosion than bare steel.
4	Li et al. [167]	201 stainless steel	FeAlCuCrCoMn	DC magnetron sputtering	Plasma power = 80 to 150 W, Pressure = 0.9 Pa, S.O. D. = 75 mm.	1.788 μm	Crystalline structures	NA	17.8 GPa	Single FCC solid solution	
19	Bobzin et al. [168]	WC-Co	(Cr, Al)N (Cr, Al)ON	High-speed PVD	Ar flow rate = 6000 to 12,000 sccm, N <sub>2</sub> flow rate = 600–1200 sccm, Pressure = 28.1 to 53.2 Pa and Tem. = 200 °C Ar flow rate = 6000 sccm, N <sub>2</sub> flow rate = 300–1200 sccm, Pressure = 28.5 to 31.4 Pa and Tem. = 200 °C	21.2 μm to 56.5 μm	Dense structure	NA	NA	Crystalline phase	The chromium and aluminium ratio has a significant effect on the microstructure of the coatings.
6	Chang et al. [169]	Cermet T1200A, TNMG160404R-UM & glass substrate	(AlCrNbSiTiV)N	Reactive magnetron sputtering	DC power = 200 W, gas flow rate = 30 sccm, Pressure = 1.5 × 10 <sup>-2</sup> Torr, Deposition time = 25 min.	360–451 nm	Columnar microstructure	NA	2493 HV	FCC phase	The coating was helpful in reducing the porosity, and crack and improving adhesion strength and hardness.
7	Sha et al. [170]	M2 steel	(FeMnNiCoCr)N <sub>x</sub> (at N <sub>2</sub> flow rate = 4 sccm) (FeMnNiCoCr)N <sub>x</sub> (at N <sub>2</sub> flow rate = 8 sccm) (FeMnNiCoCr)N <sub>x</sub> (at N <sub>2</sub> flow rate = 15 sccm) (FeMnNiCoCr)N <sub>x</sub> (at N <sub>2</sub> flow rate = 25 sccm)	DC magnetron sputtering	The flow rate of Ar = 50 sccm, Bias voltage = -60 V, DC target current = 4.0 A, and the flow rate of N <sub>2</sub> = 4,8,15 and 25 sccm.	1–2 μm	Refined columnar structure	NA	11 GPa 13 GPa 14 GPa 17 GPa	FCC to BCC structure	Grain boundaries are the main factor that aids in overcoming the incompatibility of scratch response, wear resistance and hardness.

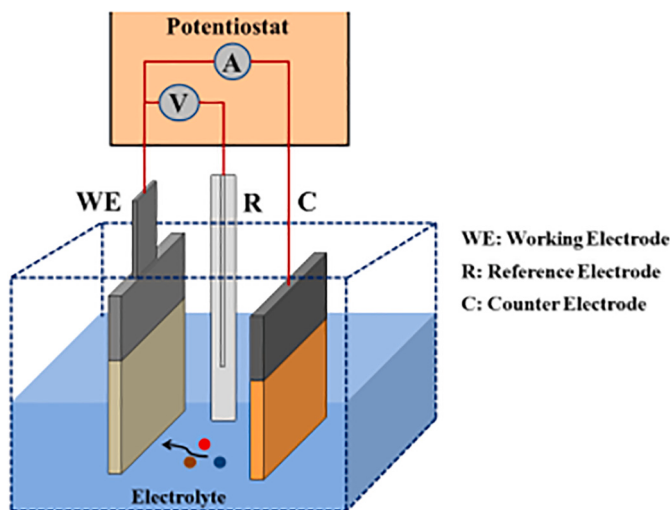


**Fig. 26.** Schematic illustration of the electro-deposition method [181].

(c) Variable coating properties: The coating properties can be tailored by adjusting plasma parameters and powder characteristics [212].

**3.4.1.3. Arc SPRAY (AS).** Arc spray involves melting and atomizing HEA powder or wire material using an electric arc, depositing the molten droplets onto the substrate to form the coating. This method offers:

- (a) Simple and robust equipment: Arc spray systems are relatively simple and robust, making them suitable for industrial applications [213].
- (b) High deposition rates: Arc spray enables the deposition of thick coatings at high speeds.
- (c) Cost-effectiveness: Arc spray is generally considered a cost-effective coating technique [214].

**3.4.1.4. High-velocity oxygen-fuel (HVOF) spray.** HVOF spray utilizes a combustion process to accelerate and heat HEA powder particles, depositing them onto the substrate at high speeds. This method offers:

- (a) Dense coatings: HVOF spray produces dense coatings with low porosity, enhancing their wear resistance and corrosion resistance [215].
- (b) Fine-grained microstructures: The high particle velocities associated with HVOF spray promote the formation of fine grains, improving the coating's strength and hardness.
- (c) Tailored coating properties: HVOF spray parameters can be adjusted to control the coating thickness, composition, and microstructure [216].

**3.4.1.5. Cold spray (CS).** Cold spray utilizes high-pressure gas to accelerate HEA powder particles at near-sonic velocities, depositing them onto the substrate without melting. This method offers:

- (a) Low-temperature deposition: Cold spray occurs at temperatures significantly lower than the melting points of the HEA components, minimizing substrate distortion and enabling deposition on temperature-sensitive materials [217].
- (b) Strong adhesion: The high particle velocities associated with cold spray promote strong mechanical bonding between the coating and the substrate.

- (c) Minimal surface oxidation: The absence of melting during deposition minimizes surface oxidation and preserves the original HEA composition [218].

The features of HEA coatings produced by thermal spray methods depend on the specific spraying parameters, the HEA composition, and the substrate material. However, general features include:

- (a) Variable coating thickness: Thermal spray methods can produce HEA coatings with a wide range of thicknesses, from a few micrometres to several millimetres [219].
- (b) Strong adhesion: The splatting and fusion of HEA particles during thermal spray create strong mechanical bonds between the coating and the substrate.
- (c) Tailored properties: The coating properties, such as wear resistance, corrosion resistance, and hardness, can be tailored by adjusting spraying parameters and HEA composition [220].

In summary, thermal spray fabrication methods provide a versatile and scalable approach to producing HEA coatings with enhanced properties, including high deposition rates, broad HEA compatibility, variable coating properties, simple and robust equipment, dense coatings, fine-grained microstructures, tailored coating properties, low-temperature deposition, strong adhesion, and minimal surface oxidation. The choice of thermal spray method depends on the specific coating requirements, the desired properties of the HEA coating, and the available equipment and expertise.

### 3.5. Powder metallurgy

Grain refinement, compact structures, and improved surface performance can all be obtained by modifying coating processing parameters and compositions using powder metallurgy techniques [221–224]. To get these findings, mechanical alloying, a hot press sintering furnace, and a graphite mould can be used. Ge et al. [225] evaluated the properties of the CuZrAlTiNi HEA coating on T10 steel achieved by mechanical alloying (MA) and vacuum hot pressing sintering (VHPS) technique. The schematic illustration of the VHPS furnace and graphite mould is represented in Fig. 28.

The vacuum hot pressing procedure was carried out at a temperature of 950 °C at a rate of 5 °C/min, at a pressure of 30 MPa, for 30 min. The interface strength between the coating and the substrate was determined to be 355.5 MPa after the coating was applied, as evaluated by a three-point bending test. In addition, the CuZrAlTiNi HEA coating outperformed the substrate in the seawater solution in terms of hardness and corrosion resistance.

The summary of various HEA coatings fabricated by powder metallurgy methods is given in Table 7.

**3.5.1.1. Summary of the relationship between powder metallurgy methods and their features.** Powder metallurgy methods, including hot pressing, high-energy ball milling, and combustion synthesis, offer unique advantages for producing high-entropy alloy (HEA) coatings with tailored properties and enhanced performance.

**3.5.1.2. Hot pressing.** Hot pressing involves compressing and heating a mixture of HEA powders to consolidate them into a dense coating. This method offers:

- (a) Dense coatings: Hot pressing produces dense HEA coatings with minimal porosity, enhancing their wear resistance and corrosion resistance [229].

**Table 5**

High entropy alloy coatings fabricated by chemical methods (electro-deposition).

S. no.	Authors /reference	Substrate	Coating material	Coating Process	Processing parameter	Coating thickness	Microstructure	Hardness		Phase	Conclusions
								Bare	Coated		
1	Aliyu et al. [182]	Mild steel (polished surface)	AlCrFeCoNiCu/ GO	Electro-deposition	Current density = 50 mA/cm <sup>2</sup> , Temperature = 30 °C, Coating area = 4 cm <sup>2</sup> , Deposition time = 15 min., p <sup>H</sup> = 1.5, Agitation speed = 850 rpm.	2.8 ± 0.5 nm	Granular microstructure	NA	NA	FCC + BCC	The resistance against corrosion was improved with the addition of graphene oxide.
2	Aliyu et al. [183]	Mild steel (polished surface)	CuFeNiCoCr	Electro-deposition	Current density = 40 mA/cm <sup>2</sup> , Temperature = 30 °C, Deposition time = 15 min., p <sup>H</sup> = 1.5, Under stirring.	3.16 ± 0.57 nm	Layered microstructure	NA	NA	FCC + BCC	The corrosion resistance of the coating increased with the addition of graphene oxide.
3	Soare et al. [184]	Pure Cu	AlCrCuFeMnNi	Electro-deposition	Time = 30, 60 and 90 min., Voltage = -1.5 V to -2.7 V	287–416 nm	Spherical and flaky	NA	NA	Amorphous + BCC	For the synthesis of multi-element HEAs, an electro-deposition process is a practical approach
4	Yoosefan et al. [185]	Copper	CoCrFeMnNi	Electrochemical deposition	DC Power = 298 K, Time = 1 h, Voltage = 1 to 6 V,	NA	Smooth	NA	NA	FCC Solid solution	The morphology of the deposited coating was found to be cracked, smooth and compacted.
5	Yao et al. [186]	Cu	Bi–Fe–Co–Ni–Mn	Potentiostatic electro-deposition	Temperature = 298 K, Voltage = -2.0 V, (Electrodeposition was done in DMF–CH <sub>3</sub> CN solution)	NA	Amorphous	NA	NA	FCC	The as-sprayed coating shows soft magnetic behaviour.
6	Malatji et al. [187]	Mild steel	Zn-Cr <sub>2</sub> O <sub>3</sub> -SiO <sub>2</sub>	Electro-deposition (electrolytic chloride bath solution)	Cathode: mild steel, Anode: Zinc, pH: 3.8, Current: 1.5A, Temperature: 25 °C	NA	Flake like crystalline	161 HVN	228 HVN	NA	From the experimental result, it is clear that Cr <sub>2</sub> O <sub>3</sub> & SiO <sub>2</sub> nanoparticles offered an excellent synergistic effect on the resistance against corrosion of Zinc based coatings
7	Malatji, N. et al. [188]	Mild steel	Zinc ZAC 1 ZAC 2 ZAC 3	Electro-deposition	Cathode: mild steel, Anode: Zinc, pH: 3.8, Current: 1.5A, Temperature: 25 °C.	NA	Uniform, compact, & agglomerated crystal grains.	122	132 238 275 239	NA	Improvement in wear resistance, micro-hardness, and thermal stability was observed.

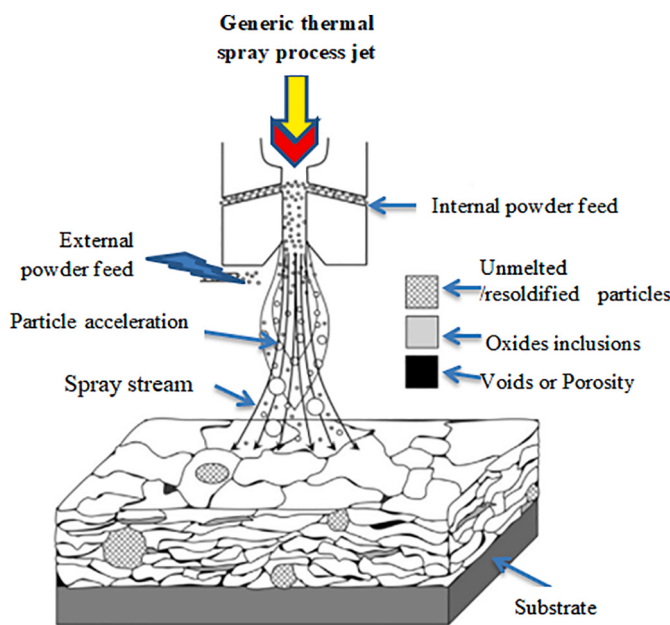


Fig. 27. Schematic illustration of thermal spraying [197].

- (b) Controlled microstructures: The hot pressing temperature and pressure can be controlled to tailor the microstructure and grain size of the HEA coating.
- (c) Scalability: Hot pressing can be used to produce HEA coatings on a variety of substrates and in various shapes and sizes [230].

**3.5.1.3. High-energy ball milling.** High-energy ball milling involves mechanically grinding and mixing HEA powders to produce a homogeneous mixture with a fine-grained microstructure. This method offers:

- (a) Fine-grained microstructures: The intense mechanical action of ball milling refines the grain size of the HEA powder, improving the coating's strength, hardness, and toughness [231].
- (b) Enhanced mixing: Ball milling ensures uniform mixing of the HEA constituents, promoting the formation of a single-phase HEA structure.
- (c) Tailored particle morphology: The ball milling process can be optimized to control the shape and morphology of the HEA particles, influencing the coating's properties [232].

**3.5.1.4. Combustion synthesis.** Combustion synthesis involves a self-propagating reaction between a mixture of HEA precursor powders, resulting in the rapid formation of a HEA coating. This method offers:

- (a) Rapid coating formation: Combustion synthesis produces HEA coatings in a short time frame, making it an efficient fabrication method [233].
- (b) High-purity coatings: The high temperatures generated during combustion synthesis ensure the formation of high-purity HEA coatings with minimal impurities.
- (c) Tailored coating composition: The composition of the HEA coating can be controlled by adjusting the precursor powder mixture [234].

The features of HEA coatings produced by powder metallurgy methods depend on the specific processing parameters, the HEA composition, and the substrate material. However, general features include

- (a) Strong adhesion: The mechanical interlocking of HEA particles during powder metallurgy processes creates strong bonds between the coating and the substrate [235].
- (b) Tunable properties: The microstructural and compositional control achieved through powder metallurgy methods allows for tailoring the properties of HEA coatings to meet specific requirements.
- (c) Scalability: Powder metallurgy methods can be adapted to produce HEA coatings on a range of substrates and in various sizes and shapes [236].

In summary, powder metallurgy methods provide a versatile and effective approach to producing HEA coatings with enhanced properties, including dense microstructures, controlled grain sizes, fine-grained microstructures, enhanced mixing, tailored particle morphology, rapid coating formation, high-purity coatings, tailored coating composition, strong adhesion, and tunable properties. The choice of powder metallurgy method depends on the specific coating requirements, the desired properties of the HEA coating, and the available equipment and expertise.

#### 4. Summary of HEA-based coatings fabricated by different methods

There are various fabrication methods for HEA coatings. The most widely used methods include laser cladding, vacuum arc melting, mechanical alloying, powder metallurgy, thermal spraying and electrochemical deposition [237–241]. However, laser cladding and electrochemical deposition are the foremost methods for coating and thin film high-entropy alloys. At the beginning of the study, researchers used magnetron sputtering and electrochemical deposition to prepare HEA coatings, but the thickness of the coating obtained by the above methods can only reach the micron scale, which is difficult to meet the requirements of high strength service environment, thus HEA coatings are usually synthesized through laser cladding process.

Laser cladding technology has more advantages than traditional HEA preparation methods. In the process of powder metallurgy, laser cladding has almost no restrictions on the selection of forming elements of HEAs, especially on the surface of low melting point metal, and the cladding powder has the advantage of easy adjustment of alloy composition. In addition, laser cladding has the characteristics of high energy density, fast heating and cooling speed ( $10^6 \text{ }^\circ\text{C/s}$ ), and less thermal effect on the substrate, which contributes to forming uniform, dense coating with fewer micro defects, and obtaining a fully dense metallurgical bonding layer between the coating and the substrate [242,243].

In addition, Laser-based methods offered attractive features including high heat input, less material wastage, rapid process, and eco-friendly method [244–246]. Although the process's quick heating and cooling rates result in less thermal damage, it also helps to create a homogeneous microstructure and robust coating substrate bonding. The creation of the heat-affected zone, high residual stresses, and elemental dilution of the HEA coating and the substrate are the main disadvantages of laser surface alloying [247]. The microstructure of high entropy alloys is significantly impacted by their production process. Depending on the thermal history, such as in laser cladding, laser surface alloying, and plasma spray techniques, a variety of microstructural characteristics of the HEA coatings are documented, including equiaxed, columnar grains, dendritic, and lamellar structures. HEA coatings produced chemically feature grainy structures that are granular and spherical.

The use of thermal spraying at high temperatures is another often-used method for HEA coatings. The most commonly used thermal spray processes are cold spray, HVOF and plasma spray [248]. Atmospheric plasma spray is appropriate for porous coatings in the case of bioimplants, while the cold gas dynamic spray is appropriate in low-temperature processing of coatings on Al, Mg alloys, or ceramics on

**Table 6**  
HEA coatings fabricated by thermal spray methods.

S. no.	Authors /reference	Substrate	Coating material	Coating process	Processing parameters	Coating thickness	Microstructure	Hardness		Phase	Conclusions		
								Bare	Coated				
1	Lobel et al. [198]	Mild steel	AlCrFeCoNi	High-velocity air fuel (HVAF)	Air pressure: 110 psi, Flow rate of N <sub>2</sub> gas: 40 l/min., SOD: 300 mm, powder feed rate: 100 g/min.	Coating layer: 15	Lamellar structure	680 ± 20 HV <sub>0.1</sub>		BCC	Higher corrosion resistance was observed in the case of HVAF coating than in HVOF coating.		
				High-velocity oxy-fuel (HVOF)	O <sub>2</sub> : 850 l/min., Kerosene (l/h): 22.5 l/h, Ar gas flow rate: 2 × 11 l/min., SOD: 360 mm	Coating layer: 23	600 ± 50 HV <sub>0.1</sub>						
				AlCoCrFeNi	Current = 300 A, Voltage = 65 V, Primary Gas Flow (Ar) = 42.1 slpm, Secondary Gas Flow rate = 2.35slpm, Powder Feed Rate = 17 to 21 g/min., Powder Carrier Gas Flow (Ar) = 6 slpm, SOD = 90 mm.	4.13 ± 0.43 GPa		BCC					
2	Ang et al. [199]	Mild steel	MnCoCrFeNi	Plasma spraying	Plasma spraying rate = 2.35slpm, Powder Feed Rate = 17 to 21 g/min., Powder Carrier Gas Flow (Ar) = 6 slpm, SOD = 90 mm.	–	Lamellar and composite-type microstructure	4.42 ± 0. + 0.60 GPa		FCC	Both the as-sprayed coating showed anisotropic mechanical behaviour		
23	Hsu et al. [200]	Incoloy-800H	Ni <sub>0.2</sub> Co <sub>0.6</sub> Fe <sub>0.2</sub> CrSi <sub>0.2</sub> AlTi <sub>0.2</sub>	HVOF	Barrel length = 100 mm, SOD = 200 mm, Powder feed rate = 2.5 r.p.m., transverse speed of spray gun = 700 mm/s and pitch = 4 mm	450 ± 19 HV		BCC structure (grey phase) + crystalline structure of Cr <sub>3</sub> Si (white phase)	The heat-treated HEA coating showed high hardness (800 HV) & good resistance against wear (20 m/mm <sup>3</sup> )				
				APS	pitch = 4 mm Current = 800 A, SOD = 80 mm, Powder feed rate = 1.6 rpm, Transverse speed of spray gun = 200 mm/s. And pitch = 4 mm	Approx. 1.5 mm	Crystalline structure	429 ± 8 HV					
				Atmospheric plasma spray	Primary gas pressure (Ar) = 0.4 MPa, Secondary gas pressure (N <sub>2</sub> ) = 0.3 MPa, Rotating speed of powder feeder = 0.8 rpm, Spray angle = 90°, Plasma power = 45KW, transverse speed = 200 mm/s and SOD = 100 mm	220 μm	Dense and uniform	612 ± 41 HV		BCC	The as-sprayed coating showed high resistance against wear.		
4	Tian et al. [201]	316 stainless steel	AlCoCrFeNiSi										
5	Yin et al. [202]	Al6082	FeCoNiCrMn	Cold spray	Propulsive gas = Helium, Inlet pressure = 3 MPa, temp. = 300 °C, S.O.D. = 30 mm, nozzle traverse speed = 100 mm/s.	1.5 mm	Dislocations and coarse-grained.	124.01 ± 38.92 HV	332.91 ± 34.74 HV	FCC	The lower wear rate of cold sprayed HEA coating than laser cladded HEA coatings		
6	Lin et al. [203]	304 stainless steel	FeCoCrNiAl	Plasma Spray	Current = 500 A, Voltage = 40 V	–	Uniform microstructure	177 HV		BCC + AlNi <sub>3</sub>	The coating after laser remelting exhibited the highest wear resistance.		

(continued on next page)

Table 6 (continued)

S. no.	Authors /reference	Substrate	Coating material	Coating process	Processing parameters	Coating thickness	Microstructure	Hardness		Phase	Conclusions
								Bare	Coated		
7	Lobel et al. [204]	S235 steel	AlCoCrFeNiTi	HVOF	Flow rate of O <sub>2</sub> , N <sub>2</sub> and Kerosin = 810 l/min., 11 l/min. and 22.5 l/h, Powder feed rate = 80 g/min., SOD = 360 mm, nozzle length = 100 mm and Relative transverse speed = 70 m/min. Arc power = 30KW, Current = 500 A, Flow rate of main gas (Ar) = 45 l/min., SOD = 100 mm	210 µm	Lamellar structure	730 ± 82 HV <sub>0.1</sub>		BCC	High resistance against wear is achieved after applying compositionally complex alloys for HVOF.
8	Wang et al. [205]	Q235 steel	(CoCrFeNi) <sub>95</sub> Nb <sub>5</sub>	Plasma Spray	Arc Current = 500 A, Power = 30Kw, Gas flow rate of primary gas (Ar) = 50 l/min., Gas flow rate of secondary gas (H <sub>2</sub> ) = 6 l/min., Powder feed rate = 30 g/min., SOD = 120 mm.	500 µm	Dendritic and interdendritic structure	310 to 325 HV		FCC + Laves phase	The coatings showed excellent resistance to corrosion
9	Xiao et al. [206]	304 stainless steel	FeCoNiCrSiAl <sub>1.5</sub>	Atmospheric Plasma Spray	Arc Current = 500 A, Power = 30Kw, Gas flow rate of primary gas (Ar) = 50 l/min., Gas flow rate of secondary gas (H <sub>2</sub> ) = 6 l/min., Powder feed rate = 30 g/min., SOD = 120 mm.	160 µm	Lamellar microstructure	418 ± 61 HV 439 ± 63 HV		BCC + FCC phase (minor)	The wear rates of as-sprayed coating underwater sliding conditions are much lower as compared to dry sliding conditions.
10	Li et al. [207]	45# steel	FeCoCrNiMo <sub>0.2</sub>	HVOF	Arc Current = 300 A, Voltage = 28–32 V, Flow rate of Ar = 2600 l/h, Flow rate of hydrogen = 50 l/h, Powder feed rate = 1 kg/h, SOD = 100 mm.	–	Lamellar structure	356HV <sub>0.2</sub>		FCC+ Fe <sub>2</sub> O <sub>3</sub> , Fe <sub>3</sub> O <sub>4</sub> , and AB <sub>2</sub> O <sub>4</sub>	The oxide content of the HVOF and APS sprayed coating was found to be 12.7 % and 47.0 %, respectively.
11	Li et al. [208]	Carbon steel	Al <sub>0.2</sub> Co <sub>1.5</sub> CrFeNi <sub>1.5</sub> Ti-Ag	Plasma Spray	Primary gas (Ar) flow rate = 90 l/min., Secondary gas flow rate = 5 l/min, Arc Voltage = 110 V, Arc Current = 330 A, Powder feeding rate = 30 g/min., SOD = 100 mm	400 µm	Lamellar structure	620.06 HV		BCC	Tribological property improved.
12	Yue et al. [209]	Pure Mg	AlCoCrCuFeNi	Plasma spray	–	–	–	390HV <sub>0.2</sub>		BCC + FCC	After re-melting, the microporosity present in the plasma sprayed coating was eliminated.

(continued on next page)

Table 6 (continued)

S. no.	Authors /reference	Substrate	Coating material	Coating process	Processing parameters	Coating thickness	Microstructure	Hardness Bare	Hardness Coated	Phase	Conclusions
13	Tian et al. [210]	316 stainless steel	AlCoCrFeNiTi/Ni-60 coating	Atmospheric Plasma Spraying	power = 15kW, Pressure (Ar) = 0.41 MPa, Pressure of secondary gas (N <sub>2</sub> ) = 0.45 MPa, Powder carrier gas (Ar) pressure = 0.28 MPa, Rotating speed of powder feeder = 0.8 r.p.m., SOD = 1.00 mm and transverse speed of gun = 200 mm/s,	240 μm	Lamellar structure	636 to 727 HV	BCC + FCC		The bonding strength of this coating (AlCoCrFeNiTi/ Ni-60) was higher than HEA coating by 60.1 MPa.

Ni-based superalloys. Nakonechnyi et al. [249] effectively deposited up to 470 μm of the thickness of cold-sprayed AlNiCoFeCrTi HEA milled powder on the steel substrate. Their findings verified that low-temperature processes generated HEA coatings with minimal porosity and that HEA coatings did not undergo phase transition or alter in phase composition.

Lu et al. [250] investigated plasma-cladded CrCuFexNiTi on Q235 and observed enhancement in hardness from 650 to 730HV<sub>0.2</sub>. Few researchers used magnetron sputtering (where HEA is atomically sputtered layer-by-layer over a substrate) to deposit HEA coatings (HEA carbide, nitride, and boride coatings). The coatings offered excellent resistance against oxidation, and irradiation resistance characteristics [251–253]. In contrast to conventional thermally sprayed coatings, the majority of these sputtered coatings feature BCC or FCC solid solution phases with amorphous morphologies. A dense (HfNbTiVZr)Nx HEA coating with a maximum thickness of 800 nm was created by sputtering, according to Tuten et al. [254]. Another method to deposit HEA coating is powder metallurgy, which does not engage any fusion of the substrate material. Numerous authors have utilized mechanically alloyed HEA powder for plasma spraying on a harder base material [255–257]. Compared to milled HEA, plasma-sprayed HEA consisted of an ordered BCC phase [257]. However, for the fabrication of HEA coatings at low temperatures, the electro-deposition method is suitable owing to its attractive properties such as lower cost, and lower energy consumption than solid state and laser-based processes [258,259]. Aliyu et al. [260] used electroplating to prepare graphene oxide-reinforced AlCrFeCoNiCu coatings. The addition of graphene oxide enhanced the homogeneity of the HEA coating matrix and reduced localized corrosion, according to the researchers, who also observed a significant increase in the coatings' resistance to corrosion. The electroplated HEAs are still in the emerging stage, nevertheless, despite all of this advancement, because of the intricate processing parameters and multicomponent alloy deposition, which is a laborious procedure given the linked pulse deposition factors [261–263].

The summary of micro-structural and coating thickness of HEA-based coatings fabricated by different methods is given in Table 8.

Hence, the choice of HEA coating method depends on the specific application requirements, the desired coating properties, and the available equipment and expertise.

In the next section, the mechanical and tribological properties of HEAs-based coatings are discussed. Multi-component and equiatomic metal components such as Fe, Ni, Co, Cr, Mn, Al, Mo, and Ti make up HEAs. The configurational entropy of mixing elements in high entropy allotrope results in the formation of single or many solid solutions with the FCC or BCC structure. This breaks the “one primary element” design concept of conventional alloys. Thus, high entropy alloys generally offer excellent mechanical and tribological properties (high strength, ductility, wear resistance, corrosion/oxidation resistance etc.) [282,283].

Among distinct high entropy alloys, FeCoNiCrMn (HEAs) with face-centred cubic structures have great interest in high-temperature applications, and cryogenic and wear resistance fields [284–288]. Xiao et al. [289] investigated the tribological characteristics of FeCoNiCrMn coatings before and after annealing using plasma spray. The results showed that examined coatings offered high resistance against wear. However, this wear resistance can be enhanced by applying heat treatment on coatings. Various authors [290–293] also reported that thermal sprayed CoNiCrMn coatings offered excellent tribological properties. Recently, Zhang et al. [292] deposited plasma sprayed CoNiCrMn composite coating reinforced by TiO<sub>2</sub> and Al<sub>2</sub>O<sub>3</sub> particles to investigate the microstructure, tribological and mechanical properties. The authors observed that the composite coatings had significantly enhanced the tribological properties compared to pure high entropy alloy coatings. This may be owing to the reinforcing particle that leads to increased resistance against crack propagation and deformation. Further, Zhang et al. [294] compared two thermal sprayed processes (atmospheric

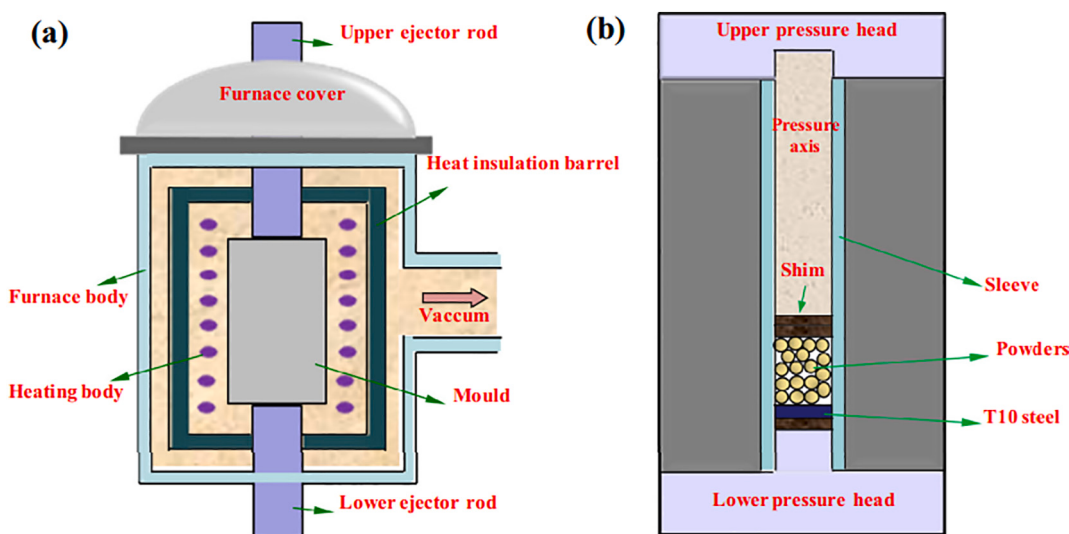


Fig. 28. Schematic illustration (a). hot pressing setup (b). mould [225].

plasma spray and cold spray). They concluded that cold-sprayed Inconel 718 coatings were harder, and denser with less oxidation than plasma sprayed. In 2022, Zou et al. [295] investigated the tribological and mechanical properties of Al<sub>2</sub>O<sub>3</sub>-reinforced FeCoNiCrMn HEA composite coating using cold spray. Pure FeCoNiCrMn and composite coatings (composite 1: 11 wt% Al<sub>2</sub>O<sub>3</sub> reinforced coating and composite 2: 20 wt% Al<sub>2</sub>O<sub>3</sub> reinforced coating) with a thickness of over 1.5 mm were deposited on 6082aluminum alloy substrate using a cold spray process as shown in Fig. 29.

Fig. 29 (a-c) indicates the SEM images at the interface b/w the substrate and as-sprayed coatings. From the images, it is clear that all of the coatings demonstrated good bonding with the substrate (aluminium alloy), as evidenced by a smooth interface devoid of fractures and gaps. Mechanical interlocking develops due to significant plastic deformation of soft material (Al alloy as substrate) when hard FeCoNiCrMn particles strike it. However, as seen in Fig. 29 (d-f), FeCoNiCrMn coatings have a dense microstructure with few pores, as indicated by yellow arrows, and red arrows indicate inter-particle boundaries. The composite coatings also possessed a thick microstructure, as illustrated in Fig. 29 (e) and (f).

The results show that the cold spray process is an effective method to fabricate high-entropy alloy coatings. The fabricated composite offered higher hardness and wear resistance (50 % reduction in wear rate) than pure FeCoNiCrMn coating (Figs. 30 and 31). The creation of a tribo-layer that can efficiently endure material loss was credited with the increased wear resistance.

Moreover, the investigated value of wear rate and micro-hardness of different HEAs coatings fabricated by a distinct thermal spray process are summarized in Table 9.

## 5. Post processing of HEAs coatings

Due to rapid cooling, severe matrix deformation, and phase shifts, several non-equilibrium phenomena occur during the manufacturing of high entropy alloy coatings. These changes may lead to reduced adhesion and result in the premature failure of the base material [158,314,315]. In addition, weak interfacial forces and other defects occur due to the development of voids caused by thermal stresses. This results in a decrease in the overall surface integrity and coating adhesion. As a result, to improve the adhesion and surface properties of HEA coatings, some post-processing techniques are used [316,317].

The commonly used post-processing techniques of HEA coatings are shown in Fig. 32.

### 5.1. Heat treatment

The grain refinement of HEA coatings is influenced by heat treatments. Zhang et al. [318] "effectively refined grain and boundary misorientation transition by annealing in the laser rapid solidified 6FeNiCoCrAlTiSi multicomponent ferrous alloy coating. The abnormal microstructure refinement and grain boundary misorientation transition in the coating after annealing at 500 °C were investigated using electron backscatter diffraction. The microstructure of the coating, however, was predominantly made up of directionally solidified columnar grains with low-angle grain boundaries spread as networks before the annealing treatment. However, following annealing, the microhardness and primary phase were determined to be nearly identical. With the grain boundary misorientation transitioning from low to high, the columnar grains transform into equiaxed refined grains. Fig. 33 indicates the cross-sectional microstructure of HEA coating (6FeNiCoCrAlTiSi) before and after annealing treatment.

After the annealing treatment, the interdendritic morphology changed into polygonal grains, as in the marked circles (represented in Fig. 33).

In brief, the interdendritic morphology became polygonal grains, as shown in the marked circles (Fig. 33). The results showed that columnar grains transition to equiaxed after annealing without a significant decrease in microhardness (Fig. 33 a, b).

In addition, columnar grains changed to equiaxed after annealing. Further, the electron backscatter diffraction maps of the high entropy alloy coating (6FeNiCoCrAlTiSi) are shown in Fig. 34.

The grain size of the coating in the electron backscatter diffraction image is substantially refined after annealing at 500 °C, as shown in Fig. 34. The arrow-marked red and green boundaries in Fig. 34 (d) indicate that with the boundary misorientation transition from low to high angles, the refined grains are predominantly modified from the subgrains in the parent columnar grain.

These findings show that the reheating process in the post-solidification stage considerably impacts grain refining during the quick solidification phase." [318] Several publications [315,316,319–321] reported comparable findings and stated that heat treatment, typically annealing in most cases, is commonly used to alter applied coatings to a roughly thermodynamic equilibrium condition.

### 5.2. Friction stir processing

Friction stir processing is a relatively new solid-state surface

**Table 7**  
HEA coatings fabricated by powder metallurgy methods.

S. no.	Authors /reference	Substrate	Coating material	Coating process	Processing parameters	Coating thickness	Microstructure		Hardness	Phases	Conclusions
							Bare	Coated			
1	Ge et al. [225]	TiO steel	CuZrAlTiNi	MA and VHPS	Vacuum level of the VHPS furnace = $3 \times 10^{-3}$ Pa, Temperature = 950 °C, Heating rate = 5 °C/min, Pressure = 30 MPa and Holding time = 30 min.	0.9 mm	Homogenous	270HV <sub>0.2</sub>	943HV <sub>0.2</sub> and AlNi <sub>2</sub> Zr	FCC + BCC	The hardness of the coated sample was found to be 3.5 times higher than the substrate. This leads to an increase the wear resistance.
2	Shang et al. [226]	Q235 steel	CoCrFeNi	MA and VHPS	200 h milled powders by VHPS, Dia. Of graphite die = 35 mm, Temp. = 950 °C, Time = 1 h, Axial pressure = 30 MPa, Cooling media = furnace.	Approx. 700 $\mu$ m	—	160 HV	450 HV	Single FCC	CoCrFeNi HEA offered higher hardness, corrosion and wear resistance than CoCrFeNiCu coating.
3	Shang et al. [227]	Q235 steel	CoCrFeNiW <sub>0.5</sub> Mn <sub>0.5</sub>	MA and VHPS	Used 200 h as-milled powders, Inner dia. of graphite die = 35 mm, Temperature = 1000 °C, time = 1 h, Axial pressure = 30 MPa and Cooling media = furnace.	600 $\mu$ m	Crystalline	669 HV	400 HV	Duplex FCC	CoCrFeNiW coating offered excellent mechanical characteristics than Mo addition coating.
4	Tian et al. [228]	Ti-6Al-4V	CrMnFeCoMoW/Al	HEMA	A Fritsch Pulverisette six-planetary ball mill was used.	650 $\mu$ m	Equiaxed	160 HV	600 HV	FCC + BCC	Al-Cr-Mn-Fe-Co-Mo-W composite coatings offered better oxidation resistance than traditional Al-Cr and Al-Si coatings.

\*Here MA = Mechanical Alloying, VHPS=Vacuum Hot Pressing Sintering, HEMA = High Energy Mechanical Alloying.

modification technique with a wide range of applications, including as-cast parts, thermally sprayed, cold-sprayed, and laser-cladded coatings or bulk composites [322–326].

Grain refining and homogeneous distributions of brittle phases or reinforcements are all benefits of this process. This may be owing to the mass frictional heat, severe plastic deformation and large forging force caused by friction stir processing [327].

Li et al. [328] used a friction stir processing technique to improve the HEAs microstructure (CrFeCoNiMoWC). The nano-structured CrFeCo-NiMoWC HEA layer was established using severe plastic deformation and laser melting deposition. The microstructure of the laser-melted HEA was primarily composed of subeutectic and dendritic structures (having grain sizes of 3  $\mu$ m to 4  $\mu$ m). After, Friction-stir processing (FSP), improvement in the micro-hardness of the plastic zone was observed. The strengthening mechanism includes dispersion/twinning strengthening, work hardening, and dislocation strengthening. In addition, FSP also improved electrochemical corrosion characteristics owing to the partial dissolution and breakage of the carbide particles. Huang et al. [329] studied the mechanical properties and dynamic recrystallization of friction stir-processed Mg-Zn-Y-Zr alloys. The author reported that during friction stir processing of as-cast test samples, greater dynamic recrystallization and more dispersed particles contribute to the development of finer & more uniform grains. This results in attaining excellent mechanical characteristics with an ultimate tensile strength of 300 MPa, yield strength of 170 MPa and elongation of 27 %. In other words, FSP improved maximum tensile strength, yield strength and elongation by 50 %, 90 % and 150 %, respectively.

FSP is feasible to induce crack-free and dense high entropy alloy coating-related surface coatings with nano-sized particles and homogeneous microstructures. This leads to the improvement of surface performance. It is worth mentioning, however, that the friction stir processing tool wears out quickly, and the worn debris will be integrated into the coatings. This affects the friction stir processing tool's lifetime and the technical usefulness of the friction stir processing procedure to modify high entropy alloy-based coatings with high hardness [328].

Overall, FSP treatment diminishes or eliminates the existing voids, pores, and micro-cracks in the as-sprayed coating. This leads to modifying the surface microstructures and improving the resistance against corrosion and wear.

### 5.3. Laser re-melting

This process improves the microstructure of high entropy alloy coatings developed by ultrafast melting and solidification. This process eliminates the internal defects, and the interfacial interaction with the high entropy alloy elements can be restricted on the alloy having low melting temperature (aluminium, magnesium and Zinc alloy) [330,331]. In addition, this technique has been utilized for the post-modification of distinct HEA coatings in the past developed by distinct thermal spray techniques, laser cladding, etc. Jin et al. [132] analyzed the properties and microstructure of plasma sprayed FeCoCrNiAl0.5Si<sub>x</sub> (x: molar ratio; x = 0.5, 1.0, and 2.0 % at.%) HEA coatings on Q235 steel and subsequently subjected them to laser remelting. In addition, the effect of distinct Si molar concentrations on the micro-hardness, microstructure evolution, phase constituents and the characteristics of high entropy alloy coating was also analyzed. The results show that with the increase of Si content (from 0 to 2), the microstructure of as-deposited HEA coating transforms gradually from BCC, FCC solid solution & Cr<sub>3</sub>Si phase to BCC solid solution and Cr<sub>3</sub>Si phase. The formation of the hard phase (Cr<sub>3</sub>Si) enhanced the coating hardness (500 HV to 1085 HV). Furthermore, after laser remelting, there was a significant improvement in bonding and surface performance.

Various authors [203,332–337] also used various post-processing techniques to improve the coating quality (improved coating hardness, microstructure, fracture toughness) and reduced porosity, surface roughness, renovation of microstructure and fragmentation of splat

**Table 8**

Comparison of micro-structural and coating thickness of HEA-based coatings fabricated by different methods.

S. no.	Authors	Substrate	Coating material	Fabrication method	Coating thickness (μm)	Micro-structure
1	Li et al. [264]	Q235 steel	AlCoCrFeNi/NbC	Laser cladding	1200	Rod-like and blocky particles with equiaxed fine structure
2	Li et al. [265]	AZ31Mg	AlCoCrCuFeNiSi <sub>0.5</sub> /Y <sub>2</sub> O <sub>3</sub>	Laser cladding	1500	Core-shell
3	Zhang et al. [266]	Q235 steel	FeCoNiCrCu+Si, Mo, Mn	Laser cladding	2000	Equiaxed and columnar grains
4	Fang et al. [267]	Pure titanium	FeCoCrNiNb <sub>x</sub>	Plasma cladding	1500	Dendritic
5	Cai et al. [268]	AISI 1045	FeCoNiAlCu	Plasma cladding	1000	Equiaxed and columnar grains
6	Shu et al. [269]	H13 steel	FeCoCrBNiSi	Laser cladding	200	Equiaxed
7	Meng et al. [270]	AZ91D Mg	AlCoCrCuFeNi	Laser melt injection	400	Dendritic eutectic
8	Cai et al. [271]	Ti64	AlCoCrNiTiV	Laser surface Allooying	800	Dendritic
9	Wu et al. [272]	Pure Copper	FeCoCrAlCuNiX	Laser surface Allooying	500	Dendritic
10	Lobel et al. [273]	S235 steel	AlCoCrFeNiTi	HVOF	210	Lamellar
11	Tian et al. [274]	316 SS	AlCoCrFeNiTi	APS	240	Lamellar
12	Yue et al. [275]	Pure Magnesium	AlCoCrCuFeNi	PS	275	Lamellar
13	Yin et al. [276]	Al6082	FeCoNiCrMn	CS	1500	Coarse-grained
14	Braic et al. [277]	C45 steel	(TiZrNbHfTa)N	Magnetron Sputtering	2	Fine-grained
15	Tuten et al. [278]	Ti64	TiTaHfNbZr	Magnetron sputtering	0.8	Couli-flower shaped
16	Pogrebnyak et al. [279]	Stainless steel	(TiZrNbAlYCr)N	Vacuum arc evaporation	7	Fine-grained droplet
17	Shang et al. [280]	Q235 steel	CoCrFeNiCu	Hot press sintering	700	Nanoscale grains
18	Aliyu et al. [260]	Mild steel	AlCrFeCoNiCu/GO	Electro-deposition	4	Granular
19	Soare et al. [281]	Pure Copper	AlCrCuFeMnNi	Electro-deposition	400	Flaky and spherical

boundaries.

Overall, it is concluded that the coatings composed of ceramic particles, laser re-melting, heat treatment procedures, and friction stir processing are all useful in surface engineering of high entropy alloy coatings that enhance the overall coating performance in terms of improving the quality and reducing the defects and porosity.

## 6. Applications of HEAs coatings

Over the last few years, high entropy materials (HEMs), such as high entropy alloys (HEAs), high entropy compounds, various high entropy oxides (HEOs), and high entropy alloy coatings, have attracted a lot of attention.

The most common applications of HEAs coating are discussed below:

### 6.1. Energy-related applications

The diverse applications of HEMs, including HEAs, HEOs, and other high entropy compounds, are shown in Fig. 35.

#### 6.1.1. Hydrogen storage

High entropy-coated alloys (HEAs) have emerged as promising materials for hydrogen storage applications due to their unique combination of properties, including:

- (a) High hydrogen absorption capacity: HEAs can absorb a significant amount of hydrogen due to their disordered atomic arrangement, which creates interstitial sites for hydrogen to occupy [339].
- (b) Enhanced hydrogen diffusion: The disordered structure of HEAs facilitates the diffusion of hydrogen atoms through the material, enabling rapid uptake and release of hydrogen [340].
- (c) Improved reversibility: HEAs exhibit good reversibility, allowing for repeated hydrogen absorption and desorption cycles without significant degradation in performance.
- (d) Thermal stability: HEAs maintain their structural integrity and hydrogen storage properties over a wide range of temperatures,

making them suitable for applications in various environments [341].

- (e) Corrosion resistance: HEAs generally exhibit good corrosion resistance in hydrogen environments, reducing the risk of material degradation and hydrogen embrittlement.
- (f) Tailorable properties: The composition of HEAs can be customized to tailor their properties for specific hydrogen storage applications, such as optimizing hydrogen absorption capacity, diffusion rate, and operating temperature range.
- (g) Versatility: HEAs can be employed in various forms, including bulk materials, thin films, and coatings, catering to diverse hydrogen storage applications [342,343].

Overall, HEAs offer a promising avenue for developing advanced hydrogen storage materials with enhanced performance and versatility, making them attractive candidates for future energy storage solutions [344–347].

#### 6.1.2. Supercapacitor

High entropy alloys (HEAs) are a class of materials that have emerged as promising candidates for supercapacitor electrodes due to their unique combination of properties, including:

- (a) High electrical conductivity: HEAs exhibit high electrical conductivity, which is essential for facilitating electron transport during the charge-discharge processes in supercapacitors [348].
- (b) Large surface area: HEAs can be engineered to have a large surface area, which provides more active sites for electrochemical reactions, leading to increased capacitance.
- (c) Enhanced electrochemical stability: HEAs generally show good electrochemical stability in various electrolyte environments, reducing the risk of material degradation and ensuring long-term performance [349].
- (d) Mechanical robustness: HEAs possess good mechanical strength, which is crucial for maintaining structural integrity during the repeated charge-discharge cycles experienced in supercapacitors.

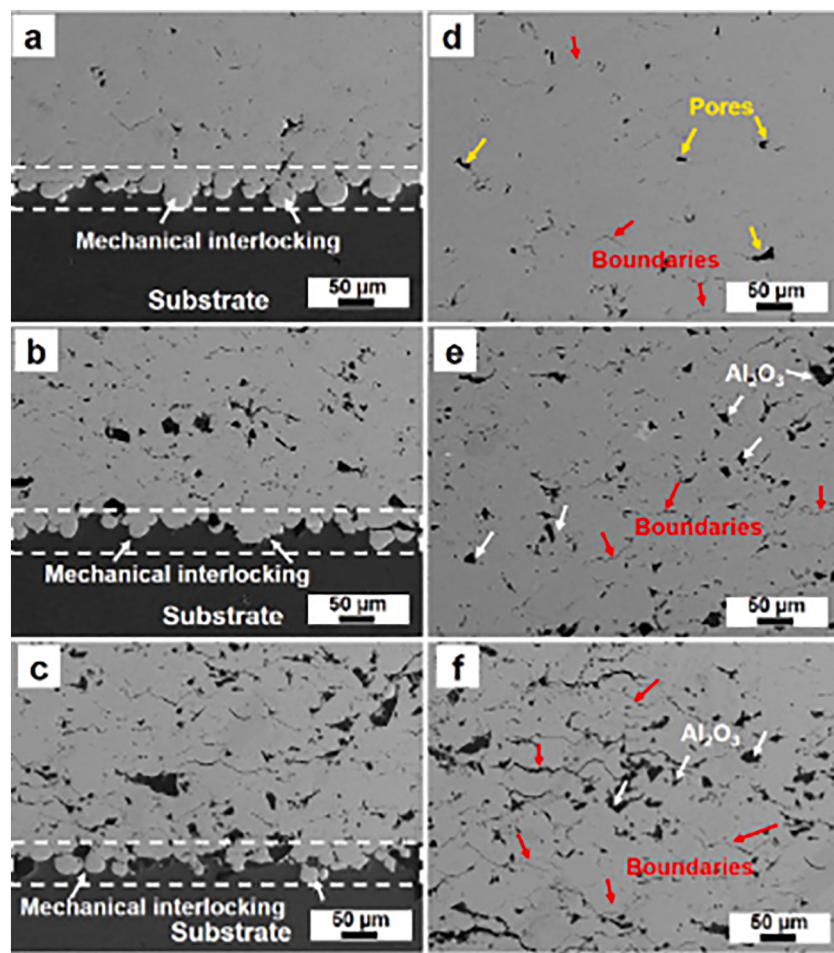


**Fig. 29.** SEM images (cross-sectional) of the coating-substrate interface & the coatings, (a), (d): Pure FeCoNiCrMn coating (b), (e): Composite coating-1 (11 wt% Al<sub>2</sub>O<sub>3</sub> reinforced coating) (c), (f): composite coating –2: (20 wt% Al<sub>2</sub>O<sub>3</sub> reinforced coating) [295].

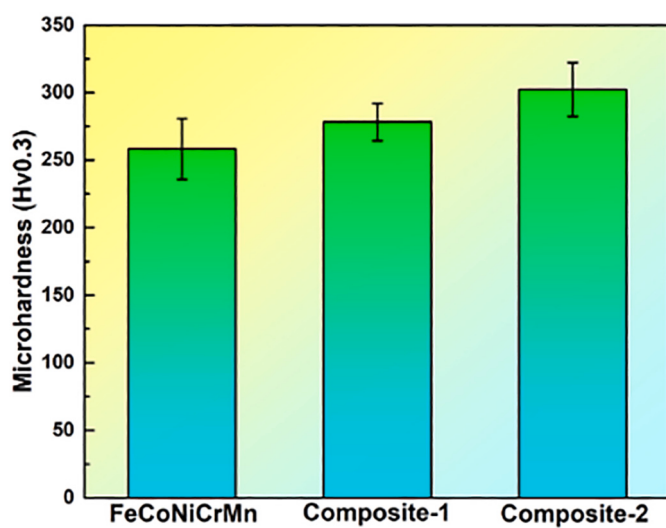


**Fig. 30.** Microhardness comparison of the pure FeCoNiCrMn and composite coatings [295].

(e) Tailorable properties: The composition of HEAs can be tailored to optimize their electrochemical properties, such as capacitance, energy density, and power density, for specific supercapacitor applications [350].

(f) Potential for cost-effectiveness: HEAs can be produced using various synthesis techniques, including mechanical alloying, arc melting, and laser processing, offering potential cost advantages compared to traditional supercapacitor electrode materials.

(g) Versatility: HEAs can be employed in various forms, including bulk materials, thin films, and coatings, allowing for their integration into different supercapacitor designs [351].

Overall, HEAs hold promise as a new generation of supercapacitor electrode materials due to their favourable combination of electrical, electrochemical, and mechanical properties. With further research and development, HEAs have the potential to revolutionize supercapacitor technology, leading to high-performance energy storage devices for various applications [352–355].

#### 6.1.3. Magnetic devices

Magnetic ions in high-entropy materials could be used to create a tunable platform for magnetic properties. High entropy alloy-based devices can be studied for applications such as magnetometers, magnetic memory, and magneto-optic devices by properly integrating HEMs with other functional compounds [338].

High entropy alloys (HEAs) are a class of materials that have emerged as promising candidates for magnetic devices due to their unique combination of properties, including:

(a) Tunable magnetic properties: The composition of HEAs can be tailored to achieve desired magnetic properties, such as saturation magnetization, coercivity, and Curie temperature. This

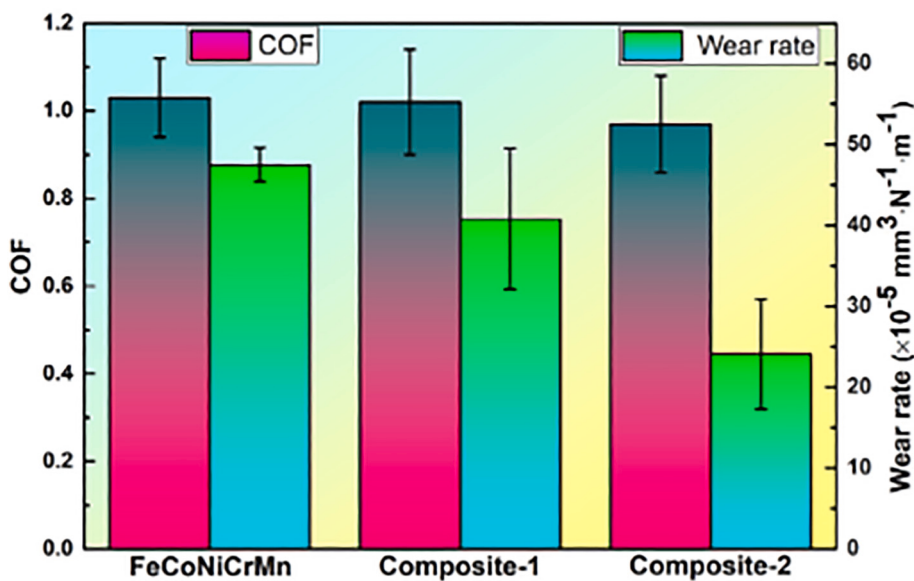


**Fig. 31.** Wear rate and coefficient of friction for the pure FeCoNiCrMn coating and composite coatings [295].

- tunability allows for the development of HEAs with specific magnetic characteristics suitable for various applications [356].
- (b) High saturation magnetization: HEAs can exhibit high saturation magnetization, which is the maximum magnetization a material can achieve at a given applied magnetic field. This property is crucial for applications where strong magnetic fields are required, such as actuators and sensors [357].
  - (c) Enhanced magnetic anisotropy: HEAs can display enhanced magnetic anisotropy, which refers to the material's preference to align its magnetization in a particular direction. High magnetic anisotropy is essential for applications where magnetic stability is critical, such as permanent magnets.
  - (d) Favourable mechanical properties: HEAs generally possess good mechanical strength and toughness, which are important for applications where magnetic devices are subjected to mechanical stress or impact [358].
  - (e) Corrosion resistance: HEAs can exhibit good corrosion resistance in various environments, reducing the risk of material degradation and ensuring long-term performance. (f) Versatility: HEAs can be employed in various forms, including bulk materials, thin films, and coatings, catering to diverse magnetic device designs [359].

Overall, HEAs hold promise as a new generation of magnetic materials due to their favourable combination of magnetic, mechanical, and corrosion resistance properties. With further research and development, HEAs have the potential to revolutionize magnetic device technology, leading to high-performance devices for various applications [360–363].

Here are some specific examples of how HEAs are being used in magnetic devices:

- (a) Permanent magnets: HEAs are being investigated for their potential to develop high-performance permanent magnets with stronger magnetic fields and higher energy product values compared to traditional materials like neodymium-iron-boron (NdFeB). [364].
- (b) Actuators: HEAs are being explored for the development of actuators that can generate precise and controlled movements in response to magnetic fields. Their tunable magnetic properties and high saturation magnetization make them promising candidates for this application [365].

- (c) Sensors: HEAs are being studied for their potential use in magnetic sensors that can detect and measure magnetic fields with high sensitivity. Their enhanced magnetic anisotropy and favourable mechanical properties make them suitable for this application [366].

As research on HEAs continues, we can expect to see even more innovative applications emerge, further demonstrating the potential of these materials in the field of magnetic devices.

#### 6.1.4. Dielectric devices

In the presence of an external electric field, the dielectric compound can store the electric energy by its polarization. Hence, dielectric materials may be utilized in distinct dielectric devices, including capacitors, storage devices, energy harvesting and high-power electronic transducers [338,367].

Recently, HEAs have emerged as promising candidates for dielectric devices due to their unique combination of properties, including:

- (a) High dielectric constant: HEAs can exhibit high dielectric constants due to their disordered atomic arrangement, which leads to a large polarization response to an applied electric field. This property is crucial for applications where high capacitance is required, such as capacitors and energy storage devices [368].
- (b) Low dielectric loss: HEAs generally demonstrate low dielectric loss, which indicates efficient energy storage and minimal dissipation during charge-discharge cycles. This property is essential for applications where low energy loss is critical, such as high-frequency electronics [369–371].
- (c) Tunable dielectric properties: The composition of HEAs can be tailored to achieve desired dielectric properties, such as dielectric constant, dielectric loss, and temperature stability. This tunability allows for the development of HEAs with specific dielectric characteristics suitable for various applications [372,373].
- (d) Enhanced electrical conductivity: HEAs can exhibit enhanced electrical conductivity compared to traditional dielectric materials, which can improve the overall performance of dielectric devices [374–376].
- (e) Thermal stability: HEAs generally possess good thermal stability, which is important for applications where dielectric devices are subjected to high temperatures [377,378].

**Table 9**

Tribological and mechanical properties of HEAs-based coating fabricated by a distinct coating process.

S. no.	Authors (years/ref.)	Substrate	Coatings	Process	Wear rate	Micro-hardness	Conclusions
1	Tian et al. [296]	316 stainless steel	AlCoCrFeNiTi/Ni60	Plasma spray	$0.55 \pm 0.06 \times 10^{-4} \text{ mm}^3 \cdot \text{N}^{-1} \cdot \text{m}^{-1}$ (at 25°C) and $0.66 \pm 0.02 \times 10^{-4} \text{ mm}^3 \cdot \text{N}^{-1} \cdot \text{m}^{-1}$ (at 500°C)	676 HV	Ni-60 is a suitable reinforcement to increase the resistance against wear.
2.	Zhang et al. [297]	Q235 steel	6FeNiCoSiCrAlTi	Laser cladding	–	780 HV0.2	The coatings offered soft magnetic properties.
3.	Hsu et al. [200]	316 SS	Ni <sub>0.2</sub> Co <sub>0.6</sub> Fe <sub>0.2</sub> CrSi <sub>0.2</sub> AlTi <sub>0.2</sub>	Atmospheric plasma spray HVOF	21 ± 3 (m/mm <sup>3</sup> ) 20 ± 2 (m/mm <sup>3</sup> )	800 HV0.5 790 ± 13 HV0.5	Lamellar morphology and FCC + BCC+ Cr <sub>3</sub> Si phase were observed.
4	Tian et al. [298]	316 SS	AlCoCrFeNiTi	Atmospheric plasma spray	$0.77 \pm 0.01 \times 10^{-4} \text{ mm}^3 \text{ N}^{-1} \text{ m}^{-1}$	642 HV0.2	The higher bonding strength was observed (50.3 ± 8.5 MPa)
5	Ge et al. [225]	T10 steel	CuZrAlTiNi	Hot-pressing sintering	Slightly improved	943 HV0.2	Improved wear resistance and hardness.
6	Lobel et al. [204]	S235 steel	AlCoCrFeNiTi	HVOF	Wear depth 120 μm	730 ± 82 HV <sub>0.1</sub>	Lamellar structure with BCC phase and higher wear resistance was observed.
7	Yin et al. [299]	6082 Al	FeCoNiCrMn	Cold spraying	$4.76 \pm 0.22) \times 10^{-4} \text{ mm}^3 / \text{Nm}$	332.91 ± 34.74 HV	FCC phase with low porosity was observed
8	Ni et al. [137]	5083 Al	Al0.5FeCu0.7NiCoCr	Laser cladding	–	750 HV0.2	The hardness of the coating was eight times higher than the substrate and Crack/porosity-free coating was attained.
9	Li et al. [47]	Q235 steel	AlCoCrFeNi/NbC (0 wt% NbC particle) AlCoCrFeNi/NbC (10 wt% NbC particle) AlCoCrFeNi/NbC (20 wt% NbC particle) AlCoCrFeNi/NbC (30 wt% NbC particle) FeCoCrNiNb(x = 0.25) FeCoCrNiNb(x = 0.60)	Laser cladding	Wear loss = 1.66 mg Wear loss = 1.31 mg Wear loss = 1.05 mg Wear loss = 1.17 mg Wear mass loss = 2.3 mg Wear mass loss = 1.7 mg	210 HV0.2 405 HV0.2 585 HV0.2 530 HV0.2 550 HV0.2 600 HV0.2	The addition of 20 wt% NbC particle showed promising results.
10	Fang et al. [129]	Pure Ti	FeCoCrNiNb(x = 0.80)	Plasma cladding	Wear mass loss = 2.1 mg	580 HV0.2	The wear resistance and hardness of the coating first increase and then decrease with the addition of Nb content.
11	Cao et al. [300]	M2 steel	CoCrNi/Ti	Magnetron sputtering	–	7.6 GPa	A high elastic modulus of about 233 GPa was measured.
12	Pogrebniak et al. [301]	Stainless-steel	(TiZrNbAlYCr)N	Vacuum-arc deposition	–	47 GPa	At the lowest pressure, a BCC lattice with crystallites (15 nm) was formed.
13	Wang et al. [302]	304 stainless steel	Ni <sub>0.2</sub> Co <sub>0.6</sub> Fe <sub>0.2</sub> CrSi <sub>0.2</sub> AlTi <sub>0.2</sub> NiCo <sub>0.6</sub> Fe <sub>0.2</sub> CrSiAlTi <sub>0.2</sub> NiCo <sub>0.6</sub> Fe <sub>0.2</sub> Cr <sub>1.5</sub> SiAlTi <sub>0.2</sub> NiCo <sub>0.6</sub> Fe <sub>0.2</sub> Cr <sub>1.5</sub> AlTi <sub>0.2</sub> MnNiCo <sub>0.6</sub> Fe <sub>0.2</sub> Cr <sub>1.5</sub> SiAlTi <sub>0.2</sub> MnCo <sub>0.6</sub> Fe <sub>0.2</sub> Cr <sub>1.5</sub> SiAlTi <sub>0.2</sub>	Plasma spray	880 ± 10 HV 888 ± 23 HV 1045 ± 12 HV 633 ± 10 HV 479 ± 7 HV 540 ± 8 HV	880 ± 10 HV 888 ± 23 HV 1045 ± 12 HV 633 ± 10 HV 479 ± 7 HV 540 ± 8 HV	The hardness of HEAs after thermal spray and heat treatment at 1100 °C for ten hours is significantly enhanced to a nearly casted state (1045 Hv). In addition, it provides excellent coarsening resistance performance resulting from the several unidentified phases and Cr <sub>3</sub> Si.
14	Xiao et al. [303]	Steel	FeCoNiCrMn-3	Plasma spray	$5.3 \times 10^{-4} \text{ mm}^3 / \text{Nm}$	273 ± 35 HV	The wear rate of the as-sprayed FeCoNiCrMn high entropy alloy coating was decreased by half when the H <sub>2</sub> flow rate enhanced from 3 to 6 l/min
15	Hsu et al. [304]	304 stainless steel	NiCo <sub>0.6</sub> Fe <sub>0.2</sub> Cr <sub>1.5</sub> SiAlTi <sub>0.2</sub>	Atmospheric plasma spraying	–	1045 HV	The high hardness and wear resistance make the examined coating a promising overlay coating for high-temperature applications
16	Qiu et al. [63]	Q235 steel	Al <sub>2</sub> CrFeNiCoCuTi <sub>x</sub>	Laser cladding	$3.80 \times 10^{-4} \text{ mm}^3 / \text{Nm}$	–	The examined HEA exhibited excellent corrosion and wear resistance.

(continued on next page)

**Table 9 (continued)**

S. no.	Authors (years)/ref.	Substrate	Coatings	Process	Wear rate	Micro-hardness	Conclusions
17	Zhang et al. [305]	Q235 steel	FeCoNiCrCu+Si, Mn, Mo  (Fe <sub>x</sub> Co <sub>100-52</sub> ) <sub>42</sub> Cr <sub>29</sub> Ni <sub>8</sub> Si <sub>7</sub> B <sub>14</sub> (Fe <sub>x</sub> Co <sub>100-57</sub> ) <sub>42</sub> Cr <sub>29</sub> Ni <sub>8</sub> Si <sub>7</sub> B <sub>14</sub> (Fe <sub>x</sub> Co <sub>100-62</sub> ) <sub>42</sub> Cr <sub>29</sub> Ni <sub>8</sub> Si <sub>7</sub> B <sub>14</sub>	Laser cladding	–  6 × 10 <sup>-4</sup> mm <sup>3</sup> /Nm 7 × 10 <sup>-4</sup> mm <sup>3</sup> /Nm 7.5 × 10 <sup>-4</sup> mm <sup>3</sup> /Nm	375 HV <sub>0.5</sub>  850 HV 820 HV 790 HV	The HEAs coating has high micro-hardness, high corrosion resistance and excellent resistance to softening in 5 % H <sub>2</sub> SO <sub>4</sub> solution.
18	Shu et al. [306]	H13 steel	(Fe <sub>x</sub> Co <sub>100-67</sub> ) <sub>42</sub> Cr <sub>29</sub> Ni <sub>8</sub> Si <sub>7</sub> B <sub>14</sub>	Laser cladding	8 × 10 <sup>-4</sup> mm <sup>3</sup> /Nm	700 HV	The coating achieved with the lowest Fe-to-Co ratio (1: 1) offered the highest amorphous content (66.7 %), while the lowest amorphous content (59.2 %) was achieved in the coating with the highest Fe-to-Co ratio (2: 1). The mean friction coefficient of high entropy alloy coating is ~0.58, which is about 66 % that of the substrate. Results showed that higher wear resistance could be attained by employing compositionally complex alloys for HVOF.
19	Zhang et al. [307]	Q235 steel	FeCoCrAlCu	Laser surface alloying	2.98 × 10 <sup>-6</sup> mm <sup>3</sup> /N m	826 HV	Coated samples exhibited 4 times more hardness than the substrate. Based upon results, examined HEA coating can effectively protect against cracking and wear, mainly for long-term orthopaedic implants.
20	Lobel et al. [308]	S235 steel	AlCoCrFeNiTi	HVOF	Wear depth = 25–40 µm	730 ± 82 HV <sub>0.1</sub>	Due to their good wear and friction performance, the achieved multi-element coatings are promising candidates for different tribological applications.
21	Tian et al. [309]	316 stainless steel	AlCoCrFeNiTi	Atmospheric plasma spray	0.77 ± 0.01 × 10 <sup>-4</sup> mm <sup>3</sup> /Nm	642 HV	Ni10 high entropy alloy coating developed with cold spray had very low porosity and completely retained the high entropy alloy phase structure without any phase transformation.
22	Tuten et al. [310]	Ti64	TiTaHfNbZr	Magnetron sputtering	Negligible wear loss	12.51 ± 0.34 GPa	The addition of copper lowers the wear, corrosion and hardness.
23	Braic et al. [311]	C45 and M2 steel	TiZrNbHfTa (TiZrNbHfTa)N (TiZrNbHfTa)C TiN TiC	Magnetron sputtering	17 ± 1 × 10 <sup>-6</sup> mm <sup>3</sup> N <sup>-1</sup> m <sup>-1</sup> 2.9 ± 0.2 × 10 <sup>-6</sup> mm <sup>3</sup> N <sup>-1</sup> m <sup>-1</sup> 0.8 ± 0.05 × 10 <sup>-6</sup> mm <sup>3</sup> N <sup>-1</sup> m <sup>-1</sup> 4.4 ± 0.2 × 10 <sup>-6</sup> mm <sup>3</sup> N <sup>-1</sup> m <sup>-1</sup> 9.4 ± 0.6 × 10 <sup>-6</sup> mm <sup>3</sup> N <sup>-1</sup> m <sup>-1</sup>	636 HV 600 HV	High-entropy alloy coatings developed with cold spray had very low porosity and completely retained the high entropy alloy phase structure without any phase transformation.
24	Wu et al. [312]	Pure Cu	FeCoCrAlCuNi <sub>05</sub> FeCoCrAlCuNi <sub>10</sub> FeCoCrAlCuNi <sub>15</sub>	Laser surface alloying	2.49 × 10 <sup>-4</sup> mm <sup>3</sup> /Nm 9.31 × 10 <sup>-4</sup> mm <sup>3</sup> /Nm 2.6 × 10 <sup>-4</sup> mm <sup>3</sup> /Nm	522 HV	Here are some of the reasons why HEAs are used in alcohol oxidation
25	Yin et al. [313]	Al6082	FeCoNiCrMn	Cold spray	4.76 ± 0.22 × 10 <sup>-4</sup> mm <sup>3</sup> /Nm	332.91 + 34.74 HV	High-entropy alloys (HEAs) are a class of materials that are composed of multiple elements in equiatomic or near-equiatomic proportions. They have attracted significant attention in recent years due to their unique properties, including high strength, hardness, toughness, and corrosion resistance. These properties make them promising candidates for a variety of applications, including alcohol oxidation [386].
26	Shang et al. [226]	Q235 steel	CoCrFeNi CoCrFeNiCu AlCrCuFeMnNi	Hot press sintering	– –	450 HV 400 HV	Overall, HEAs hold promise as a new generation of dielectric materials due to their favourable combination of dielectric, electrical,

- (f) Mechanical robustness: HEAs can exhibit good mechanical strength and toughness, which are crucial for maintaining the structural integrity of dielectric devices during operation [379–381].
- (g) Corrosion resistance: HEAs can demonstrate good corrosion resistance in various environments, reducing the risk of material degradation and ensuring long-term performance [382–384].
- (h) Versatility: HEAs can be employed in various forms, including bulk materials, thin films, and coatings, catering to diverse dielectric device designs [385].

Overall, HEAs hold promise as a new generation of dielectric materials due to their favourable combination of dielectric, electrical,

thermal, mechanical, and corrosion resistance properties. With further research and development, HEAs have the potential to revolutionize dielectric device technology, leading to high-performance devices for various applications.

#### 6.1.5. Alcohols oxidation

High-entropy alloys (HEAs) are a class of materials that are composed of multiple elements in equiatomic or near-equiatomic proportions. They have attracted significant attention in recent years due to their unique properties, including high strength, hardness, toughness, and corrosion resistance. These properties make them promising candidates for a variety of applications, including alcohol oxidation [386].

Here are some of the reasons why HEAs are used in alcohol oxidation

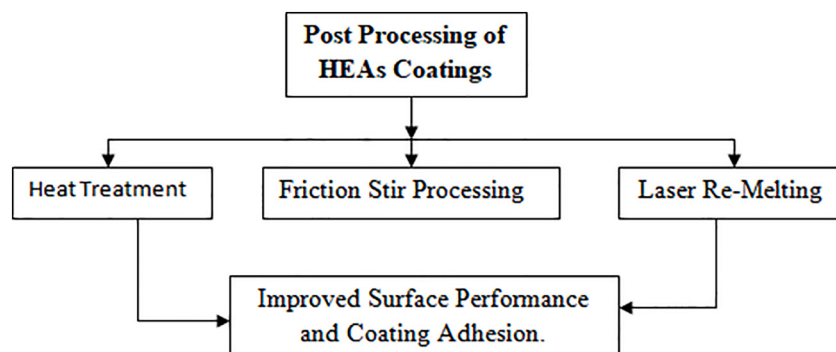


Fig. 32. Post-processing techniques of HEA coatings [317].

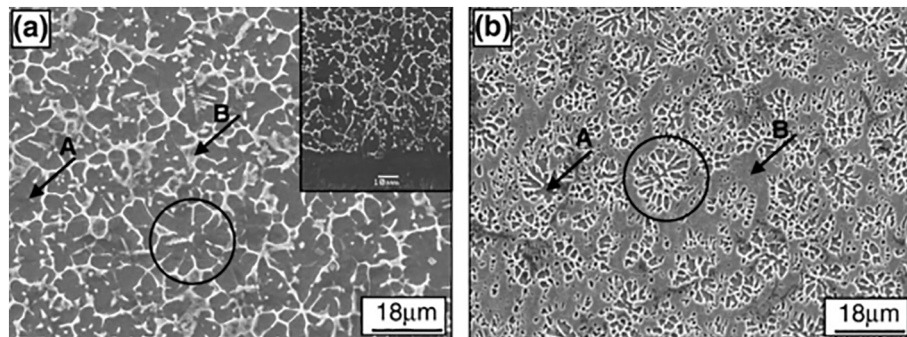


Fig. 33. Cross-section microstructure of the HEA coating (6FeNiCoCrAlTiSi) (a). before annealing treatment (b). after annealing treatment [318].

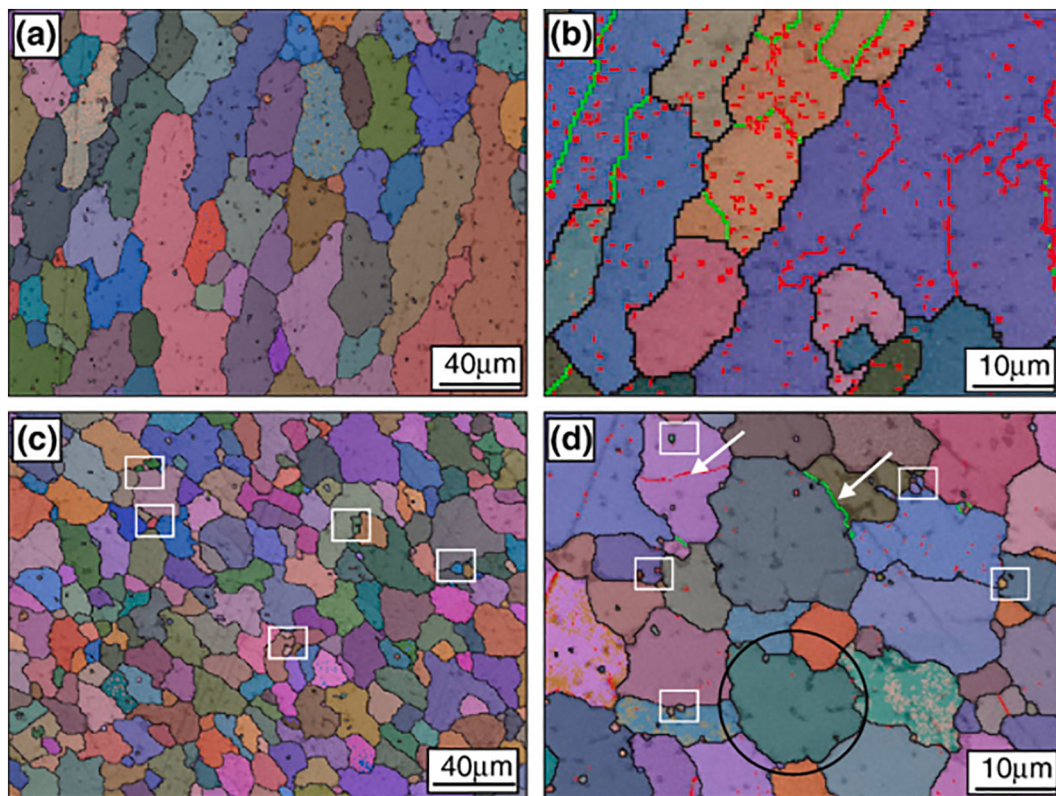
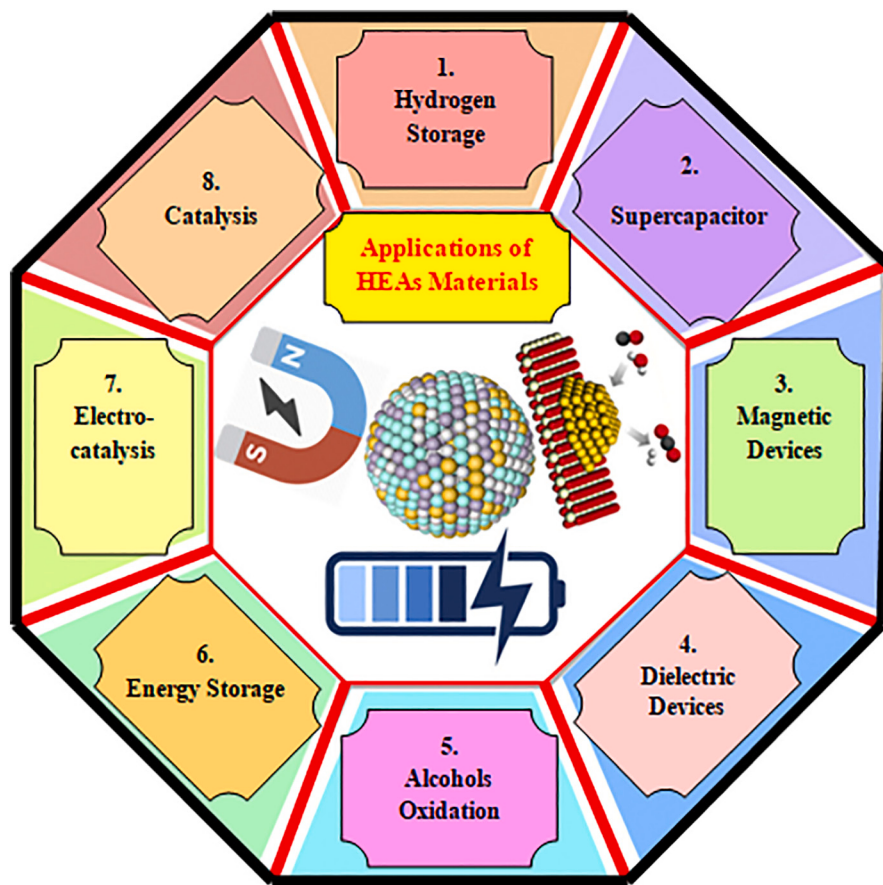


Fig. 34. “Electron Backscatter Diffraction maps of the HEA coating (6FeNiCoCrAlTiSi). (a) and (c) represents the orientation maps with the boundary misorientation larger than 5° before and after annealing at 500°C, respectively; (b) and (d) represents the orientation map with the angle of grain boundaries ranging from 1° to 3° (red) and larger than 3° (black) before and after annealing”[318].



**Fig. 35.** Diverse applications of HEMs, including HEAs, HEOs and other high entropy compounds in the energy sector [338].

applications:

- (a) Enhanced catalytic activity: HEAs can exhibit significantly enhanced catalytic activity compared to traditional catalysts. This is due to their unique electronic structure and the synergistic effects of their multiple elements [387,388].
- (b) Improved stability: HEAs are often more stable than traditional catalysts, which can lead to longer lifetimes and reduced operating costs. This is because they are less susceptible to deactivation by reaction intermediates and poisoning by impurities [389–391].
- (c) Tunable properties: The properties of HEAs can be tuned by varying the composition of the alloy. This allows for the development of HEAs with specific properties that are tailored to the desired application [392].

Some researchers reported that a HEA composed of Pt, Pd, Cu, Ag, and Au exhibited significantly enhanced electrocatalytic activity for ethanol oxidation compared to traditional Pt-based catalysts. The HEA catalyst also showed superior stability and durability [393–395].

However, HEA composed of Al, Nb, Ta, Zr, and Ti exhibited excellent catalytic activity for the oxidation of 2-propanol. The HEA catalyst was also found to be highly resistant to oxidation and corrosion [396–398].

These studies demonstrate the potential of HEAs as catalysts for alcohol oxidation. Further research is needed to optimize the composition and structure of HEAs for specific applications, but they hold promise for replacing traditional catalysts in a variety of industrial processes.

#### 6.1.6. Energy storage

Due to its appealing features, such as high capacity and high ionic/

electronic conductivity, many authors have used high entropy oxides for energy storage devices. Electrodes for lithium/sodium ion batteries, lithium/Sulfur batteries, and solid electrolytes are among them [338].

Recently, High-entropy alloys (HEAs) have emerged as promising materials for energy storage applications due to their unique properties, including:

- (a) Enhanced electrochemical performance: HEAs exhibit exceptional electrochemical properties, including high specific capacity, excellent cycle stability, and fast rate capability. These properties are attributed to their disordered atomic arrangement and synergistic interactions among multiple elements [399,400].
- (b) Improved thermal stability: HEAs possess high thermal stability, enabling them to withstand the harsh operating conditions of energy storage devices, such as high temperatures and cycling stresses. This stability arises from their unique lattice structure and strong interatomic bonding [401–403].
- (c) Tunable properties: The composition of HEAs can be tailored to achieve desired properties, offering a versatile platform for material design. By adjusting the elemental ratios and types, HEAs can be optimized for specific energy storage applications [404,405].

Here are some specific applications of HEAs in energy storage:

- (a) Lithium-ion batteries (LIBs): HEAs are being explored as anode and cathode materials for LIBs due to their high specific capacity, excellent cycle stability, and enhanced lithium diffusion kinetics [406,407].

- (b) Sodium-ion batteries (SIBs): HEAs are promising alternatives to conventional SIB electrode materials, offering improved sodium storage capacity, cycling stability, and rate capability [408,409].
- (c) Supercapacitors: HEAs are being investigated as electrode materials for supercapacitors due to their high electrical conductivity, large specific capacitance, and excellent rate performance [410,411].

In particular, the applications in supercapacitors exhibited a promising capacitive performance. For instance, Jin et al. [412] reported a new class of high entropy metal nitrides operated as a favourable candidate for supercapacitors, with a specific capacitance of  $230 \text{ F g}^{-1}$  at a scan rate of  $10 \text{ mVs}^{-1}$ . In addition, Lal and Sundara [413] reported high entropy oxides and CNT composite with a high capacitance of  $286.6 \text{ F g}^{-1}$  ( $10 \text{ mV s}^{-1}$ ). These new alloys involve the mixing of multiple metallic elements and have attracted considerable attention due to their distinctive physicochemical properties [414]. Such distinctive physicochemical properties covering excellent magnetic and electrical properties, high mechanical and thermal stability, and corrosion and oxidation resistance are greatly enhanced when their size is reduced to the nanoregime [415]. Thus, these studies suggest a promising potential of HEAs in supercapacitors.

- (d) Hydrogen storage: HEAs exhibit promising hydrogen storage properties, including high hydrogen absorption capacity, favourable thermodynamics, and enhanced reversibility [416,417].
- (e) Redox flow batteries: HEAs are being explored as electrode materials for redox flow batteries due to their high redox activity, stability in electrolyte solutions, and tunable electrochemical properties [418,419].

In summary, HEAs offer a promising avenue for developing advanced energy storage materials with enhanced performance, stability, and tunability. Their potential to revolutionize energy storage technologies is being actively investigated, and their applications are expected to expand significantly in the future.

#### 6.1.7. Electro-catalysis

High entropy alloys have recently been discovered to have considerable potential as electro-catalysts for the oxygen reduction reaction. A near-continuum of adsorption energies can be found on the surface of a high-entropy alloy. This could be owing to a large number of surface configurations and the fact that a simple model can project the entire range of adsorption energies. The surface structure can then be engineered to maximize catalytic activity for the oxygen reduction reaction [420].

However, the unique composition leads to several advantages that make HEAs attractive for electrocatalysis:

- (a) Enhanced Catalytic Activity: The multi-element composition of HEAs can create synergistic effects that enhance their catalytic activity compared to traditional catalysts. The presence of multiple elements with different electronic properties and d-band positions can lead to the formation of active sites with optimized binding energies for reactants and intermediates, facilitating efficient electrocatalytic reactions [421,422].

In simple words, due to rational adsorption energy, HEAs have excellent electrocatalytic active, then they can be employed to prepare electrodes. The overpotential of high-entropy alloys (HEAs) for various electrochemical reactions is typically lower than that of commercial electrodes, indicating their superior catalytic performance [423]. Here's a comparison of the overpotential of HEAs and commercial electrodes for different electrochemical reactions, specifically in millivolts (mV) is given in Table 10.

As you can see, HEAs consistently exhibit lower overpotentials compared to commercial electrodes, demonstrating their enhanced catalytic activity. This is attributed to their unique structure and composition, which allows for more efficient electron transfer and active site availability.

- (b) Improved Stability: HEAs often exhibit exceptional stability under harsh electrocatalytic conditions, such as high temperatures, acidic or alkaline environments, and reactive species. This stability is attributed to their high configurational entropy, which reduces the driving force for phase decomposition and segregation. As a result, HEAs can maintain their structural integrity and catalytic activity over extended periods, even under demanding operating conditions [424–426].
- (c) Tunable Properties: The properties of HEAs can be precisely tailored by adjusting the composition and arrangement of their constituent elements. This versatility allows for the development of HEAs with specific properties that are optimized for different electrocatalytic applications. By varying the elemental ratios and types, HEAs can be fine-tuned to achieve desired catalytic activity, selectivity, and stability [427,428].
- (d) Synergistic Effects: The presence of multiple elements in HEAs can lead to synergistic effects that enhance their overall performance. These interactions can modify the electronic structure, lattice parameters, and surface properties of the alloy, leading to improved catalytic activity, stability, and resistance to poisoning [429–431].
- (e) Cost-Effectiveness: HEAs often offer a cost-effective alternative to traditional catalysts, particularly those based on precious metals. By utilizing a combination of more abundant and less expensive elements, HEAs can provide comparable or even superior catalytic performance at a lower cost [432,433].

Due to these advantages, HEAs are being actively explored for various electrocatalytic applications, including:

- (a) Fuel Cells: HEAs are being investigated as catalysts for both the hydrogen evolution reaction (HER) and the oxygen reduction reaction (ORR), which are crucial processes in fuel cell technology. Their ability to enhance catalytic activity and stability can improve fuel cell efficiency and durability [434,435].
- Liu et al. [436] summarized the performance of distinct high-entropy alloys and high-entropy compounds for hydrogen evolution reaction as depicted in Table 11.
- (b) Water Electrolysis: HEAs are showing promise as electrocatalysts for water electrolysis, a process that splits water into hydrogen and oxygen using electrical energy. Their enhanced activity and stability can contribute to more efficient and cost-effective hydrogen production [437].

**Table 10**  
Overpotential of HEAs and commercial electrodes for different electrochemical reactions.

Reaction	HEA Overpotential (mV)	Commercial Electrode Overpotential (mV)
Oxygen Reduction Reaction (ORR)	40	80
Hydrogen Evolution Reaction (HER)	50	70
Nitrogen Reduction Reaction (NRR)	340	400
Formic Acid Oxidation Reaction (FAOR)	100	250

**Table 11**

Summary of distinct high entropy alloys and high entropy compounds for hydrogen evolution reaction performance.

Components	Methods	Electrolyte	Tafel slope (mV dec <sup>-1</sup> )	Overpotential (mV) at 10 mA cm <sup>-2</sup>
CuAlNiMoFe (High entropy alloys)	Arc-melting + dealloying	1 M KOH	60	9.7
PdFeCoNiCu (High entropy alloys)	Oil phase	1 M KOH	39	18
PtNiFeCoCu (High entropy alloys)	Oil phase	1 M KOH	30	11
IrPdPtRhRu (High entropy alloys)	One-pot polyol	1 M KOH/ 0.5 M H <sub>2</sub> SO <sub>4</sub>	–	17/ 33
CoCrFeNiAl (High entropy alloys)	Mechanical alloying + spark plasma sintering	0.5 M H <sub>2</sub> SO <sub>4</sub>	39.7	73
AlNiCoIrMo (High entropy alloys)	Alloying + dealloying	0.5 M H <sub>2</sub> SO <sub>4</sub>	33.2	18.5
PdPtCuNiP (High-entropy metallic glasses)	Melt-spinning	1 M KOH/ 0.5 M H <sub>2</sub> SO <sub>4</sub>	37.4/ 44.6	32/ 62
NiCoFeMnCrP (High-entropy phosphides)	Sol-gel	1 M KOH	94.5	220

(c) Metal-Air Batteries: HEAs are being explored as catalysts for metal-air batteries, such as zinc-air and aluminium-air batteries, which offer high energy density and potential applications in electric vehicles. Their ability to improve oxygen reduction activity can enhance battery performance [438,439].

(d) Organic Electrosynthesis: HEAs are being investigated as catalysts for organic electrosynthesis, a process that converts organic compounds using electrical energy. Their tunable properties can enable the selective synthesis of valuable organic products [440,441].

(e) CO<sub>2</sub> Reduction: HEAs are being explored as catalysts for CO<sub>2</sub> reduction, a process that converts carbon dioxide into valuable fuels and chemicals using electrical energy. Their enhanced activity and selectivity can contribute to more efficient and sustainable CO<sub>2</sub> utilization [442–444].

Overall, HEAs hold significant promise for revolutionizing various electrocatalytic applications due to their unique properties, tunability, and potential for cost-effective performance. As research continues to advance, HEAs are expected to play an increasingly important role in developing next-generation electrocatalysts for a wide range of applications. Recently, HEAs have great potential for distinct electrocatalysis applications owing rich elemental composition, unique physical and chemical properties and adjustable electronic structure [445,446]. The recent advances in HEAs for electrolysis are shown in Fig. 36.

#### 6.1.8. Catalysis

HEAs offer various properties that make them promising candidates for catalysis. These properties are

- (a) Enhanced catalytic activity: The multi-element composition of HEAs can create synergistic effects that enhance their catalytic activity compared to traditional catalysts. This is due to the fact that the different elements in HEAs can interact with each other to modify the electronic structure of the material, which can in turn affect its catalytic activity [447,448].
- (b) Improved stability: HEAs are often more stable than traditional catalysts, which can lead to longer lifetimes and reduced operating costs. This is because HEAs are less susceptible to deactivation by reaction intermediates and poisoning by impurities [449,450].

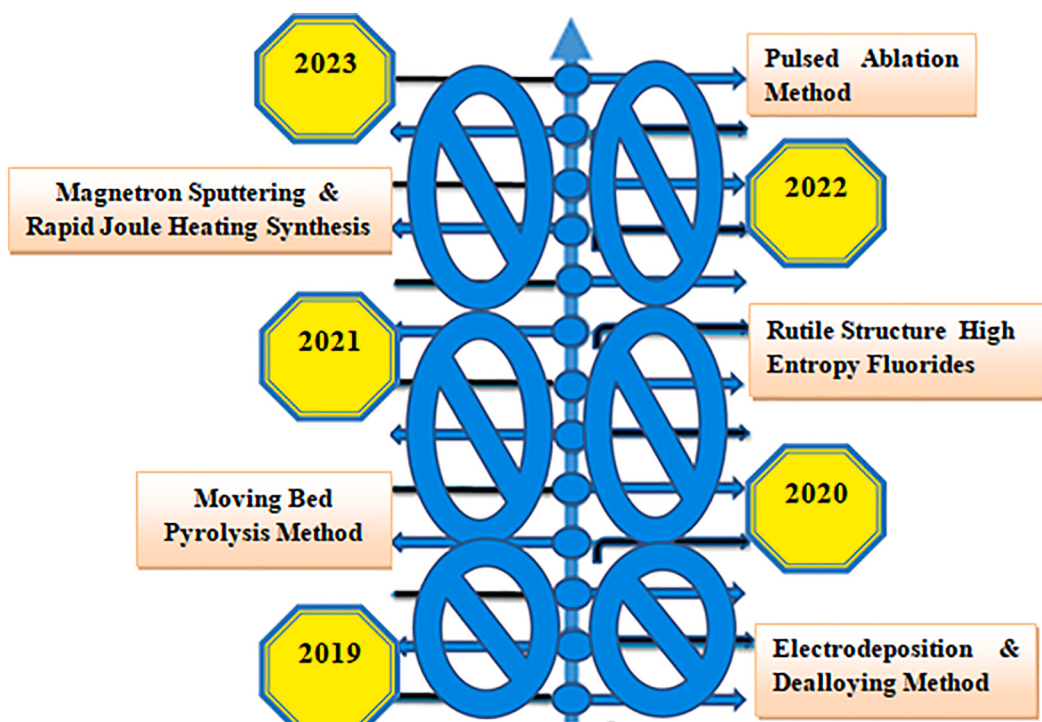


Fig. 36. Recent advances in HEAs for electrocatalysis.

- (c) Tunable properties: The properties of HEAs can be tuned by varying the composition of the alloy. This allows for the development of HEAs with specific properties that are tailored to the desired application [451].
- (d) Synergistic effects: The presence of multiple elements in HEAs can lead to synergistic effects that enhance their overall performance. This is because the different elements in HEAs can interact with each other to create new and improved properties [452].

As a result of these properties, HEAs are being used in a variety of catalysis applications, including:

- (a) Hydrogenation reactions: HEAs are being used to catalyze the hydrogenation of a variety of organic compounds, such as alkenes and alkynes [453].
- (b) Oxidation reactions: HEAs are being used to catalyze the oxidation of a variety of organic compounds, such as alcohols and aldehydes [454].

Yao et al. [455] synthesized PtPdRhRuCe, PtCoNiFeCuAu, PtPdCo-NiCuAu, and PtPdCoNiFeCuAuSn nanocrystals with FCC lattice via the carbothermal shock method. They found that PtPdRhRuCeNPs exhibit excellent activity for ammonia oxidation with 100 % conversion and > 99 % nitrogen oxide selectivity toward NO<sub>x</sub> (NO + NO<sub>2</sub>). The enhanced catalytic selectivity is suggested due to the highly atomically homogeneous nature of the solid-solution NPs, compared with the lower activity of the phase-separated heterostructures. In addition, PtPdRhRuCeNPs show no activity degradation owing to their high-entropy nature preventing phase separation or elemental segregation [456].

## 6.2. Cutting tools

High entropy-based coatings deposited on the surface of the cutting tool improve the machining performance and decrease the frictional forces induced during machining. Further, this increased the life of the tool and improved the surface integrity of the machined surface [457].

Guo et al. [458] analyzed the wear resistance of high-melting-point AlCrFeMoNb<sub>x</sub>TiW ( $x = 1, 3, 5$  and  $7$ ) high-entropy alloy coatings with industrial annealed W<sub>6</sub>Mo<sub>5</sub>Cr<sub>4</sub>V<sub>2</sub> tool steel as the substrate. With the increase in Nb content, the hardness of the coatings increased, and the friction coefficient and wear rate decreased. Due to the increase in Nb content, the content of carbides and intermetallic compounds in the coatings increased significantly, and the hardness increased, this reduced the plastic contact between friction pairs and improved the adhesive wear resistance. In addition, the overall hardness of each Nb<sub>x</sub> coating is much higher than that of the substrate. AlCrFeMoNb<sub>x</sub>TiW high-entropy alloy coatings can be used to improve the surface wear resistance of high-speed cutting tools. Recently, High Entropy Alloy (HEA) coatings are a promising new technology for cutting tools that offer several advantages over traditional coatings [459], such as:

- (a) Increased hardness and wear resistance: HEAs are typically much harder than traditional coatings, such as TiN or TiAlN, which can lead to significantly longer tool life. Overall, HEA coatings exhibit exceptional wear resistance due to their high hardness and strong grain boundaries. They can withstand abrasive wear, adhesive wear, and erosive wear, making them ideal for applications involving friction and sliding contact [460].

The superior wear resistance of HEAs has been the subject of study in recent years [461–463]. Firstov et al. [464] compared the wear resistance of Fe–Cr–Ni–Mn–Co–Al HEA with that of 65G steel. The results demonstrated the higher wear resistance of HEAs even at high temperatures, which is attributed to the formation of an ordered  $\beta$ -phase with a

BCC lattice structure on the friction surface of the HEA. The microstructure of the wear subsurface of HEAs, which is highly dependent on load and temperature, is an essential factor in their wear resistance.

- (a) Improved thermal stability: HEAs have a high melting point and can withstand high temperatures without degradation, making them suitable for use in high-speed machining applications [464].
- (b) Enhanced corrosion resistance: HEAs are generally more resistant to corrosion than traditional coatings, which can help to prevent tool failure in corrosive environments.

Their high entropy leads to a disordered microstructure that hinders the diffusion of corrosive agents, while their ability to form passive oxide films further enhances their corrosion resistance [465].

Lin et al. [466] investigated the corrosion behaviour of FeCoCrNi-based HEA coating. The authors reported that FeCoCrNi-based HEA coating offered excellent corrosion resistance owing to the presence of chromium and nickel elements. These elements form protective oxides (Cr<sub>2</sub>O<sub>3</sub> and NiO) and improve the corrosion resistance in the alloys by encouraging the forming of a passive film.

HEA coatings are typically applied to cutting tools using physical vapour deposition (PVD) or chemical vapour deposition (CVD) techniques. The thickness of the coating is typically in the range of a few micrometres [467].

HEA coatings have been shown to improve the performance of cutting tools in a variety of applications, including:

Milling: HEA coatings can increase tool life by up to 50 % in milling applications [468].

Turning: HEA coatings can increase tool life by up to 30 % in turning applications [469].

Drilling: HEA coatings can increase tool life by up to 20 % in drilling applications [470].

HEA coatings are a relatively new technology, and research is ongoing to develop new HEA compositions and coating techniques. However, the initial results are promising, and HEA coatings are expected to have a significant impact on the cutting tool industry in the years to come [471].

Here are some of the specific applications of HEA coatings for cutting tools:

End mills: HEA coatings can be used to protect the cutting edges of end mills from wear and abrasion, which can extend tool life and improve machining accuracy [472].

Turning tools: HEA coatings can be used to protect the cutting edges of turning tools from wear and heat, which can extend tool life and improve surface finish [473].

Drilling tools: HEA coatings can be used to protect the cutting edges of drilling tools from wear and impact, which can extend tool life and improve hole quality. Wang et al. [474] successfully deposited high-entropy alloy coatings (CoCrFeNiMn) on offshore drilling equipment using HVOF and cold spraying. Then, the coatings were subjected to vacuum heat treatment at distinct temperatures (500 °C, 700 °C and 900 °C). The friction and wear experiments of the coatings before and after vacuum heat treatment were carried out in simulated seawater drilling fluid. The results show that CoCrFeNiMn high-entropy alloy coatings prepared by CS and HVOF have dense structures and bond well with the substrate. They are all single-FCC solid solution structures and the porosity is <1.5 %. Compared with the CS coating, the HVOF coating has higher porosity. The wear rate for the CS and HVOF coatings reaches its lowest point after vacuum heat treatment at 500 °C. Overall, HEA coatings are a promising new technology that has the potential to significantly improve the performance of cutting tools in a variety of applications.

### 6.3. To resist chemical corrosion

The HEA-based coating is suitable for protecting the material from corrosion in an aggressive environment [475]. This is due to their unique microstructure and properties, which include:

- (a) *High entropy*: HEAs have large configurational entropy, which results in a disordered microstructure. This microstructure makes it difficult for corrosive agents to penetrate the coating and reach the substrate [476].
- (b) *Passive film formation*: Many HEAs form a passive oxide film on their surface when exposed to corrosive environments. This passive film acts as a barrier to corrosion and can self-heal if it is damaged [477].
- (c) *Low diffusivity*: HEAs have a low diffusivity for corrosive agents. This means that corrosive agents can only slowly diffuse through the coating and reach the substrate [478].

As a result of these properties, HEA-based coatings can provide excellent corrosion protection for a wide range of materials, including metals, polymers, and ceramics. They are being used in a variety of applications, such as

- (a) *Marine applications*: HEA-based coatings can be used to protect ships and offshore structures from corrosion [479].
- (b) *Chemical processing*: HEA-based coatings can be used to protect equipment from corrosion in chemical processing plants [480].
- (c) *Power generation industry*: HEA-based coatings can be used to protect power plant components from corrosion [481].
- (d) *Aerospace*: HEA-based coatings can be used to protect aircraft parts from corrosion [482].
- (e) HEA-based coatings are a promising new technology for corrosion protection. They have the potential to replace traditional coatings, such as chromium and nickel plating, which can be hazardous to the environment.

Lin et al. [483] reported that FeCoCrNi-based HEA coatings usually have excellent corrosion resistance owing to the content of passive elements chromium and nickel. Also, the addition of aluminium and titanium has a better effect on improving the mechanical characteristics (plasticity and density) and wear resistance of high entropy alloy coatings.

### 6.4. High temperature (thermal barrier) application

The HEA-based coating is used to develop high-quality golf-hitting surfaces and to increase the hardness of turbine blades and steel pipes which are exposed to elevated temperatures.

In addition, HEAs materials find wide application in nuclear, chemical power plants, aerospace and other sectors [484].

High entropy alloy-based coatings can provide thermal protection for underlying substrates by reflecting heat and reducing thermal conductivity. Their high melting temperatures and low thermal expansion coefficients make them suitable for applications involving high temperatures and thermal cycling [485].

### 6.5. Biomedical applications

HEA coatings are generally biocompatible and can be used in biomedical applications such as implants and prosthetics. Their corrosion resistance and wear resistance make them suitable for long-term implantation, while their biocompatibility minimizes the risk of adverse tissue reactions [486].

Various studies have reported superior biocompatibility of Ti–Nb–Ta–Zr–Mo, Ti–Nb–Ta–Zr–Fe, Ti–Nb–Ta–Zr–W, Ti–Nb–Ta–Zr–Cr, and Ti–Nb–Ta–Zr–Hf HEAs in comparison with pure titanium [487,488].

The remarkable biocompatibility characteristics of HEAs, along with their outstanding mechanical characteristics and corrosion resistance, make them promising candidates for biomedical applications [489].

### 6.6. Traditional applications of HEA coatings

HEA coatings have been successfully applied in various industries, including:

- (a) *Marine industry*: HEA coatings protect ships and offshore structures from corrosion in seawater environments [490].
- (b) *Chemical industry*: HEA coatings protect equipment from corrosion in harsh chemical environments [491].
- (c) *Power generation industry*: HEA coatings protect power plant components from corrosion and erosion [492].
- (d) *Aerospace industry*: HEA coatings protect aircraft parts from corrosion and wear [493].
- (e) *Automotive industry*: HEA coatings protect automotive components from wear and corrosion [494].
- (f) *Medical industry*: HEA coatings are used in implants and prosthetics to improve biocompatibility and wear resistance [495].

#### 6.6.1. Recent progress in HEA coatings

Researchers are continuously developing new HEA compositions and coating techniques to further enhance the performance of HEA coatings. Some of the recent advancements in HEA coatings include:

- (A) Development of new HEA compositions with improved properties: Researchers are exploring new HEA compositions with even higher hardness, strength, and corrosion resistance [496].

Based on the concept of HEAs, several types of new alloy systems have been developed with promising properties for engineering applications. This section reviews the current state of the art of various special HEAs.

- (i) Low-stacking-fault-energy high-entropy alloys (LSF-HEAs): CoCrFeMnNi and related FCC-type HEAs have been found to possess relatively low stacking fault energies, which generally attributed to both high strength and good ductility [497]. Zadach et al. [498] reported that for CoCrFeMnNi, both its tensile strength and ductility can be increased at cryogenic temperatures, as deformation-induced twinning becomes a more prominent deformation mechanism [498].
- (ii) High-entropy superalloys (HESAs): Superalloys are important materials for gas turbine engines in aerospace and energy industries [499]. Traditional superalloys have relied on ordered Ni<sub>3</sub>(Al, Ti)-based L12-structured ( $\gamma'$ ) coherent precipitates to strengthen the FCC-structured ( $\gamma$ ) matrix. During the development of advanced superalloys, Ru and Re elements are of interest due to their contributions to phase stability and creep resistance. The addition of these two elements in the Ni-based system can be seen as a “quasi-cocktail effect” [500–505]. Although creep properties of Ni-based alloys can be improved by adding Ru and Re, high density and high cost prohibit a large scale of applications. Furthermore, the homologous temperature of superalloys has appeared to reach the limit, and efforts on superalloy development have focused on improving the cost performance by reducing the use of expensive elements.
- (iii) High-entropy metallic glasses (HEMGs).

Metallic glasses are regarded as promising materials due to their high hardness, strength, and elasticity. However, the tensile brittleness after elastic deformation limits the use of metallic glasses as structural materials. Studies have reported that the HEAs can be fully amorphous

without crystalline phases after solidification [506]. Interestingly, HEMGs could combine the features of both metallic glasses and high-entropy alloys and may provide a new direction to develop materials with high strength and high ductility. Gong et al. [507] demonstrated that TiZrHfBeCu can possess excellent compressive plasticity. Li et al. [508] reported that the  $(\text{Fe}_{1/3}\text{Co}_{1/3}\text{Ni}_{1/3})_{80}(\text{P}_{1/2}\text{B}_{1/2})_{20}$  HEMGs have superior magneto-caloric properties in a wide temperature range compared with those of conventional crystalline materials. Chen et al. [509] reported that the magnetic properties of HEMGs can be superior to conventional materials and might be promising candidates for magnetic refrigeration applications.

#### (iv) Refractory high-entropy alloys (RHEAs)

Senkov et al. [510] proposed the MoNbTaW and MoNbTaVW RHEAs with a simple BCC solid solution phase. These two kinds of RHEAs possess high hardness and high-temperature strength. To further improve the ductility, niobium and tantalum were retained; hafnium, titanium, and zirconium were added; and the result was HfNbTaTiZr RHEA, which is also a stable BCC solid solution. This RHEA possesses superior room-temperature strength and can retain high hardness as well as high-temperature strength [511–513].

#### (v) Eutectic high-entropy alloys (EHEAs)

Eutectic alloys are known to possess good castability and excellent mechanical strength [514]. Since the eutectic reaction is associated with isothermal transformation, both chemical segregation and shrinkage cavity can be alleviated. Eutectic HEAs (EHEAs) with composite FCC/BCC structures can possess the advantages of good mechanical properties and excellent castability.

Ding et al. [515] reported that AlCoCrFeNi2.1 EHEA possessed excellent mechanical properties and good corrosion resistance properties. There is a limited study on the solidification of EHEAs with complete eutectic microstructure; this could be due to the complicated solidification mechanism associated with HEA effects. The underlying mechanism of the solidification behaviours of EHEAs still needs to be further clarified in the future.

#### (vi) High-entropy intermetallic compounds (HEICs).

High-entropy intermetallic compounds (HEICs) are a new class of high-entropy materials, which may fill the knowledge gap between the metallic HEAs and intermetallic HEA compounds. These new HEICs are mostly metallic but also have crystal structures resembling the ionic solid. Zhou et al. [516] fabricated the HEICs  $(\text{Fe}_{0.2}\text{Co}_{0.2}\text{Ni}_{0.2}\text{Mn}_{0.2}\text{Cu}_{0.2})\text{Al}_1$  with a B<sub>2</sub> structure and  $(\text{Ti}_{0.25}\text{Nb}_{0.25}\text{V}_{0.25}\text{Zr}_{0.25})\text{Al}_3$  with a D<sub>022</sub> structure.

#### (vii) High-entropy coatings (HE-Coatings).

HEA-based coatings have the potential to be applied as a diffusion barrier and high-temperature protective coating. Chang et al. [517] reported the suppressed interdiffusion kinetics in high-entropy coating film and it could be a diffusion barrier to improve the Cu/TaN interface in the IC technology. Hsu et al. [518,519] studied the NiC-0.6Fe-0.2Cr<sub>x</sub>SiAl<sub>y</sub> system as a high-temperature protective coating. The results indicated that HE-Coatings could possess high hardness and excellent wear resistance due to the formation of Nb<sub>d</sub>Si compounds at the interface.

#### (B) Development of novel coating techniques: New coating techniques, such as laser cladding and magnetron sputtering, are being developed to produce HEA coatings with improved adhesion, uniformity, and thickness control [520].

(C) Tailoring HEA coatings for specific applications: Researchers are tailoring HEA coatings to meet the specific requirements of different applications. For instance, HEA coatings are being designed with enhanced biocompatibility for biomedical applications and with superior thermal barrier properties for high-temperature applications [521].

The future of HEA coatings is bright, and they are poised to play an increasingly important role in a wide range of applications. As research continues to advance, HEA coatings are expected to become even more versatile and effective, offering solutions to some of the most challenging material problems in various industries.

### 6.7. Other applications

There are some projects led by companies in collaboration with various research institutes and universities investigating the diverse applications of high entropy alloys. For example, The energy department of Directed Vapour Technologies International, Inc. (DVTI) has been exploring the use of high entropy alloys in thermal barrier coating systems since 2015 [522]. In addition, the energy department of QuesTek Innovations LLC has been exploring the use of HEAs for turbine applications in collaboration with the University of Tennessee since 2016 [523].

However, the potential functional and structural applications of high entropy alloys in bulks, powder forms and thin films are summarized in Fig. 37.

Various authors suggested a particular type of high entropy alloy, along with their critical properties for potential applications, which are summarized in Table 12.

#### 6.7.1. Structural properties and applications

**6.7.1.1. Bulk alloys.** Bulk HEAs are widely used in distinct industries such as aerospace, automotive, energy, machining, moulding, soldering, mining, nuclear, thermal, and biomedical.

Developing low-cost, lightweight, energy-efficient structure materials that possess superior properties at high temperatures is the great interest to the researchers. Presently, the maximum service temperature of conventional nickel-based superalloys, which are mostly utilized in thermal power plants (boiler tubes), aero engines, and gas turbine engines, has reached approx. 80 % of their melting temperature [561]. Thus, these superalloys cannot fulfil the harsher service conditions, where the working temperature is very high. In addition, nickel-based superalloys are expensive and possess high densities. This problem can be solved using novel bulk eutectic high entropy alloys (EHEAs). Because the EHEAs combine the benefits of high entropy alloys and eutectic alloys [562,563]. These EHEAs also have a controlled, near-equilibrium microstructure that can withstand temperature fluctuations up to the eutectic reaction temperature. As a result, EHEAs [564,565] are ideal materials for high-temperature applications. Lu et al. [565] produced the first EHA (AlCoCrFeNi2.1) in 2014. After that, bulk eutectic high entropy alloys have attained a great global interest owing to their superior properties (ability to withstand high temperature, strength and ductility) than traditional materials [566–571]. Further, with the advancement of new technology, various researchers [572–588] designed and investigated novel bulk eutectic high entropy alloys. These include, AlCrFeNiMo<sub>0.2</sub>, Nb<sub>25</sub>Sc<sub>25</sub>Ti<sub>25</sub>Zr<sub>25</sub>, Zr<sub>0.6</sub>CoCrFeNi<sub>2.0</sub>, CoCrFeNiMnPd, Fe<sub>20</sub>Co<sub>20</sub>Ni<sub>41</sub>Al<sub>19</sub>, CoCrFeNiTa<sub>x</sub>, Al<sub>16</sub>Co<sub>41</sub>Cr<sub>15</sub>Fe<sub>10</sub>Ni<sub>18</sub>, CrFeNi<sub>(3-x)</sub>Al<sub>x</sub>, Co<sub>25.1</sub>Cr<sub>18.8</sub>Fe<sub>23.3</sub>Ni<sub>22.6</sub>Ta<sub>8.5</sub>Al<sub>1.7</sub>, Nb<sub>25</sub>Sc<sub>25</sub>Ti<sub>25</sub>Zr<sub>25</sub>, Co<sub>20</sub>Cu<sub>20</sub>Fe<sub>20</sub>Ni<sub>20</sub>Ti<sub>20</sub>, Al<sub>1.3</sub>CrFeNi, CoCrFeNiNb<sub>0.45</sub>, CoCrFeNiTa<sub>0.395</sub>, Co<sub>30</sub>Cr<sub>10</sub>Fe<sub>10</sub>Al<sub>18</sub>Ni<sub>32-x</sub>Mo<sub>x</sub>, etc.

In 2014, Gludovatz et al. [38] reported that HEA (CoCrFeMnNi), which comprises late transition metals (iron, nickel, copper, cobalt), is suitable for cryogenic applications. Further, Senkov et al. [50]

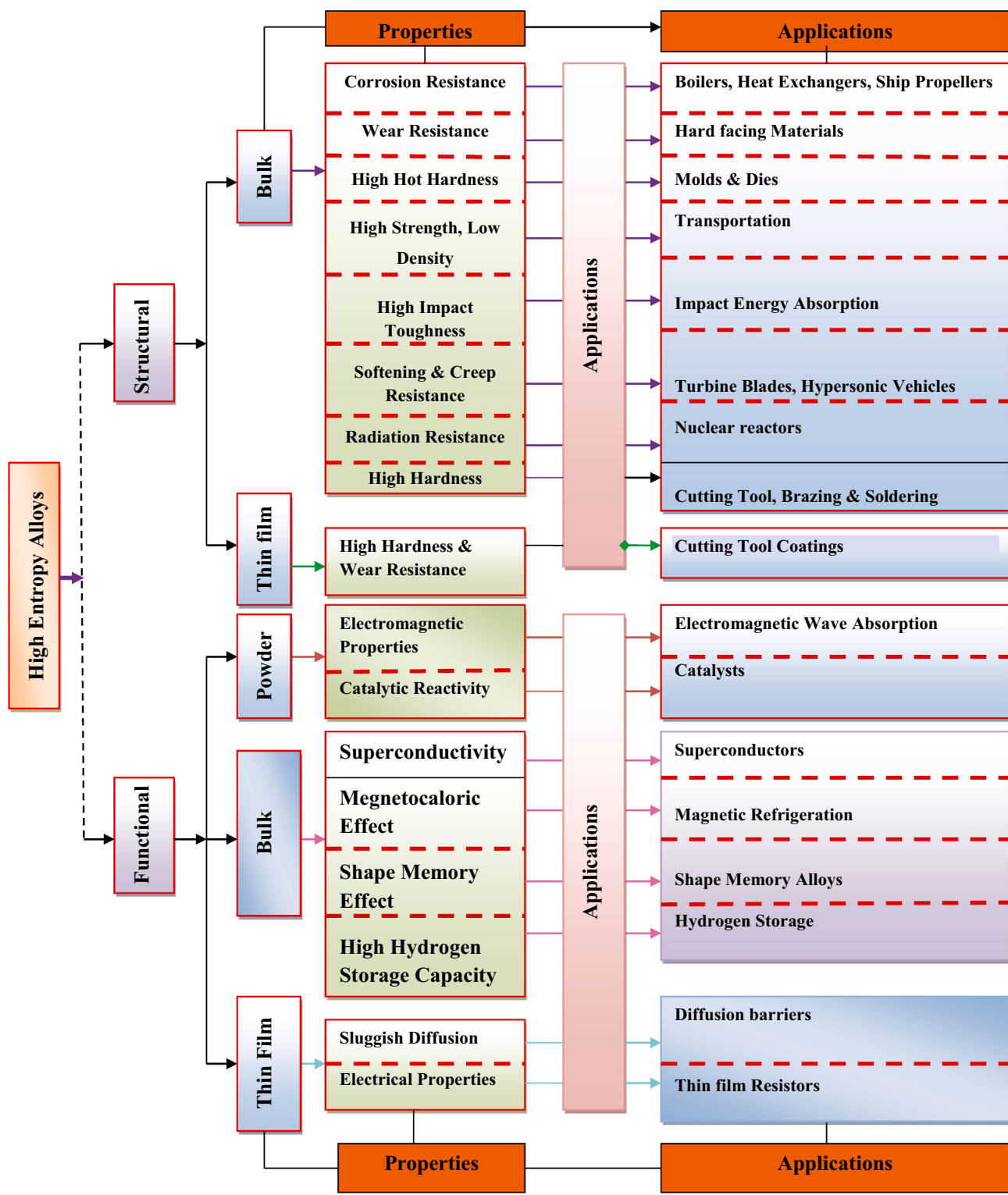


Fig. 37. Functional and structural applications of HEAs along with their properties [43].

developed refractory HEAs (W-Nb-Mo-Ta and W-Nb-Mo-Ta-V) using vacuum arc melting and suggested high-temperature applications.

**6.7.1.2. Thin films.** A thin film is a thin layer of material with a thickness ranging from a fraction of a nanometer to several micrometres. However, a coating is a layer that is deposited on the surface of the substrate, which is usually thicker than the film. To fabricate the HEA films and coating number of technologies have been employed. These

techniques include magnetron sputtering, spraying, plasma-transferred arc cladding, laser cladding, electrodeposition, etc. [13,17,589–594].

Various authors reported the structures and micro-hardness of HEA films and coating by different fabrication processes, as given in Table 13.

In the past fourteen years, HEA film and coatings have shown unique and attractive properties than conventional materials and films [613]. These HEA films exhibited superior physical and mechanical properties, such as excellent wear resistance, high resistance against corrosion, high

**Table 12**

Suggested high entropy alloy for potential applications along with their properties, fabrication process and critical results.

S. no	Author	Field	Alloy form	Fabrication process	Suggested alloy	Key properties	Applications	Conclusions
1	Bridge et al. [524]	Structural	Bulk	Laser brazing	Ni:Cu:Co:Fe: Mn (molar ratio of 1:1:1:0.25:1.75)	High hardness	Cutting tools, brazing of turbine blade, and soldering materials	After brazing, the HEA experiences four times hardness. In addition, max. Shear strength (220 MPa) was obtained by using HEA filler metal. The coated sample exhibited high hardness and young modulus by 17.5 and 186 GPa, respectively. The coating also improved the corrosion resistance than the 201 stainless steel.
2	Li et al. [167]	Structural	Bulk	DC magnetron sputtering	FeAlCuCrCoMn	Retained high hot hardness	Hot-working moulds and dies	
3	Chuang et al. [525]	Structural	Bulk	Arc-melting	Al <sub>0.2</sub> Co <sub>1.5</sub> CrFeNi <sub>1.5</sub> Ti <sub>0.5</sub> Al <sub>0</sub> Co <sub>1.5</sub> CrFeNi <sub>1.5</sub> Ti Al <sub>0.2</sub> Co <sub>1.5</sub> CrFeNi <sub>1.5</sub> Ti	Wear resistance	Hard facing materials	Wear Hardness 501 HV 250 m/ mm <sup>3</sup> 480 HV 250 m/ mm <sup>3</sup> 650 HV 2000 m/ mm <sup>3</sup> 700 HV 5500 m/ mm <sup>3</sup>
4	Youssef et al. [526]	Structural	Bulk	Mechanical alloying	Al <sub>20</sub> Li <sub>20</sub> Mg <sub>10</sub> Sc <sub>20</sub> Ti <sub>30</sub>	Low density & high strength.	Transportation and energy sector	HEA exhibited a higher strength-to-weight ratio than nano-crystalline alloys. Fabrication of HEA for aerospace applications using laser additive manufacturing can reduce noise, large fuel consumption and emissions. Thus, minimizing repair and maintenance costs of aerospace parts.
5	Dada et al. [527]	Structural	Bulk	Laser additive manufacturing	Al <sub>x</sub> -Co-Cr-Cu-Fe-Ni	Can withstand high operating temperatures, high fatigue/ creep strength, and withstand cyclic and translational movements of parts at high speed and erosion.	Aerospace sector	Laser-based manufacturing methods of HEA eliminate the defects of conventional manufacturing processes. Results showed that outstanding strain hardening ability gives rise to significant resistance to shear localization.
6	Dada et al. [528]	Structural	Bulk	Laser-based Manufacturing	Al <sub>0.5</sub> CoCrCuFeNi	Ability to withstand high environmentally induced degradation, thermal, and mechanical loads.	Suitable for aerospace gas turbines, rocket nozzles nuclear constructions etc.	(continued on next page)
7	Li et al. [529]	Structural	Bulk	Vacuum-induction melting	Al <sub>0.3</sub> CoCrFeNi	High resistance to shear localization	Used for penetration protection applications such as armours.	

Table 12 (continued)

S. no	Author	Field	Alloy form	Fabrication process	Suggested alloy	Key properties	Applications	Conclusions
8	Gludovatz et al. [38]	Structural	Bulk	Arc melting	CrMnFeCoNi	Possess high fracture toughness at cryogenic temperature.	Used for storage tanks of liquefied gases	HEA forms a single-phase FCC solid solution and OBSERVED it to have exceptional damage tolerance.
9	Yang et al. [530]	Structural	Bulk	Arc melting	Ni <sub>30</sub> Co <sub>30</sub> Fe <sub>13</sub> Cr <sub>15</sub> Al <sub>6</sub> Ti <sub>6</sub>	Excellent ductility-strength- combinations at both cryogenic and ambient temperatures.	Used in aerospace, natural gas industries and marine shipbuilding.	Ultrahigh tensile strength and large ductility of 1.7GPa and 51 % were observed.
10	Yang et al. [531]	Structural	Bulk	Arc melting	NbTiVTaAl <sub>x</sub>	High strength, good resistance to high thermal stability and wear and better room temperature ductility.	Aerospace industry	The HEA exhibit simple phase structures and possesses obvious dendrite structures. Improvement in mechanical property was observed. The alloy density and Vickers micro-hardness were measured to be 9.94 g/cm <sup>3</sup> and 3826 MPa, respectively. The HEA possess a high compression yield strength of 929 MPa and ductility ( $\epsilon > 50\%$ ).
11	Senkov et al. [100]	Structural	Bulk	Vacuum arc-melting + hot isostatic pressing	Ta <sub>20</sub> Nb <sub>20</sub> Hf <sub>20</sub> Zr <sub>20</sub> Ti <sub>20</sub>	Strain hardening and homogeneous deformation	High-temperature applications	HEA possess excellent resistance against oxidation at 700 °C and 900 °C, which is much better than Ti-6Al-4 V. Hence, the present alloy is a promising material for elevated temperature applications requiring wear-resistant, lightweight, and oxidation-resistant components.
12	Tseng et al. [532]	Structural	Bulk	Vacuum-arc melting	Al <sub>20</sub> Be <sub>20</sub> Fe <sub>10</sub> Si <sub>15</sub> Ti <sub>35</sub>	High oxidation resistance, high hardness, high fracture/fatigue resistance and excellent resistance against corrosion.	High-temperature applications	Improvement in tensile and creep properties of HEA was observed. Results showed that the yield strength of this refractory HEA is superior to the yield strength of Ni-based super-alloys from 20 °C to 1200 °C.
13	Tsao et al. [533]	Structural	Bulk	Vacuum-arc melting + directional solidification	Ni <sub>47.9</sub> Al <sub>10.2</sub> Co <sub>16.9</sub> Cr <sub>7.4</sub> Fe <sub>8.9</sub> Ti <sub>5.8</sub> Mo <sub>0.9</sub> Nb <sub>1.2</sub> W <sub>0.4</sub> C <sub>0.4</sub>	Tensile and creep properties	Turbine blades & hypersonic vehicles	At room temperature, HEA offered high yield strength (929 MPa), strong work hardening (3360 MPa), excellent compression ductility (50 %) and homogeneous macroscopic flow.
14	Senkov et al. [534]	Structural	Bulk	Vacuum arc melting	AlMo <sub>0.5</sub> NbTa <sub>0.5</sub> TiZr	Retained high strength at high temperature, possesses high creep resistance, ductile and tough	Turbine engines and future hypersonic vehicles.	(continued on next page)
15	Senkov et al. [535]	Structural	Bulk	Vacuum arc melting	Ta <sub>20</sub> Nb <sub>20</sub> Hf <sub>20</sub> Zr <sub>20</sub> Ti <sub>20</sub>	High creep resistance and high-temperature strength.	Aerospace industry	

Table 12 (continued)

S. no	Author	Field	Alloy form	Fabrication process	Suggested alloy	Key properties	Applications	Conclusions
16	Rongbin et al. [536]	Structural	Bulk	Arc-melting	FeNiMnCr <sub>0.75</sub> Al <sub>x</sub>	High strength and ductility	HEA HAS potential applications in the industry & daily life to replace conventional materials	The as-cast HEAs OFFERED superior mechanical behaviour with a good combination of high ductility and strength, which is owing to the duplex phases. The investigated HEA material offers superior radiation resistance than conventional single-phase Fe-Cr-Ni austenitic alloys (stainless steels). Electrochemical tests show the excellent corrosion resistance of examined HEAs against the attack of chloride-containing solutions.
17	Kumar et al. [537]	Structural	Bulk	Arc-melting	27%Fe-28%Ni27%Mn-18%Cr	Good mechanical and corrosion resistance properties and Radiation-damage resistance properties	High-temperature fusion or structural fission applications, Nuclear reactors and energy application	Wear resistance
18	Wang et al. [538]	Structural	Bulk	Vacuum arc melting in a water-cooled Cu crucible	Al <sub>0.1</sub> CoCrFeNi Al <sub>0.5</sub> CoCrCuFeNiV <sub>0.2</sub> Al <sub>0.5</sub> CoCrCuFeNiV <sub>0.4</sub> Al <sub>0.5</sub> CoCrCuFeNiV <sub>0.6</sub> Al <sub>0.5</sub> CoCrCuFeNiV <sub>0.8</sub>	High resistance against corrosion	Boilers and heat exchangers	Hardness 200 HV 0.910 m/ mm <sup>3</sup> 225 HV 0.875 m/ mm <sup>3</sup> 325 HV 0.850 m/ mm <sup>3</sup> 450 HV 0.900 m/ mm <sup>3</sup>
43	Chen et al. [539]	Structural	Bulk	Arc melting and casting method	Al <sub>0.5</sub> CoCrCuFeNiV <sub>1.0</sub> Al <sub>0.5</sub> CoCrCuFeNiV <sub>1.2</sub> Al <sub>0.5</sub> CoCrCuFeNiV <sub>1.4</sub> Al <sub>0.5</sub> CoCrCuFeNiV <sub>1.6</sub> Al <sub>0.5</sub> CoCrCuFeNiV <sub>1.8</sub> Al <sub>0.5</sub> CoCrCuFe20NiV <sub>2.0</sub> Al <sub>0.5</sub> CoCrCuFeNi	High wear resistance, High mechanical property	Tool alloy industry	Hardness 650 HV 0.925 m/ mm <sup>3</sup> 575 HV 1.050 m/ mm <sup>3</sup> 578 HV 1.100 m/ mm <sup>3</sup> 600 HV 1.050 m/ mm <sup>3</sup> 600 HV 1.100 m/ mm <sup>3</sup> 598 HV 1.110 m/ mm <sup>3</sup> 252 HV 0.925 m/ mm <sup>3</sup>
20	Wu et al. [540]	Structural	Bulk	Arc melting	Al <sub>1.5</sub> CoCrCuFeNi Al <sub>2.0</sub> CoCrCuFeNi	High hardness and wear resistance	Structural and tool industries	Hardness 350 HV 0.825 m/ mm <sup>3</sup> 550 HV 0.850 m/ mm <sup>3</sup>
21	Hsu et al. [541]	Structural	Bulk	An induction furnace was utilized to melt the alloy in the air	Al <sub>0.5</sub> B <sub>0</sub> CoCrCuFe Al <sub>0.5</sub> B <sub>0.2</sub> CoCrCuFe	Ease of amorphization and nanoprecipitation in the alloy, high hardness, thermal stability and excellent resistance against corrosion	High-temperature structures and working tools	Hardness 300 HV 0.8 m/ mm <sup>3</sup> 400 HV 0.9 m/ mm <sup>3</sup>

(continued on next page)

Table 12 (continued)

S. no	Author	Field	Alloy form	Fabrication process	Suggested alloy	Key properties	Applications	Conclusions			
22	Hsu et al. [542]	Structural	Bulk	Arc melting and casting method	Al <sub>0.5</sub> B <sub>0.6</sub> CoCrCuFe	High strength, excellent resistance against abrasive wear, temper-softening, oxidation and corrosion	Tribological applications	500 HV 1.0 m/ mm <sup>3</sup>			
					Al <sub>0.5</sub> B <sub>1.0</sub> CoCrCuFe			725 HV 1.6 m/ mm <sup>3</sup>			
					AlCoCrFe <sub>0.6</sub> Mo <sub>0.5</sub> Ni			675 HV 1600 m/ mm <sup>3</sup>			
					AlCoCrFe <sub>1.0</sub> Mo <sub>0.5</sub> Ni			700 HV 1500 m/ mm <sup>3</sup>			
					AlCoCrFe <sub>1.5</sub> Mo <sub>0.5</sub> Ni			525 HV 1200 m/ mm <sup>3</sup>			
					AlCoCrFe <sub>2.0</sub> Mo <sub>0.5</sub> Ni			425 HV 1250 m/ mm <sup>3</sup>			
23	Nair et al. [543]	Structural	Bulk	Vacuum arc melting + hot isostatic pressing (HIP)	Al <sub>0.1</sub> CrCoFeNi	Corrosion resistance	Boilers, ship propellers, heat exchangers etc.	Examined HEA showed a 1/9th erosion rate, and 1/4th erosion-corrosion rate compared to SS316L steel. This may be attributed to the high resistance against corrosion and work hardening. Higher biocompatibility and mechanical properties of HEA were observed than those of biomaterials that are utilized currently. In addition, a higher resistance against corrosion was observed than the presently used alloy (Ti-6Al-4 V alloy). HVOF sprayed HEA coating on flat steel (S235) substrates showed higher hardness ( $730 \pm 82 \text{ HV}_{0.1}$ ) and wear resistance. The examined HEA offered better resistance against oxidation. This may be due to the development of a protective $\text{Al}_2\text{O}_3$ oxide phase. Improvement in mechanical and magnetic properties was observed. The residual magnetization reaches a maximum for			
24	Popescu et al. [544]	Structural	Bulk	Powder metallurgy	TiZrNbTaFe	Excellent mechanical properties, oxidation and corrosion resistance and biocompatibility	Biomedical applications: (orthopaedic or dental implants)				
25	Lobel et al. [204]	Structural	Thin film	Vacuum arc melting	AlCoCrFeNiTi	High strength, ductility, hardness and resistance against wear.	Cutting tool				
26	Shen et al. [545]	Structural	Thin film	Vacuum arc melting	(Al <sub>0.34</sub> Cr <sub>0.22</sub> Nb <sub>0.11</sub> Si <sub>0.11</sub> Ti <sub>0.22</sub> ) <sub>50</sub> N <sub>50</sub>	High hardness, good wear resistance, excellent thermal stability, and diffusion resistance.	Wear-resistant coatings, such as the coating on the cutting tool				
27	Li et al. [546]	Functional	Bulk	Vacuum arc melting	FeCoNiMn <sub>0.25</sub> Al <sub>0.25</sub>	High saturated magnetization, high Curie temperature, low coercivity, and good tensile ductility.	Electric cars, aeronautics and astronautics.				
28	Ma et al. [547]	Functional	Bulk	Vacuum arc melting	AlCoCrFeNb <sub>0.1</sub> Ni AlCoCrFeNb <sub>0.25</sub> Ni AlCoCrFeNb <sub>0.5</sub> Ni AlCoCrFeAlNb <sub>0.75</sub> Ni	High yield strength, hardness and coercive forces.	Aerospace engine components				

(continued on next page)

**Table 12 (continued)**

S. no	Author	Field	Alloy form	Fabrication process	Suggested alloy	Key properties	Applications	Conclusions
29	Feng et al. [548]	Functional	Bulk	Arc melting	FeCoNi (AlSi) <sub>x</sub>	Good thermal stability, high mechanical strength, high saturation magnetization and low resistivity.	Magnetic applications	AlCoCrFeNb <sub>0.1</sub> Ni HEA, which is 6.106 emu/g Results showed that short-range order behaviour has an important effect on the mechanical and magnetic properties of HEA. HEA improve catalytic activities and electrochemical stability. Examined HEAs can be utilized as a new class of alloy for hydrogen storage that does not comprise any rare-earth metals.
30	Zhang et al. [549]	Functional	Bulk	Arc melting	Ni <sub>20</sub> Fe <sub>20</sub> Mo <sub>10</sub> Co <sub>35</sub> Cr <sub>15</sub>	High electrocatalytic activity and corrosion resistance	Solar, water and wind energy	The examined high entropy shape memory alloy is much smaller than the NiTi intermetallic compound. Results showed that introducing multicomponent ultra-high temperature shape memory alloys (SMA) is estimated to open a new research area. Further, this possibly enables new technologies that may rely on superior performance and repeated solid-state actuation at high temperatures.
31	Sahlberg et al. [550]	Functional	Bulk	Arc melting	TiVZrNbHf	Excellent hydrogen storage capacity	Hydrogen storage	Significant thermal stability was observed. The development of a superconducting gap is shared with the electronic stabilization of the high entropy alloy state at low temperatures.
32	First et al. [551]	Functional	Bulk	Arc melting	Ti <sub>16.667</sub> Zr <sub>16.667</sub> Hf <sub>16.667</sub> Ni <sub>25</sub> Cu <sub>25</sub>	Shape memory behaviour at large temperature ranges	High-temperature application	Introducing the high entropy alloy concept increases the electrical properties of Ni-Cr-based thin film.
33	Canadinc et al. [552]	Functional	Bulk	Vacuum arc melting	(Ni,Pd) <sub>50</sub> (Ti,Hf,Zr) <sub>50</sub>	Shape memory performance at elevated temperature ranges	Ultra-high temperature shape memory alloys	(continued on next page)
34	Zhao et al. [553]	Functional	Bulk	Vacuum arc melting	(NiCoFeCr) <sub>94</sub> Ti <sub>2</sub> Al <sub>4</sub>	Thermal stability and coarsening of these coherent precipitates	Structural applications at high temperatures.	
35	Kozelj et al. [554]	Functional	Bulk	Arc melting	Ta <sub>34</sub> Nb <sub>33</sub> Hf <sub>8</sub> Zr <sub>14</sub> Ti <sub>11</sub>	Superconductivity	Superconductors	
36	Lin et al. [555]	Functional	Film	DC magnetron co-sputtering	Ni-Cr-Si-Al-Ta	Good electrical properties and higher resistivity	Thin-film resistors	

**Table 12 (continued)**

S. no	Author	Field	Alloy form	Fabrication process	Suggested alloy	Key properties	Applications	Conclusions
37	Hsu et al. [556]	Functional	Film	Arc melting under Argon atmosphere	NiCo <sub>0.6</sub> Fe <sub>0.2</sub> Cr <sub>1.5</sub> SiAlTi <sub>0.2</sub>	High hardness, better thermal stability, hot hardness and resistance against heat and oxidation and thermal expansion	Thermal barrier coatings in high-temperature applications	The high entropy alloy coating shows a hot hardness of 230 Hv at 1100 °C very high hardness (1045 Hv) at room temperature.
38	Tsai et al. [557]	Functional	Film	Vacuum arc-melting	AlMoNbSiTaTi VZr	Thermal stability and sluggish diffusion	Diffusion barriers	The present HEA has the potential to operate efficiently as the diffusion barrier for Cu metallization
39	Hassan et al. [558]	Functional	Powder	Powder metallurgy	AlCoCrFeNi	High relative density, high toughness	Aerospace engine components	The toughness and formability of the fabricated materials improved by enhancing the copper's content. The excellent microwave absorption in middle and high frequency was owing to their crystal structure and unique morphologies.
40	Yang et al. [559]	Functional	Powder	Mechanical alloying	FeCoNiCrAl	Excellent magnetic properties	Electromagnetic wave absorption	The high entropy alloy sample for smaller size has a maximum total shielding of 20 dB, than 8.44 dB of the HEA of larger size.
41	Zhang et al. [560]	Functional	Powder	Mechanical alloying	AlCoCrFeNi	Superior electromagnetic wave absorption properties	Interference shielding and electromagnetic wave absorption	

**Table 13**  
Investigated structures and micro-hardness of HEA films and coating.

S. no.	Authors	Composition/substrate	Structure	Property	Fabrication process	Hardness	Elastic modulus (GPa)
1	Cheng et al. [595]	CoNiCuFeCr/ Q235 steel	FCC	Excellent wear and corrosion resistance	Plasma-transferred arc cladding	194.8HV <sub>100</sub>	211
2	Cheng et al. [596]	(AlCrMoTaTiZr)N <sub>x</sub> / Si (100) wafer	FCC	High wear resistance	Reactive RF magnetron sputtering	11.2–40.2 Gpa	193–420 GPa
3	Zhang et al. [597]	CoCrCuFeNi/ Q235 steel	FCC	Excellent thermal stability	Laser cladding	370–430 HV <sub>0.5</sub>	NA
4	Lin et al. [598]	(AlCrTaTiZrSi)N <sub>x</sub> Si <sub>y</sub> /Silicon	FCC	High mechanical and oxidation resistance property	Magnetron sputtering	30.2GPa	258
5	Huang et al. [599]	TiVCrAlSi/ Ti–6Al–4 V	(Ti, V) <sub>5</sub> Si <sub>3</sub> and a BCC solid solution	High tribological property, o High oxidation resistance	Laser cladding	750–1000HV <sub>0.2</sub>	NA
6	Huang et al. [600]	(AlCrNbSiTiV)N/ Si (100) wafer	FCC	High mechanical properties	Unbalanced magnetron sputtering	10.4–41 Gpa	177–360
7	Huo et al. [601]	CoCrFeMnNbNi/ AISI 304 steel	FCC + Nb-rich Laves phase	Excellent wear resistance	Tungsten inert gas cladding	470–500 HV <sub>0.2</sub>	NA
8	Ye et al. [602]	Al <sub>1.0</sub> FeCoNiCuCr/ AISI 1045 steel Al <sub>1.3</sub> FeCoNiCuCr/ AISI 1045 steel Al <sub>1.5</sub> FeCoNiCuCr/ AISI 1045 steel Al <sub>1.8</sub> FeCoNiCuCr/ AISI 1045 steel Al <sub>2.0</sub> FeCoNiCuCr/ AISI 1045 steel CoCrNiFeAl <sub>0.3</sub> Cu <sub>0.7</sub> B <sub>0.15</sub> Si <sub>0.1</sub> By/Steel CoCrNiFeAl <sub>0.3</sub> Cu <sub>0.7</sub> B <sub>0.3</sub> Si <sub>0.1</sub> By/Steel	BCC + FCC	High hardness at high temperature	Laser cladding	390HV <sub>0.2</sub> 540 HV <sub>0.2</sub> 640 HV <sub>0.2</sub> 660 HV <sub>0.2</sub> 687 HV <sub>0.2</sub> 312 HV <sub>0.5</sub> 342 HV <sub>0.5</sub>	NA
9	He et al. [603]	CoCrNiFeAl <sub>0.3</sub> Cu <sub>0.7</sub> B <sub>0.6</sub> Si <sub>0.1</sub> By/Steel CoCrNiFeAl <sub>2.3</sub> Cu <sub>0.7</sub> B <sub>0.15</sub> Si <sub>0.1</sub> By/Steel CoCrNiFeAl <sub>2.3</sub> Cu <sub>0.7</sub> B <sub>0.3</sub> Si <sub>0.1</sub> By/Steel CoCrNiFeAl <sub>2.3</sub> Cu <sub>0.7</sub> B <sub>0.6</sub> Si <sub>0.1</sub> By/Steel	FCC BCC	High hardness, strength	Laser cladding	502 HV <sub>0.5</sub> 694 HV <sub>0.5</sub> 732 HV <sub>0.5</sub> 756 HV <sub>0.5</sub>	NA
10	Zhang et al. [604]	TiZrNbWMo/ 45 # steel	BCC + β-Ti <sub>x</sub> W <sub>1-x</sub>	High hardness and resistance to softening	Laser cladding	700 HV <sub>0.5</sub>	NA
11	Zhang et al. [605]	FeCoNiCrCu (with the addition of Si, Mn and Mo)/ Q235 steel	BCC	High corrosion resistance and softening resistance property	Laser cladding	450 HV <sub>0.5</sub>	NA
12	Zhang et al. [606]	FeCrNiCoB <sub>1.25</sub>	FCC + (Fe, Cr) <sub>2</sub> B		Laser cladding	810–890 HV <sub>0.2</sub>	
13	Zhang et al. [607]	FeCoNiCrCu/ Q235 steel	FCC	high hardness, corrosion resistance and softening resistance property	Laser cladding	450 HV <sub>0.5</sub>	NA
14	Lin et al. [608]	FeCoCrNiAlB <sub>0</sub> /Q235 steel FeCoCrNiAlB <sub>0.25</sub> /Q235 steel FeCoCrNiAlB <sub>0.50</sub> /Q235 steel FeCoCrNiAlB <sub>0.75</sub> /Q235 steel	FCC + BCC + M <sub>2</sub> B	High micro-hardness and wear resistance	Laser cladding	344.74 HV 574.64 HV 625.48 HV 726.02 HV	NA
15	Zhang et al. [609]	6FeNiCoCrAlTiSi/ Q235 steel	BCC solid solution phase	High electrical resistivity, high micro-hardness and good resistance to softening	Laser cladding	780 HV <sub>0.5</sub>	NA
16	Hsueh et al. [610]	(AlCrSiTiZr) <sub>100-x</sub> N <sub>x</sub> /6061Al alloy (AlCrSiTiZr) <sub>100-x</sub> N <sub>x</sub> /mild steel	FCC + Amorphous	High corrosion resistance	DC reactive magnetron sputtering	11.5–17GPa	221–231.5GPa
17	Chang et al. [611]	(TiVCrAlZr)N/silicon	FCC	excellent mechanical, physical, and chemical properties	Magnetron sputtering	8.2–11 GPa	128.9–151
18	Zhang et al. [612]	6FeNiCoSiCrAlTi/ Q235 steel	BCC	Excellent soft magnetic properties.	Laser cladding	780 HV <sub>0.5</sub>	NA
19	Wu et al. [613]	Al <sub>2</sub> CrFeNiMo <sub>x</sub> /stainless steel	two BCC phases	High hardness and wear resistance	Laser cladding	678 HV <sub>0.25</sub>	NA
20	Liu et al. [614]	FeCoCrNiB <sub>x</sub> / Q245R steel	FCC + M <sub>3</sub> B phase	High tribological properties	Laser cladding	1025HV <sub>0.2</sub>	NA
21	Ren et al. [615]	(AlCrMnMoNiZr)N/ Silicon wafers (100)	FCC	High tribological properties	Magnetron sputtering	7.2–11.9 GPa	172
22	Liu et al. [616]	(FeCoNiCuVZrAl)/	Amorphous	High hardness and young modulus	Magnetron sputtering	8.6–12 GPa	153–166

elastic modulus and hardness, and the ability to withstand high temperatures, as well as magnetic and electrical properties [596,617–623].

### 6.7.2. Functional properties and application

**6.7.2.1. Bulk alloys.** The significance of HEAs should not be limited to improving the mechanical properties but exhibit some specific functional properties. High entropy alloys have made significant advances in functional applications, including irradiation resistance materials [624–627], soft-magnetic materials [628–630], diffusion barrier films [28,631,632], superconducting materials [633,634], and photo-thermal conversion materials [635,636]. Moreover, the high-concentration solid solution structure and novel alloy design concept provide high entropy alloys and many unique thermodynamic and kinetic properties, which make it feasible to develop specific functional characteristics [637]. In addition, the properties of high entropy alloys can be adjusted easily as compared to traditional alloys. This may be due to the large compositional variation in the case of HEAs. The categories, advantages and mechanisms of high entropy alloy are summarized from both functional and mechanical performances, as represented in Fig. 38.

(Here: TRIP: Transformation-induced plasticity; TWIP: Twinning-induced plasticity)

Numerous superior performances have been verified for high entropy alloys, such as excellent low-temperature plasticity, overcoming the trade-off of ductility and strength, excellent resistance against corrosion, wear, and oxidation and good thermal stability etc. [64,638–640].

**6.7.2.2. Thin films.** Many other high-entropy alloys are functionally useful in thin form. Hsu et al. [556] used a heat-resistant HEA NiC<sub>0.6</sub>Fe<sub>0.2</sub>Cr<sub>1.5</sub>SiAlTi<sub>0.2</sub> overlay coating for elevated temperature applications. The results revealed that the examined coating developed a layer of  $\alpha$ -Al<sub>2</sub>O<sub>3</sub> on the surface at 1100 °C. In addition, the examined

HEA coating exhibits better thermal stability, lower thermal conductivity, higher hardness at elevated temperatures, and smaller thermal expansion than MCrAlY coating. “Tsai et al. [641] studied the usage of AlMoNbSiTaTiVZr HEA film as a Cu metallization diffusion barrier. Then, by direct current magnetron sputtering, the copper and AlMoNbSiTaTiVZr layers are deposited sequentially on silicon substrates without breaking the vacuum. Further, to determine the diffusion barrier capabilities of this HEA material, an eight-element of the investigated high entropy alloy was introduced into a Cu/HEA/Si sandwich structure. Results showed that the prepared Cu/AlMoNbSi-TaTiVZr/Si sandwich structure can prevent interdiffusion of silicon and copper for 30 min. upto 700 °C. This recommends that the examined HEAs have a potential to operate effectively as the diffusion barrier for Cu metallization” [641]. Further, Lin et al. [555] prepared a Ni-Cr-Si-Al-Ta resistive thin film on alumina (Al<sub>2</sub>O<sub>3</sub>) and glass substrate by direct current magnetron co-sputtering from the target of Ta metal and Ni<sub>0.35</sub>Cr<sub>0.25</sub>-Si<sub>0.2</sub>-Al<sub>0.2</sub> casting alloy. The author studied the electrical properties and microstructure of Ni-Cr-Si-Al-Ta films under distinct annealing temperatures and sputtering powers. For Ni-Cr-Si-Al-Ta films at an annealing temperature of 300 °C, an amorphous structure was observed. However, at 500 °C, the Ni-Cr-Si-Al-Ta films crystallized into Ta<sub>5</sub>Si<sub>3</sub> and Cr<sub>2</sub>Ta phases. Furthermore, the Ni-Cr-Si-Al-Ta films formed at 300 °C and 100 W had a greater resistivity of 2215  $\mu\Omega\text{cm}$  with a temperature coefficient of resistance of 10 ppm/C. (TCR).

**6.7.2.3. Powders.** There are some high entropy alloys which offer excellent electromagnetic properties when they are present in powder form. These HEAs are mainly effective in interface shielding and electromagnetic wave absorption. In a planetary ball milling machine, Yang et al. [642] used mechanical alloying (for 70 h) to prepare FeCoNiCrAl HEA powder with flaky shapes. As a function of frequency (2–18 GHz), the electromagnetic wave absorption property and electromagnetic response behaviour of the powders (70 wt% powders) dispersed in the

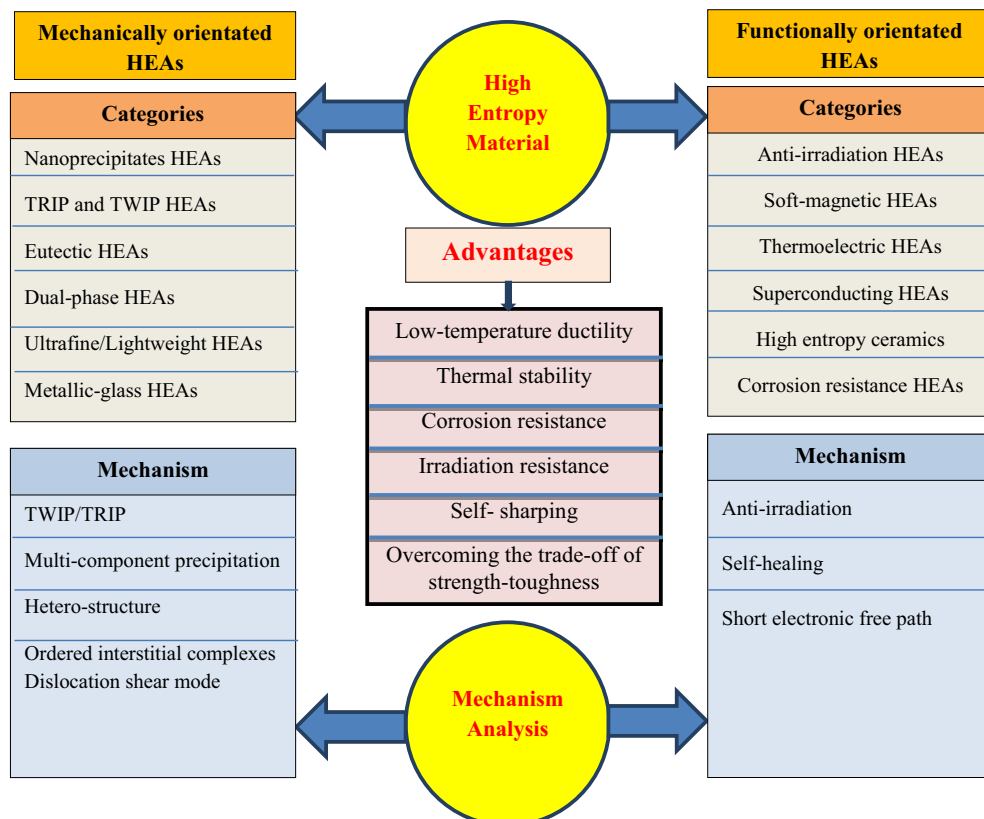


Fig. 38. The categories, advantages and mechanism of high entropy alloy [619].

paraffin matrix were investigated. It was determined that the minimal reflection loss was  $-35.3$  dB at  $10.35$  GHz, with a matching layer thickness of  $1.5$  mm, based on the computed value of reflection loss. Furthermore, a  $2.7$  GHz ( $9.2$ – $11.9$  GHz) effective absorption bandwidth was discovered. This means that the electromagnetic wave absorption properties of the FeCoNiCrAl HEA powders were outstanding. Various authors [7,643–645] successfully synthesized HEA powder using mechanical alloying. The authors reported that the ball milling parameters greatly influence the properties and microstructure. Further, it was observed that with the increase in milling time, amorphous alloy powder was fabricated, which exhibited excellent soft magnetic characteristics. Many researchers [646–650] also investigated several types of crystal structures and morphologies of cobalt particles as electromagnetic materials. They found that ferromagnetic materials with a laminated or highly symmetrical crystal structure have good electromagnetic wave absorption capabilities. Recently, the demands for structural and functional materials are increasing rapidly in distinct sectors such as transportation, mining, energy, naval, manufacturing and aviation over the traditionally utilized superalloys [29]. The existing potential applications of HEAs in the distinct sector as represented in Fig. 39.

However, the summary of distinct functional properties of HEAs and their intended application is summarized in Table 14.

## 7. Recent advances in high-entropy alloys for 3D printing

Due to the unique features of 3D printing technology, 3D printing of high entropy alloys is currently attracting significant attention from various businesses and academia. 3D printing can create complex geometries with customizable material properties. In addition, freedom of design, waste minimization, mass customization, fast prototyping, etc., are the significant advantages of 3D printing technology [683]. The main methods of 3D technology include fusion deposition modelling (FDM), Inkjet printings, Powder bed fusion (PBF), Stereolithography (SLA), Laminated object manufacturing (LOM) and Direct energy deposition(DED) etc. Among these methods, PBF and DED have been greatly explored for the 3D printing of high-entropy alloy products [684].

### 7.1. Direct energy deposition (DED)

Direct energy deposition (DED) is the most popular and effective 3D printing process to create high-entropy alloy products. This method

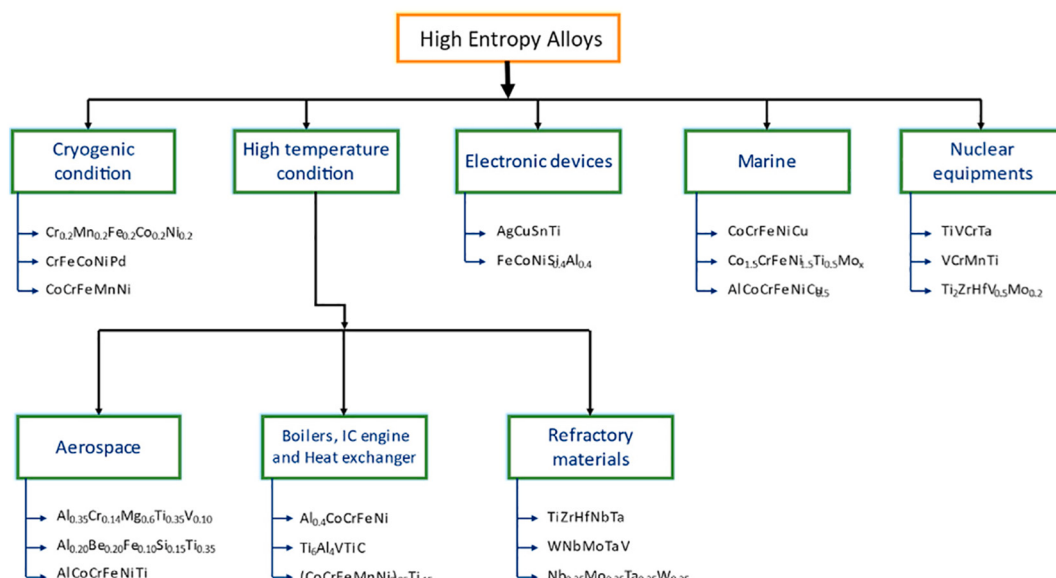
utilizes a laser, electric arc or electric beam to melt metals in the form of wires or powders upon deposition [653–688]. In addition, DED can fabricate functionally graded high entropy alloys through in situ alloying using elemental powders [689]. The schematic diagram of direct energy deposition (DED) for the fabrication of HEA products is shown in Fig. 40.

Borkar et al. [689] examined the phases and microstructures of direct energy deposition printed graded  $\text{Al}_x\text{CrCuFeNi}_2$  ( $0 \leq x \leq 1.5$ ). Further, in another investigation, Borkar et al. [690] studied the microstructures and phases of graded  $\text{AlCo}_x\text{Cr}_{1-x}\text{FeNi}$  ( $0 \leq x \leq 1$ ) high entropy alloy products produced with DED. Then, the variation of both the crystal features and phases was developed as per the predefined compositional gradient. The results revealed that with the increase in aluminium content, the printed  $\text{Al}_x\text{CrCuFeNi}_2$  high entropy alloy products attained a transition in microstructure from a disordered face-centered cubic to face-centered cubic + ordered  $\text{L}1_2$ , and to disordered body-centered cubic + ordered  $\text{B}2$  as shown in Fig. 41.

### 7.2. Selective laser melting (SLM)

SLM is a powder bed fusion printing technology that involves melting metal powders on a powder bed and printing geometrically complicated items using a high-energy laser [691–695]. The manner in which powders are fed is the crucial difference between SLM and DED. Instead of being blown from the nozzle as indirect energy deposition, high entropy alloy powders are dispersed across the building platform using a roller or blade in Selective Laser Melting. Fig. 42 shows a schematic diagram of the SLM process.

This process has been introduced to print high entropy alloy products by utilizing the developed high entropy alloy powders owing to its capability to create complex parts with excellent mechanical characteristics [696,697]. Several researchers have described SLM-printed items with a combination of high ductility and strength [698–702]. Piglione et al. [703] used the laser powder bed fusion procedure to create single-layer and multi-layer constructions. The creation of microstructure during rapid cooling and its evolution through repeated metal deposition was next investigated. According to the findings, the CrFeMnNi provided good printability, high consolidation, and consistently high hardness. Competitive grain growth and epitaxial growth determine the microstructure of the printed HEA alloy. Furthermore, the single track of studied HEA (CoCrFeMnNi) provided many grains that formed epitaxially from the base material's existing grains, with the cell

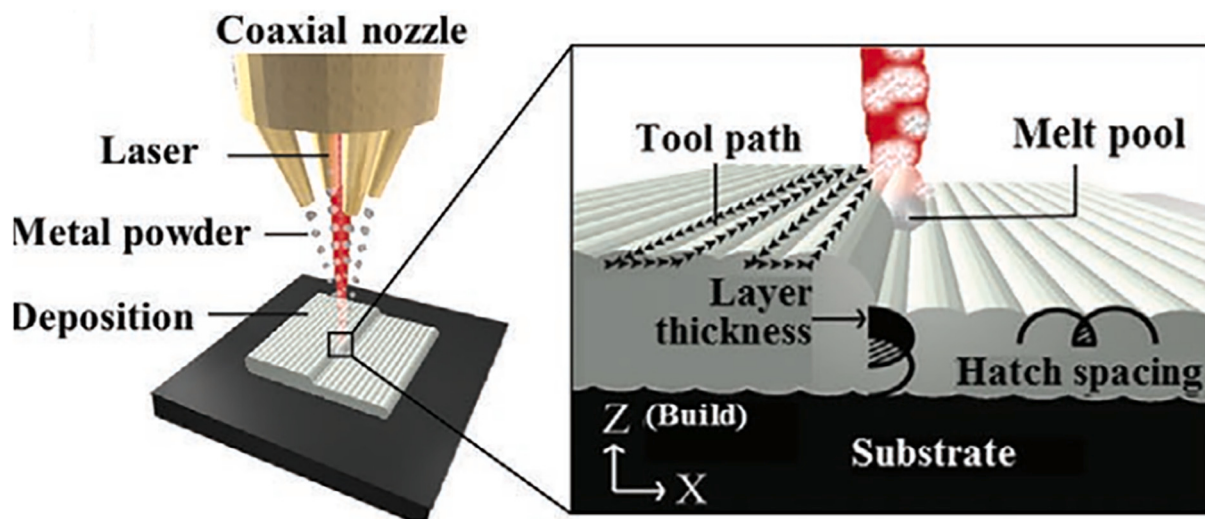


**Fig. 39.** Existing applications of distinct high entropy alloys in the diverse field [29].

**Table 14**

Summary of functional properties of HEAs and their intended application.

HEAs	Properties	Applications	Reference
YxCrFeNi, GdxCrFeNiCu, and annealed Al <sub>0.3</sub> CoCrFeNi	High strength ductility and good wear resistance.	Thermoelectric Materials, hot corrosion-resistant alloy working at high temperatures	[651–653]
AlCoCrFeNi	Al <sub>2.08</sub> CoCrFeNi offered persistent resistivity, exhibit ferromagnetic, antiferromagnetic, or paramagnetic behaviour.	electronics-based applications	[654], [655]
FeNiCoMnMg	Ultra-high-power density, long life span, and rapid energy transfer, Large storage capacity.	Used for magnetic sensors and spintronic devices.	[656]
FeNiCoMnCu	Offered high strength at room temperature and oxidation endurance	Energy storage	[657]
AlCrFeMn	Higher recyclability, Removal of contaminant by absorbing them and Low activation energy barrier. Suitable to store hydrogen fuels, Higher bulk density, better safety, and reversibility	AlCrFeMn could be used for lightweight car parts, such as body panels and wheels, aircraft parts that need to be strong and lightweight, such as landing gear and engine components.	[658]
AlFeMnTiCr, AlCrFeNi CoFeMnTiVZr, TiZrNbMoV, HfNbTiVZr, ZrTiVCrFeNi AlxCrFeNi, Ti <sub>2</sub> ZrHfV0.5Mo <sub>0.2</sub> , CrMnFeNi	Higher-strength and toughness, Withstand harsh conditions	Environmental Protection	[659], [660]
Gd <sub>20</sub> Tb <sub>20</sub> Dy <sub>20</sub> Al <sub>20</sub> M <sub>20</sub> (M <sup>1/4</sup> Co, Fe and Ni), FeCoNiCuMn, Mn <sub>27</sub> Cr <sub>7</sub> Ni <sub>33</sub> Ge <sub>25</sub> Si <sub>8</sub> Pt <sub>50</sub> Fe <sub>11</sub> Co <sub>10</sub> Ni <sub>11</sub> Cu <sub>10</sub> Ag <sub>8</sub> , Ni <sub>20</sub> Fe <sub>20</sub> Mo <sub>10</sub> Co <sub>35</sub> Cr <sub>15</sub> , AlNiCuPtPdAu	More energy efficient than traditional refrigeration mode, Economical, higher efficiency and environment friendly	Gas Storage and sensing	[661]–[664]
FeCoNiCrAl, FeCoNiSi <sub>0.4</sub> Al <sub>0.4</sub> , FeCoNiCuZn	Reduce energy consumption, progress the rate of reaction, Improve the selectivity and even change the elementary reaction	Radiation Protection	[665]–[667]
CoCrFeNiNbX	Excellent capability to absorb electromagnetic and microwave, High conductivity and better permeability	Magnetocaloric Materials	[668]–[670]
Ti <sub>16.667</sub> Zr <sub>16.667</sub> Hf <sub>16.667</sub> , Ti <sub>16.667</sub> Zr <sub>16.667</sub> , TiZrHfAlNb Ni <sub>25</sub> Cu <sub>25</sub> , Cu <sub>15</sub> Ni <sub>35</sub> Ti <sub>25</sub> Hf <sub>12.5</sub> Zr <sub>12.5</sub> , Hf <sub>16.667</sub> Co <sub>10</sub> Ni <sub>25</sub> Cu <sub>15</sub> Ta <sub>34</sub> Nb <sub>33</sub> Hf <sub>6</sub> Zr <sub>14</sub> Ti <sub>11</sub> , Hf <sub>21</sub> Nb <sub>25</sub> Ti <sub>15</sub> V <sub>15</sub> Zr <sub>24</sub>	Lightweight car parts, such as body panels and wheels, could be made from FeCoNiCuZn to improve fuel efficiency. Aircraft parts that need to be strong and lightweight, such as landing gear and engine components, could be made from FeCoNiCuZn. Medical implants, such as orthopaedic implants and dental implants, could be made from Ti <sub>16.667</sub> Zr <sub>16.667</sub> Hf due to its biocompatibility	Catalyst Materials	[671], [672]
	Improve plastic deformation ability	Electromagnetic Wave absorption	[673]–[675]
	Superconductivity, Meissner effect, and strong electron-phonon coupling	Shape memory alloy	[677]
		Superconducting materials	[678], [679]
			[680]–[682]

**Fig. 40.** Schematic diagram of the DED process for fabrication of HEA product [684,685].

axis perpendicular to the fusion line. Both the cell axis and the cell wall were visible in these grains (Fig. 43).

### 7.3. Electron beam melting (EBM)

A focused, high-energy beam interacts with powders in these processes, forming a melt pool where rapid melting and solidification occur. This rapid solidification helps to prevent element segregation, which

commonly occurs at linear or surface flaws. As a result, avoid the formation of brittle intermetallic compounds, which improves the mechanical properties of the goods [684]. Fig. 44 depicts a schematic diagram of the EBM process.

Fujieda et al. [704] provide a 1st print of AlCoCrFeNi high entropy alloy products by selective electron beam melting process and compared with the traditional casting method. The mechanical characteristics of the equiaxed AlCoCrFeNi high entropy alloy moulds developed by

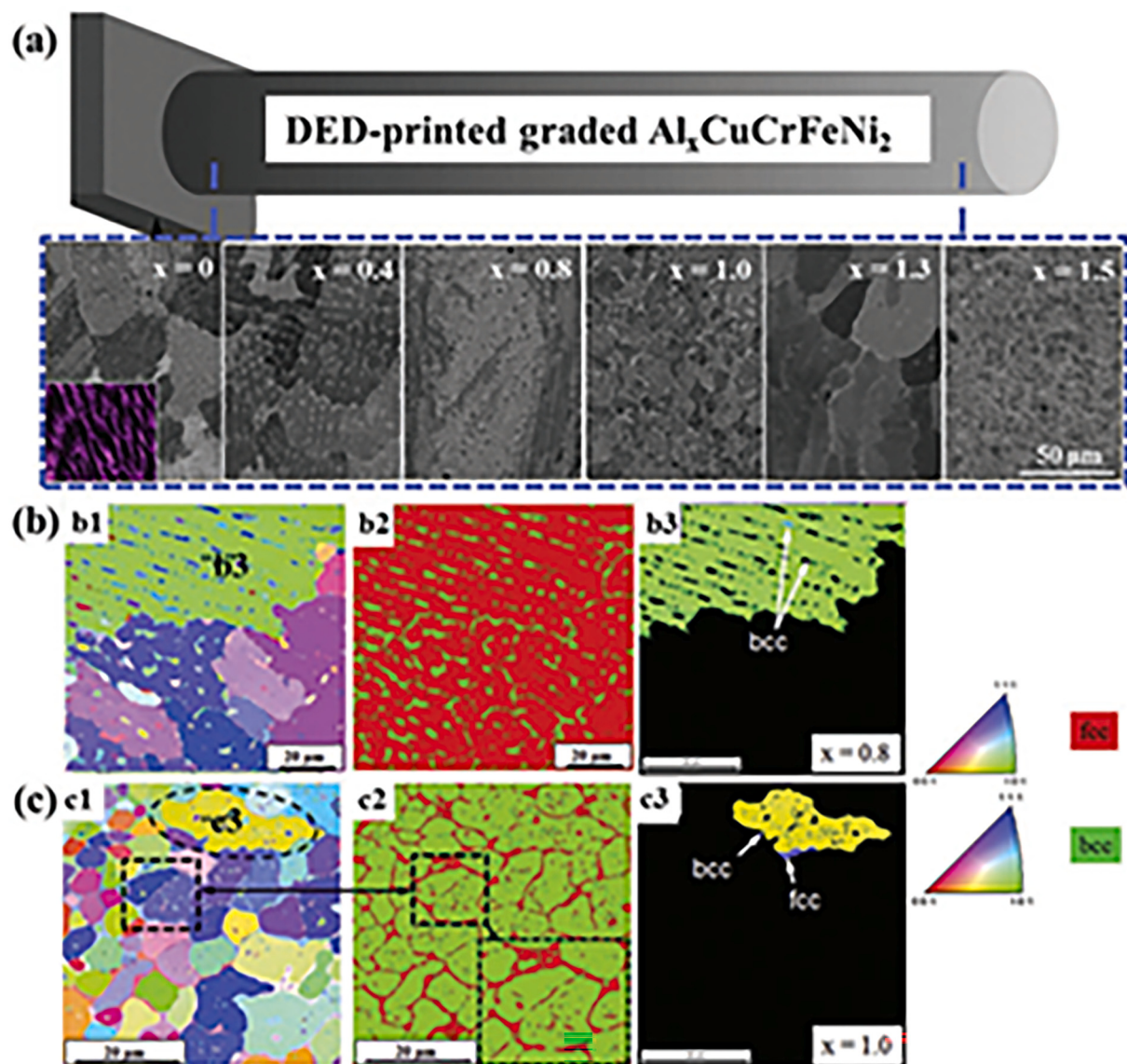


**Fig. 41.** “Microstructure of compositionally graded  $\text{Al}_x\text{CuCrFeNi}_2$  high entropy alloy products fabricated by direct energy deposition (a). Morphologies (b) EBSD results from  $\text{Al}_{0.8}\text{CuCrFeNi}_2$ , (b1) various positions and the inverse pole figure map, (b2) phase map demarking FCC and BCC regions, (b3) inverse pole figure map of a selected grain in (b1), c) EBSD results from  $\text{AlCuCrFeNi}_2$ , c1) various orientations and the inverse pole figure map, c2) phase map demarking face-centred cubic and body centred cubic regions, and c3) inverse pole figure map of a selected grain in (c1)”[689].

selective electron beam melting were far better than those of the corresponding castings. The fracture strength of the EBM part was 1400 MPa, which was 6 times higher than the conventional material (SUS304). The authors concluded that selective electron beam melting is a promising manufacturing technique for using high entropy alloys as engineering materials. Further, Shiratori et al. [705] also used selective electron beam melting to analyze the relationship b/w the mechanical properties & microstructure of an equiatomic  $\text{AlCoCrFeNi}$  HEA. Their results showed similar phase components but distinct microstructures in the high entropy alloy's bottom and top regions, owing to different temperature distributions induced by heat transfer and preheating, as shown in Fig. 45.

In Fig. 45, B2+ body-centred cubic phases with face-centred cubic precipitates were shown. Further, the (aluminium, nickel) rich and (chromium, iron-rich phases corresponded to the B2 and body-centred cubic, respectively. Following that, preheating at  $950^\circ\text{C}$  caused the face-centred cubic phase to form and precipitate along the grain boundaries of B2 and body-centred cubic. However, a modulated structure within equiaxed grains was found both in the bottom and top

regions, but the great number of equiaxed grains was higher at the bottom. The difference in experience time at the preheating temperature caused the local difference within the microstructure. Further, various researchers developed high entropy alloy products using 3D printed technology and compared their mechanical properties with those manufactured by traditional processes. (See Table 15).

## 8. Research lapses

This review describes an overview of high entropy alloys and their application in distinct sectors. The literature revealed that many research efforts are being made to develop high-entropy alloys for many structural applications. These high entropy alloys offered excellent strength, hardness, and high resistance against oxidation, corrosion and wear. However, high entropy alloys have not been explored for diverse applications. Even though recently, many novel high entropy alloys have been designed and studied. However, their tensile properties have rarely been explored. Instead, various authors only investigated the mechanical properties of HEAs/ HEAs coatings in terms of hardness or

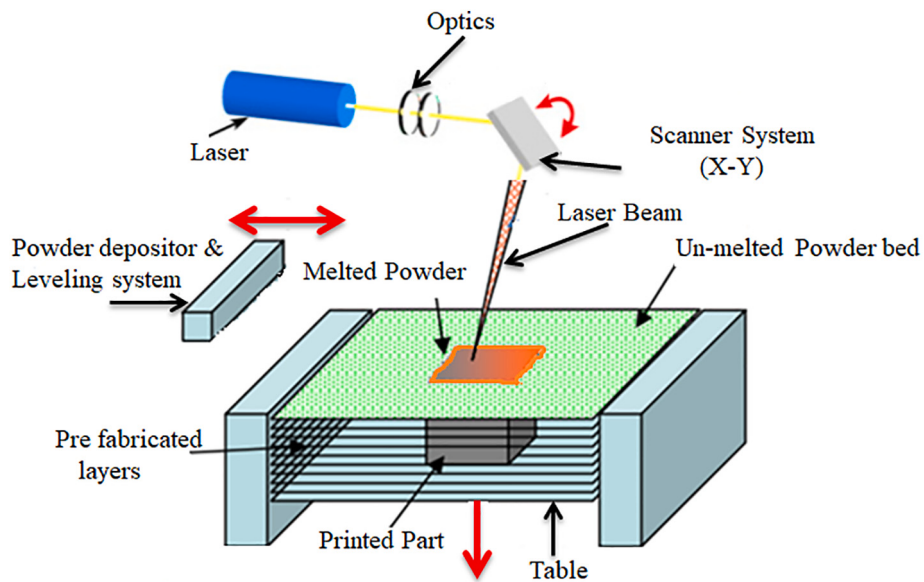


Fig. 42. Schematic diagram of SLM for fabrication of HEA product [686].

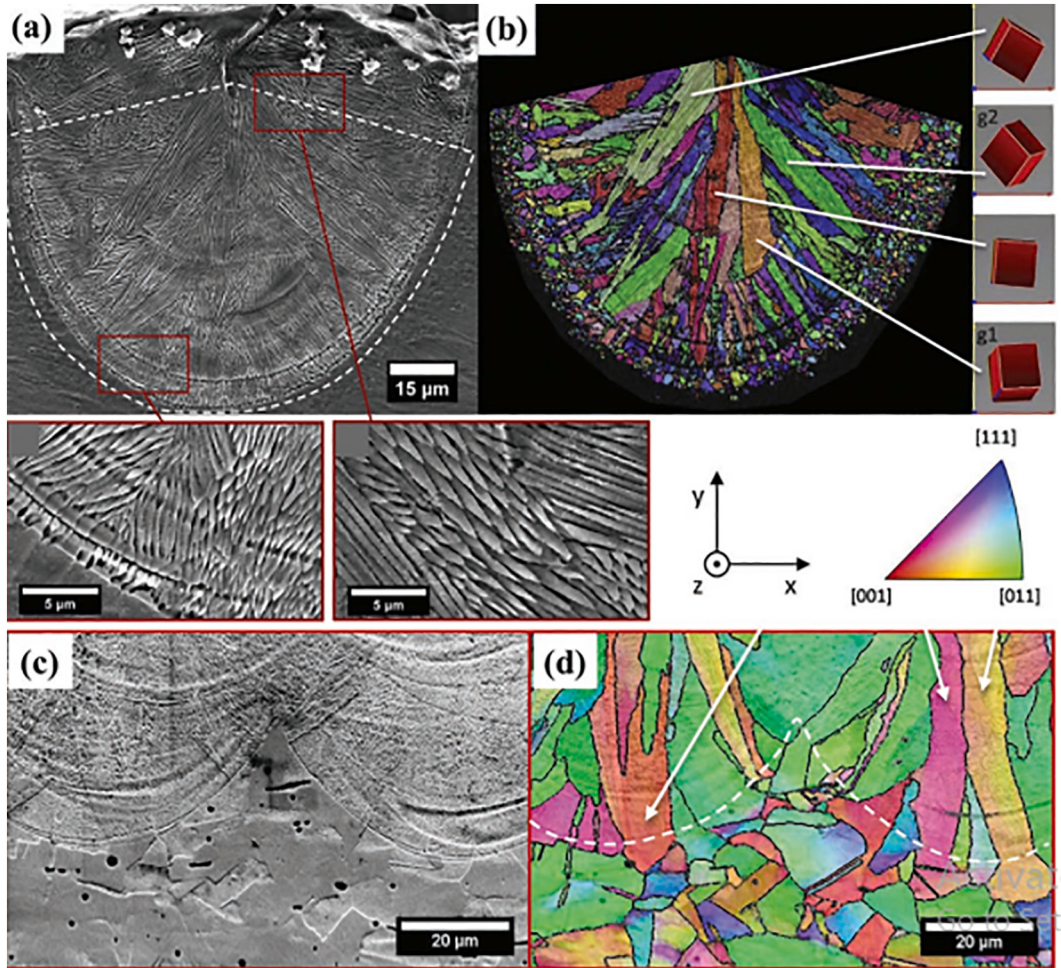
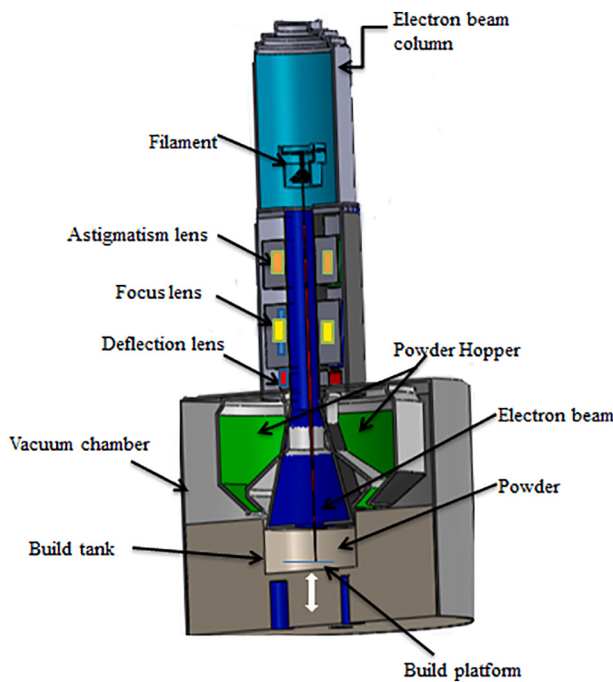


Fig. 43. “(a). Microstructure (b). Inverse pole diagram map of the cross-section of one track in the single-layer build developed by selective laser melting from a CoCrFeMnNi high entropy alloy powder through electron backscatter diffraction measurement; the cubes indicate the crystallographic orientations of selected grains, (c). Microstructure (d). Inverse pole diagram map of the cross-section in the multi-layer build”[703].



**Fig. 44.** Schematic diagram of EBM for fabrication of HEA product [686].

compression test [43,722]. Kumar A. and Gupta M. (2016) [723] also provide a detailed review of the evolution of lightweight high entropy alloys (LWHEAs) for biomedical applications. The high strength and anti-oxidation/corrosion properties of HEAs made them suitable for biomedical applications. But, at the same time, it is observed that most of the lightweight high entropy alloys designed to date exhibited very limited tensile ductility. In addition, HEAs having a density of  $<3\text{ g/cm}^3$

are extremely limited. But, the density of the high entropy alloys is the main constraint for lightweight applications, including energy, transportation and medical sectors. Hence, more research and development are needed in this area. Further, extensive research is required to fabricate porous biomedical parts of lightweight high entropy alloys using distinct additive manufacturing techniques.

Furthermore, based on the initial research on HEA, it is evident that HEAs in bulk, thin-film, and powder forms have significant structural and functional promise in a wide range of domains. Some key applications, however, are critical in resolving severe societal issues. These include transportation, hydrogen storage, nuclear reactors, aerospace, cutting tools, magnetic refrigeration, electronics and biomedical applications. But, at the same time, it was observed that despite the various applications of HEAs in distinct industries, a considerable gap still exists from laboratory explorations to practical engineering applications. From the previous laboratory investigations, it is clear that they are focused only on primary properties which are essential for a particular application. However, the practical applications of various HEAs should be justified by considering a combination of many properties.

For example, high entropy alloys are utilized for energy conversion or shape memory and also need to have good ductility and strength to maintain structural integrity in harsh environmental conditions. In this way, more application-focused or application-driven research with investigating and analyzing all necessary properties is necessary to close the gaps. In addition, more research is required to minimize the cost of HEAs for diverse applications in various sectors.

Literature also revealed that most of the work done by various researchers on high entropy alloys is still limited to their morphology, microstructure, and mechanical and tribological properties. So, futuristic researchers need to investigate and compare other properties (stiffness, creep resistance, ductility, density and wear resistance) of distinct HEAs with traditional alloys. So that more application-based high entropy alloys can be designed and developed for future applications, including aviation, energy, marine, structural and transportation

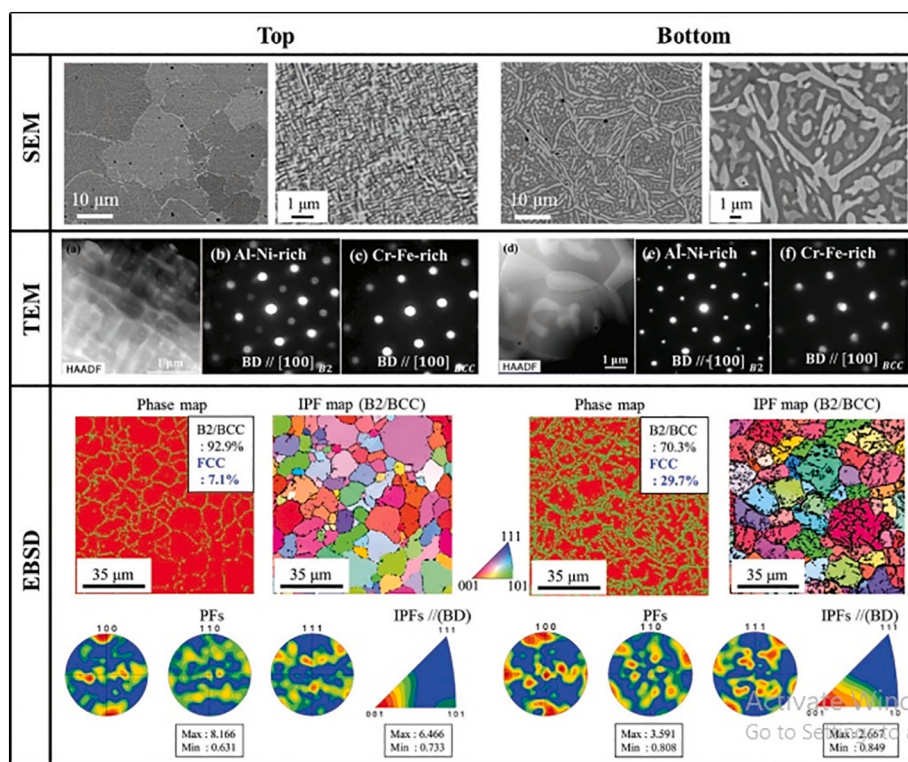


**Fig. 45.** Microstructural and phase characteristics of electron beam melting printed AlCoCrFeNi high entropy alloy products at the bottom and top regions from scanning electron microscopy (SEM), transmission electron microscope (TEM), and electron backscatter diffraction (EBSD) measurements [705].

**Table 15**

Mechanical properties of 3D printed high entropy alloy products and those fabricated by traditional processes.

S. no.	Authors	High entropy alloys	Process	Mechanical properties			Microstructure	Results
				Yield strength (MPa)	Ultimate tensile strength (MPa)	% elongation		
1	Chew et al. [706]	CoCrFeMnNi	LAAM	518	660	19.8	The as-built HEAs have directional solidification along the melt-pool boundaries, indicating dendritic columnar grains and equiaxed grains.	LAAM can be used to print high-entropy bulk material, to build larger & more complex parts.
2	Guan et al. [707]	CrMnFeCoNi	LENS™	517	650	17	Single-phase disordered FCC structure	LENS™ process has the capability to manufacture HEAs for distinct engineering applications.
3	Melia et al. [708]	CoCrFeMnNi	DED	424	651	48	A cellular microstructure was found	The fabricated HEA exhibits lower porosity and equiatomic CoCrFeMnNi alloy parts than traditional methods.
4	Xiang et al. [709]	CoCrFeMnNi	LMD	290	535	55	Columnar and equiaxed grains are formed.	The mechanical characteristics of the 1400 W samples developed by using LMD are superior as compared to those produced by casting.
			Casting	250	489	42 %	Coarse dendritic structure	Examined HEAs fabricated by SLM offered higher hardness, ductility and strength than those manufactured by the traditional method (arc melting).
5	Brif et al. [698]	FeCoCrNi	SLM (50 µm)	402	480	8	Single-phase FCC fine microstructure	
			SLM (20 µm)	600	745	32		
6	Sun et al. [710]	CoCrFeNi	Arc melting	188	457	50	Coarse microstructure	
7	Li et al. [711]	CoCrFeMnNi	SLM (by chessboard scan)	556 ± 23.6	676 ± 20.5	12.4 ± 2.1	Coarse-grained microstructure	By selecting optimum printing parameters, no hot tearing issue was observed.
			SLM (by stripe scan)	572 ± 7.5	69.10 ± 15.9	17.9 ± 0.9		
8	Zhu et al. [712]	CoCrFeNiMn	SLM	510	609	34	Laser molten pool boundary and submicro cellular grains structure	After HIP, the tensile strength and densification were improved while the elongation was reduced.
			SLM+ hot isostatic pressing	–	601	35		An outstanding combination of excellent ductility and high strength compared to those manufactured by traditional methods was attained in the as-built samples.
9	Fujieda et al. [704]	AlCoCrFeNi	SEBM (0°)	1015.0 ± 52.5	1668.3 ± 71.5 (compressive)	26.4 ± 6.7	FCC phase (finer microstructures)	The fracture strength of the SEBM printed part was above 1400 MPa, which was >6 times greater than that of SUS304, a traditional engineering material.
			SEBM (90°)	944.0 ± 55.4	1447.0 ± 135.8 (compressive)	14.5 ± 5.3		
			Casting	1308.3 ± 77.3	1425.0 ± 127.5 (compressive)	5.6 ± 1.9	Complex microstructures	
10	Fujieda et al. [713]	Co <sub>1.5</sub> CrFeNi <sub>1.5</sub> Ti <sub>0.5</sub> Mo <sub>0.1</sub>	SLM	773 ± 4.2	1178	25.8 ± 0.6 %	Uniform microstructures with no visible segregation	As-built SLM sample was superior to traditional alloys and exhibited excellent corrosion resistance and tensile properties.
11	Yang et al. [714]	Ni <sub>6</sub> Cr <sub>4</sub> WFe <sub>9</sub> Ti	SLM	742	972	12.2	Fine-grained structure	SLM process effectively refines the crystalline structure, and the coarse grain boundary precipitates to give a general pathway for fabricating fine-grained material with both ductility and high strength.
12	Yang et al. [715]	Ni <sub>6</sub> Cr <sub>4</sub> WFe <sub>9</sub> Ti	SLM	630–710	920–983	8.6–12.9	Extremely fine cellular crystals	The result showed that SLM-processed HEA alloys are simultaneously ductile and ultra-strong.
13	Wang et al. [716]	CoCrFeMnNi	EBM	205 ± 3	497 ± 2	63 ± 1	Hierarchical microstructure	EBM-built HEA Parts offered comparable tensile characteristics to their

(continued on next page)

**Table 15 (continued)**

S. no.	Authors	High entropy alloys	Process	Mechanical properties			Microstructure	Results
				Yield strength (MPa)	Ultimate tensile strength (MPa)	% elongation		
14	Kim et al. [717]	CoCrFeMnNi	as-cast	210	430	33–48	Recrystallized microstructure	conventional cast counterparts. As-cast high entropy alloy with very large grain sizes offered active twin generation even at 500 °C
15	Kenel et al. [718]		3D extrusion + sintering (1573 K) 3D extrusion + sintering (130K)	250 ± 5 388 ± 7	598 ± 8 864 ± 12	33.8 ± 1.3 37.6 ± 0.7	Higher densification (a near-fully dense structure) with equiaxed grains Dense structure with equiaxed grains	Excellent mechanical properties of examined HEA were achieved at cryogenic and ambient temperatures.
16	Wu, Z. et al. [719]	CrMnFeCoNi	Weld	270	565	30	Coarse grain microstructure.	At cryogenic and room temperature, the mechanical properties of the weld zone were comparable with the base metal. The Vickers harnesses of the parent metal & fusion zone were $145.00 \pm 2.61$ and $163.62 \pm 5.56$ HV, respectively
17	Fan, Y. et al. [720]	CoCrCuFeNi	Fiber laser welding	$262.83 \pm 36.24$	NA	NA	Cast dendritic & inter-dendritic structures	Extruded alloy offers a very high tensile strength (712.5 MPa). This may be due to the solid solution strengthening and homogenous microstructure.
18	Liu et al. [721]	FeCoCrNi	Powder extrusion	359	712.5	56	Single FCC and an equiaxed microstructure.	At cryogenic and room temperature, the mechanical properties of the weld zone were comparable with the base metal. The Vickers harnesses of the parent metal & fusion zone were $145.00 \pm 2.61$ and $163.62 \pm 5.56$ HV, respectively

Here; LAAM: laser aided additive manufacturing; LENS™: Laser engineered net shaping; DED: laser-based directed energy deposition; LMD: laser metal deposition; SLM: Selective laser melting; HIP: hot isostatic pressing; SEBM: selective electron beam melting;

applications. The futuristic researcher's focus is to reduce the cost and durability of HEAs in harsh environments and how to utilize recyclable and waste scrap material. Another research gap in the utilization of HEA is the weldability of HEA materials. Weldability is an important property that cannot be ignored. Although, there is still some work that has been carried out by some researchers on the weldability of HEAs. However, the optimization of process parameter to attain a highly efficient weld joint with enhanced mechanical properties still need to be explored. In addition, high-temperature corrosion of boiler tubes is a major problem in thermal power plants. However, various researchers [20,43,698,704,707–734] have used diverse coating on boiler tubes by distinct thermal spray processes to combat the corrosion of boiler steel. However, limited work has been done on high entropy alloy coatings on boiler steel to combat high-temperature oxidation, erosion and corrosion. Hence, futuristic researchers need to explore the behaviour of the thermally sprayed HEAs coating on distinct boiler steel. High entropy alloys have the potential to be helpful in a variety of industries. However, the impacts of stress-corrosion cracking, residual stress, corrosion fatigue, and the synergistic influences of service conditions have yet to be adequately explored. So, extensive research on the above-mentioned investigations is essential for real-world applications.

## 9. Prospects and future opportunities

Various specific issues need to be solved to promote the novel application of high entropy alloys. 1st Issue: exploring the interaction b/w enthalpy and entropy of high entropy alloys is the main issue in attaining optimal performance. 2nd issue: the internal structure of high entropy alloy is more intricate. In addition, the influence of local chemical order on the functional performance of high-entropy alloys is still an open issue. 3rd issue: the notion of high entropy ceramics is projected in the field of energy and engineering (high entropy carbides, nitrides, and oxides). In contrast to the high entropy alloys, the solid

solution unit transforms from the metal atom into a binary compound, making the traditional phase formation rules no longer applicable to high entropy ceramics. Hence, developing phase transformation rule for high entropy ceramics is also a significant research work in the field of HEAs" [29].

"Despite these issues, the high entropy alloys are observed to have novel properties (superb specific strength, exceptional ductility & fracture toughness at cryogenic temperature, excellent mechanical performance at elevated temperature, superconductivity and superparamagnetic behaviour etc.). In the energy sector and transportation industry, where high-strength and lightweight materials are in great demand, novel HEAs can be designed and developed. For example, high entropy alloys are as light as aluminium alloys but stronger than metallic glasses. In addition, the high entropy alloys that contain refractory elements (Mo, Nb, and Ta) can sustain their high strength at high temperatures ( $>1200^\circ\text{C}$ ), superior to conventional superalloys (Haynes-230 and Inconel-718). Further, the extensive research on HEAs can be utilized in high-temperature applications (boiler tubes, gas turbines, nuclear construction, rocket nozzle etc.). However, refractory lightweight HEAs having low density can be utilized in the aerospace industry. Due to their excellent cryogenic properties, these HEAs can also be used for cryogenic applications (pipework, rocket casting, and liquid nitrogen or oxygen equipment)." [735]. Overall, more novel high entropy alloys with promising properties for specific applications can be discovered with continuous research and development. Thus, it promotes the applications of high entropy alloys in diverse applications.

In the coming years, machine learning theory can be introduced to speed up the fabrication of novel HEAs for additive manufacturing. In addition, the concept of m/c learning can be used for fast prediction of novel additive manufactured HEAs products, as per the database prepared from the characterizations, numerical modelling predictions, experimental printing etc.

## 10. Conclusions

This review article provides an overview of high entropy alloy coatings, classification, fabrication methods, post-processing, and applications of HEAs coatings. Further, the tribological and mechanical properties of HEAs-based coating, including the recent advances in HEAs for 3D printing, are discussed. From the literature studies following conclusions are made:

- HEA alloy-based coating is the better option to protect the surface from oxidation, erosion, wear and corrosion. However, the adhesion and coating performance can be enhanced by applying a post-processing technique. These coatings not only enhance the mechanical properties (hardness and wear resistance) but these coating materials are being used as functional coatings, including radiation barriers, corrosion barriers and diffusion barriers.
- Most of the high-entropy alloys in the surface engineering field are processed through vapour deposition techniques and cladding. However, a developing market for thick, high entropy alloy coating exists. Various researchers used high-velocity oxy-fuel and atmospheric plasma spray methods to fabricate high entropy alloy coatings, while few researchers reported on cold spray and wire arc spray.
- Some high entropy alloys exhibit novel corrosion performance in high-temperature/high-pressure water environments. This depicts that high entropy alloys can be employed in supercritical service conditions.
- The mechanical characteristics of high entropy alloy films & coating are summarized, which shows that the high entropy alloy film and coatings offered high elastic modulus, high hardness, and superior resistance against wear.
- High entropy alloy films also offered superior electrical, electrochemical and magnetic properties. Due to these properties, HEA films become suitable for diffusion, radiation barrier and corrosion protection applications.
- High-velocity oxy-fuel high entropy alloy coatings offered dense microstructure and high hardness. In addition, in most cases, the wear resistance and hardness were found to be better than traditional materials owing to the formation of supersaturated multi-component phases & distinct strengthening mechanisms.
- The high entropy alloy parts fabricated by DED offered lower strength as compared to parts fabricated by using EBM and SLM.
- Extensive research and development on the fabrication method of HEAs, HEAs coating material, and coating process is required for corrosion-resistant applications.

Overall, the study shows that only some of the investigated HEA coatings exhibited better or enhanced surface protection ability. Hence, there is a significant requirement to develop a basic understanding of HEA materials so that futuristic researchers can consistently continue designing and developing a novel and superior HEA coating for diverse applications.

## CRediT authorship contribution statement

**Santosh Kumar:** Conceptualization, Investigation, Methodology, Supervision, Validation, Visualization, Writing – original draft, Writing – review & editing.

## Declaration of competing interest

The authors report no declarations of interest.

## Data availability

No data was used for the research described in the article.

## Acknowledgement

The author is thankful to Chandigarh Group of Colleges Landran for their motivation to write the research paper.

## References

- [1] J. Li, Y. Huang, X. Meng, Y. Xie, A review on high entropy alloys coatings: fabrication processes and property assessment, *Adv. Eng. Mater.* 21 (8) (2019) 1900343, <https://doi.org/10.1002/adem.201900343>.
- [2] F. Otto, A. Dlouhý, C. Somsen, H. Bei, G. Eggerle, E. George, The influences of temperature and microstructure on the tensile properties of a CoCrFeMnNi high-entropy alloy, *Acta Mater.* 61 (15) (2013) 5743–5755, <https://doi.org/10.1016/j.actamat.2013.06.018>.
- [3] C. Tong, M. Chen, J. Yeh, S. Lin, S. Chen, T. Shun, S. Chang, Mechanical performance of the al X CoCrCuFeNi high-entropy alloy system with multiprincipal elements, *Metall. Mater. Trans. A* 36 (5) (2005) 1263–1271, <https://doi.org/10.1007/s11661-005-0218-9>.
- [4] Z. Ang, T. Yuan, C. Tsai, J. Yeh, C.D. Lundin, P.K. Liaw, Fatigue behavior of a wrought Al0.5CoCrCuFeNi two-phase high-entropy alloy, *Acta Mater.* 99 (2015) 247–258, <https://doi.org/10.1016/j.actamat.2015.07.004>.
- [5] C. Liu, H. Wang, S. Zhang, H. Tang, A. Zhang, Microstructure and oxidation behavior of new refractory high entropy alloys, *J. Alloys Compd.* 583 (2014) 162–169, <https://doi.org/10.1016/j.jallcom.2013.08.102>.
- [6] Y. Hsu, W. Chiang, J. Wu, Corrosion behavior of FeCoNiCrCux high-entropy alloys in 3.5% sodium chloride solution, *Mater. Chem. Phys.* 92 (1) (2005) 112–117, <https://doi.org/10.1016/j.matchemphys.2005.01.001>.
- [7] Y. Kao, S. Chen, T. Chen, P. Chu, J. Yeh, S. Lin, Electrical, magnetic, and hall properties of AlxCoCrFeNi high-entropy alloys, *J. Alloys Compd.* 509 (5) (2011) 1607–1614, <https://doi.org/10.1016/j.jallcom.2010.10.210>.
- [8] Tsai, M.H., Wang, C.W., Tsai, C.W., Shen, W.J., Yeh, J.W., Gan, J.Y., Wu, W.W. (2011). Thermal stability and performance of NbSiTaTiZr high-entropy alloy barrier for copper metallization. *J. Electrochem. Soc.*, 158:H1161–H1165.
- [9] Y. Zhang, T. Zuo, Y. Cheng, P.K. Liaw, High-entropy alloys with high saturation magnetization, electrical resistivity and malleability, *Sci. Rep.* 3 (1) (2013), <https://doi.org/10.1038/srep01455>.
- [10] W. Li, P. Liu, P.K. Liaw, Microstructures and properties of high-entropy alloy films and coatings: a review, *Mater. Res. Lett.* 6 (4) (2018) 199–229, <https://doi.org/10.1080/21663831.2018.1434248>.
- [11] G. Abadias, E. Chason, J. Keckes, M. Sebastiani, G.B. Thompson, E. Barthel, G. L. Doll, C.E. Murray, C.H. Stoessel, L. Martinu, Review article: stress in thin films and coatings: current status, challenges, and prospects, *J. Vac. Sci. Technol. A* 36 (2) (2018) 020801, <https://doi.org/10.1116/1.5011790>.
- [12] Z. An, H. Jia, Y. Wu, P.D. Rack, A.D. Patchen, Y. Liu, Y. Ren, N. Li, P.K. Liaw, Solid-solution CrCoCuFeNi high-entropy alloy thin films synthesized by sputter deposition, *Mater. Res. Lett.* 3 (4) (2015) 203–209, <https://doi.org/10.1080/21663831.2015.1048904>.
- [13] Ji, X., Duan, H., Zhang, H., & Ma, J. (2015). Slurry erosion resistance of laser clad NiCoCrFeAl3high-entropy alloy coatings. *Tribol. Trans.*, 58(6), 1119–1123. <https://doi.org/10.1080/10402004.2015.1044148>.
- [14] H. Zhang, W. Wu, Y. He, M. Li, S. Guo, Formation of core-shell structure in high entropy alloy coating by laser cladding, *Appl. Surf. Sci.* 363 (2016) 543–547, <https://doi.org/10.1016/j.apsusc.2015.12.059>.
- [15] T. Yue, H. Xie, X. Lin, H. Yang, G. Meng, Microstructure of laser re-melted AlCoCrCuFeNi high entropy alloy coatings produced by plasma spraying, *Entropy* 15 (12) (2013) 2833–2845, <https://doi.org/10.3390/e15072833>.
- [16] C. Yao, P. Zhang, M. Liu, G. Li, J. Ye, P. Liu, Y. Tong, Electrochemical preparation and magnetic study of Bi–FE–Co–Ni–Mn high entropy alloy, *Electrochim. Acta* 53 (28) (2008) 8359–8365, <https://doi.org/10.1016/j.electacta.2008.06.036>.
- [17] D. Liu, J.B. Cheng, H. Ling, Electrochemical behaviours of (NiCoFeCrCu)95B5 high entropy alloy coatings, *Mater. Sci. Technol.* 31 (10) (2014) 1159–1164, <https://doi.org/10.1179/1743284714y.0000000739>.
- [18] O. Oluwatosin Abegunde, E. Titilayo Akinlabi, O. Philip Oladipo, S. Akinlabi, A. Uchenwa Ude, Overview of thin film deposition techniques, *AIMS Materials Science* 6 (2) (2019) 174–199, <https://doi.org/10.3934/matersci.2019.2.174>.
- [19] S. Kumar, A. Handa, V. Chawla, N.K. Grover, R. Kumar, Performance of thermal-sprayed coatings to combat hot corrosion of coal-fired boiler tube and effect of process parameters and post-coating heat treatment on coating performance: A review, *Surf. Eng.* 37 (7) (2021) 833–860, <https://doi.org/10.1080/02670844.2021.1924506>.
- [20] S. Kumar, M. Kumar, A. Handa, High temperature oxidation and erosion-corrosion behaviour of wire arc sprayed Ni-CR coating on boiler steel, *Mater. Res. Express* 6 (12) (2020) 125533, <https://doi.org/10.1088/2053-1591/ab5fae>.
- [21] S. Kumar, R. Kumar, S. Singh, H. Singh, A. Handa, The role of thermal spray coating to combat hot corrosion of boiler tubes: a study, *J. Xidian Univ.* 14 (5) (2020) 229–239, <https://doi.org/10.37896/jxu14.5/024>.
- [22] R. Kumar, S. Kumar, Thermal spray coating: a study, *Int. J. Eng. Sci. Res. Technol.* 7 (3) (2018) 610–617, <https://doi.org/10.5281/zenodo.1207005>.
- [23] M. Renner, Thermal spray coating applications in the chemical process industries. MTI publication No. 42. VonR. P. Krepki, 252 S., 30 abb., 3 tab., the materials technology Institute of the chemical industry Inc., 1993, St. Louis, USA, \$85,00 (NACE member \$60,00), ISBN 1-877914-59-2, Mater. Corros. Werkstoffe Korrosion 46 (11) (1995) 657, <https://doi.org/10.1002/maco.19950461115>.

- [24] A.S. Ang, C.C. Berndt, A review of testing methods for thermal spray coatings, *Int. Mater. Rev.* 59 (4) (2014) 179–223, <https://doi.org/10.1179/1743280414y.0000000029>.
- [25] X.H. Yan, J.S. Li, W.R. Zhang, Y. Zhang, A brief review of high-entropy films, *Mater. Chem. Phys.* 210 (2018) 12–19, <https://doi.org/10.1016/j.matchemphys.2017.07.078>.
- [26] W. Sheng, X. Yang, C. Wang, Y. Zhang, Nano-crystallization of high-entropy amorphous NbTiAlSiVxNy films prepared by magnetron sputtering, *Entropy* 18 (6) (2016) 226, <https://doi.org/10.3390/e18060226>.
- [27] Q.F. He, Z.Y. Ding, Y.F. Ye, Y. Yang, Design of high-entropy alloy: a perspective from nonideal mixing, *JOM* 69 (11) (2017) 2092–2098, <https://doi.org/10.1007/s11837-017-2452-1>.
- [28] S. Chang, C. Li, S. Chiang, Y. Huang, 4-nm thick multilayer structure of multi-component (AlCrRuTaTiZr)Nx as robust diffusion barrier for Cu interconnects, *J. Alloys Compd.* 515 (2012) 4–7, <https://doi.org/10.1016/j.jallcom.2011.11.082>.
- [29] A. Kumar, A. Singh, A. Suhane, Mechanically alloyed high entropy alloys: existing challenges and opportunities, *J. Mater. Res. Technol.* 17 (2022) 2431–2456, <https://doi.org/10.1016/j.jmrt.2022.01.141>.
- [30] B.L. Musicó, D. Gilbert, T.Z. Ward, K. Page, E. George, J. Yan, V. Keppens, The emergent field of high entropy oxides: design, prospects, challenges, and opportunities for tailoring material properties, *APL Mater.* 8 (4) (2020) 040912, <https://doi.org/10.1063/5.00003149>.
- [31] Y. Huang, L. Chen, H. Lui, M. Cai, J. Yeh, Microstructure, hardness, resistivity and thermal stability of sputtered oxide films of AlCoCrCu0.5NiFe high-entropy alloy, *Mater. Sci. Eng. A* 457 (1–2) (2007) 77–83, <https://doi.org/10.1016/j.msea.2006.12.001>.
- [32] M. Tsai, J. Yeh, J. Gan, Diffusion barrier properties of AlMoNbSiTaTiVZr high-entropy alloy layer between copper and silicon, *Thin Solid Films* 516 (16) (2008) 5527–5530, <https://doi.org/10.1016/j.tsf.2007.07.109>.
- [33] X. Ye, M. Ma, W. Liu, L. Li, M. Zhong, Y. Liu, Q. Wu, Synthesis and characterization of high-entropy alloy FeCoNiCuCr by laser cladding, *Adv. Mater. Sci. Eng.* 2011 (2011) 1–7, <https://doi.org/10.1155/2011/485942>.
- [34] X. Yin, S. Xu, Properties and preparation of high entropy alloys, in: *MATEC Web of Conferences* 142, 2018 03003, <https://doi.org/10.1051/matecconf/201814203003>.
- [35] Z. Li, S. Zhao, R.O. Ritchie, M.A. Meyers, Mechanical properties of high-entropy alloys with emphasis on face-centered cubic alloys, *Prog. Mater. Sci.* 102 (2019) 296–345, <https://doi.org/10.1016/j.pmatsci.2018.12.003>.
- [36] R.S. Mishra, N. Kumar, M. Komarasamy, Lattice strain framework for plastic deformation in complex concentrated alloys including high entropy alloys, *Mater. Sci. Technol.* 31 (10) (2015) 1259–1263, <https://doi.org/10.1179/1743284715y.0000000050>.
- [37] S. Ranganathan, Alloyed pleasures: multimetallic cocktails, *Curr. Sci.* 85 (10) (2003) 1404–14066. <https://asset-pdf.scinapse.io/prod/41078916/41078916.pdf>.
- [38] B. Gludovatz, A. Hohenwarter, D. Catoor, E.H. Chang, E.P. George, R.O. Ritchie, A fracture-resistant high-entropy alloy for cryogenic applications, *Science* 345 (6201) (2014) 1153–1158, <https://doi.org/10.1126/science.1254581>.
- [39] S.A. Al-Fozan, A.U. Malik, Effect of seawater level on corrosion behavior of different alloys, *Desalination* 228 (1–3) (2008) 61–67, <https://doi.org/10.1016/j.desal.2007.08.007>.
- [40] W. Li, P.K. Liaw, Y. Gao, Fracture resistance of high entropy alloys: a review, *Intermetallics* 99 (2018) 69–83, <https://doi.org/10.1016/j.intermet.2018.05.013>.
- [41] Z. Li, F. Körmann, B. Grabowski, J. Neugebauer, D. Raabe, AB initio assisted design of quinary dual-phase high-entropy alloys with transformation-induced plasticity, *Acta Mater.* 136 (2017) 262–270, <https://doi.org/10.1016/j.actamat.2017.07.023>.
- [42] D. Raabe, C.C. Tasan, H. Springer, M. Bausch, From high-entropy alloys to high-entropy steels, *Steel Res. Int.* 86 (10) (2015) 1127–1138, <https://doi.org/10.1002/srin.201500133>.
- [43] W. Li, D. Xie, D. Li, Y. Zhang, Y. Gao, P.K. Liaw, Mechanical behavior of high-entropy alloys, *Prog. Mater. Sci.* 118 (2021) 100777, <https://doi.org/10.1016/j.pmatsci.2021.100777>.
- [44] P. Zarras, J.D. Stenger-Smith, Smart inorganic and organic pretreatment coatings for the inhibition of corrosion on metals/alloys, *Intell. Coat. Corros. Control* 59–91 (2015), <https://doi.org/10.1016/b978-0-12-411467-8.00003-9>.
- [45] M.A. Jafar Mazumder, Global impact of corrosion: occurrence, cost and mitigation, *Glob. J. Eng. Sci.* 5 (4) (2020), <https://doi.org/10.33552/gjes.2020.05.000618>.
- [46] S.D. Cramer, B.S. Covino Jr., *ASM Handbook*, Volume 13A—Fundamentals, testing, and protection 2003, ASM International: Novelty, OH, USA, 2003, <https://doi.org/10.31399/asm.hb.v13a.9781627081825>.
- [47] X. Li, Y. Feng, B. Liu, D. Yi, X. Yang, W. Zhang, P. Bai, Influence of NbC particles on microstructure and mechanical properties of AlCoCrFeNi high-entropy alloy coatings prepared by laser cladding, *J. Alloys Compd.* 788 (2019) 485–494, <https://doi.org/10.1016/j.jallcom.2019.02.223>.
- [48] Y. Wang, J. Han, H. Wu, B. Yang, X. Wang, Effect of sigma phase precipitation on the mechanical and wear properties of Z3CN20.09M cast duplex stainless steel, *Nucl. Eng. Des.* 259 (2013) 1–7, <https://doi.org/10.1016/j.nucengdes.2013.02.037>.
- [49] B. Cantor, I. Chang, P. Knight, A. Vincent, Microstructural development in equiaxed multicomponent alloys, *Mater. Sci. Eng. A* 375–377 (2004) 213–218, <https://doi.org/10.1016/j.msea.2003.10.257>.
- [50] O. Senkov, G. Wilks, D. Miracle, C. Chuang, P. Liaw, Refractory high-entropy alloys, *Intermetallics* 18 (9) (2010) 1758–1765, <https://doi.org/10.1016/j.intermet.2010.05.014>.
- [51] J. Yeh, S. Chen, S. Lin, J. Gan, T. Chin, T. Shun, S. Chang, Nanostructured high-entropy alloys with multiple principal elements: novel alloy design concepts and outcomes, *Adv. Eng. Mater.* 6 (5) (2004) 299–303, <https://doi.org/10.1002/adem.200300567>.
- [52] M. Feuerbacher, M. Heidelmann, C. Thomas, Hexagonal high-entropy alloys, *Mater. Res. Lett.* 3 (1) (2014) 1–6, <https://doi.org/10.1080/21663831.2014.951493>.
- [53] M.C. Gao, Design of high-entropy alloys, *High-Entropy Alloys* 369–398 (2016), [https://doi.org/10.1007/978-3-319-27013-5\\_11](https://doi.org/10.1007/978-3-319-27013-5_11).
- [54] Y. Zhang, T.T. Zuo, Z. Tang, M.C. Gao, K.A. Dahmen, P.K. Liaw, Z.P. Lu, Microstructures and properties of high-entropy alloys, *Prog. Mater. Sci.* 61 (2014) 1–93, <https://doi.org/10.1016/j.pmatsci.2013.10.001>.
- [55] Y. Zhang, Y. Zhou, J. Lin, G. Chen, P. Liaw, Solid-solution phase formation rules for multi-component alloys, *Adv. Eng. Mater.* 10 (6) (2008) 534–538, <https://doi.org/10.1002/adem.200700240>.
- [56] M.C. Gao, B. Zhang, S.M. Guo, J.W. Qiao, J.A. Hawk, High-entropy alloys in hexagonal close-packed structure, *Metall. Mater. Trans. A* 47 (7) (2015) 3322–3332, <https://doi.org/10.1007/s11661-015-3091-1>.
- [57] K.M. Youssef, A.J. Zaddach, C. Niu, D.L. Irving, C.C. Koch, A novel low-density, high-hardness, high-entropy alloy with close-packed single-phase Nanocrystalline structures, *Mater. Res. Lett.* 3 (2) (2014) 95–99, <https://doi.org/10.1080/21663831.2014.985855>.
- [58] H. Diao, L.J. Santodonato, Z. Tang, T. Egami, P.K. Liaw, Local structures of high-entropy alloys (HEAs) on atomic scales: an overview, *JOM* 67 (10) (2015) 2321–2325, <https://doi.org/10.1007/s11837-015-1591-5>.
- [59] Y. Chen, T. Duval, U. Hung, J. Yeh, H. Shih, Microstructure and electrochemical properties of high entropy alloys—a comparison with type-304 stainless steel, *Corros. Sci.* 47 (9) (2005) 2257–2279, <https://doi.org/10.1016/j.corrsci.2004.11.008>.
- [60] Y. Chen, U. Hung, H. Shih, J. Yeh, T. Duval, Electrochemical kinetics of the high entropy alloys in aqueous environments—a comparison with type 304 stainless steel, *Corros. Sci.* 47 (11) (2005) 2679–2699, <https://doi.org/10.1016/j.corrsci.2004.09.026>.
- [61] Z. Tang, L. Huang, W. He, P. Liaw, Alloying and processing effects on the aqueous corrosion behavior of high-entropy alloys, *Entropy* 16 (2) (2014) 895–911, <https://doi.org/10.3390/e16020895>.
- [62] Y. Liu, C. Cheng, J. Shang, R. Wang, P. Li, J. Zhao, Oxidation behavior of high-entropy alloys Al<sub>x</sub>CoCrFeNi (x=0.15, 0.4) in supercritical water and comparison with HR3C steel, *Trans. Nonferrous Metals Soc. China* 25 (4) (2015) 1341–1351, [https://doi.org/10.1016/s1003-6326\(15\)63733-5](https://doi.org/10.1016/s1003-6326(15)63733-5).
- [63] X. Qiu, Y. Zhang, C. Liu, Effect of Ti content on structure and properties of Al<sub>2</sub>CrFeNiCoCuTix high-entropy alloy coatings, *J. Alloys Compd.* 585 (2014) 282–286, <https://doi.org/10.1016/j.jallcom.2013.09.083>.
- [64] Z. Li, K.G. Pradeep, Y. Deng, D. Raabe, C.C. Tasan, Metastable high-entropy dual-phase alloys overcome the strength–ductility trade-off, *Nature* 534 (7606) (2016) 227–230, <https://doi.org/10.1038/nature17981>.
- [65] O. Senkov, S. Senkova, C. Woodward, Effect of aluminum on the microstructure and properties of two refractory high-entropy alloys, *Acta Mater.* 68 (2014) 214–228, <https://doi.org/10.1016/j.actamat.2014.01.029>.
- [66] M. Hemphill, T. Yuan, G. Wang, P. Liaw, J. Yeh, C. Tsai, A. Chuang, Fatigue behavior of Al<sub>0.5</sub>CoCrFeNi high entropy alloys, *Acta Mater.* 60 (16) (2012) 5723–5734, <https://doi.org/10.1016/j.actamat.2012.06.046>.
- [67] M. Seifi, D. Li, Z. Yong, P.K. Liaw, J.J. Lewandowski, Fracture toughness and fatigue crack growth behavior of as-cast high-entropy alloys, *JOM* 67 (10) (2015) 2288–2295, <https://doi.org/10.1007/s11837-015-1563-9>.
- [68] Z. Zhang, M.M. Mao, J. Wang, B. Gludovatz, Z. Zhang, S.X. Mao, R.O. Ritchie, Nanoscale origins of the damage tolerance of the high-entropy alloy CrMnFeCoNi, *Nat. Commun.* 6 (1) (2015), <https://doi.org/10.1038/ncomms10143>.
- [69] Z. Tang, T. Yuan, C. Tsai, J. Yeh, C.D. Lundin, P.K. Liaw, Fatigue behavior of a wrought Al<sub>0.5</sub>CoCrCuFeNi two-phase high-entropy alloy, *Acta Mater.* 99 (2015) 247–258, <https://doi.org/10.1016/j.actamat.2015.07.004>.
- [70] B. Gludovatz, A. Hohenwarter, D. Catoor, E.H. Chang, E.P. George, R.O. Ritchie, A fracture-resistant high-entropy alloy for cryogenic applications, *Science* 345 (6201) (2014) 1153–1158, <https://doi.org/10.1126/science.1254581>.
- [71] L.J. Santodonato, Y. Zhang, M. Feygenson, C.M. Parish, M.C. Gao, R.J. Weber, P. K. Liaw, Deviation from high-entropy configurations in the atomic distributions of a multi-principal-element alloy, *Nat. Commun.* 6 (1) (2015), <https://doi.org/10.1038/ncomms6964>.
- [72] C. Lee, C. Chang, Y. Chen, J. Yeh, H. Shih, Effect of the aluminium content of Al<sub>x</sub>CrFe<sub>1-x</sub>MnNi<sub>0.5</sub> high-entropy alloys on the corrosion behaviour in aqueous environments, *Corros. Sci.* 50 (7) (2008) 2053–2060, <https://doi.org/10.1016/j.corrsci.2008.04.011>.
- [73] Y. Chou, J. Yeh, H. Shih, The effect of molybdenum on the corrosion behaviour of the high-entropy alloys Co<sub>1.5</sub>CrFeNi<sub>1.5</sub>Ti<sub>0.5</sub>Mox in aqueous environments, *Corros. Sci.* 52 (8) (2010) 2571–2581, <https://doi.org/10.1016/j.corrsci.2010.04.004>.
- [74] Y. Kao, T. Lee, S. Chen, Y. Chang, Electrochemical passive properties of Al<sub>x</sub>CoCrFeNi (x=0, 0.25, 0.50, 1.00) alloys in sulfuric acids, *Corros. Sci.* 52 (3) (2010) 1026–1034, <https://doi.org/10.1016/j.corrsci.2009.11.028>.
- [75] C.P. Lee, Y.Y. Chen, C.Y. Hsu, J.W. Yeh, H.C. Shih, The effect of boron on the corrosion resistance of the high entropy alloys Al<sub>[sub 0.5]CoCrCuFeNiB<sub>[sub 0.5]</sub></sub> in *J. Electrochem. Soc.* 154 (8) (2007) C424, <https://doi.org/10.1149/1.2744133>.

- [76] X. Ye, M. Ma, Y. Cao, W. Liu, X. Ye, Y. Gu, The property research on high-entropy alloy Al<sub>x</sub>FeCoNiCuCr coating by laser cladding, *Phys. Procedia* 12 (2011) 303–312, <https://doi.org/10.1016/j.phpro.2011.03.039>.
- [77] X. Qiu, C. Liu, Microstructure and properties of Al<sub>2</sub>CrFeCoCuTiNi<sub>x</sub> high-entropy alloys prepared by laser cladding, *J. Alloys Compd.* 553 (2013) 216–220, <https://doi.org/10.1016/j.jallcom.2012.11.100>.
- [78] Y. Shi, B. Yang, P. Liaw, Corrosion-resistant high-entropy alloys: a review, *Metals* 7 (2) (2017) 43, <https://doi.org/10.3390/met7020043>.
- [79] C. Kwok, F. Cheng, H. Man, Synergistic effect of cavitation erosion and corrosion of various engineering alloys in 3.5% NaCl solution, *Mater. Sci. Eng. A* 290 (1–2) (2000) 145–154, [https://doi.org/10.1016/s0921-5093\(00\)00899-6](https://doi.org/10.1016/s0921-5093(00)00899-6).
- [80] C. Zhang, F. Zhang, H. Diao, M.C. Gao, Z. Tang, J.D. Poplawsky, P.K. Liaw, Understanding phase stability of Al-Co-Cr-Fe-Ni high entropy alloys, *Mater. Des.* 109 (2016) 425–433.
- [81] H. Ezuber, A. El-Houd, F. El-Shawesh, A study on the corrosion behavior of aluminum alloys in seawater, *Mater. Des.* 29 (4) (2008) 801–805, <https://doi.org/10.1016/j.matdes.2007.01.021>.
- [82] P. Sarkar, P. Kumar, M.K. Manna, P. Chakraborti, Microstructural influence on the electrochemical corrosion behaviour of dual-phase steels in 3.5% NaCl solution, *Mater. Lett.* 59 (19–20) (2005) 2488–2491, <https://doi.org/10.1016/j.matlet.2005.03.030>.
- [83] C. Delgado-Alvarado, P. Sundaram, A study of the corrosion behavior of gamma titanium aluminide in 3.5wt% NaCl solution and seawater, *Corros. Sci.* 49 (9) (2007) 3732–3741, <https://doi.org/10.1016/j.corsci.2007.04.001>.
- [84] X. Peng, Y. Zhang, J. Zhao, F. Wang, Electrochemical corrosion performance in 3.5% NaCl of the electrodeposited nanocrystalline Ni films with and without dispersions of CR nanoparticles, *Electrochim. Acta* 51 (23) (2006) 4922–4927, <https://doi.org/10.1016/j.electacta.2006.01.035>.
- [85] Y.Q. Wang, N. Li, B. Yang, Effect of ferrite on pitting corrosion of Fe20Cr9Ni cast austenite stainless steel for nuclear power plant pipe, *Corros. Eng. Sci. Technol.* 50 (4) (2014) 330–337, <https://doi.org/10.1179/1743278214y.0000000229>.
- [86] E. McCafferty, Validation of corrosion rates measured by the Tafel extrapolation method, *Corros. Sci.* 47 (12) (2005) 3202–3215, <https://doi.org/10.1016/j.corsci.2005.05.046>.
- [87] S. Park, S. Lee, J. Kim, Effect of chromium on the corrosion behavior of low alloy steel in sulfuric acid, *Met. Mater. Int.* 18 (6) (2012) 975–987, <https://doi.org/10.1007/s12540-012-6009-0>.
- [88] G. Lu, G. Zangari, Corrosion resistance of ternary Ni-P based alloys in sulfuric acid solutions, *Electrochim. Acta* 47 (18) (2002) 2969–2979, [https://doi.org/10.1016/s0013-4686\(02\)00198-6](https://doi.org/10.1016/s0013-4686(02)00198-6).
- [89] G. Moretti, F. Guidi, Tryptophan as copper corrosion inhibitor in 0.5 M aerated sulfuric acid, *Corros. Sci.* 44 (9) (2002) 1995–2011, [https://doi.org/10.1016/s0010-938x\(02\)00020-3](https://doi.org/10.1016/s0010-938x(02)00020-3).
- [90] J. Hong, S. Lee, J. Kim, J. Yoon, Corrosion behaviour of copper containing low alloy steels in sulphuric acid, *Corros. Sci.* 54 (2012) 174–182, <https://doi.org/10.1016/j.corsci.2011.09.012>.
- [91] S. Baik, The study of corrosion behavior for solution and aging heat treated Ti alloy, *Journal of the Korean Society of Marine Environment and Safety* 22 (1) (2016) 138–144, <https://doi.org/10.7837/kosmeso.2016.22.1.138>.
- [92] Y. Zhang, J. Qiao, P.K. Liaw, A brief review of high entropy alloys and serration behavior and flow units, *J. Iron Steel Res. Int.* 23 (1) (2016) 2–6, [https://doi.org/10.1016/s1006-706x\(16\)30002-4](https://doi.org/10.1016/s1006-706x(16)30002-4).
- [93] J. Li, W. Jia, J. Wang, H. Kou, D. Zhang, E. Beaugnon, Enhanced mechanical properties of CoCrFeNi high entropy alloy by supercooling method, *Mater. Des.* 95 (2016) 183–187, <https://doi.org/10.1016/j.matdes.2016.01.112>.
- [94] C. Lin, H. Tsai, Evolution of microstructure, hardness, and corrosion properties of high-entropy Al<sub>0.5</sub>CoCrFeNi alloy, *Intermetallics* 19 (3) (2011) 288–294, <https://doi.org/10.1016/j.intermet.2010.10.008>.
- [95] Q. Chen, Y. Lu, Y. Dong, T. Wang, T. Li, Effect of minor B addition on microstructure and properties of AlCoCrFeNi multi-component alloy, *Trans. Nonferrous Metals Soc. China* 25 (9) (2015) 2958–2964, [https://doi.org/10.1016/s1003-6326\(15\)63922-x](https://doi.org/10.1016/s1003-6326(15)63922-x).
- [96] Z. Tang, O.N. Senkov, C.M. Parish, C. Zhang, F. Zhang, L.J. Santodonato, P. K. Liaw, Tensile ductility of an AlCoCrFeNi multi-phase high-entropy alloy through hot isostatic pressing (HIP) and homogenization, *Mater. Sci. Eng. A* 647 (2015) 229–240, <https://doi.org/10.1016/j.msea.2015.08.078>.
- [97] Y. Liu, N. Qu, X. Zhao, J. Chen, J. Zhu, Z. Lai, Stability of FeCrNiTiAl high-entropy alloy at high temperature, *Heat Treatm. Surf. Eng.* 3 (1) (2021) 29–36, <https://doi.org/10.1080/25787616.2021.2019390>.
- [98] A. Takeuchi, T. Wada, H. Kato, Solid solutions with bcc, hcp, and FCC structures formed in a composition line in multicomponent Ir–Rh–Ru–W–Mo system, *Mater. Trans.* 60 (11) (2019) 2267–2276, <https://doi.org/10.2320/matertrans.mtm2019212>.
- [99] A. Takeuchi, T. Wada, H. Kato, Solid solutions with bcc, hcp, and FCC structures formed in a composition line in multicomponent Ir–Rh–Ru–W–Mo system, *Mater. Trans.* 60 (11) (2019) 2267–2276, <https://doi.org/10.2320/matertrans.mtm2019212>.
- [100] O. Senkov, J. Scott, S. Senkova, D. Miracle, C. Woodward, Microstructure and room temperature properties of a high-entropy TaNbHfZrTi alloy, *J. Alloys Compd.* 509 (20) (2011) 6043–6048, <https://doi.org/10.1016/j.jallcom.2011.02.171>.
- [101] Y. Wu, Y. Cai, T. Wang, J. Si, J. Zhu, Y. Wang, X. Hui, A refractory Hf<sub>25</sub>Nb<sub>25</sub>Ti<sub>25</sub>Zr<sub>25</sub> high-entropy alloy with excellent structural stability and tensile properties, *Mater. Lett.* 130 (2014) 277–280, <https://doi.org/10.1016/j.matlet.2014.05.134>.
- [102] S. Veselkov, O. Samoilova, N. Shaburova, E. Trofimov, High-temperature oxidation of high-entropic alloys: a review, *Materials (Basel)* 14 (10) (2021) 1–25, <https://doi.org/10.3390/ma1410259>.
- [103] X. Xu, P. Liu, A. Hirata, S. Song, T. Nieh, M. Chen, Microstructural origins for a strong and ductile Al<sub>0.1</sub>CoCrFeNi high-entropy alloy with ultrafine grains, *Materialia* 4 (2018) 395–405, <https://doi.org/10.1016/j.mtla.2018.10.015>.
- [104] X. Xu, S. Chen, Y. Ren, A. Hirata, T. Fujita, P. Liaw, M. Chen, Temperature-dependent compression behavior of an Al<sub>0.5</sub>CoCrCuFeNi high-entropy alloy, *Materialia* 5 (2019) 100243, <https://doi.org/10.1016/j.mtla.2019.100243>.
- [105] S.Y. Lee, S. Byeon, H.S. Kim, H. Jin, S. Lee, Deep learning-based phase prediction of high-entropy alloys: optimization, generation, and explanation, *Mater. Des.* 197 (2021) 109260, <https://doi.org/10.1016/j.matdes.2020.109260>.
- [106] X. Fu, C. Schuh, E. Olivetti, Materials selection considerations for high entropy alloys, *Scr. Mater.* 138 (2017) 145–150, <https://doi.org/10.1016/j.scriptamat.2017.03.014>.
- [107] A. Sharma, M.C. Oh, B. Ahn, Microstructural evolution and mechanical properties of non-cancor AlCuSiZnFe lightweight high entropy alloy processed by advanced powder metallurgy, *Mater. Sci. Eng. A* 797 (2020) 140066, <https://doi.org/10.1016/j.msea.2020.140066>.
- [108] K.M. Youssef, A.J. Zaddach, C. Niu, D.L. Irving, C.C. Koch, A novel low-density, high-hardness, high-entropy alloy with close-packed single-phase nanocrystalline structures, *Mater. Res. Lett.* 3 (2) (2014) 95–99, <https://doi.org/10.1080/21663831.2014.985855>.
- [109] M.J. Chae, A. Sharma, M.C. Oh, B. Ahn, Lightweight AlCuFeMnMgTi high entropy alloy with high strength-to-density ratio processed by powder metallurgy, *Met. Mater. Int.* 27 (4) (2020) 629–638, <https://doi.org/10.1007/s12540-020-00823-5>.
- [110] K. Tseng, Y. Yang, C. Juan, T. Chin, C. Tsai, J. Yeh, A light-weight high-entropy alloy Al20Be20Fe10Si15Ti35, *SCIENCE CHINA Technol. Sci.* 61 (2) (2017) 184–188, <https://doi.org/10.1007/s11431-017-9073-0>.
- [111] P. Barron, A. Carruthers, J. Fellowes, N. Jones, H. Dawson, E. Pickering, Towards V-based high-entropy alloys for nuclear fusion applications, *Scr. Mater.* 176 (2020) 12–16, <https://doi.org/10.1016/j.scriptamat.2019.09.028>.
- [112] A. Pogrebnyak, V. Beresnev, K. Smyrnova, Y. Kravchenko, P. Zukowski, G. Bondarenko, The influence of nitrogen pressure on the fabrication of the two-phase superhard nanocomposite (Ti<sub>2</sub>ZrNbAlYCr)N coatings, *Mater. Lett.* 211 (2018) 316–318, <https://doi.org/10.1016/j.matlet.2017.09.121>.
- [113] A. Bagdasaryan, A. Pshyk, L. Coy, P. Konarski, M. Misnik, V. Ivashchenko, S. Jurga, A new type of (Ti<sub>2</sub>ZrNbTaHf)N/MON nanocomposite coating: microstructure and properties depending on energy of incident ions, *Compos. Part B Eng.* 146 (2018) 132–144, <https://doi.org/10.1016/j.compositesb.2018.04.015>.
- [114] S. Chang, S. Lin, Y. Huang, C. Wu, Mechanical properties, deformation behaviors and interface adhesion of (AlCr<sub>x</sub>Ti<sub>y</sub>Zr<sub>z</sub>)Nx multi-component coatings, *Surf. Coat. Technol.* 204 (20) (2010) 3307–3314, <https://doi.org/10.1016/j.surfcoat.2010.03.041>.
- [115] S. Lin, S. Chang, Y. Huang, F. Shieh, J. Yeh, Mechanical performance and nanoindenting deformation of (AlCr<sub>x</sub>Ti<sub>y</sub>Zr<sub>z</sub>)Ny multi-component coatings co-sputtered with bias, *Surf. Coat. Technol.* 206 (24) (2012) 5096–5102, <https://doi.org/10.1016/j.surfcoat.2012.06.035>.
- [116] H. Wan, D. Song, X. Shi, Y. Cai, T. Li, C. Chen, Corrosion behavior of Al<sub>0.4</sub>CoCu<sub>0.6</sub>Ni<sub>0.2</sub>Ti<sub>0.25</sub> high-entropy alloy coating via 3D printing laser cladding in a sulphur environment, *J. Mater. Sci. Technol.* 60 (2021) 197–205, <https://doi.org/10.1016/j.jmst.2020.07.001>.
- [117] Y. Guo, X. Li, Q. Liu, A novel biomedical high-entropy alloy and its laser-clad coating designed by a cluster-plus-glue-atom model, *Mater. Des.* 196 (2020) 109085, <https://doi.org/10.1016/j.matdes.2020.109085>.
- [118] Y. Guo, X. Shang, Q. Liu, Microstructure and properties of in-situ tin reinforced laser cladding CoCr<sub>2</sub>FeNi<sub>7</sub> high-entropy alloy composite coatings, *Surf. Coat. Technol.* 344 (2018) 353–358, <https://doi.org/10.1016/j.surfcoat.2018.03.035>.
- [119] J. Cheng, D. Liu, X. Liang, Y. Chen, Evolution of microstructure and mechanical properties of in situ synthesized tic-tb<sub>2</sub>/CoCr<sub>2</sub>FeNi high entropy alloy coatings, *Surf. Coat. Technol.* 281 (2015) 109–116, <https://doi.org/10.1016/j.surfcoat.2015.09.049>.
- [120] L. Tian, Z. Feng, W. Xiong, Microstructure, microhardness, and wear resistance of Al<sub>0.4</sub>CoCr<sub>0.6</sub>Ni<sub>0.2</sub>Ti<sub>0.25</sub> coating by plasma spraying, *Coatings* 8 (3) (2018) 112, <https://doi.org/10.3390/coatings8030112>.
- [121] D. Tsai, Z. Chang, L. Kuo, T. Lin, T. Lin, F. Shieh, Solid solution coating of (Ti<sub>2</sub>VCr<sub>2</sub>ZrHf)N with unusual structural evolution, *Surf. Coat. Technol.* 217 (2013) 84–87, <https://doi.org/10.1016/j.surfcoat.2012.11.077>.
- [122] A. Sharma, High entropy alloy coatings and technology, *Coatings* 11 (4) (2021) 372, <https://doi.org/10.3390/coatings11040372>.
- [123] Q. Sun, H. Di, J. Li, X. Wang, Effect of pulse frequency on microstructure and properties of welded joints for dual phase steel by pulsed laser welding, *Mater. Des.* 105 (2016) 201–211, <https://doi.org/10.1016/j.matdes.2016.05.071>.
- [124] Q. Sun, H. Di, J. Li, B. Wu, R. Misra, A comparative study of the microstructure and properties of 800 MPa microalloyed C-mn steel welded joints by laser and gas metal arc welding, *Mater. Sci. Eng. A* 669 (2016) 150–158, <https://doi.org/10.1016/j.msea.2016.05.079>.
- [125] S. Nam, C. Kim, Y. Kim, Recent studies of the laser cladding of high entropy alloys, *J. Weld. Join.* 35 (4) (2017) 58–66, <https://doi.org/10.5781/jwj.2017.35.4.9>.
- [126] L. Zhu, P. Xue, Q. Lan, G. Meng, Y. Ren, Z. Yang, Z. Liu, Recent research and development status of laser cladding: a review, *Opt. Laser Technol.* 138 (2021) 106915, <https://doi.org/10.1016/j.optlastec.2021.106915>.

- [127] B.B. Straumal, L. Klinger, A. Kuzmin, G.A. Lopez, A. Korneva, A.B. Straumal, A. S. Goranova, High entropy alloys coatings deposited by laser cladding: a review of grain boundary wetting phenomena, *Coatings* 12 (3) (2022) 343, <https://doi.org/10.3390/coatings12030343>.
- [128] Z. Cai, Y. Wang, X. Cui, G. Jin, Y. Li, Z. Liu, M. Dong, Design and microstructure characterization of FeCoNiAlCu high-entropy alloy coating by plasma cladding: in comparison with thermodynamic calculation, *Surf. Coat. Technol.* 330 (2017) 163–169, <https://doi.org/10.1016/j.surfocoat.2017.09.083>.
- [129] Q. Fang, Y. Chen, J. Li, Y. Liu, Y. Liu, Microstructure and mechanical properties of FeCoCrNb high-entropy alloy coatings, *Phys. B Condens. Matter* 550 (2018) 112–116, <https://doi.org/10.1016/j.physb.2018.08.044>.
- [130] J. Lu, B. Wang, X. Qiu, Z. Peng, M. Ma, Microstructure evolution and properties of CrCuFe X NiTi high-entropy alloy coating by plasma cladding on Q235, *Surf. Coat. Technol.* 328 (2017) 313–318, <https://doi.org/10.1016/j.surfoat.2017.08.019>.
- [131] J. Wang, B. Zhang, Y. Yu, Z. Zhang, S. Zhu, X. Lou, Z. Wang, Study of high temperature friction and wear performance of (CoCrFeMnNi)8ST15 high-entropy alloy coating prepared by plasma cladding, *Surf. Coat. Technol.* 384 (2020) 125337, <https://doi.org/10.1016/j.surfoat.2020.125337>.
- [132] B. Jin, N. Zhang, S. Guan, Y. Zhang, D. Li, Microstructure and properties of laser re-melting FeCoCrNiAl0.5Six high-entropy alloy coatings, *Surf. Coat. Technol.* 349 (2018) 867–873, <https://doi.org/10.1016/j.surfoat.2018.06.032>.
- [133] C. Han, L. Ma, X. Sui, B. Ma, G. Huang, Influence of low energy density laser remelting on the properties of cold sprayed FeCoCrMoBCY amorphous alloy coatings, *Coatings* 11 (6) (2021) 695, <https://doi.org/10.3390/coatings11060695>.
- [134] Z. Cai, X. Cui, Z. Liu, Y. Li, M. Dong, G. Jin, Microstructure and wear resistance of laser cladded Ni-CR-Co-Ti-V high-entropy alloy coating after laser remelting processing, *Opt. Laser Technol.* 99 (2018) 276–281, <https://doi.org/10.1016/j.optlastec.2017.09.012>.
- [135] K.M. Doleker, The examination of microstructure and thermal oxidation behavior of laser-remelted high-velocity oxygen liquid fuel FE/Al coating, *J. Mater. Eng. Perform.* 29 (5) (2020) 3220–3232, <https://doi.org/10.1007/s11665-020-04873-z>.
- [136] S. Zhang, C. Wu, C. Zhang, M. Guan, J. Tan, Laser surface alloying of FeCoCrAlNi high-entropy alloy on 304 stainless steel to enhance corrosion and cavitation erosion resistance, *Opt. Laser Technol.* 84 (2016) 23–31, <https://doi.org/10.1016/j.optlastec.2016.04.011>.
- [137] C. Ni, Y. Shi, J. Liu, G. Huang, Characterization of Al0.5FeCu0.7NiCoCr high-entropy alloy coating on aluminum alloy by laser cladding, *Opt. Laser Technol.* 105 (2018) 257–263, <https://doi.org/10.1016/j.optlastec.2018.01.058>.
- [138] H. Zhang, W. Wu, Y. He, M. Li, S. Guo, Formation of core-shell structure in high entropy alloy coating by laser cladding, *Appl. Surf. Sci.* 363 (2016) 543–547, <https://doi.org/10.1016/j.apsusc.2015.12.059>.
- [139] X. Ye, M. Ma, Y. Cao, W. Liu, X. Ye, Y. Gu, The property research on high-entropy alloy AlFeCoNiCr coating by laser cladding, *Phys. Procedia* 12 (2011) 303–312, <https://doi.org/10.1016/j.phpro.2011.03.039>.
- [140] H. Zhang, Y. Pan, Y. He, H. Jiao, Microstructure and properties of 6FeNiCoSiCrAlTi high-entropy alloy coating prepared by laser cladding, *Appl. Surf. Sci.* 257 (6) (2011) 2259–2263, <https://doi.org/10.1016/j.apsusc.2010.09.084>.
- [141] H. Zhang, Y. Pan, Y. He, Synthesis and characterization of FeCoNiCrCu high-entropy alloy coating by laser cladding, *Mater. Des.* 32 (4) (2011) 1910–1915, <https://doi.org/10.1016/j.matdes.2010.12.001>.
- [142] G. Zhang, H. Liu, X. Tian, , et al.G. Zhang, H. Liu, X. Tian, P. Chen, H. Yang, J. Hao, Microstructure and properties of AlCoCrFeNiSi high-entropy alloy coating on AISI 304 stainless steel by laser cladding, *J. Mater. Eng. Perform.* 29 (1) (2020) 278–288, <https://doi.org/10.1007/s11665-020-04586-3>.
- [143] C. Cui, M. Wu, X. Miao, Z. Zhao, Y. Gong, Microstructure and corrosion behavior of CeO<sub>2</sub>/FeCoNiCrMo high-entropy alloy coating prepared by laser cladding, *J. Alloys Compd.* 890 (2022) 161826, <https://doi.org/10.1016/j.jallcom.2021.161826>.
- [144] F. Shu, B. Yang, S. Dong, H. Zhao, B. Xu, F. Xu, J. Feng, Effects of FE-to-C ratio on microstructure and mechanical properties of laser cladded FeCoCrBniSi high-entropy alloy coatings, *Appl. Surf. Sci.* 450 (2018) 538–544, <https://doi.org/10.1016/j.apsusc.2018.03.128>.
- [145] D. Xiang, Y. Liu, T. Yu, D. Wang, X. Leng, K. Wang, L. Liu, J. Pan, Y. Sun, Z. Chen, Review on wear resistance of laser cladding high-entropy alloy coatings, *J. Mater. Res. Technol.* (2023), <https://doi.org/10.1016/j.jmrt.2023.11.138>.
- [146] M. Arshad, M. Amer, Q. Hayat, V. Janik, X. Zhang, M. Moradi, M. Bai, High-entropy coatings (HEC) for high-temperature applications: materials, processing, and properties, *Coatings* 12 (5) (2022) 691, <https://doi.org/10.3390/coatings12050691>.
- [147] A.-C. Mocanu, Florin Miculescu, G. Stan, T. Tite, M. Miculescu, Mircea Horia Tiorean, A. Pascau, R. Ciocoiu, Tudor Mihai Butte, Lucian Toma Ciocan, Development of ceramic coatings on titanium alloy substrate by laser cladding with pre-placed natural derived-slurry: influence of hydroxyapatite ratio and beam power, *Ceram. Int.* vol. 49 (7) (2023) 10445–10454, <https://doi.org/10.1016/j.ceramint.2022.11.227>.
- [148] Z. Cai, Y. Wang, X. Cui, G. Jin, Y. Li, Z. Liu, M. Dong, Design and microstructure characterization of FeCoNiAlCu high-entropy alloy coating by plasma cladding, in: Comparison with Thermodynamic Calculation, *Surface & Coatings Technology*, vol. 330, 2017, pp. 163–169, <https://doi.org/10.1016/j.surfoat.2017.09.083>.
- [149] A. Rashidy Ahmady, A. Ekhlasi, A. Nouri, M. Haghbin Nazarpak, P. Gong, A. Solouk, High entropy alloy coatings for biomedical applications: a review, *Smart Mater. Manuf.* 1 (2023) 100009, <https://doi.org/10.1016/j.smmp.2022.100009>.
- [150] C. Lin, Y. Yao, Corrosion-resistant coating based on high-entropy alloys, *Metals* 13 (2) (2023) 205–228, <https://doi.org/10.3390/met13020205>.
- [151] I. Bunaviz, O.M. Akselsen, X. Ren, B. Nyhus, M. Eriksson, Laser beam and laser-arc hybrid welding of aluminium alloys, *Metals* 11 (8) (2021) 1150, <https://doi.org/10.3390/met11081150>.
- [152] A. Erdogan, K.M. Döleker, S. Zeytin, Effect of laser re-melting on electric current assistive sintered CoCrFeNiAlxTiy high entropy alloys: formation, micro-hardness and wear behaviors, *Surf. Coat. Technol.* 399 (2020) 126179, <https://doi.org/10.1016/j.surfoat.2020.126179>.
- [153] K. Yang, J. Li, Q. Wang, Z. Li, Y. Jiang, Y. Bao, Effect of laser remelting on microstructure and wear resistance of plasma sprayed Al2O3-40%TiO2 coating, *Wear* 426–427 (2019) 314–318, <https://doi.org/10.1016/j.wear.2019.01.100>.
- [154] Z.U. Arif, M.Y. Khalid, A. Al Rashid, E. Ur Rehman, M. Atif, Laser deposition of high-entropy alloys: a comprehensive review, *Opt. Laser Technol.* 145 (2022) 107447, <https://doi.org/10.1016/j.optlastec.2021.107447>.
- [155] M. Daroonparvar, M.U.F. Khan, Y. Saadeh, C.M. Kay, A.K. Kasar, P. Kumar, L. Esteves, M. Misra, P. Menezes, P.R. Kalvala, H.R. Bakhshehi-Rad, R.K. Gupta, Modification of surface hardness, wear resistance and corrosion resistance of cold spray al coated AZ31B Mg alloy using cold spray double layered Ta/Ti coating in 3.5 wt % NaCl solution, *Corros. Sci.* 176 (2020) 109029, <https://doi.org/10.1016/j.corsci.2020.109029>.
- [156] A. Ahmad Siddiqui, A. Kumar Dubey, Laser surface treatment, in: *Engineering Steels and High Entropy-alloys*, 2020, <https://doi.org/10.5772/intechopen.91800>.
- [157] A. Pogrebniak, I. Yakushchenko, A. Bagdasaryan, O. Bondar, R. Krause-Rehberg, G. Abadias, O. Sobol, Microstructure, physical and chemical properties of nanostructured (Ti-Hf-Zr-V-Nb)N coatings under different deposition conditions, *Mater. Chem. Phys.* 147 (3) (2014) 1079–1091, <https://doi.org/10.1016/j.matchemphys.2014.06.062>.
- [158] A. Meghwal, A. Anupam, B.S. Murty, C.C. Berndt, R.S. Kottada, A.S. Ang, Thermal spray high-entropy alloy coatings: a review, *J. Therm. Spray Technol.* 29 (5) (2020) 857–893, <https://doi.org/10.1007/s11666-020-01047-0>.
- [159] R.L. Boxman, V.N. Zhitomirsky, Vacuum arc deposition devices, *Rev. Sci. Instrum.* 77 (2) (2006) 021101, <https://doi.org/10.1063/1.2169539>.
- [160] S.K. Padamata, A. Yasinskiy, V. Yanov, G. Saevardsdottir, Magnetron sputtering high-entropy alloy coatings: a mini-review, *Metals* 12 (2) (2022) 319, <https://doi.org/10.3390/met12020319>.
- [161] S. Calderon Velasco, A. Cavaleiro, S. Carvalho, Functional properties of ceramic-ag nanocomposite coatings produced by magnetron sputtering, *Prog. Mater. Sci.* 84 (2016) 158–191, <https://doi.org/10.1016/j.pmatsci.2016.09.005>.
- [162] D.A. Golosov, Balanced magnetic field in magnetron sputtering systems, *Vacuum* 139 (2017) 109–116, <https://doi.org/10.1016/j.vacuum.2017.02.018>.
- [163] Y. Zhang, Q. Xing, High entropy alloys: manufacturing routes, *Encyclopedia of Materials: Metals and Alloys* 327–338 (2022), <https://doi.org/10.1016/b978-0-12-803581-8.12123-x>.
- [164] M.A. Baker, P.J. Kench, C. Tsotsos, P.N. Gibson, A. Leyland, A. Matthews, Investigation of the nanostructure and wear properties of physical vapor deposited CrCuN nanocomposite coatings, *J. Vac. Sci. Technol. A* 23 (3) (2005) 423–433, <https://doi.org/10.1116/1.1875212>.
- [165] W. Shen, M. Tsai, J. Yeh, Machining performance of sputter-deposited (Al<sub>0.34</sub>Cr<sub>0.22</sub>Nb<sub>0.11</sub>Si<sub>0.11</sub>Ti<sub>0.22</sub>)<sub>50</sub>N<sub>50</sub> high-entropy nitride coatings, *Coatings* 5 (3) (2015) 312–325, <https://doi.org/10.3390/coatings5030312>.
- [166] N.A. Khan, RF Magnetron Sputtered AlCoCrCu0.5FeNi High Entropy Alloy (HEA) and High Entropy Ceramic (HEC) Thin Films (Doctoral dissertation), 2021. Retrieved from file:///C:/Users/CVcomputers.infotech/Downloads/Aziz%20Khan\_N\_Thesis.pdf.
- [167] X. Li, Z. Zheng, D. Dou, J. Li, Microstructure and properties of coating of FeAlCuCrCoMn high entropy alloy deposited by direct current magnetron sputtering, *Mater. Res. 19* (4) (2016) 802–806, <https://doi.org/10.1590/1980-5373-mr-2015-0536>.
- [168] K. Bobzin, T. Brögelmann, C. Kalscheuer, T. Liang, High-rate deposition of thick (Cr,Al)ON coatings by high speed physical vapor deposition, *Surf. Coat. Technol.* 322 (2017) 152–162, <https://doi.org/10.1016/j.surfoat.2017.05.034>.
- [169] C.H. Chang, P.W. Li, Q.Q. Wu, M.H. Wang, C.C. Sung, C. Hsu, Nanostructured and mechanical properties of high-entropy alloy nitride films prepared by magnetron sputtering at different substrate temperatures, *Mater. Technol.* 34 (6) (2018) 343–349, <https://doi.org/10.1080/10667857.2018.1557411>.
- [170] C. Sha, Z. Zhou, Z. Xie, P. Munroe, Femnnicocr-based high entropy alloy coatings: effect of nitrogen additions on microstructural development, mechanical properties and tribological performance, *Appl. Surf. Sci.* 507 (2020) 145101, <https://doi.org/10.1016/j.apsusc.2019.145101>.
- [171] Y.F. Ivanov, Kh. Akhmadeev Yurii, N.A. Prokopenko, O.B. Крысина, N.N. Koval, E.A. Петрикова, О.С. Толкачев, В.В. Шугуров, В.В. Углов, А.Н. Shmakov, Structure and properties of NbMoCrTiAl high-entropy alloy coatings formed by plasma-assisted vacuum arc deposition, *Coatings* 13 (7) (2023) 1191–1204, <https://doi.org/10.3390/coatings13071191>.
- [172] J.P. Riviere, Formation of hard coatings for tribological and corrosion protection by dynamic ion mixing, *Surf. Coat. Technol.* 108–109 (1998) 276–283, [https://doi.org/10.1016/s0257-8972\(98\)00563-5](https://doi.org/10.1016/s0257-8972(98)00563-5).
- [173] B. Schultrich, Structure and characterization of vacuum arc deposited carbon films—a critical overview, *Coatings* 12 (2) (2022) 109, <https://doi.org/10.3390/coatings12020109>.
- [174] M. Makówka, A. Sobczyk-Guzenda, W. Pawlak, B. Wendler, M. Gazicki-Lipman, H. Szymanowski, Correlation between plasma parameters and structure of thin

- TiO<sub>2</sub> films deposited by conventional and pulsed magnetron sputtering methods, *Appl. Surf. Sci.* 578 (2022) 151808–151820, <https://doi.org/10.1016/j.apsusc.2021.151808>.
- [175] S.K. Padamata, A. Yasinsky, V. Yanov, G. Saevarsottir, Magnetron sputtering high-entropy alloy coatings: a mini-review, *Metals* 12 (2) (2022) 319, <https://doi.org/10.3390/met12020319>.
- [176] F. Otto, A. Dlouhý, C. Sonnen, H. Bei, G. Eggeler, E.P. George, The influences of temperature and microstructure on the tensile properties of a CoCrFeMnNi high-entropy alloy, *Acta Mater.* 61 (2013) 5743–5755.
- [177] S. Calderon Velasco, A. Cavaleiro, S. Carvalho, Functional properties of ceramic-ag nanocomposite coatings produced by magnetron sputtering, *Prog. Mater. Sci.* 84 (2016) 158–191.
- [178] A. Sharma, S. Das, K. Das, Pulse electrodeposition of lead-free tin-based composite for microelectronic packaging, *Electrodeposition of Composite Materials*. 253–274 (2016), <https://doi.org/10.5772/62036>.
- [179] A. Sharma, S. Das, K. Das, Pulse electroplating of ultrafine grained tin coating, *Electroplating of Nanostructures*. (2015), <https://doi.org/10.5772/61255>.
- [180] A. Sharma, S. Bhattacharya, S. Das, K. Das, Fabrication of Sn nanostructures by template assisted pulse electrodeposition, *Surf. Eng.* 32 (5) (2016) 378–384, <https://doi.org/10.1179/1743294415y.0000000091>.
- [181] H. Soomin, A review of nanostructured thin films for gas sensing and corrosion protection, *Mediterranean Journal of Chemistry* 7 (6) (2018) 433–451, <https://doi.org/10.13171/mjc7618111916hs>.
- [182] A. Aliyu, C. Srivastava, Microstructure-corrosion property correlation in electrodeposited AlCrFeCoNi high entropy alloys-graphene oxide composite coatings, *Thin Solid Films* 686 (2019) 137434, <https://doi.org/10.1016/j.tsf.2019.137434>.
- [183] A. Aliyu, M.Y. Rekha, C. Srivastava, Microstructure-electrochemical property correlation in electrodeposited CuFeNiCoCr high-entropy alloy-graphene oxide composite coatings, *Philos. Mag.* 99 (6) (2018) 718–735, <https://doi.org/10.1080/14786435.2018.1554915>.
- [184] V. Soare, M. Burada, I. Constantin, D. Mitrićă, V. Bădiliță, A. Caragea, M. Tărcolea, Electrochemical deposition and microstructural characterization of AlCrFeMnNi and AlCrCuFeMnNi high entropy alloy thin films, *Appl. Surf. Sci.* 358 (2015) 533–539, <https://doi.org/10.1016/j.apsusc.2015.07.142>.
- [185] F. Yoosefan, A. Ashrafi, S. Monir Vaghefi, The feasibility of producing CoCrFeMnNi high entropy alloy coatings by electrochemical deposition method and its characterization, *J. Metall. Mater. Eng.* 31 (2) (2020) 109–120, <https://doi.org/10.22067/ma.v31i1.72033>.
- [186] C. Yao, P. Zhang, M. Liu, G. Li, J. Ye, P. Liu, Y. Tong, Electrochemical preparation and magnetic study of Bi–FE–Co–Ni–Mn high entropy alloy, *Electrochim. Acta* 53 (28) (2008) 8359–8365, <https://doi.org/10.1016/j.electacta.2008.06.036>.
- [187] N. Malatji, A.P.I. Popoola, Electrodeposition of ternary Zn-Cr<sub>2</sub>O<sub>3</sub>-SiO<sub>2</sub> nanocomposite coating on mild steel for extended applications, *Int. J. Electrochem. Sci.* 10 (2015) 3988–4003.
- [188] N. Malatji, A. Popoola, O. Fayomi, The effect of nanoparticulate loading on the fabrication and characterization of multi-doped Zn-Al<sub>2</sub>O<sub>3</sub>-Cr<sub>2</sub>O<sub>3</sub> hybrid coatings on mild steel, *Int. J. Adv. Manuf. Technol.* 90 (9–12) (2016) 2443–2452, <https://doi.org/10.1007/s00170-016-9525-0>.
- [189] J.Y. He, H. Wang, H.L. Huang, X.D. Xu, M.W. Chen, Y. Wu, X.J. Liu, T.G. Nieh, K. An, Z.P. Lu, A precipitation-hardenable high-entropy alloy with outstanding tensile properties, *Acta Mater.* 102 (2016) 187–196, <https://doi.org/10.1016/j.actamat.2015.08.076>.
- [190] C. Lin, Y. Yao, Corrosion-resistant coating based on high-entropy alloys, *Metals* 13 (2) (2023) 205–228, <https://doi.org/10.3390/met13020205>.
- [191] M. Alioofkhazraei, F.C. Walsh, G. Zangari, H. Köçkar, M. Alper, C. Rizal, L. Magagnin, V. Protsenko, R. Arunachalam, A. Rezvaniyan, A. Moein, S. Assareh, M.H. Allahyarzadeh, Development of electrodeposited multilayer coatings: a review of fabrication, microstructure, properties and applications, *Appl. Surf. Sci. Adv.* 6 (2021) 100141, <https://doi.org/10.1016/j.apsadv.2021.100141>.
- [192] M. Xiao, Y. Wang, Z. Zhang, Y. Li, Micro-arc oxidation in titanium and its alloys: development and potential of implants, *Coatings* 13 (12) (2023) 2064–2100, <https://doi.org/10.3390/coatings13122064>.
- [193] V. Harish, M.M. Ansari, D. Tewari, M. Gaur, A.B. Yadav, M.-L. García-Betancourt, F.M. Abdel-Haleem, M. Bechelany, A. Barhoum, Nanoparticle and nanostructure synthesis and controlled growth methods, *Nanomaterials* 12 (18) (2022) 3226, <https://doi.org/10.3390/nanow12183226>.
- [194] N. Ma, S. Liu, W. Liu, L. Xie, D. Wei, L. Wang, L. Li, B. Zhao, Y. Wang, Research progress of titanium-based high entropy alloy: methods, properties, and applications, *Front. Bioeng. Biotechnol.* (2020) 8, <https://doi.org/10.3389/fbioe.2020.603522>.
- [195] J. Zhang, M. Liu, J. Song, C. Deng, C. Deng, Microstructure and corrosion behavior of Fe-based amorphous coating prepared by HVOF, *J. Alloys Compd.* 721 (2017) 506–511, <https://doi.org/10.1016/j.jallcom.2017.06.046>.
- [196] Q. Li, P. Song, X. Yu, X. He, A. Khan, K. Cheng, J. Lu, Heat-induced interface-coupling behaviour of thermally sprayed Cu/ceramic coatings, *Ceram. Int.* 44 (10) (2018) 11918–11922, <https://doi.org/10.1016/j.ceramint.2018.03.212>.
- [197] D. Tejero-Martin, M. Rezvani Rad, A. McDonald, T. Hussain, Beyond traditional coatings: a review on thermal-sprayed functional and smart coatings, *J. Therm. Spray Technol.* 28 (4) (2019) 598–644, <https://doi.org/10.1007/s11666-019-00857-1>.
- [198] M. Löbel, T. Lindner, T. Mehner, L. Rymer, S. Björklund, S. Joshi, T. Lampke, Microstructure and corrosion properties of AlCrFeCoNi high-entropy alloy coatings prepared by HVAF and HVOF, *J. Therm. Spray Technol.* 31 (1–2) (2021) 247–255, <https://doi.org/10.1007/s11666-021-01255-2>.
- [199] A.S. Ang, C.C. Berndt, M.L. Sesso, A. Anupam, S. P., Kottada, R. S., & Murty, B. S., Plasma-sprayed high entropy alloys: microstructure and properties of AlCoCrFeNi and MnCoCrFeNi, *Metall. Mater. Trans. A* 46 (2) (2014) 791–800, <https://doi.org/10.1007/s11661-014-2644-z>.
- [200] W. Hsu, H. Murakami, J. Yeh, A. Yeh, K. Shimoda, On the study of thermal-sprayed Ni 0.2 Co 0.6 FE 0.2 CrSi 0.2 AlTi 0.2 HEA overlay coating, *Surf. Coat. Technol.* 316 (2017) 71–74, <https://doi.org/10.1016/j.surfcoat.2017.02.073>.
- [201] L. Tian, M. Fu, W. Xiong, Microstructural evolution of AlCoCrFeNiSi high-entropy alloy powder during mechanical alloying and its coating performance, *Materials* 11 (2) (2018) 320, <https://doi.org/10.3390/ma11020320>.
- [202] S. Yin, W. Li, B. Song, X. Yan, M. Kuang, Y. Xu, R. Lupoi, Deposition of FeCoNiCrMn high entropy alloy (HEA) coating via cold spraying, *J. Mater. Sci. Technol.* 35 (6) (2019) 1003–1007, <https://doi.org/10.1016/j.jmst.2018.12.015>.
- [203] D. Lin, N. Zhang, B. He, B. Jin, Y. Zhang, D. Li, F. Dong, Influence of laser remelting and vacuum heat treatment on plasma-sprayed FeCoCrNiAl alloy coatings, *J. Iron Steel Res. Int.* 24 (12) (2017) 1199–1205, [https://doi.org/10.1016/s1006-706x\(18\)30018-9](https://doi.org/10.1016/s1006-706x(18)30018-9).
- [204] M. Löbel, T. Lindner, T. Mehner, T. Lampke, Microstructure and wear resistance of AlCoCrFeNiTi high-entropy alloy coatings produced by HVOF, *Coatings* 7 (9) (2017) 144, <https://doi.org/10.3390/coatings7090144>.
- [205] W. Wang, W. Qi, L. Xie, X. Yang, J. Li, Y. Zhang, Microstructure and corrosion behavior of (CoCrFeNi)95Nb5 high-entropy alloy coating fabricated by plasma spraying, *Materials* 12 (5) (2019) 694, <https://doi.org/10.3390/ma12050694>.
- [206] J. Xiao, Y. Wu, J. Chen, C. Zhang, Microstructure and tribological properties of plasma sprayed FeCoNiCrSiAlx high entropy alloy coatings, *Wear* 448–449 (2020) 203209, <https://doi.org/10.1016/j.wear.2020.203209>.
- [207] T. Li, Y. Liu, B. Liu, W. Guo, L. Xu, Microstructure and wear behavior of FeCoCrNiMo0.2 high entropy coatings prepared by air plasma spray and the high velocity oxy-fuel spray processes, *Coatings* 7 (9) (2017) 151, <https://doi.org/10.3390/coatings7090151>.
- [208] H. Li, J. Li, C. Yan, X. Zhang, D. Xiong, Microstructure and tribological properties of plasma-sprayed Al0.2Co1.5CrFeNi1.5Ti-Ag composite coating from 25 to 750 °C, *J. Mater. Eng. Perform.* 29 (3) (2020) 1640–1649, <https://doi.org/10.1007/s11665-020-04700-5>.
- [209] T. Yue, H. Xie, X. Lin, H. Yang, G. Meng, Microstructure of laser re-melted AlCoCrCuFeNi high entropy alloy coatings produced by plasma spraying, *Entropy* 15 (12) (2013) 2833–2845, <https://doi.org/10.3390/e15072833>.
- [210] L. Tian, Z. Feng, W. Xiong, Microstructure, microhardness, and wear resistance of AlCoCrFeNiTi/Ni60 coating by plasma spraying, *Coatings* 8 (3) (2018) 112, <https://doi.org/10.3390/coatings8030112>.
- [211] C. Li, X.T. Luo, X.Y. Dong, et al., Recent research advances in plasma spraying of bulk-like dense metal coatings with metallurgically bonded lamellae, *J. Therm. Spray Tech.* 31 (2022) 5–27, <https://doi.org/10.1007/s11666-022-01327-x>.
- [212] Y. Zhao, J. Wen, F. Peyraud, M.-P. Planche, S. Misra, B. Lenoir, J. Ilavsky, H. Liao, G. Montavon, Porous architecture and thermal properties of thermal barrier coatings deposited by suspension plasma spray, *Surf. Coat. Technol.* 386 (2020) 125462, <https://doi.org/10.1016/j.surfcoat.2020.125462>.
- [213] Y. Korobov, S. Nevezhin, and M. Filippov, "Study of high velocity arc sprayed heat resistant coatings from FeCrAlBY cored wire. Thermal spray. Fostering a sustainable world for a better life," in the Int. Thermal Spray Conf. and Exposition ITSC 2016 (10–13 May, 2016, Shanghai, China), 2016, 852–856.
- [214] Muhamad Hafiz Abd Malek, et al., Critical process and performance parameters of thermal arc spray coating, *Int. J. Mater. Eng. Innov.* 5 (1) (2014) 12–27.
- [215] Bernhard Wielage, et al., Development and trends in HVOF spraying technology, *Surf. Coat. Technol.* 201 (5) (2006) 2032–2037.
- [216] C.-J. Li, Relationships between Feedstock Structure, Particle Parameter, Coating Deposition, Microstructure and Properties for Thermally Sprayed Conventional and Nanostructured WC-Co, 39, 2013, pp. 2–17, <https://doi.org/10.1016/j.ijrmhm.2012.03.014>.
- [217] P. Poza, M.Á. Garrido-Maneiro, Cold-sprayed coatings: microstructure, mechanical properties, and wear behaviour, *Prog. Mater. Sci.* 123 (2022) 100839, <https://doi.org/10.1016/j.pmatsci.2021.100839>.
- [218] S. Singh, R.K.S. Ramam, C.C. Berndt, H. Singh, Influence of cold spray parameters on bonding mechanisms: a review, *Metals* 11 (12) (2021) 2016, <https://doi.org/10.3390/met11122016>.
- [219] R. Bhaskaran Nair, R. Supekar, S. Morteza Javid, W. Wang, Y. Zou, A. McDonald, J. Mostaghimi, P. Stoyan, High-entropy alloy coatings deposited by thermal spraying: a review of strengthening mechanisms, performance assessments and perspectives on future applications, *Metals* 13 (3) (2023) 579, <https://doi.org/10.3390/met13030579>.
- [220] A. Rashidy Ahmady, A. Ekhlasí, A. Nouri, M. Haghbin Nazarpak, P. Gong, A. Solouk, High entropy alloy coatings for biomedical applications: a review, *Smart Mater. Manuf.* 1 (2023) 100009, <https://doi.org/10.1016/j.smmf.2022.100009>.
- [221] Y. Tian, Y. Shen, C. Lu, X. Feng, Microstructures and oxidation behavior of al-crmnfecomow composite coatings on ti-6al-4v alloy substrate via high-energy mechanical alloying method, *J. Alloys Compd.* 779 (2019) 456–465, <https://doi.org/10.1016/j.jallcom.2018.11.266>.
- [222] J. Kozlík, D. Preisler, J. Stráský, T. Košutová, C.A. Corrèa, J. Veselý, L. Bodnárová, F. Lukáč, T. Chráška, M. Janeček, Manufacturing of biomedical Ti alloys with controlled oxygen content by blended elemental powder metallurgy, *J. Alloys Compd.* 905 (2022) 164259, <https://doi.org/10.1016/j.jallcom.2022.164259>.
- [223] Y. Lin, K. Kang, F. Chen, L. Zhang, E.J. Lavernia, 4.13 gradient metal matrix composites, Editor(s): Peter W.R. Beaumont, Carl H. Zweben, Comprehensive Composite Materials II, Elsevier 2018 (2018) 331–346, <https://doi.org/10.1016/B978-0-12-803581-8.09975-6>.

- [224] O.A. Waseem, H.J. Ryu, Powder metallurgy processing of a WxTaTiVCr high-entropy alloy and its derivative alloys for fusion material applications, *Sci. Rep.* 7 (1) (2017), <https://doi.org/10.1038/s41598-017-02168-3>.
- [225] W. Ge, B. Wu, S. Wang, S. Xu, C. Shang, Z. Zhang, Y. Wang, Characterization and properties of CuZrAlTiNi high entropy alloy coating obtained by mechanical alloying and vacuum hot pressing sintering, *Adv. Powder Technol.* 28 (10) (2017) 2556–2563, <https://doi.org/10.1016/j.apptech.2017.07.006>.
- [226] C. Shang, E. Axinte, W. Ge, Z. Zhang, Y. Wang, High-entropy alloy coatings with excellent mechanical, corrosion resistance and magnetic properties prepared by mechanical alloying and hot pressing sintering, *Surf. Interfaces* 9 (2017) 36–43, <https://doi.org/10.1016/j.surfin.2017.06.012>.
- [227] C. Shang, E. Axinte, J. Sun, X. Li, P. Li, J. Du, Y. Wang, CoCrFeNi(W<sub>1</sub>–xMox) high-entropy alloy coatings with excellent mechanical properties and corrosion resistance prepared by mechanical alloying and hot pressing sintering, *Mater. Des.* 117 (2017) 193–202, <https://doi.org/10.1016/j.matdes.2016.12.076>.
- [228] Y. Tian, Y. Shen, C. Lu, X. Feng, Microstructures and oxidation behavior of al-cr-mn-fecomow composite coatings on ti-6al-4v alloy substrate via high-energy mechanical alloying method, *J. Alloys Compd.* 779 (2019) 456–465, <https://doi.org/10.1016/j.jallcom.2018.11.266>.
- [229] Caiyun Shang, et al., High-entropy alloy coatings with excellent mechanical, corrosion resistance and magnetic properties prepared by mechanical alloying and hot pressing sintering, *Surf. Interfaces* 9 (2017) 36–43.
- [230] M. Vaidya, G.M. Muralikrishna, B.S. Murty, High-entropy alloys by mechanical alloying: A review, *J. Mater. Res.* 34 (5) (2019) 664–686, <https://doi.org/10.1557/jmr.2019.37>.
- [231] Cheenepalli Nagarjuna, et al., Strengthening the mechanical properties and wear resistance of CoCrFeMnNi high entropy alloy fabricated by powder metallurgy, *Adv. Powder Technol.* 33 (4) (2022) 103519.
- [232] Alireza Nouri, P.D. Hodgson, Cui'E. Wen, Effect of process control agent on the porous structure and mechanical properties of a biomedical Ti-Sn-Nb alloy produced by powder metallurgy, *Acta Biomater.* 6 (4) (2010) 1630–1639.
- [233] Junchen Li, et al., A review on high entropy alloys coatings: fabrication processes and property assessment, *Adv. Eng. Mater.* 21 (8) (2019) 1900343.
- [234] Ashok Meghwal, et al., Thermal spray high-entropy alloy coatings: a review, *J. Therm. Spray Technol.* 29 (2020) 857–893.
- [235] Jia-Jia Tian, et al., An effective approach for creating metallurgical self-bonding in plasma-spraying of NiCr-Mo coating by designing shell-core-structured powders, *Acta Mater.* 110 (2016) 19–30.
- [236] José Manuel Torralba, Paula Alvaredo, Andrea García-Junceda, High-entropy alloys fabricated via powder metallurgy. A critical review, *Powder Metall.* 62 (2) (2019) 84–114.
- [237] P. Zhang, Z. Li, H. Liu, Y. Zhang, H. Li, C. Shi, P. Liu, D. Yan, Recent progress on the microstructure and properties of high entropy alloy coatings prepared by laser processing technology: a review, *J. Manuf. Process.* 76 (2022) 397–411, <https://doi.org/10.1016/j.jmapro.2022.02.006>.
- [238] A. Erdogan, M.S. Gök, S. Zeytin, Analysis of the high-temperature dry sliding behavior of CoCrFeNiTi0.5Al<sub>x</sub> high-entropy alloys, *Friction* (2019), <https://doi.org/10.1007/s40544-019-0278-2>.
- [239] X. Liu, H. Cheng, Z. Li, H. Wang, F. Chang, W. Wang, Q. Tang, P. Dai, Microstructure and mechanical properties of FeCoCrNiMnTi0.1Co0.1 high-entropy alloy produced by mechanical alloying and vacuum hot pressing sintering, *Vacuum* 165 (2019) 297–304, <https://doi.org/10.1016/j.vacuum.2019.04.043>.
- [240] H. Cheng, W. Chen, X. Liu, Q. Tang, Y. Xie, P. Dai, Effect of Ti and c additions on the microstructure and mechanical properties of the FeCoCrNiMn high-entropy alloy, *Mater. Sci. Eng. A* 719 (2018) 192–198, <https://doi.org/10.1016/j.msea.2018.02.040>.
- [241] J.Y. He, W.H. Liu, H. Wang, Y. Wu, Z.P. Lu, Effects of al addition on structural evolution and tensile properties of the FeCoNiCrMn high-entropy alloy system, *Acta Mater.* 62 (2014) 105–113, <https://doi.org/10.1016/j.actamat.2013.09.037>.
- [242] S. Sun, Y. Durandet, M. Brandt, Parametric investigation of pulsed Nd: YAG laser cladding of Stellite 6 on stainless steel, *Surf. Coat. Technol.* 194 (2–3) (2005) 225–231, <https://doi.org/10.1016/j.surfcoat.2004.03.058>.
- [243] J. Menghani, A. Vyas, P. Patel, H. Natu, S. More, Wear, erosion and corrosion behavior of laser cladded high entropy alloy coatings – a review, *Mater. Today: Proc.* 38 (2021) 2824–2829, <https://doi.org/10.1016/j.matpr.2020.08.763>.
- [244] D. Tsai, Z.-C. Chang, L.-Y. Kuo, T.-Y. Lin, T.-Y. Lin, Fuh-Sheng Shieh, Solid solution coating of Ti(V,Cr,Zr)HfN with unusual structural evolution, *Surf. Coat. Technol.* 217 (2013) 84–87, <https://doi.org/10.1016/j.surfcoat.2012.11.077>.
- [245] S.-Y. Chang, C.-E. Li, S. Chiang, Y.-C. Huang, 4-nm thick multilayer structure of multi-component (AlCrRuTaTiZr)N as robust diffusion barrier for cu interconnects, *J. Alloys Compd.* 515 (2012) 4–7, <https://doi.org/10.1016/j.jallcom.2011.11.082>.
- [246] Y. Guo, X. Li, Q. Liu, A novel biomedical high-entropy alloy and its laser-clad coating designed by a cluster-plus-glue-atom model, *Mater. Des.* 196 (2020) 109085, <https://doi.org/10.1016/j.matdes.2020.109085>.
- [247] S. Nam, C. Kim, Y.-M. Kim, Recent studies of the laser cladding of high entropy alloys, *J. Weld. Join.* 35 (4) (2017) 58–66, <https://doi.org/10.5781/jwj.2017.35.4.9>.
- [248] N. Espallargas, Introduction to thermal spray coatings, *Future Development of Thermal Spray Coatings* 1–13 (2015), <https://doi.org/10.1016/b978-0-85709-769-9.00001-4>.
- [249] S. Nakonechnyi, A. Yurkova, Nanostructural AlNiCoFeCrTi high-entropy coatings performed by cold spraying. 2021 IEEE 11th International Conference Nanomaterials: Applications & Properties (NAP), 2021, <https://doi.org/10.1109/nap51885.2021.9568613>.
- [250] J. Lu, B. Wang, X. Qiu, Z. Peng, M. Ma, Microstructure evolution and properties of CrCuFeNiTi high-entropy alloy coating by plasma cladding on Q235, *Surf. Coat. Technol.* 328 (2017) 313–318, <https://doi.org/10.1016/j.surfcoat.2017.08.019>.
- [251] T. Chen, T. Shun, J. Yeh, M. Wong, Nanostructured nitride films of multi-element high-entropy alloys by reactive DC sputtering, *Surf. Coat. Technol.* 188–189 (2004) 193–200, <https://doi.org/10.1016/j.surfcoat.2004.08.023>.
- [252] D. Tsai, M. Deng, Z. Chang, B. Kuo, E. Chen, S. Chang, F. Shieh, Oxidation resistance and characterization of (alcrrotati)-six-N coating deposited via magnetron sputtering, *J. Alloys Compd.* 647 (2015) 179–188, <https://doi.org/10.1016/j.jallcom.2015.06.025>.
- [253] W. Zhang, R. Tang, Z. Yang, C. Liu, H. Chang, J. Yang, J. Liao, Y. Yang, N. Liu, Preparation, structure, and properties of high-entropy alloy multilayer coatings for nuclear fuel cladding: a case study of AlCrMoNbZr/(AlCrMoNbZr)N, *J. Nucl. Mater.* 512 (2018) 15–24, <https://doi.org/10.1016/j.jnucmat.2018.10.001>.
- [254] N. Tütün, D. Canadinc, A. Motallebzadeh, B. Bal, Microstructure and tribological properties of TiTaHfNbZr high entropy alloy coatings deposited on Ti 6Al 4V substrates, *Intermetallics* 105 (2019) 99–106, <https://doi.org/10.1016/j.intermet.2018.11.015>.
- [255] A. Sharma, High entropy alloy coatings and technology, *Coatings* 11 (4) (2021) 372, <https://doi.org/10.3390/coatings11040372>.
- [256] D.V. Hushchyk, A.I. Yurkova, V.V. Cherniavsky, I.I. Bilyk, S.O. Nakonechnyy, Nanostructured AlNiCoFeCrTi high-entropy coating performed by cold spray, *Appl. Nanosci.* 10 (12) (2020) 4879–4890, <https://doi.org/10.1007/s13204-020-01364-4>.
- [257] L. Tian, M. Fu, W. Xiong, Microstructural evolution of AlCoCrFeNiSi high-entropy alloy powder during mechanical alloying and its coating performance, *Materials* 11 (2) (2018) 320, <https://doi.org/10.3390/matl11020320>.
- [258] A. Sharma, S. Das, Pulse electroplating of ultrafine grained tin coating, *Electroplating of Nanostructures*. (2015), <https://doi.org/10.5772/61255>.
- [259] A. Sharma, S. Bhattacharya, S. Das, K. Das, Fabrication of Sn nanostructures by template assisted pulse electrodeposition, *Surf. Eng.* 32 (5) (2016) 378–384, <https://doi.org/10.1179/1743294415y.0000000091>.
- [260] A. Aliyu, C. Srivastava, Microstructure-corrosion property correlation in electrodeposited AlCrFeCoNiCu high-entropy alloys-graphene oxide composite coatings, *Thin Solid Films* 686 (2019) 137434, <https://doi.org/10.1016/j.tsf.2019.137434>.
- [261] S. Bhattacharya, A. Sharma, S. Das, K. Das, Synthesis and properties of pulse electrodeposited lead-free tin-based Sn/ZrSiO<sub>4</sub> nanocomposite coatings, *Mettal. Mater. Trans. A* 47 (3) (2016) 1292–1312, <https://doi.org/10.1007/s11661-015-3313-6>.
- [262] A. Sharma, S. Bhattacharya, S. Das, K. Das, A study on the effect of pulse electrodeposition parameters on the morphology of pure tin coatings, *Mettal. Mater. Trans. A* 45 (10) (2014) 4610–4622, <https://doi.org/10.1007/s11661-014-2389-8>.
- [263] F. Yoosfan, A. Ashrafi, Monir vaghefi, S. M., & Constantin, I., Synthesis of CoCrFeMnNi high entropy alloy thin films by pulse electrodeposition: part 1: effect of pulse electrodeposition parameters, *Met. Mater. Int.* 26 (8) (2019) 1262–1269, <https://doi.org/10.1007/s12540-019-00404-1>.
- [264] Xiaofeng Li, Yinghao Feng, Bin Liu, Denghao Yi, Xiaohui Yang, Weidong Zhang, Gang Chen, Yong Liu, Peikang Bai, Influence of NbC particles on microstructure and mechanical properties of AlCoCrFeNi high-entropy alloy coatings prepared by laser cladding, *J. Alloys Compd.* 788 (2019) 485–494, <https://doi.org/10.1016/j.jallcom.2019.02.223>.
- [265] X. Li, Y. Feng, B. Liu, D. Yi, X. Yang, W. Zhang, G. Chen, Y. Liu, P. Bai, Influence of NbC particles on microstructure and mechanical properties of AlCoCrFeNi high-entropy alloy coatings prepared by laser cladding, *J. Alloys Compd.* 788 (2019) 485–494, <https://doi.org/10.1016/j.jallcom.2019.02.223>.
- [266] Hui Zhang, Ye Pan, Yi-Zhu He, Synthesis and characterization of FeCoNiCrCu high-entropy alloy coating by laser cladding, *Mater. Des.* 32 (4) (2011) 1910–1915, <https://doi.org/10.1016/j.matdes.2010.12.001>.
- [267] Qihong Fang, Yang Chen, Jia Li, Yanbin Liu, Yong Liu, Microstructure and mechanical properties of FeCoCrNiNbX high-entropy alloy coatings, *Phys. B Condens. Matter* 550 (2018) 112–116. ISSN 0921-4526,, <https://doi.org/10.1016/j.physb.2018.08.044>.
- [268] Z. Cai, Y. Wang, X. Cui, G. Jin, Y. Li, Z. Liu, M. Dong, Design and microstructure characterization of FeCoNiAlCu high-entropy alloy coating by plasma cladding: in comparison with thermodynamic calculation, *Surf. Coat. Technol.* 330 (2017) 163–169, <https://doi.org/10.1016/j.surfcoat.2017.09.083>.
- [269] F. Shu, B. Yang, S. Dong, H. Zhao, B. Xu, F. Xu, B. Liu, P. He, J. Feng, Effects of Fe-to-carbon ratio on microstructure and mechanical properties of laser cladded FeCoCrB<sub>2</sub>NiSi high-entropy alloy coatings, *J. Appl. Surf. Sci.* 450 (2018) 538–544, <https://doi.org/10.1016/j.japsusc.2018.03.128>.
- [270] G.H. Meng, X. Lin, H. Xie, T.M. Yue, X. Ding, L. Sun, M. Qi, The effect of cu rejection in laser forming of AlCoCrCuFeNi/Mg composite coating, *Mater. Des.* 108 (2016) 157–167, <https://doi.org/10.1016/j.matdes.2016.06.094>.
- [271] Z. Cai, X. Cui, G. Jin, B. Lu, D. Zhang, Z. Zhang, In situ TEM tensile testing on high-entropy alloy coating by laser surface alloying, *J. Alloys Compd.* 708 (2017) 380–384, <https://doi.org/10.1016/j.jallcom.2017.03.049>.
- [272] C.L. Wu, S. Zhang, C.H. Zhang, H. Zhang, S.Y. Dong, Phase evolution and properties in laser surface alloying of FeCoCrAlCuNiX high-entropy alloy on copper substrate, *Surf. Coat. Technol.* 315 (2017) 368–376, <https://doi.org/10.1016/j.surfcoat.2017.02.068>.
- [273] M. Löbel, T. Lindner, T. Mehner, L. Thomas, Microstructure and wear resistance of AlCoCrFeNiTi high-entropy alloy coatings produced by HVOF, *Coatings* 7 (2017) 144, <https://doi.org/10.3390/coatings7090144>.

- [274] Tian, L.H., Xiong, W., Liu, C. et al. Microstructure and Wear behavior of atmospheric plasma-sprayed AlCoCrFeNiTi high-entropy alloy coating. *J. Mater. Eng. Perform.* 25, 5513–5521 (2016). doi:<https://doi.org/10.1007/s11665-016-2396-6>.
- [275] T.M. Yue, H. Xie, X. Lin, H. Yang, G. Meng, Microstructure of laser re-melted AlCoCrCuFeNi high entropy alloy coatings produced by plasma spraying, *Entropy* 15 (2013) 2833–2845, <https://doi.org/10.3390/e15072833>.
- [276] S. Yin, W. Li, B. Song, X. Yan, M. Kuang, Y. Xu, K. Wen, R. Lupoi, Deposition of FeCoNiCrMn high entropy alloy (HEA) coating via cold spraying, *J. Mater. Sci. Technol.* 35 (2019) 1003–1007, <https://doi.org/10.1016/j.jmst.2018.12.015>.
- [277] V. Braic, A. Vladescu, M. Balaceanu, C.R. Luculescu, M. Braic, Nanostructured multi-element (TiZrNbHfTa)N and (TiZrNbHfTa)C hard coatings, *Surf. Coat. Technol.* 211 (2012) 117–121, <https://doi.org/10.1016/j.surcoat.2011.09.033>.
- [278] N. Tütün, D. Canadinc, A. Motallebzadeh, B. Bal, Microstructure and tribological properties of TiTaHfNbZr high entropy alloy coatings deposited on Ti-6Al-4V substrates, *Intermetallics* 105 (2019) 99–106, <https://doi.org/10.1016/j.intermet.2018.11.015>.
- [279] A.D. Pogrebnyak, V.M. Beresnev, K.V. Smyrnova, Y.O. Kravchenko, P. V. Zukowski, G.G. Bondarenko, The influence of nitrogen pressure on the fabrication of the two-phase superhard nanocomposite (TiZrNbAlYCr)N coatings, *Mater. Lett.* 211 (2018) 316–318, <https://doi.org/10.1016/j.matlet.2017.09.121>.
- [280] C. Shang, E. Axinte, W. Ge, Z. Zhang, Y. Wang, High-entropy alloy coatings with excellent mechanical, corrosion resistance and magnetic properties prepared by mechanical alloying and hot pressing sintering, *Surf. Interface* 9 (2017) 36–43.
- [281] V. Soare, M. Burada, I. Constantin, D. Mitrica, V. Badilin, A. Caragea, M. Tărcolea, Electrochemical deposition and microstructural characterization of AlCrFeMnNi and AlCrCuFeMnNi high entropy alloy thin films, *Appl. Surf. Sci.* 358 (2015) 533–539.
- [282] D. Miracle, O. Senkov, A critical review of high entropy alloys and related concepts, *Acta Mater.* 122 (2017) 448–511, <https://doi.org/10.1016/j.actamat.2016.08.081>.
- [283] M. Tsai, J. Yeh, High-entropy alloys: a critical review, *Mater. Res. Lett.* 2 (3) (2014) 107–123, <https://doi.org/10.1080/21663831.2014.912690>.
- [284] Y. Wu, F. Zhang, X. Yuan, H. Huang, X. Wen, Y. Wang, Z. Lu, Short-range ordering and its effects on mechanical properties of high-entropy alloys, *J. Mater. Sci. Technol.* 62 (2021) 214–220, <https://doi.org/10.1016/j.jmst.2020.06.018>.
- [285] J.M. Park, J. Choe, J.G. Kim, J.W. Bae, J. Moon, S. Yang, H.S. Kim, Superior tensile properties of 1%Co-CrFeMnNi high-entropy alloy additively manufactured by selective laser melting, *Mater. Res. Lett.* 8 (1) (2019) 1–7, <https://doi.org/10.1080/21663831.2019.1638844>.
- [286] Z. Li, Interstitial equiatomic CoCrFeMnNi high-entropy alloys: carbon content, microstructure, and compositional homogeneity effects on deformation behavior, *Acta Mater.* 164 (2019) 400–412, <https://doi.org/10.1016/j.actamat.2018.10.050>.
- [287] H. Luo, Z. Li, A.M. Mingers, D. Raabe, Corrosion behavior of an equiatomic CoCrFeMnNi high-entropy alloy compared with 304 stainless steel in sulfuric acid solution, *Corros. Sci.* 134 (2018) 131–139, <https://doi.org/10.1016/j.corsci.2018.02.031>.
- [288] R. Li, P. Niu, T. Yuan, P. Cao, C. Chen, K. Zhou, Selective laser melting of an equiatomic CoCrFeMnNi high-entropy alloy: processability, non-equilibrium microstructure and mechanical property, *J. Alloys Compd.* 746 (2018) 125–134, <https://doi.org/10.1016/j.jallcom.2018.02.298>.
- [289] J. Xiao, H. Tan, Y. Wu, J. Chen, C. Zhang, Microstructure and wear behavior of FeCoNiCrMn high entropy alloy coating deposited by plasma spraying, *Surf. Coat. Technol.* 385 (2020) 125430, <https://doi.org/10.1016/j.surcoat.2020.125430>.
- [290] F. Ye, Z. Jiao, Y. Yuan, Precipitation behaviors and properties of micro-beam plasma arc cladded CoCrFeMnNi high-entropy alloy at elevated temperatures, *Mater. Chem. Phys.* 236 (2019) 121801, <https://doi.org/10.1016/j.matchemphys.2019.121801>.
- [291] S. Zhu, Z. Zhang, B. Zhang, Y. Yu, Z. Wang, X. Zhang, B. Lu, Microstructure and properties of  $\text{Al}_2\text{O}_3$ -3wt.% $\text{TiO}_2$ -reinforced CoCrFeMnNi high-entropy alloy composite coatings prepared by plasma spraying, *J. Therm. Spray Technol.* 30 (3) (2021) 772–786, <https://doi.org/10.1007/s11666-021-01170-6>.
- [292] Z. Zhang, B. Zhang, S. Zhu, Y. Yu, Z. Wang, X. Zhang, B. Lu, Microstructural characteristics and enhanced wear resistance of nanoscale  $\text{Al}_2\text{O}_3$ /3 wt% $\text{TiO}_2$ -reinforced CoCrFeMnNi high entropy coatings, *Surf. Coat. Technol.* 412 (2021) 127019, <https://doi.org/10.1016/j.surcoat.2021.127019>.
- [293] Y. Peng, W. Zhang, T. Li, M. Zhang, L. Wang, Y. Song, Y. Hu, Microstructures and mechanical properties of FeCoCrNi high entropy alloy/WC reinforcing particles composite coatings prepared by laser cladding and plasma cladding, *Int. J. Refract. Met. Hard Mater.* 84 (2019) 105044, <https://doi.org/10.1016/j.ijrmhm.2019.105044>.
- [294] Z. Zhang, D.H. Seng, M. Lin, S.L. Teo, T.L. Meng, C.J. Lee, J. Pan, Cold spray deposition of Inconel 718 in comparison with atmospheric plasma spray deposition, *Appl. Surf. Sci.* 535 (2021) 147704, <https://doi.org/10.1016/j.apsusc.2020.147704>.
- [295] Y. Zou, Z. Qiu, C. Huang, D. Zeng, R. Lupoi, N. Zhang, S. Yin, Microstructure and tribological properties of  $\text{Al}_2\text{O}_3$  reinforced FeCoNiCrMn high entropy alloy composite coatings by cold spray, *Surf. Coat. Technol.* 434 (2022) 128205, <https://doi.org/10.1016/j.surcoat.2022.128205>.
- [296] L. Tian, Z. Feng, W. Xiong, Microstructure, microhardness, and wear resistance of AlCoCrFeNiTi/Ni60 coating by plasma spraying, *Coatings* 8 (3) (2018) 112, <https://doi.org/10.3390/coatings8030112>.
- [297] H. Zhang, Y. Pan, Y. He, H. Jiao, Microstructure and properties of 6FeNiCoSiCrAlTi high-entropy alloy coating prepared by laser cladding, *Appl. Surf. Sci.* 257 (6) (2011) 2259–2263, <https://doi.org/10.1016/j.apusc.2010.09.084>.
- [298] L. Tian, W. Xiong, C. Liu, S. Lu, M. Fu, Microstructure and wear behavior of atmospheric plasma-sprayed AlCoCrFeNiTi high-entropy alloy coating, *J. Mater. Eng. Perform.* 25 (12) (2016) 5513–5521, <https://doi.org/10.1007/s11665-016-2396-6>.
- [299] S. Yin, W. Li, B. Song, X. Yan, M. Kuang, Y. Xu, R. Lupoi, Deposition of FeCoNiCrMn high entropy alloy (HEA) coating via cold spraying, *J. Mater. Sci. Technol.* 35 (6) (2019) 1003–1007, <https://doi.org/10.1016/j.jmst.2018.12.015>.
- [300] F. Cao, P. Munroe, Z. Zhou, Z. Xie, Microstructure and mechanical properties of a multilayered CoCrNi/Ti coating with varying crystal structure, *Surf. Coat. Technol.* 350 (2018) 596–602, <https://doi.org/10.1016/j.surcoat.2018.07.066>.
- [301] A. Pogrebnyak, V. Beresnev, K. Smyrnova, Y. Kravchenko, P. Zukowski, G. Bondarenko, The influence of nitrogen pressure on the fabrication of the two-phase superhard nanocomposite (TiZrNbAlYCr)N coatings, *Mater. Lett.* 211 (2018) 316–318, <https://doi.org/10.1016/j.matlet.2017.09.121>.
- [302] L. Wang, C. Chen, J. Yeh, S. Ke, The microstructure and strengthening mechanism of thermal spray coating Ni<sub>x</sub>Co<sub>0.6</sub>Fe<sub>0.2</sub>CrySizAlTi<sub>0.2</sub> high-entropy alloys, *Mater. Chem. Phys.* 126 (3) (2011) 880–885, <https://doi.org/10.1016/j.mcp.2010.12.022>.
- [303] J. Xiao, H. Tan, Y. Wu, J. Chen, C. Zhang, Microstructure and wear behavior of FeCoNiCrMn high entropy alloy coating deposited by plasma spraying, *Surf. Coat. Technol.* 385 (2020) 125430, <https://doi.org/10.1016/j.surcoat.2020.125430>.
- [304] W. Hsu, Y. Yang, C. Chen, J. Yeh, Thermal sprayed high-entropy NiCo 0.6 Fe 0.2 Cr 1.5 SiAlTi 0.2 coating with improved mechanical properties and oxidation resistance, *Intermetallics* 89 (2017) 105–110, <https://doi.org/10.1016/j.intermet.2017.05.015>.
- [305] H. Zhang, Y. Pan, Y. He, Synthesis and characterization of FeCoNiCrCu high-entropy alloy coating by laser cladding, *Mater. Des.* 32 (4) (2011) 1910–1915, <https://doi.org/10.1016/j.matdes.2010.12.001>.
- [306] F. Shu, B. Yang, S. Dong, H. Zhao, B. Xu, F. Xu, J. Feng, Effects of FE-to-C ratio on microstructure and mechanical properties of laser cladded FeCoCrBnSi high-entropy alloy coatings, *Appl. Surf. Sci.* 450 (2018) 538–544, <https://doi.org/10.1016/j.apsusc.2018.03.128>.
- [307] S. Zhang, C. Wu, J. Yi, C. Zhang, Synthesis and characterization of FeCoCrAlCu high-entropy alloy coating by laser surface alloying, *Surf. Coat. Technol.* 262 (2015) 64–69, <https://doi.org/10.1016/j.surcoat.2014.12.013>.
- [308] M. Löbel, T. Lindner, T. Mehner, T. Lampke, Microstructure and wear resistance of AlCoCrFeNiTi high-entropy alloy coatings produced by HVOF, *Coatings* 7 (9) (2017) 144, <https://doi.org/10.3390/coatings7090144>.
- [309] L. Tian, W. Xiong, C. Liu, S. Lu, M. Fu, Microstructure and wear behavior of atmospheric plasma-sprayed AlCoCrFeNiTi high-entropy alloy coating, *J. Mater. Eng. Perform.* 25 (12) (2016) 5513–5521, <https://doi.org/10.1007/s11665-016-2396-6>.
- [310] N. Tütün, D. Canadinc, A. Motallebzadeh, B. Bal, Microstructure and tribological properties of TiTaHfNbZr high entropy alloy coatings deposited on Ti 6Al 4V substrates, *Intermetallics* 105 (2019) 99–106, <https://doi.org/10.1016/j.intermet.2018.11.015>.
- [311] V. Braic, A. Vladescu, M. Balaceanu, C. Luculescu, M. Braic, Nanostructured multi-element (TiZrNbHfTa)N and (TiZrNbHfTa)C hard coatings, *Surf. Coat. Technol.* 211 (2012) 117–121, <https://doi.org/10.1016/j.surcoat.2011.09.033>.
- [312] C. Wu, S. Zhang, C. Zhang, H. Zhang, S. Dong, Phase evolution and properties in laser surface alloying of FeCoCrAlCuNi high-entropy alloy on copper substrate, *Surf. Coat. Technol.* 315 (2017) 368–376, <https://doi.org/10.1016/j.surcoat.2017.02.068>.
- [313] S. Yin, W. Li, B. Song, X. Yan, M. Kuang, Y. Xu, R. Lupoi, Deposition of FeCoNiCrMn high entropy alloy (HEA) coating via cold spraying, *J. Mater. Sci. Technol.* 35 (6) (2019) 1003–1007, <https://doi.org/10.1016/j.jmst.2018.12.015>.
- [314] J. Zhao, Q. Gao, H. Wang, F. Shu, H. Zhao, W. He, Z. Yu, Microstructure and mechanical properties of Co-based alloy coatings fabricated by laser cladding and plasma arc spray welding, *J. Alloys Compd.* 785 (2019) 846–854, <https://doi.org/10.1016/j.jallcom.2019.01.056>.
- [315] Y. Lin, Y. Cho, Elucidating the microstructure and wear behavior for multicomponent alloy clad layers by in situ synthesis, *Surf. Coat. Technol.* 202 (19) (2008) 4666–4672, <https://doi.org/10.1016/j.surcoat.2008.03.033>.
- [316] Y. Chen, U. Hong, J. Yeh, H. Shih, Selected corrosion behaviors of a Cu<sub>0.5</sub>NiAlCoFeSi bulk glassy alloy in 288°C high-purity water, *Scr. Mater.* 54 (12) (2006) 1997–2001, <https://doi.org/10.1016/j.scriptamat.2006.03.021>.
- [317] H. Zhang, Y. Pan, Y. He, H. Jiao, Microstructure and properties of 6FeNiCoSiCrAlTi high-entropy alloy coating prepared by laser cladding, *Appl. Surf. Sci.* 257 (6) (2011) 2259–2263, <https://doi.org/10.1016/j.apusc.2010.09.084>.
- [318] H. Zhang, Y. Pan, Y. He, Grain refinement and boundary misorientation transition by annealing in the laser rapid solidified 6FeNiCoCrAlTiSi multicomponent ferrous alloy coating, *Surf. Coat. Technol.* 205 (16) (2011) 4068–4072, <https://doi.org/10.1016/j.surcoat.2011.02.054>.
- [319] Y. Liu, Y. Wu, Y. Ma, W. Gao, G. Yang, H. Fu, H. Chen, High temperature wear performance of laser cladding Co06 coating on high-speed train brake disc, *Appl. Surf. Sci.* 481 (2019) 761–766, <https://doi.org/10.1016/j.apusc.2019.02.235>.
- [320] C. Bezençon, Epitaxial deposition of MCrAlY coatings on a Ni-base superalloy by laser cladding, *Scr. Mater.* 49 (7) (2003) 705–709, [https://doi.org/10.1016/s1359-6462\(03\)00369-5](https://doi.org/10.1016/s1359-6462(03)00369-5).
- [321] H. Zhang, Y. Pan, Y. He, H. Jiao, Microstructure and properties of 6FeNiCoSiCrAlTi high-entropy alloy coating prepared by laser cladding, *Appl. Surf. Sci.* 257 (6) (2011) 2259–2263, <https://doi.org/10.1016/j.apusc.2010.09.084>.

- [322] Y. Wang, Y. Huang, X. Meng, L. Wan, J. Feng, Microstructural evolution and mechanical properties of Mg Zn Y Zr alloy during friction stir processing, *J. Alloys Compd.* 696 (2017) 875–883, <https://doi.org/10.1016/j.jallcom.2016.12.068>.
- [323] T. Peat, A. Galloway, A. Toumpis, R. Steel, W. Zhu, N. Iqbal, Enhanced erosion performance of cold spray co-deposited AlSi316 MMCs modified by friction stir processing, *Mater. Des.* 120 (2017) 22–35, <https://doi.org/10.1016/j.matdes.2017.01.099>.
- [324] Y. Huang, J. Li, L. Wan, X. Meng, Y. Xie, Strengthening and toughening mechanisms of CNTs/Mg-6zn composites via friction stir processing, *Mater. Sci. Eng. A* 732 (2018) 205–211, <https://doi.org/10.1016/j.msea.2018.07.011>.
- [325] K. Yang, W. Li, Y. Xu, X. Yang, Using friction stir processing to augment corrosion resistance of cold sprayed AA2024/Al2O3 composite coatings, *J. Alloys Compd.* 774 (2019) 1223–1232, <https://doi.org/10.1016/j.jallcom.2018.09.386>.
- [326] S. Xie, R. Li, T. Yuan, C. Chen, M. Zhang, M. Wang, P. Cao, Laser deposition technology assisted by friction stir processing for preparation of nanostructured Fe-CR-Si alloy layer, *Surf. Coat. Technol.* 337 (2018) 426–433, <https://doi.org/10.1016/j.surfcoat.2018.01.031>.
- [327] A. Heidarzadeh, S. Mironov, R. Kaibyshev, G. Çam, A. Simar, A. Gerlich, F. Khodabakhshi, A. Mostafaei, D.P. Field, J.D. Robson, A. Deschamps, P. J. Withers, Friction stir welding/processing of metals and alloys: a comprehensive review on microstructural evolution, *Prog. Mater. Sci.* 117 (2021) 100752, <https://doi.org/10.1016/j.pmatsci.2020.100752>.
- [328] R. Li, M. Wang, T. Yuan, B. Song, Y. Shi, Microstructural modification of laser-deposited high-entropy CrFeCoNiMoWC alloy by friction stir processing: nanograins formation and deformation mechanism, *Metall. Mater. Trans. A* 48 (2) (2016) 841–854, <https://doi.org/10.1007/s11661-016-3875-y>.
- [329] Y. Huang, Y. Wang, X. Meng, L. Wan, J. Cao, L. Zhou, J. Feng, Dynamic recrystallization and mechanical properties of friction stir processed mg-zn-Y-Zr alloys, *J. Mater. Process. Technol.* 249 (2017) 331–338, <https://doi.org/10.1016/j.jmatprot.2017.06.021>.
- [330] R. Li, Y. Jin, Z. Li, Y. Zhu, M. Wu, Effect of the remelting scanning speed on the amorphous forming ability of Ni-based alloy using laser cladding plus a laser remelting process, *Surf. Coat. Technol.* 259 (2014) 725–731, <https://doi.org/10.1016/j.surfcoat.2014.09.067>.
- [331] B. Yilbas, S. Akhtar, Laser re-melting of HVOF coating with WC blend: thermal stress analysis, *J. Mater. Process. Technol.* 212 (12) (2012) 2569–2577, <https://doi.org/10.1016/j.jmatprot.2012.07.012>.
- [332] B. Huang, Y. Kaynak, Y. Sun, I. Jawahir, Surface layer modification by cryogenic burnishing of al 7050-T7451 alloy and validation with FEM-based burnishing model, *Procedia CIRP* 31 (2015) 1–6, <https://doi.org/10.1016/j.procir.2015.03.097>.
- [333] T. Peat, A. Galloway, A. Toumpis, P. McNutt, N. Iqbal, The erosion performance of cold spray deposited metal matrix composite coatings with subsequent friction stir processing, *Appl. Surf. Sci.* 396 (2017) 1635–1648, <https://doi.org/10.1016/j.apsusc.2016.10.156>.
- [334] E. Broszeit, V. Hauk, R. Oudelhoven, H. Steindorf, Residual stress state after roll-peening of sintered Fe-Cu material, *International Conference on Residual Stresses* 46–51 (1989), [https://doi.org/10.1007/978-94-009-1143-5\\_5](https://doi.org/10.1007/978-94-009-1143-5_5).
- [335] M. Rani, G. Perumal, M. Roy, H.S. Grewal, H. Singh, H.S. Arora, Post-processing of Ni-CR-Al2O3 thermal spray coatings through friction stir processing for enhanced erosion-corrosion performance, *J. Therm. Spray Technol.* 28 (7) (2019) 1466–1477, <https://doi.org/10.1007/s11666-019-00891-z>.
- [336] Y. Morisada, H. Fujii, T. Mizuno, G. Abe, T. Nagaoka, M. Fukusumi, Modification of thermally sprayed cemented carbide layer by friction stir processing, *Surf. Coat. Technol.* 204 (15) (2010) 2459–2464, <https://doi.org/10.1016/j.surfcoat.2010.01.021>.
- [337] K. Yang, W. Li, P. Niu, X. Yang, Y. Xu, K. Yang, W. Li, P. Niu, X. Yang, Y. Xu, Cold sprayed AA2024/Al 2 O 3 metal matrix composites improved by friction stir processing: microstructure characterization, mechanical performance and strengthening mechanisms, *J. Alloys Compd.* 736 (2018) 115–123, <https://doi.org/10.1016/j.jallcom.2017.11.132>.
- [338] M. Fu, X. Ma, K. Zhao, X. Li, D. Su, High-entropy materials for energy-related applications, *iScience* 24 (3) (2021) 102177, <https://doi.org/10.1016/j.isci.2021.102177>.
- [339] Thakur Prasad Yadav, et al., High-entropy alloys for solid hydrogen storage: potentials and prospects, *Trans. Indian Natl. Acad. Eng.* (2022) 1–10.
- [340] Thakur Prasad Yadav, et al., High-entropy alloys for solid hydrogen storage: potentials and prospects, *Trans. Indian Natl. Acad. Eng.* (2022) 1–10.
- [341] Niklas Heinemann, et al., Enabling large-scale hydrogen storage in porous media—the scientific challenges, *Energy Environ. Sci.* 14 (2) (2021) 853–864.
- [342] F. marques, M. Balcerzak, F. Winkelmann, G. Zepon, M. Felderhoff, Review and outlook on high-entropy alloys for hydrogen storage, *Energy Environ. Sci.* 1 (10) (2021) 1–10, <https://doi.org/10.1039/DIEE01543E>.
- [343] Eklas Hossain, et al., A comprehensive review on energy storage systems: types, comparison, current scenario, applications, barriers, and potential solutions, policies, and future prospects, *Energies* 13 (14) (2020) 3651.
- [344] X. Yin, S. Xu, Properties and preparation of high entropy alloys, in: MATEC Web of Conferences 142, 2018 03003, <https://doi.org/10.1051/matecconf/201814203003>.
- [345] Thabang R. Somo, Mykhaylo V. Lototskyy, Volodymyr A. Yartys, Moegamat Wafeeq Davids, Serge Nyallang Nyamsi, Hydrogen storage behaviours of high entropy alloys: a review, *J. Energy Storage*, volume 73, Part B 108969 (2023), <https://doi.org/10.1016/j.est.2023.108969>.
- [346] Felipe Marques, Mateusz Balcerzak, Frederik Winkelmann, Guilherme Zepon, Michael Felderhoff, Review and outlook on high-entropy alloys for hydrogen storage, *Energy Environ. Sci.* (2021), <https://doi.org/10.1039/DIEE01543E>.
- [347] JorgeMonteroBanuelos., Refractory high entropy alloys for hydrogen storage, *Chemicalengineering*, UniversitéParis-Est, 2020. English. NNT:2020PESC2078. tel-03382754, <https://theses.hal.science/tel-03382754>.
- [348] Iftilkar Hussain, et al., High entropy alloys as electrode material for supercapacitors: a review, *J. Energy Storage* 44 (2021) 103405.
- [349] Xin Wang, Wei Guo, Fu Yongzhu, High-entropy alloys: emerging materials for advanced functional applications, *J. Mater. Chem. A* 9 (2) (2021) 663–701.
- [350] Yitong Wang, YuHua Wang, High-entropy alloys in catalyze and supercapacitors: A review, *Nano Energy* 107958 (2022).
- [351] Tian Liu, et al., A micromolding method for transparent and flexible thin-film supercapacitors and hybrid supercapacitors, *Adv. Funct. Mater.* 30 (46) (2020) 2004410.
- [352] T. Jin, X. Sang, R.R. Unocic, R.T. Kinch, X. Liu, J. Hu, S. Dai, Mechanochemical-assisted synthesis of high-entropy metal nitride via a soft urea strategy, *Adv. Mater.* 30 (23) (2018) 1707512, <https://doi.org/10.1002/adma.201707512>.
- [353] Yitong Wang, Yuhua Wang, High-entropy alloys in catalyses and supercapacitors: Progress, prospects, *Nano Energy*, Volume 104, Part A 107958 (2022), <https://doi.org/10.1016/j.nanoen.2022.107958>.
- [354] P. Forouzandeh, V. Kumaravel, S.C. Pillai, Electrode materials for supercapacitors: a review of recent advances, *Catalysts* 10 (2020) 969, <https://doi.org/10.3390/catal10090969>.
- [355] B. Senthilkumar, K.V. Sankar, L. Vasylechko, Y.-S. Lee, R.K. Selvan, Synthesis and electrochemical performances of maricite-NaMPO<sub>4</sub> (M = Ni, Co, Mn) electrodes for hybrid supercapacitors, *RSC Adv.* 4 (2014) 53192–53200, <https://doi.org/10.1039/C4RA06050D>.
- [356] Brianna L. Musicó, et al., The emergent field of high entropy oxides: design, prospects, challenges, and opportunities for tailoring material properties, *APL Mater.* 8 (4) (2020), <https://doi.org/10.1063/5.0003149>.
- [357] James Lenz, S. Edelstein, Magnetic sensors and their applications, *IEEE Sensors J.* 6 (3) (2006) 631–649, <https://doi.org/10.1109/JSEN.2006.874493>.
- [358] E-Wen Huang, et al., Mechanical and magnetic properties of the high-entropy alloys for combinatorial approaches, *Crystals* 10 (3) (2020) 200, <https://doi.org/10.3390/cryst10030200>.
- [359] Akshay Kumar, Alok Singh, Amit Suhane, Mechanically alloyed high entropy alloys: existing challenges and opportunities, *J. Mater. Res. Technol.* 17 (2022) 2431–2456, <https://doi.org/10.1016/j.jmrt.2022.01.141>.
- [360] Priyanka Kumari, Amit K. Gupta, Rajesh K. Mishra, M.S. Ahmad, Rohit R. Shahi, A comprehensive review: recent progress on magnetic high entropy alloys and oxides, *J. Magn. Magn. Mater.* 554 (2022) 169142, <https://doi.org/10.1016/j.jmmm.2022.169142>.
- [361] R.B. Mishra, R.R. Shahi, Magnetic Characteristics of High Entropy Alloys, InTech eBooks, 2018, <https://doi.org/10.5772/intechopen.74235>.
- [362] J. Duan, M. Wang, R. Huang, et al., A novel high-entropy alloy with an exceptional combination of soft magnetic properties and corrosion resistance, *Sci. China Mater.* 66 (2023) 772–779, <https://doi.org/10.1007/s40843-022-2171-5>.
- [363] E.-W. Huang, G.-Y. Hung, S.Y. Lee, J. Jain, K.-P. Chang, J.J. Chou, W.-C. Yang, P. K. Liaw, Mechanical and magnetic properties of the high-entropy alloys for combinatorial approaches, *Crystals* 10 (2020) 200, <https://doi.org/10.3390/cryst10030200>.
- [364] S.R. Trout, Material selection of permanent magnets, considering thermal properties correctly, in: Proceedings: Electrical Insulation Conference and Electrical Manufacturing and Coil Winding Conference (Cat. No.01CH37264), Cincinnati, OH, USA, 2001, pp. 365–370, <https://doi.org/10.1109/EIIC.2001.965683>.
- [365] Shaohui Li, Daoyong Cong, Zhen Chen, Shengwei Li, Chao Song, Yuxian Cao, Zhihua Nie, Yandong Wang, A high-entropy high-temperature shape memory alloy with large and complete superelastic recovery, *Mater. Res. Lett.* 9 (6) (2021) 263–269, <https://doi.org/10.1080/21663831.2021.1893233>.
- [366] E.-W. Huang, G.-Y. Hung, S.Y. Lee, J. Jain, K.-P. Chang, J.J. Chou, W.-C. Yang, P. K. Liaw, Mechanical and magnetic properties of the high-entropy alloys for combinatorial approaches, *Crystals* 10 (2020) 200, <https://doi.org/10.3390/cryst10030200>.
- [367] D. Bérdaran, S. Franger, D. Dragoe, A.K. Meena, N. Dragoe, Colossal dielectric constant in high entropy oxides. *Phys. Status Solidi (RRL)*, Rapid Res. Lett. 10 (4) (2016) 328–333, <https://doi.org/10.1002/pssr.201600043>.
- [368] Rui Hu Mi, Bu Hang Chen, Xiao Li Zhu, Xiang Ming Chen, Dielectric and ferroelectric characteristics of Ba(Ti0.25Zr0.25Hf0.25Sn0.25)O3 high-entropy ceramics, *J. Mater.* 9 (4) (2023) 634–641, <https://doi.org/10.1016/j.jmat.2023.01.005>.
- [369] L. Eric Cross, Relaxorferroelectrics: an overview, *Ferroelectrics* 151 (1) (1994) 305–320, <https://doi.org/10.1080/00150199408244755>.
- [370] Kenji Uchino, Shioichiro Nomura, Critical exponents of the dielectric constants in diffused-phase-transition crystals, *Ferroelectrics* 44 (1) (1982) 55–61, <https://doi.org/10.1080/00150198208260644>.
- [371] Xiangyan Yu, Muhammad Rehan Bhatti, Xintong Ren, Pietro Steiner, Federico Di Sacco, Ming Dong, Han Zhang, Dimitrios Papageorgiou, Giuseppe Portale, Coskun Kocabas, Cees W.M. Bastiaansen, Mike Reece, Haixue Yan, Emiliano Bilotti, Dielectric polymer composites with ultra-high thermal conductivity and low dielectric loss, *Compos. Sci. Technol.* 229 (2022) 109695, <https://doi.org/10.1016/j.compscitech.2022.109695>.
- [372] Shiyi Zhou, Pu Yongping, Qianwen Zhang, Xu Ruike Shi, Wen Wang Guo, Jiamin Ji, Tianchen Wei, Tao Ouyang, Microstructure and dielectric properties of high entropy Ba(Zr0.2Ti0.2Sn0.2Hf0.2)O3 perovskite oxides, *Ceram. Int.* 46 (6) (2020) 7430–7437, <https://doi.org/10.1016/j.ceramint.2019.11.239>.
- [373] Mingjun Xie, Xiao Li, Yuanming Lai, Cong Qi, Jun Yin, Weiping Gong, Yuanxun Li, Qian Liu, Chongsheng Wu, Phase evolution and microwave dielectric

- properties of high-entropy spinel-type ( $Mg_0.2Co_0.2Ni_0.2Li_0.4Zn_0.2Al_2O_4$ ) ceramics, *J. Eur. Ceram. Soc.* 44 (1) (2024) 284–292, <https://doi.org/10.1016/j.jeurceramsoc.2023.09.017>.
- [374] M.-H. Tsai, Physical properties of high entropy alloys, *Entropy* 15 (2013) 5338–5345, <https://doi.org/10.3390/e15125338>.
- [375] S.K. Chen, Y.F. Kao, Near-constant resistivity in 4.2–360 K in a  $B2$   $Al_2.08CoCrFeNi$ , *AIP Adv.* (2012) 2, <https://doi.org/10.1063/1.3679072>.
- [376] H.P. Chou, Y.S. Chang, S.K. Chen, J.W. Yeh, Microstructure, thermophysical and electrical properties in  $Al_xCoCrFeNi$  ( $0 \leq x \leq 2$ ) high-entropy alloys, *Mater. Sci. Eng. B* 163 (2009) 184–189.
- [377] H.P. Chou, Y.S. Chang, S.K. Chen, J.W. Yeh, Microstructure, thermophysical and electrical properties in  $Al_xCoCrFeNi$  ( $0 \leq x \leq 2$ ) high-entropy alloys, *Mater. Sci. Eng. B* 163 (2009) 184–189.
- [378] C.L. Lu, S.Y. Lu, J.W. Yeh, W.K. Hsu, Thermal expansion and enhanced heat transfer in high-entropy alloys, *J. Appl. Crystallogr.* 46 (2013) 736–739.
- [379] Y.F. Ye, Q. Wang, J. Lu, C.T. Liu, Y. Yang, High-entropy alloy: challenges and prospects, *Mater. Today* 19 (6) (2016) 349–362, <https://doi.org/10.1016/j.mattod.2015.11.026>.
- [380] X. Gao, R. Chen, T. Liu, et al., High-entropy alloys: a review of mechanical properties and deformation mechanisms at cryogenic temperatures, *J. Mater. Sci.* 57 (2022) 6573–6606, <https://doi.org/10.1007/s10853-022-07066-2>.
- [381] M. Nagini, B.S. Murty, Advanced high-entropy alloys: a next generation materials, *Trans Indian Natl. Acad. Eng.* (2023), <https://doi.org/10.1007/s41403-023-00435-6>.
- [382] Y. Shi, B. Yang, P.K. Liaw, Corrosion-resistant high-entropy alloys: a review, *Metals* 7 (2017) 43, <https://doi.org/10.3390/met7020043>.
- [383] Yu Chang Liu, Kai Chong Gao, Fuqiang Guo, Wu Dongting, Yong Zou, Effect of Nb content on the microstructure and corrosion resistance of FeCoCrNiNb high-entropy alloys in chloride ion environment, *J. Compounds*, Volume 935, Part 1 (2023) 168013, <https://doi.org/10.1016/j.jallcom.2022.168013>.
- [384] Ram Mohan Rao, K., Corrosion resistance of high entropy alloys, in: K. Kumar, B. S. Babu, J.P. Davim (Eds.), *Coatings, Materials Forming, Machining and Tribology*, Springer, Cham, 2021, [https://doi.org/10.1007/978-3-030-62163-6\\_4](https://doi.org/10.1007/978-3-030-62163-6_4).
- [385] N.I. Muhammad Nadzri, D.S.C. Halin, M.M. Al Bakri Abdullah, S. Joseph, M.A. A. Mohd Salleh, P. Vizureanu, D.-P. Burduhos-Nergis, A.V. Sandu, High-entropy alloy for thin film application: a review, *Coatings* 12 (2022) 1842, <https://doi.org/10.3390/coatings12121842>.
- [386] D. Feng, Y. Dong, L. Zhang, X. Ge, W. Zhang, S. Dai, Z. Qiao, Holey lamellar high-entropy oxide as an ultra-high-activity heterogeneous catalyst for solvent-free aerobic oxidation of benzyl alcohol, *Angew. Chem. Int. Ed.* 59 (44) (2020) 19503–19509, <https://doi.org/10.1002/anie.202004892>.
- [387] B. Rafael, Araujo, Ilknur Bayrak Pehlivan, Tomas Edvinsson, high-entropy alloy catalysts: fundamental aspects, promises towards electrochemical NH<sub>3</sub> production, and lessons to learn from deep neural networks, *Nano Energy* 105 (2023) 108027, <https://doi.org/10.1016/j.nanoen.2022.108027>.
- [388] Irmal Kumar Katiyar, Krishnan Biswas, Jien-Wei Yeh, Sudhanshu Sharma, Chandra Sekhar Tiwary, A perspective on the catalysis using the high entropy alloys, *Nano Energy* 88 (2021) 106261, <https://doi.org/10.1016/j.nanoen.2021.106261>.
- [389] Tobias Löffler, Alfred Ludwig, Jan Rossmeisl, What Makes High-Entropy Alloys Exceptional Electrocatalysts?, doi:<https://doi.org/10.1002/anie.202109212>.
- [390] Thomas A.A. Batchelor, Jack K. Pedersen, Simon H. Winther, Ivano E. Castelli, Karsten W. Jacobsen, Jan Rossmeisl, High-entropy alloys as a discovery platform for electrocatalysis, *Joule* 3 (3) (2019) 834–845, <https://doi.org/10.1016/j.joule.2018.12.015>.
- [391] Attila Kormányos, Q. Dong, B. Xiao, T. Li, A. Savan, K.J. Jennewein, T. Priamushko, A. Körner, B. Böhm, A. Hutzler, L. Hu, A. Ludwig, Serhiy Cherevko, Stability of high-entropy alloys under electrocatalytic conditions, *iScience* 26 (10) (2023) 107775–107793, <https://doi.org/10.1016/j.isci.2023.107775>.
- [392] Hung Yen, An-Chou Yeh, Jien-Wei Yeh, High-entropy alloys: an overview on the fundamentals, development, and future perspective, in: Tapash Chakraborty (Ed.), *Encyclopedia of Condensed Matter Physics*, Second edition, Academic Press, 2024, pp. 647–658, <https://doi.org/10.1016/B978-0-323-90800-9.00117-7>.
- [393] Y. Wang, S. Zou, W.-B. Cai, Recent advances on electro-oxidation of ethanol on Pt- and Pd-based catalysts: from reaction mechanisms to catalytic materials, *Catalysts* 5 (2015) 1507–1534, <https://doi.org/10.3390/catal5031507>.
- [394] A.F. Shao, Z.B. Wang, Y.Y. Chu, Z.Z. Jiang, G.P. Yin, Y. Liu, Evaluation of the performance of carbon supported Pt-Ru-Ni-P as anode catalyst for methanol electrooxidation, *Fuel Cells* 10 (2010) 472–477.
- [395] X. Teng, Anodic Catalyst Design for the Ethanol Oxidation Fuel Cell, Available online, <http://www.formatech.info/energymaterialsbook/book/473-484.pdf>. (Accessed 17 August 2015).
- [396] L. Ke, L. Meng, S. Fang, C. Lin, M. Tan, T. Qi, High-temperature oxidation behaviors of  $AlCrTiSi_0.2$  high-entropy alloy doped with rare earth La and Y, *Crystals* 13 (2023) 1169, <https://doi.org/10.3390/cryst13081169>.
- [397] Research progress of titanium-based high entropy alloy: methods, properties, and applications, *Front. Bioeng. Biotechnol.* 8 (2020) (11 November 2020), <https://doi.org/10.3389/fbioe.2020.603522>. Sec. Biomaterials.
- [398] R. Gawel, Ł. Rogal, K. Przybylski, Oxidation resistance of Ti-Al-Cr-Nb-based high-entropy alloys in air at 1073 K, *J. Mater. Eng. Perform.* 28 (2019) 4163–4170, <https://doi.org/10.1007/s11665-019-04177-x>.
- [399] M. Fu, X. Ma, K. Zhao, X. Li, D. Su, High-entropy materials for energy-related applications, *iScience* 24 (3) (2021 Feb 12) 102177, <https://doi.org/10.1016/j.isci.2021.102177>. PMID: 33718829; PMCID: PMC7921604.
- [400] Chen Liu, Jiangjiang Bi, Lulin Xie, Xicheng Gao, Jiacheng Rong, High entropy spinel oxides ( $CrFeMnNiCox$ ) $3O_4$  ( $x = 2, 3, 4$ ) nanoparticles as anode material towards electrochemical properties, *J. Energy Storage* 71 (2023) 108211, <https://doi.org/10.1016/j.est.2023.108211>.
- [401] Sheetal Kumar Dewangan, Anandev Mangish, Sunny Kumar, Ashutosh Sharma, Byungmin Ahn, Vinod Kumar, A review on high-temperature applicability: a milestone for high entropy alloys, *Eng. Sci. Technol.* 35 (2022) 101211, <https://doi.org/10.1016/j.jestech.2022.101211>.
- [402] W. Huo, H. Zhou, F. Fang, Z. Xie, J. Jiang, Microstructure and mechanical properties of  $CoCrFeNiZrx$  eutectic high-entropy alloys, *Mater. Des.* 134 (2017) 226–233, <https://doi.org/10.1016/j.matdes.2017.08.030>.
- [403] Y. Zhang, X. Wang, J. Li, Y. Huang, Y. Lu, X. Sun, Deformation mechanism during high-temperature tensile test in an eutectic high-entropy alloy  $AlCoCrFeNi_2.1$ , *Mater. Sci. Eng. A* 724 (2018) 148–155, <https://doi.org/10.1016/j.msea.2018.03.078>.
- [404] Novel Alloy Design Concepts Enabling Enhanced Mechanical Properties of High Entropy Alloys doi:<https://doi.org/10.3389/fmats.2022.868721>.
- [405] S. Mooraj, W. Chen, A review on high-throughput development of high-entropy alloys by combinatorial methods, *J. Mater. Inf.* 3 (2023) 4, <https://doi.org/10.20517/jmi.2022.41>.
- [406] Bin Xiao, Wu Gang, Tongde Wang, Zhengang Wei, Yanwei Sui, Baolong Shen, Jiqiu Qi, Fuxiang Wei, Junchao Zheng, High-entropy oxides as advanced anode materials for long-life lithium-ion batteries, *Nano Energy* 95 (2022) 106962, <https://doi.org/10.1016/j.nanoen.2022.106962>.
- [407] Review: High-Entropy Materials for Lithium-Ion Battery Electrodes, doi:<https://doi.org/10.3389/fenrg.2022.862551>.
- [408] Du Xing-Yu, Yan Meng, Hongyan Yuan, Dan Xiao, High-entropy substitution: a strategy for advanced sodium-ion cathodes with high structural stability and superior mechanical properties, *Energy Storage Mater.* 56 (2023) 132–140, <https://doi.org/10.1016/j.ensm.2023.01.010>.
- [409] T.P. Nguyen, I.T. Kim, Recent advances in sodium-ion batteries: cathode materials, *Materials* 16 (2023) 6869, <https://doi.org/10.3390/ma16216869>.
- [410] Yu Jing, Fu Ning, Jing Zhao, Rui Liu, Feng Li, Du Yuchuan, A.C.S. Zhenglong Yang, *Omega* 4 (14) (2019) 15904–15911, <https://doi.org/10.1021/acsomega.9b01916>.
- [411] Iftikhar Hussain, Charmaine Lamiel, Muhammad Ahmad, Yatu Chen, Shuo Shuang, Muhammad Sufyan Javed, Yong Yang, Kaili Zhang, High entropy alloys as electrode material for supercapacitors: a review, *J. Energy Storage*, Volume 44, Part A 103405 (2021), <https://doi.org/10.1016/j.est.2021.103405>. ISSN 2352-152X.
- [412] T. Jin, X. Sang, R.R. Unocic, R.T. Kinch, X. Liu, J. Hu, H. Liu, S. Dai, *Adv. Mater.* 30 (2018) 1707512.
- [413] M.S. Lal, R. Sundara, A.C.S. Appl. Mater. Interfaces 11 (2019) 30846–30857.
- [414] Irum Shaheen, Iftikhar Hussain, Taghazal Zahra, Muhammad Sufyan Javed, Syed Shoab Ahmad Shah, Karim Khan, Muhammad Bilal Hanif, Mohammed A. Assiri, Zafar Said, Waqas Ul Arifeen, Bhargav Akkinapally, Kaili Zhang, Recent advancements in metal oxides for energy storage materials: design, classification, and electrodes configuration of supercapacitor, *J. Energy Storage* 72 (Part E) (2023) 108719, <https://doi.org/10.1016/j.est.2023.108719>.
- [415] M. El Garah, L. Patout, A. Bouissil, A. Charai, F. Sanchezette, The effect of yttrium addition on microstructure and mechanical properties of refractory  $TiTaZrHfW$  high-entropy films, *Coatings* 13 (2023) 1380, <https://doi.org/10.3390/coatings13081380>.
- [416] Xiangfeng Ma, Xin Ding, Ruirui Chen, Jiaxin Zhang, Qiang Song, Hongzhi Cui, Microstructural features and improved reversible hydrogen storage properties of  $TiTiVFe$  high-entropy alloy via Cu alloying, *Int. J. Hydrog. Energy* 48 (7) (2023) 2718–2730, <https://doi.org/10.1016/j.ijhydene.2022.10.130>.
- [417] Rohit R. Shahi, Amit K. Gupta, Priyanka Kumari, Perspectives of high entropy alloys as hydrogen storage materials, *Int. J. Hydrog. Energy* 48 (56) (2023) 21412–21428, <https://doi.org/10.1016/j.ijhydene.2022.02.113>.
- [418] R. Chen, S. Kim, Z. Chang, Redox Flow Batteries: Fundamentals and Applications, InTech, 2017, <https://doi.org/10.5772/intechopen.68752>.
- [419] Yitong Wang, Yuhua Wang, High-entropy alloys in catalyses and supercapacitors: progress, prospects, *Nano Energy*, Volume 104, Part A 107958 (2022), <https://doi.org/10.1016/j.nanoen.2022.107958>.
- [420] T.A. Batchelor, J.K. Pedersen, S.H. Winther, I.E. Castelli, K.W. Jacobsen, J. Rossmeisl, High-entropy alloys as a discovery platform for electrocatalysis, *Joule* 3 (3) (2019) 834–845, <https://doi.org/10.1016/j.joule.2018.12.015>.
- [421] J. Ren, L. Chen, H. Wang, Z. Yuan, High-entropy alloys in electrocatalysis: from fundamentals to applications, *Chem. Soc. Rev.* 52 (23) (2023) 8319–8373, <https://doi.org/10.1039/d3cs00557g>.
- [422] Junhua You, Ruyue Yao, Wuren Ji, Yao Zhao, Zhaoyu Wang, Corrigendum to “Research of high entropy alloys as electrocatalyst for oxygen evolution reaction” [J. Alloy. Compd. 908 (2022) 164669], *J. Alloys Compd.*, Volume 912, 2022, 164921, doi:<https://doi.org/10.1016/j.jallcom.2022.164921>.
- [423] Chang Deng, Tao Wang, Wu Peiwen, Wenshuai Zhu, Sheng Dai, High entropy materials for catalysis: a critical review of fundamental concepts and applications, *Nano Energy* 109153 (2023), <https://doi.org/10.1016/j.nanoen.2023.109153>.
- [424] X. Zhao, X. Liu, B. Huang, et al., Hydroxyl group modification improves the electrocatalytic ORR and OER activity of graphene supported single and bi-metal atomic catalysts (Ni, Co, and Fe), *J. Mater. Chem. A* 7 (2019) 24583, <https://doi.org/10.1039/C9TA08661G>.

- [425] Y. Sun, J. Wang, Q. Liu, et al., Itinerant ferromagnetic half metallic cobalt-iron couples: promising bifunctional electrocatalysts for ORR and OER, *J. Mater. Chem. A* 7 (2019) 27175, <https://doi.org/10.1039/C9TA08616A>.
- [426] S. Wang, A. Lu, C.J. Zhong, Hydrogen production from water electrolysis: role of catalysts, *Nano Convergence* 8 (2021) 4, <https://doi.org/10.1186/s40580-021-00254-x>.
- [427] D.B. Miracle, O.N. Senkov, A critical review of high entropy alloys and related concepts, *Acta Mater.* 122 (2017) 448–511, <https://doi.org/10.1016/j.actamat.2016.08.081>.
- [428] ACS Omega 8 (31) (2023) 28333–28343. Publication Date: July 26, 2023, <https://doi.org/10.1021/acsomega.3c02222>.
- [429] Urszula Szeluga, Bogumiła Kumanek, Barbara Trzebińska, Synergy in hybrid polymer/nanocarbon composites. A review, *Compos. A: Appl. Sci. Manuf.* 73 (2015) 204–231, <https://doi.org/10.1016/j.compositesa.2015.02.021>.
- [430] M. Nagini, B.S. Murty, Advanced high-entropy alloys: a next generation materials, *Trans Indian Natl. Acad. Eng.* (2023), <https://doi.org/10.1007/s41403-023-00435-6>.
- [431] Hangwei Song, Haitao Li, Peiwen Liu, Mengye Duan, Xianghe Peng, Dynamic shock response of high-entropy alloy with elemental anomaly distribution, *Int. J. Mech. Sci.* 253 (2023) 108408, <https://doi.org/10.1016/j.ijmecsci.2023.108408>.
- [432] Thomas A.A. Batchelor, Jack K. Pedersen, Simon H. Winther, Ivano E. Castelli, Karsten W. Jacobsen, Jan Rossmeisl, High-entropy alloys as a discovery platform for Electrocatalysis, *Joule* 3 (3) (2019) 834–845, <https://doi.org/10.1016/j.joule.2018.12.015>.
- [433] D. Bridges, D. Fieser, J.J. Santiago, A. Hu, Novel frontiers in high-entropy alloys. *Metals* 13 (2023) 1193, <https://doi.org/10.3390/met13071193>.
- [434] B. Sharma, S. Harini, A possibility of Pd based high entropy alloy for hydrogen gas sensing applications, *Mater. Res. Express* 6 (11) (2019) 1165d7, <https://doi.org/10.1088/2053-1591/ab4fae>.
- [435] Q.Y. Cheng, M.F. Wang, J.J. Ni, et al., High-entropy alloys for accessing hydrogen economy via sustainable production of fuels and direct application in fuel cells, *Rare Metals* 42 (2023) 3553–3569, <https://doi.org/10.1007/s12598-023-02343-8>.
- [436] H. Liu, L. Syama, L. Zhang, C. Lee, C. Liu, Z. Dai and Q. Yan, High-entropy alloys and compounds for electrocatalytic energy conversion applications, 1 (4), 482–505. <https://doi.org/10.1002/sus2.32>.
- [437] Q. Zhang, K. Lian, G. Qi, et al., High-entropy alloys in water electrolysis: recent advances, fundamentals, and challenges, *Sci. China Mater.* 66 (2023) 1681–1701, <https://doi.org/10.1007/s40843-022-2379-8>.
- [438] Pucheng Pei, Shangwei Huang, Dongfang Chen, Yuehua Li, Wu Ziyao, Peng Ren, Keliang Wang, Xiaoning Jia, A high-energy-density and long-stable-performance zinc-air fuel cell system, *Appl. Energy* 241 (2019) 124–129, <https://doi.org/10.1016/j.apenergy.2019.03.004>.
- [439] Aderemi B. Haruna, Edwin U. Onoh, Kenneth I. Ozoemena, Emerging high-entropy materials as electrocatalysts for rechargeable zinc-air batteries, *Curr. Opin. Electrochem.* 39 (2023) 101264, <https://doi.org/10.1016/j.coelec.2023.101264>.
- [440] M.W. Glasscott, A.D. Pendergast, S. Goines, et al., Electrosynthesis of high-entropy metallic glass nanoparticles for designer, multi-functional electrocatalysis, *Nat. Commun.* 10 (2019) 2650, <https://doi.org/10.1038/s41467-019-10303-z>.
- [441] Yunan Wang, Hao Yang, Zhe Zhang, Xiangying Meng, Tao Cheng, Gaowu Qin, Song Li, Far-from-equilibrium electrosynthesis ramifies high-entropy alloy for alkaline hydrogen evolution, *J. Mater. Sci. Technol.* 166 (2023) 234–240, <https://doi.org/10.1016/j.jmst.2023.05.040>.
- [442] J.K. Pedersen, T.A.A. Batchelor, A. Bagger, J. Rossmeisl, High-entropy alloys as catalysts for the CO<sub>2</sub> and CO reduction reactions, *ACS Catal.* 10 (3) (2020) 2169–2176, <https://doi.org/10.1021/acscatal.9b04343>.
- [443] Diptendu Roy, Amitabha Das, Souvik Manna, Biswarup Pathak, A route map of machine learning approaches in heterogeneous CO<sub>2</sub> reduction reaction, *J. Phys. Chem. C* 127 (2) (2023) 871–881, <https://doi.org/10.1021/acs.jpcc.2c06924>.
- [444] Jasmin S. Shaikh, Meena Rittiruaum, Tinnakorn Saelee, Victor Márquez, Navajsharif S. Shaikh, Patcharaporn Khajondetchairit, Sumayya C. Pathan, Noppakhate Jiraborvorpompsa, Supareak Praserthdam, Piyasan Praserthdam, High entropy materials frontier and theoretical insights for logistics CO<sub>2</sub> reduction and hydrogenation: Electrocatalysis, photocatalysis and thermocatalysis, *J. Alloys Compd.* 969 (2023) 172232, <https://doi.org/10.1016/j.jallcom.2023.172232>.
- [445] L. Xiao, Z. Wang, J. Guan, Optimization strategies of high-entropy alloys for electrocatalytic applications, *Chem. Sci.* 14 (45) (2023) 12850–12868, <https://doi.org/10.1039/d3sc04962k>.
- [446] M.W. Glasscott, A.D. Pendergast, S. Goines, A.R. Bishop, A.T. Hoang, C. Renault, J.E. Dick, *Nat. Commun.* 10 (2019) 2650.
- [447] ACS Catal. 10 (19) (2020) 11280–11306. Publication Date: September 17, 2020, <https://doi.org/10.1021/acscatal.0c03617>.
- [448] L. Xiao, Z. Wang, J. Guan, Optimization strategies of high-entropy alloys for electrocatalytic applications, *Chem. Sci.* 14 (45) (2023) 12850–12868, <https://doi.org/10.1039/d3sc04962k>.
- [449] Hao Liu, Hongye Qin, Jianli Kang, Liying Ma, Guoxin Chen, Qin Huang, Zhijia Zhang, Enzuo Liu, Lu Huanming, Jianxin Li, Naiqin Zhao, A freestanding nanoporous NiCoFeMoMn high-entropy alloy as an efficient electrocatalyst for rapid water splitting, *Chem. Eng. J.*, Volume 435, Part 1 (2022) 134898, <https://doi.org/10.1016/j.cej.2022.134898>.
- [450] D.B. Miracle, J.D. Miller, O.N. Senkov, C. Woodward, M.D. Uchic, J. Tiley, Exploration and development of high entropy alloys for structural applications, *Entropy* 16 (2014) 494–525, <https://doi.org/10.3390/e16010494>.
- [451] Hung Yen, An-Chou Yeh, Jien-Wei Yeh, High-entropy alloys: an overview on the fundamentals, development, and future perspective, in: Tapash Chakraborty (Ed.), *Encyclopedia of Condensed Matter Physics*, Second edition, Academic Press, 2024, pp. 647–658, <https://doi.org/10.1016/B978-0-323-90800-9.00117-7>.
- [452] Urszula Szeluga, Bogumiła Kumanek, Barbara Trzebińska, Synergy in hybrid polymer/nanocarbon composites. A review, *Compos. A: Appl. Sci. Manuf.* 73 (2015) 204–231, <https://doi.org/10.1016/j.compositesa.2015.02.021>.
- [453] Akshay Kumar, Alok Singh, Amit Suhane, Mechanically alloyed high entropy alloys: existing challenges and opportunities, *J. Mater. Res. Technol.* 17 (2022) 2431–2456, <https://doi.org/10.1016/j.jmrt.2022.01.141>.
- [454] Bi-Zeng Zhan, Alison Thompson, Recent developments in the aerobic oxidation of alcohols, *Tetrahedron* 60 (13) (2004) 2917–2935, <https://doi.org/10.1016/j.tet.2004.01.043>.
- [455] Yao, Y., Huang, Z., Xie, P., Lacey, S.D., Jacob, R.J., Xie, H., Chen, F., Nie, A., Pu, T., Rehwoldt, M., et al. (2018). Carbothermalshocksynthesisof high-entropy-alloynanoparticles. *Science* 359, 1489–1494, doi:<https://doi.org/10.1126/science.aan5412>.
- [456] M. Fu, X. Ma, K. Zhao, X. Li, D. Su, High-entropy materials for energy-related applications, *iScience* 24 (3) (2021) 102177, <https://doi.org/10.1016/j.isci.2021.102177>.
- [457] E. Holmström, R. Lizárraga, D. Linder, A. Salmasi, W. Wang, B. Kaplan, L. Vitos, High entropy alloys: substituting for cobalt in cutting edge technology, *Appl. Mater. Today* 12 (2018) 322–329, <https://doi.org/10.1016/j.apmt.2018.07.001>.
- [458] Y.X. Guo, Q.B. Liu, F. Zhou, Misstructure and wear resistance of high-melting-point AlCrFeMoNbTiW high-entropy alloy coating by laser cladding, *Chin. J. Rare Met.* 41 (2017) 1327–1332.
- [459] K. Cui, Y. Zhang, High-entropy alloy films, *Coatings* 13 (2023) 635, <https://doi.org/10.3390/coatings13030635>.
- [460] Panpan Cui, Wei Li, Ping Liu, Ke Zhang, Fengcang Ma, Xiaohong Chen, Rui Feng, Peter K. Liaw, Effects of nitrogen content on microstructures and mechanical properties of Al(CrTiZrHf)N high-entropy alloy nitride films, *J. Alloys Compd.* 834 (2020) 155063, <https://doi.org/10.1016/j.jallcom.2020.155063>.
- [461] B. Jin, N. Zhang, H. Yu, D. Hao, Y. Ma, AlxCrFeNiSi high entropy alloy coatings with high microhardness and improved Wear resistance, *Surf. Coat. Technol.* 402 (2020) 126328, <https://doi.org/10.1016/j.surfcoat.2020.126328>.
- [462] E.N. Eremin, Wear resistance and tribological properties of high entropy coatings CrNiTiZrCu, *Eurasian Phys. Tech.* 17 (1) (2020) 13–18, <https://doi.org/10.31489/2020no1/13-18>.
- [463] H. Cheng, Y. Fang, J. Xu, C. Zhu, P. Dai, S. Xue, Tribological properties of nano/ultrafine-grained FeCoCrNiMnAlx high-entropy alloys over a wide range of temperatures, *J. Alloys Compd.* 817 (2020) 153305, <https://doi.org/10.1016/j.jallcom.2019.153305>.
- [464] S.A. Firstov, Gorban', V.F., Krapivka, N.A., et al., Wear resistance of high-entropy alloys, *Powder Metall. Ceram.* 56 (2017) 158–164, <https://doi.org/10.1007/s11106-017-9882-8> DOI:10.1007/S1003-6326(22)66035-7.
- [465] K. Guo, Y. Sun, W. Cheng, J. Gu, Y. Chen, S. Zhang, Effect of rare earth La<sub>2</sub>O<sub>3</sub> on the microstructure and corrosion resistance of CoCrFeNiMoSi high entropy alloys, *Surf. Interfaces* 44 (2024) 103683–103693, <https://doi.org/10.1016/j.surf.2023.103683>.
- [466] C. Lin, Y. Yao, Corrosion-resistant coating based on high-entropy alloys, *Metals* 13 (2023) 205, <https://doi.org/10.3390/met13020205>.
- [467] Nina Schalk, Michael Tkadletz, Christian Mitterer, Hard coatings for cutting applications: physical vs. chemical vapor deposition and future challenges for the coatings community, *Surf. Coat. Technol.* 429 (2022) 127949, <https://doi.org/10.1016/j.surfcoat.2021.127949>.
- [468] G. Constantin, E. Balan, I. Voiculescu, V. Geanta, V. Craciun, Cutting behavior of Al<sub>0.6</sub>CoCrFeNi high entropy alloy, *Materials* 13 (2020) 4181, <https://doi.org/10.3390/ma13184181>.
- [469] A. Rizzo, S. Goel, M. Luisa Grilli, R. Iglesias, L. Jaworska, V. Lapkovskis, P. Novak, B.O. Postolnyi, D. Valerini, The critical raw materials in cutting tools for machining applications: a review, *Materials* 13 (6) (2020) 1377, <https://doi.org/10.3390/ma13061377>.
- [470] S.N. Grigoriev, M.S. Migranov, Y.A. Melnik, A.A. Okunkova, S.V. Fedorov, V. D. Gurin, M.A. Volosova, Application of adaptive materials and coatings to increase cutting tool performance: efficiency in the case of composite powder high speed steel, *Coatings* 11 (2021) 855, <https://doi.org/10.3390/coatings11070855>.
- [471] A.K. Das, A review on coating with high entropy alloy developed by laser energy based surfacing process, *Mater. Today: Proc.* 52 (2022) 1551–1557, <https://doi.org/10.1016/j.mtpr.2021.11.234>.
- [472] X. Liang, C. Wang, C. Zhang, Chi Fai Cheung, Physical-metallurgical properties and micro-milling machinability evaluation of high entropy alloy FeCoNiCrAl, *J. Mater. Res. Technol.* 21 (2022) 3285–3300, <https://doi.org/10.1016/j.jmrt.2022.10.123>.
- [473] G. Constantin, E. Balan, I. Voiculescu, V. Geanta, V. Craciun, Cutting behavior of Al<sub>0.6</sub>CoCrFeNi high entropy alloy, *Materials* 13 (2020) 4181, <https://doi.org/10.3390/ma13184181>.
- [474] H. Wang, J. Kang, W. Yue, G. Jin, R. Li, Y. Zhou, J. Liang, Y. Yang, Microstructure and corrosive wear properties of CoCrFeNiMn high-entropy alloy coatings, *Materials* 16 (2023) 55, <https://doi.org/10.3390/ma16010055>.
- [475] Nascimentoa, C.B., Donatusb, U., Ríosa, C.T., de Oliveiraaa, M.C.L., Antune, R.A. (2022). A review on corrosion of high entropy alloys: exploring the interplay between corrosion properties, alloy composition, passive film stability and materials selection, *Mater. Res. 25:e20210442*. DOI:<https://doi.org/10.1590/1980-5373-MR-2021-0442>.

- [476] D.B. Miracle, O.N. Senkov, A critical review of high entropy alloys and related concepts, *Acta Mater.* 122 (2017) 448–511, <https://doi.org/10.1016/j.actamat.2016.08.081>.
- [477] X. Zhang, Z. Chen, H. Luo, T. Zhou, Y. Zhao, Z. Ling, Corrosion resistances of metallic materials in environments containing chloride ions: a review, *Trans. Nonferrous Metals Soc. China* 32 (2) (2022) 377–410, [https://doi.org/10.1016/s1003-6326\(22\)65802-3](https://doi.org/10.1016/s1003-6326(22)65802-3).
- [478] Z. Sun, M. Zhang, G. Wang, X. Yang, S. Wang, Wear and corrosion resistance analysis of FeCoNiTiAl<sub>x</sub> high-entropy alloy coatings prepared by laser cladding, *Coatings* 11 (2021) 155, <https://doi.org/10.3390/coatings11020155>.
- [479] K.A. Kuptsov, M.N. Antonyuk, A.N. Sheveyko, A.V. Bondarev, S.G. Ignatov, P. V. Slukin, P. Dwivedi, A. Fraile, T. Polcar, D.V. Shtansky, High-entropy Fe-Cr-Ni-Co-(Cu) coatings produced by vacuum electro-spark deposition for marine and coastal applications, *Surf. Coat. Technol.* 453 (2023) 129136, <https://doi.org/10.1016/j.surfcoat.2022.129136>.
- [480] C. Lin, Y. Yao, Corrosion-resistant coating based on high-entropy alloys, *Metals* 13 (2023) 205, <https://doi.org/10.3390/met13020205>.
- [481] Gifty Oppong Boakye, Erlend Oddvin Straume, Baldur Geir Gunnarsson, Danyil Kovalov, S.N. Karlssdóttir, Corrosion behaviour of HVOF developed Mo-based high entropy alloy coating and selected hard coatings for high temperature geothermal applications, *Mater. Des.* 235 (2023) 112431–112450, <https://doi.org/10.1016/j.matdes.2023.112431>.
- [482] B. Kocsis, Gábor Gulyás; Varga, L. K., Development of high-entropy alloy coating by additive technology, *Front. Mater.* (2022) 8, <https://doi.org/10.3389/fmats.2021.802076>.
- [483] C. Lin, Y. Yao, Corrosion-resistant coating based on high-entropy alloys, *Metals* 13 (2) (2023) 205–228, <https://doi.org/10.3390/met13020205>.
- [484] X. Yin, S. Xu, Properties and preparation of high entropy alloys, in: MATEC Web of Conferences 142, 2018 03003, <https://doi.org/10.1051/matecconf/201814203003>.
- [485] R. Bhaskaran Nair, R. Supekar, S. Morteza Javid, W. Wang, Y. Zou, A. McDonald, J. Mostaghimi, P. Stoyanov, High-entropy alloy coatings deposited by thermal spraying: a review of strengthening mechanisms, performance assessments and perspectives on future applications, *Metals* 13 (2023) 579, <https://doi.org/10.3390/met13030579>.
- [486] A. Rashidy Ahmady, A. Ekhlasí, A. Nouri, M. Haghbin Nazarpak, P. Gong, A. Solouk, High entropy alloy coatings for biomedical applications: a review, *Smart Mater. Manuf.* 1 (2023) 100009, <https://doi.org/10.1016/j.smmf.2022.100009>.
- [487] M. Todai, T. Nagase, T. Hori, A. Matsugaki, A. Sekita, T. Nakano, Novel TiNbTaZrMo high-entropy alloys for metallic biomaterials, *Scr. Mater.* 129 (2017) 65–68, <https://doi.org/10.1016/j.scriptamat.2016.10.028>.
- [488] S. Wang, J. Xu, TiZrNbTaMo High-entropy Alloy Designed for Orthopedic Implants: As-cast Microstructure and Mechanical Properties. 73, 2017, pp. 80–89, <https://doi.org/10.1016/j.msec.2016.12.057>.
- [489] Parisa Edalati, R. Floriano, Y. Tang, A. Mohammadi, K. Pereira, Augusto Ducati Luchessi, Kaveh Edalati, Ultrahigh Hardness and Biocompatibility of High-entropy Alloy TiAlFeCoNi Processed by High-pressure Torsion 112, 2020, pp. 110908–110918, <https://doi.org/10.1016/j.msec.2020.110908>.
- [490] A. López-Ortega, R. Bayón, J.L. Arana, Evaluation of protective coatings for offshore applications. Corrosion and tribocorrosion behavior in synthetic seawater, *Surf. Coat. Technol.* 349 (2018) 1083–1097, <https://doi.org/10.1016/j.surfcoat.2018.06.089>.
- [491] C. Lin, Y. Yao, Corrosion-resistant coating based on high-entropy alloys, *Metals* 13 (2023) 205, <https://doi.org/10.3390/met13020205>.
- [492] C. Lin, Y. Yao, Corrosion-resistant coating based on high-entropy alloys, *Metals* 13 (2) (2023) 205–228, <https://doi.org/10.3390/met13020205>.
- [493] T. Zhang, T. Zhang, Y. He, Y. Wang, Y. Bi, Corrosion and aging of organic aviation coatings: a review, *Chin. J. Aeronaut.* 36 (4) (2022), <https://doi.org/10.1016/j.cja.2022.12.003>.
- [494] C. Lin, Y. Yao, Corrosion-resistant coating based on high-entropy alloys, *Metals* 13 (2) (2023) 205–228, <https://doi.org/10.3390/met13020205>.
- [495] M. Hussain, S.H. Askari Rizvi, N. Abbas, U. Sajjad, M.R. Shah, M.A. Badshah, A. I. Malik, Recent developments in coatings for orthopedic metallic implants, *Coatings* 11 (2021) 791, <https://doi.org/10.3390/coatings11070791>.
- [496] E. Prieto, A. Vaz-Romero, Jesús González-Julián, S. Guo, P. Alvaredo, Novel high entropy alloys as binder in Cermets: from design to sintering, *Int. J. Refract. Met. Hard Mater.* 99 (2021) 105592–105610, <https://doi.org/10.1016/j.ijrmhm.2021.105592>.
- [497] K.M. Youssef, et al., A novel low-density, high-hardness, high-entropy alloy with close-packed single-phase nanocrystalline structures, *Mater. Res. Lett.* 3 (2) (2015) 95–99, <https://doi.org/10.1080/21663831.2014.985855>.
- [498] A.J. Zaddach, et al., Mechanical properties and stacking fault energies of NiFeCrCoMn high-entropy alloy, *JOM* 65 (12) (2013) 1780–1789, <https://doi.org/10.1007/s11837-013-0771-4>.
- [499] R.C. Reed, The Superalloys: Fundamentals and Applications, Cambridge University Press, Cambridge, 2006, <https://doi.org/10.1017/CBO9780511541285.online> ISBN 9780511541285.
- [500] A.C. Yeh, et al., High temperature creep of Ru-bearing Ni-base single crystal superalloys, in: *Superalloys 2004, 2004*, pp. 677–685 [Online]. Available: :://WOS:000228231000077.
- [501] A.C. Yeh, et al., On the creep and phase stability of advanced Ni-base single crystal superalloys, *Mater. Sci. Eng. A-Struct. Mater. Prop. Microstruct. Process.* 490 (1–2) (2008) 445–451, <https://doi.org/10.1016/j.msea.2008.02.008>.
- [502] A.C. Yeh, S. Tin, Effects of Ru and Re additions on the high temperature flow stresses of Ni-base single crystal superalloys, *Scr. Mater.* 52 (6) (2005) 519–524, <https://doi.org/10.1016/j.scriptamat.2004.10.039>.
- [503] A.C. Yeh, S. Tin, Effects of Ru on the high-temperature phase stability of Ni-base single-crystal superalloys, *Metall. Mater. Trans. A: Phys. Metall. Mater. Sci.* 37a (9) (2006) 2621–2631, <https://doi.org/10.1007/BF02586097>.
- [504] H. Jiang, et al., Direct solidification of bulk ultrafine-microstructure eutectic high-entropy alloys with outstanding thermal stability, *Scr. Mater.* 165 (2019) 145–149, <https://doi.org/10.1016/j.scriptamat.2019.02.035>.
- [505] K. Kawagishi, et al., Development of an oxidation-resistant high-strength sixth-generation single-crystal superalloy Tms-238, in: *Superalloys 2012, 2012*, pp. 189–195 [Online]. Available: :://WOS:000324518300021.
- [506] A. Takeuchi, et al., Alloy designs of high-entropy crystalline and bulk glassy alloys by evaluating mixing enthalpy and delta parameter for quinary to decimal equiatomic alloys, *Mater. Trans.* 55 (1) (2014) 165–170, <https://doi.org/10.2320/matertrans.M2013352>.
- [507] P. Gong, et al., Influence of deep cryogenic cycling on the rejuvenation and plasticization of TiZrHfBeCu high-entropy bulk metallic glass, *Mater. Sci. Eng. A-Struct. Mater. Prop. Microstruct. Process.* 797 (2020), <https://doi.org/10.1016/j.msea.2020.140078.ARTN 140078>.
- [508] C.Z. Li, et al., New ferromagnetic (Fe1/3Co1/3Ni1/3)(80)(P1/2B1/2)(20) high entropy bulk metallic glass with superior magnetic and mechanical properties, *J. Alloys Compd.* 791 (2019) 947–951, <https://doi.org/10.1016/j.jallcom.2019.03.375>.
- [509] Y. Chen, et al., High entropy metallic glasses: glass formation, crystallization and properties, *J. Alloys Compd.* 866 (2021), <https://doi.org/10.1016/j.jallcom.2021.158852.ARTN 158852>.
- [510] O.N. Senkov, et al., Refractory high-entropy alloys, *Intermetallics* 18 (9) (2010) 1758–1765, <https://doi.org/10.1016/j.intermet.2010.05.014>.
- [511] O.N. Senkov, et al., Microstructure and room temperature properties of a high-entropy TaNbHfZrTi alloy, *J. Alloys Compd.* 509 (20) (2011) 6043–6048, <https://doi.org/10.1016/j.jallcom.2011.02.171>.
- [512] O.N. Senkov, et al., Microstructure and elevated temperature properties of a refractory TaNbHfZrTi alloy, *J. Mater. Sci.* 47 (9) (2012) 4062–4074, <https://doi.org/10.1007/s10853-012-6260-2>.
- [513] O.N. Senkov, et al., Mechanical properties of low-density, refractory multi-principal element alloys of the Cr-Nb-Ti-V-Zr system, *Mater. Sci. Eng. A-Struct. Mater. Prop. Microstruct. Process.* 565 (2013) 51–62, <https://doi.org/10.1016/j.msea.2012.12.018>.
- [514] B.S. Murty, J.W. Yeh, S. Ranganathan, *High-Entropy Alloys*, 1st edn, p. 2, ISBN: 9780128002513, doi:10.1016/B978-0-12-800251-3.00001-8. Otarawanna S and Dahle AK (2011) 6 - Casting of aluminium alloys, in: R. Lumley (Ed.), *Fundamentals of Aluminium Metallurgy*, Woodhead Publishing, 2014, pp. 141–154.
- [515] P.P. Ding, et al., Preparation, characterization and properties of multicomponent Al1CoCrFeNi(2.1) powder by gas atomization method, *J. Alloys Compd.* 721 (2017) 609–614, <https://doi.org/10.1016/j.jallcom.2017.06.020>.
- [516] N.X. Zhou, et al., Single-phase high-entropy intermetallic compounds (HEICs): bridging high-entropy alloys and ceramics, *Sci. Bull.* 64 (12) (2019) 856–864, <https://doi.org/10.1016/j.scib.2019.05.007>.
- [517] S.Y. Chang, et al., Structural and thermodynamic factors of suppressed interdiffusion kinetics in multi-component high-entropy materials, *Sci. Rep.* 4 (2014), <https://doi.org/10.1038/srep04162.ARTN 4162>.
- [518] W.L. Hsu, et al., A heat-resistant NiCo0.6Fe0.2CrxSiAlTi0.2 overlay coating for high-temperature applications, *J. Electrochem. Soc.* 163 (13) (2016) C752–C758, <https://doi.org/10.1149/2.0821613jes>.
- [519] W.L. Hsu, et al., A study of NiCo0.6Fe0.2CrxSiAlTiy high-entropy alloys for applications as a high-temperature protective coating and a bond coat in thermal barrier coating systems, *J. Electrochem. Soc.* 165 (9) (2018) C524–C531, <https://doi.org/10.1149/2.1191809jes>.
- [520] J. Yang, C. Wang, D. Xie, H. Qin, W. Liu, M. Liang, X. Li, C. Liu, M. Huang, A new type of gradient structure FeCoCrNiWMo high entropy alloy layer by plasma solid-state surface metallurgy, *Surf. Coat. Technol.* 457 (2023) 129320–129335, <https://doi.org/10.1016/j.surfcoat.2023.129320>.
- [521] A. Rashidy Ahmady, A. Ekhlasí, A. Nouri, M. Haghbin Nazarpak, P. Gong, A. Solouk, High entropy alloy coatings for biomedical applications: a review, *Smart Mater. Manuf.* 1 (2023) 100009, <https://doi.org/10.1016/j.smmf.2022.100009>.
- [522] Advanced Bond Coats for Thermal Barrier Coating Systems Based on High Entropy Alloys. (n.d.). Retrieved from <https://www.sbir.gov/sbirsearch/detail/890837>.
- [523] Exploration of high entropy alloys for turbine applications. (n.d.). Retrieved from <https://www.sbir.gov/sbirsearch/detail/1212591>.
- [524] D. Bridges, S. Zhang, S. Lang, M. Gao, Z. Yu, Z. Feng, A. Hu, Laser brazing of a nickel-based superalloy using a Ni-mn-Fe-Co-Cu high entropy alloy filler metal, *Mater. Lett.* 215 (2018) 11–14, <https://doi.org/10.1016/j.matlet.2017.12.003>.
- [525] M. Chuang, M. Tsai, W. Wang, S. Lin, J. Yeh, Microstructure and wear behavior of AlxCu1.5CrFeNi1.5Tiy high-entropy alloys, *Acta Mater.* 59 (16) (2011) 6308–6317, <https://doi.org/10.1016/j.actamat.2011.06.041>.
- [526] K.M. Youssef, A.J. Zaddach, C. Niu, D.L. Irving, C.C. Koch, A novel low-density, high-hardness, high-entropy alloy with close-packed single-phase Nanocrystalline structures, *Mater. Res. Lett.* 3 (2) (2014) 95–99, <https://doi.org/10.1080/21663831.2014.985855>.
- [527] M. Dada, P. Popoola, S. Adeosun, N. Mathe, High entropy alloys for aerospace applications, *Aerodynamics* (2021), <https://doi.org/10.5772/intechopen.84982>.

- [528] M. Dada, P. Popoola, N. Mathe, Recent advances of high entropy alloys for aerospace applications: a review, *World J. Eng.* (2021), <https://doi.org/10.1108/wje-01-2021-0040>.
- [529] Z. Li, S. Zhao, H. Diao, P.K. Liaw, M.A. Meyers, High-velocity deformation of Al0.3CoCrFeNi high-entropy alloy: remarkable resistance to shear failure, *Sci. Rep.* 7 (1) (2017), <https://doi.org/10.1038/srep42742>.
- [530] T. Yang, Y. Zhao, J. Luan, B. Han, J. Wei, J. Kai, C. Liu, Nanoparticles-strengthened high-entropy alloys for cryogenic applications showing an exceptional strength-ductility synergy, *Scr. Mater.* 164 (2019) 30–35, <https://doi.org/10.1016/j.scriptamat.2019.01.034>.
- [531] X. Yang, Y. Zhang, P. Liaw, Microstructure and compressive properties of NbTiVAlx high entropy alloys, *Procedia Engineering* 36 (2012) 292–298, <https://doi.org/10.1016/j.proeng.2012.03.043>.
- [532] K. Tseng, Y. Yang, C. Juan, T. Chin, C. Tsai, J. Yeh, A light-weight high-entropy alloy Al20Be20Fe10Si15Ti35, *Sci. China Technol. Sci.* 61 (2) (2017) 184–188, <https://doi.org/10.1007/s11431-017-9073-0>.
- [533] T. Tsao, A. Yeh, C. Kuo, K. Kakehi, H. Murakami, J. Yeh, S. Jian, The high temperature tensile and creep behaviors of high entropy superalloy, *Sci. Rep.* 7 (1) (2017), <https://doi.org/10.1038/s41598-017-13026-7>.
- [534] O. Senkov, D. Isheim, D. Seidman, A. Pilchak, Development of a refractory high entropy superalloy, *Entropy* 18 (3) (2016) 102, <https://doi.org/10.3390/e18030102>.
- [535] O.N. Senkov, J.M. Scott, S.V. Senkova, F. Meisenkothen, D.B. Miracle, C. Woodward, Microstructure and elevated temperature properties of a refractory TaNbHfZrTi alloy, *J. Mater. Sci.* 47 (9) (2012) 4062–4074, <https://doi.org/10.1007/s10853-012-6260-2>.
- [536] R. Li, W. Zhang, Y. Zhang, P.K. Liaw, The effects of phase transformation on the microstructure and mechanical behavior of FeNiMnCr.75Al high-entropy alloys, *Mater. Sci. Eng. A* 725 (2018) 138–147, <https://doi.org/10.1016/j.msea.2018.04.007>.
- [537] N.K. Kumar, C. Li, K. Leonard, H. Bei, S. Zinkle, Microstructural stability and mechanical behavior of FeNiMnCr high entropy alloy under ion irradiation, *Acta Mater.* 113 (2016) 230–244, <https://doi.org/10.1016/j.actamat.2016.05.007>.
- [538] K. Wang, A.D. Lan, J.W. Qiao, Corrosion behavior of Al0.1CoCrFeNi high entropy alloy in various chloride-containing solutions, *Front. Mater.* 7 (2021), <https://doi.org/10.3389/fmats.2020.533843>.
- [539] M. Chen, S. Lin, J. Yeh, M. Chuang, S. Chen, Y. Huang, Effect of vanadium addition on the microstructure, hardness, and wear resistance of Al0.5CoCrCuFeNi high-entropy alloy, *Metall. Mater. Trans. A* 37 (5) (2006) 1363–1369, <https://doi.org/10.1007/s11661-006-0081-3>.
- [540] J. Wu, S. Lin, J. Yeh, S. Chen, Y. Huang, H. Chen, Adhesive wear behavior of AlxCrCrCuFeNi high-entropy alloys as a function of aluminum content, *Wear* 261 (5–6) (2006) 513–519, <https://doi.org/10.1016/j.wear.2005.12.008>.
- [541] C. Hsu, J. Yeh, S. Chen, T. Shun, Wear resistance and high-temperature compression strength of FCC CuCoNiCrAl0.5Fe alloy with boron addition, *Metall. Mater. Trans. A* 35 (5) (2004) 1465–1469, <https://doi.org/10.1007/s11661-004-0254-x>.
- [542] C. Hsu, T. Sheu, J. Yeh, S. Chen, Effect of iron content on wear behavior of AlCoCrFeMo0.5Ni high-entropy alloys, *Wear* 268 (5–6) (2010) 653–659, <https://doi.org/10.1016/j.wear.2009.10.013>.
- [543] R. Nair, H. Arora, S. Mukherjee, S. Singh, H. Singh, H. Grewal, Exceptionally high cavitation erosion and corrosion resistance of a high entropy alloy, *Ultrason. Sonochem.* 41 (2018) 252–260, <https://doi.org/10.1016/j.ulsonch.2017.09.044>.
- [544] G. Popescu, B. Ghiban, C.A. Popescu, L. Rosu, R. Trusca, I. Carcea, B.A. Carlan, New TiZrNbTaFe high entropy alloy used for medical applications, *IOP Conf. Ser.: Mater. Sci. Eng.* 400 (2018) 022049, <https://doi.org/10.1088/1757-899x/400/2/022049>.
- [545] W.J. Shen, M.H. Tsai, K.Y. Tsai, C.C. Juan, C.W. Tsai, J.W. Yeh, Y.S. Chang, Superior oxidation resistance of (Al0.34Cr0.22Nb0.11Si0.11Ti0.22) 50N50 high-entropy nitride, *J. Electrochem. Soc.* 160 (11) (2013) C531–C535, <https://doi.org/10.1149/2.028311jjes>.
- [546] P. Li, A. Wang, C. Liu, A ductile high entropy alloy with attractive magnetic properties, *J. Alloys Compd.* 694 (2017) 55–60, <https://doi.org/10.1016/j.jallcom.2016.09.186>.
- [547] S. Ma, Y. Zhang, Effect of NB addition on the microstructure and properties of AlCoCrFeNi high-entropy alloy, *Mater. Sci. Eng. A* 532 (2012) 480–486, <https://doi.org/10.1016/j.msea.2011.10.110>.
- [548] W. Feng, Y. Qi, S. Wang, Effects of short-range order on the magnetic and mechanical properties of FeCoNi(AlSi)x high entropy alloys, *Metals* 7 (11) (2017) 482, <https://doi.org/10.3390/met7110482>.
- [549] G. Zhang, K. Ming, J. Kang, Q. Huang, Z. Zhang, X. Zheng, X. Bi, High entropy alloy as a highly active and stable electrocatalyst for hydrogen evolution reaction, *Electrochim. Acta* 279 (2018) 19–23, <https://doi.org/10.1016/j.electacta.2018.05.035>.
- [550] M. Sahlberg, D. Karlsson, C. Zlatea, U. Jansson, Superior hydrogen storage in high entropy alloys, *Sci. Rep.* 6 (1) (2016), <https://doi.org/10.1038/srep36770>.
- [551] G. Firstov, T. Kosorukova, Y. Koval, V. Odnosum, High entropy shape memory alloys, *Mater. Today: Proc.* 2 (2015) S499–S503, <https://doi.org/10.1016/j.matpr.2015.07.335>.
- [552] D. Canadinc, W. Treherne, J. Ma, I. Karaman, F. Sun, Z. Chaudhry, Ultra-high temperature multi-component shape memory alloys, *Scr. Mater.* 158 (2019) 83–87, <https://doi.org/10.1016/j.scriptamat.2018.08.019>.
- [553] Y. Zhao, H. Chen, Z. Lu, T. Nieh, Thermal stability and coarsening of coherent particles in a precipitation-hardened (NiCoFeCr)94Ti2Al4 high-entropy alloy, *Acta Mater.* 147 (2018) 184–194, <https://doi.org/10.1016/j.jactamat.2018.01.049>.
- [554] P. Koželj, S. Vrtnik, A. Jelen, S. Jazbec, Z. Jagličić, S. Maiti, J. Dolinšek, Discovery of a superconducting high-entropy alloy, *Phys. Rev. Lett.* 113 (10) (2014), <https://doi.org/10.1103/physrevlett.113.107001>.
- [555] R. Lin, T. Lee, D. Wu, Y. Lee, A study of thin film resistors prepared using Ni-CR-Si-Al-Ta high entropy alloy, *Adv. Mater. Sci. Eng.* 2015 (2015) 1–7, <https://doi.org/10.1155/2015/847191>.
- [556] W. Hsu, H. Murakami, J. Yeh, A. Yeh, K. Shimoda, A heat-resistant NiCo0.6Fe0.2Cr1.5SiAlTi0.2. Overlay coating for high-temperature applications, *J. Electrochem. Soc.* 163 (13) (2016) C752–C758, <https://doi.org/10.1149/2.0821613jes>.
- [557] M. Tsai, J. Yeh, J. Gan, Diffusion barrier properties of AlMoNbSiTaTiVZr high-entropy alloy layer between copper and silicon, *Thin Solid Films* 516 (16) (2008) 5527–5530, <https://doi.org/10.1016/j.tsf.2007.07.109>.
- [558] M.A. Hassan, H.M. Yehia, A.S. Mohamed, A.E. El-Nikhaily, O.A. Elkady, Effect of copper addition on the AlCoCrFeNi high entropy alloys properties via the Electroless plating and powder metallurgy technique, *Crystals* 11 (5) (2021) 540, <https://doi.org/10.3390/cryst11050540>.
- [559] P. Yang, Y. Liu, X. Zhao, J. Cheng, H. Li, Electromagnetic wave absorption properties of mechanically alloyed FeCoNiCrAl high entropy alloy powders, *Adv. Powder Technol.* 27 (4) (2016) 1128–1133, <https://doi.org/10.1016/j.apert.2016.03.023>.
- [560] Y. Zhang, B. Zhang, K. Li, G. Zhao, S. Guo, Electromagnetic interference shielding effectiveness of high entropy AlCoCrFeNi alloy powder Laden composites, *J. Alloys Compd.* 734 (2018) 220–228, <https://doi.org/10.1016/j.jallcom.2017.11.044>.
- [561] P.C. Gasson, The superalloys: Fundamentals and applications R. C. Reed Cambridge University press, the Edinburgh building, Shaftesbury road, Cambridge, cb2 2ru, UK, 2006. 372pp. Illustrated. £80. ISBN 0-521-85904-2, *Aeronaut. J.* 112 (1131) (2008) 291, <https://doi.org/10.1017/s0001924000087509>.
- [562] J. Yeh, S. Chen, S. Lin, J. Gan, T. Chin, T. Shun, S. Chang, Nanostructured high-entropy alloys with multiple principal elements: novel alloy design concepts and outcomes, *Adv. Eng. Mater.* 6 (5) (2004) 299–303, <https://doi.org/10.1002/adem.200300567>.
- [563] Y. Zhang, T.T. Zuo, Z. Tang, M.C. Gao, K.A. Dahmen, P.K. Liaw, Z.P. Lu, Microstructures and properties of high-entropy alloys, *Prog. Mater. Sci.* 61 (2014) 1–93, <https://doi.org/10.1016/j.pmatsci.2013.10.001>.
- [564] Y. Lu, Y. Dong, S. Guo, L. Jiang, H. Kang, T. Wang, T. Li, A promising new class of high-temperature alloys: eutectic high-entropy alloys, *Sci. Rep.* 4 (1) (2014), <https://doi.org/10.1038/srep06200>.
- [565] Y. Lu, Y. Dong, H. Jiang, Z. Wang, Z. Cao, S. Guo, P.K. Liaw, Promising properties and future trend of eutectic high entropy alloys, *Scr. Mater.* 187 (2020) 202–209, <https://doi.org/10.1016/j.scriptamat.2020.06.022>.
- [566] I.S. Wani, T. Bhattacharjee, S. Sheikh, Y.P. Lu, S. Chatterjee, P.P. Bhattacharjee, N. Tsuji, Ultrafine-grained AlCoCrFeNi2.1 eutectic high-entropy alloy, *Mater. Res. Lett.* 4 (3) (2016) 174–179, <https://doi.org/10.1080/21663831.2016.1160451>.
- [567] T. Bhattacharjee, I.S. Wani, S. Sheikh, I.T. Clark, T. Okawa, S. Guo, N. Tsuji, Simultaneous strength-ductility enhancement of a nano-lamellar AlCoCrFeNi2.1 eutectic high entropy alloy by cryo-rolling and annealing, *Sci. Rep.* 8 (1) (2018), <https://doi.org/10.1038/s4198-018-21385-y>.
- [568] P. Shi, W. Ren, T. Zheng, Z. Ren, X. Hou, J. Peng, P.K. Liaw, Enhanced strength-ductility synergy in ultrafine-grained eutectic high-entropy alloys by inheriting microstructural lamellae, *Nat. Commun.* 10 (1) (2019), <https://doi.org/10.1038/s41467-019-08460-2>.
- [569] H. Zheng, R. Chen, G. Qin, X. Li, Y. Su, H. Ding, H. Fu, Phase separation of AlCoCrFeNi2.1 eutectic high-entropy alloy during directional solidification and their effect on tensile properties, *Intermetallics* 113 (2019) 106569, <https://doi.org/10.1016/j.intermet.2019.106569>.
- [570] S. Shukla, T. Wang, S. Cotton, R.S. Mishra, Hierarchical microstructure for improved fatigue properties in a eutectic high entropy alloy, *Scr. Mater.* 156 (2018) 105–109, <https://doi.org/10.1016/j.scriptamat.2018.07.022>.
- [571] T. Bhattacharjee, R. Zheng, Y. Chong, S. Sheikh, S. Guo, I.T. Clark, N. Tsuji, Effect of low temperature on tensile properties of AlCoCrFeNi2.1 eutectic high entropy alloy, *Mater. Chem. Phys.* 210 (2018) 207–212, <https://doi.org/10.1016/j.matchemphys.2017.06.023>.
- [572] Y. Dong, L. Jiang, H. Jiang, Y. Lu, T. Wang, T. Li, Effects of annealing treatment on microstructure and hardness of bulk AlCrFeNiMo0.2 eutectic high-entropy alloy, *Mater. Des.* 82 (2015) 91–97, <https://doi.org/10.1016/j.matdes.2015.05.046>.
- [573] Ł. Rogal, J. Morygiel, Z. Świątek, F. Czerwiński, Microstructure and mechanical properties of the new Nb2Sc25Cr25Zr25 eutectic high entropy alloy, *Mater. Sci. Eng. A* 651 (2016) 590–597, <https://doi.org/10.1016/j.msea.2015.10.071>.
- [574] Y. Lu, H. Jiang, S. Guo, T. Wang, Z. Cao, T. Li, A new strategy to design eutectic high-entropy alloys using mixing enthalpy, *Intermetallics* 91 (2017) 124–128, <https://doi.org/10.1016/j.intermet.2017.09.001>.
- [575] Y. Tan, J. Li, J. Wang, H. Kou, Seaweed eutectic-dendritic solidification pattern in a CoCrFeNiMnPd eutectic high-entropy alloy, *Intermetallics* 85 (2017) 74–79, <https://doi.org/10.1016/j.intermet.2017.02.004>.
- [576] P. Shi, Y. Zhong, Y. Li, W. Ren, T. Zheng, Z. Shen, Y. Zhu, Multistage work hardening assisted by multi-type twinning in ultrafine-grained heterostructural eutectic high-entropy alloys, *Mater. Today* 41 (2020) 62–71, <https://doi.org/10.1016/j.matto.2020.09.029>.
- [577] H. Jiang, D. Qiao, Y. Lu, Z. Ren, Z. Cao, T. Wang, T. Li, Direct solidification of bulk ultrafine-microstructure eutectic high-entropy alloys with outstanding thermal stability, *Scr. Mater.* 165 (2019) 145–149, <https://doi.org/10.1016/j.jscriptamat.2019.02.035>.

- [578] C. Ai, F. He, M. Guo, J. Zhou, Z. Wang, Z. Yuan, L. Liu, Alloy design, micromechanical and macromechanical properties of CoCrFeNiTax eutectic high entropy alloys, *J. Alloys Compd.* 735 (2018) 2653–2662, <https://doi.org/10.1016/j.jallcom.2017.12.015>.
- [579] W. Huo, H. Zhou, F. Fang, X. Zhou, Z. Xie, J. Jiang, Microstructure and properties of novel CoCrFeNiTax eutectic high-entropy alloys, *J. Alloys Compd.* 735 (2018) 897–904, <https://doi.org/10.1016/j.jallcom.2017.11.075>.
- [580] A. Shafeei, S. Rajabi, A cobalt-rich eutectic high-entropy alloy in the system Al–Co–Cr–Fe–Ni, *Appl. Phys. A* 125 (11) (2019), <https://doi.org/10.1007/s00339-019-3084-9>.
- [581] Z. Yang, Z. Wang, Q. Wu, T. Zheng, P. Zhao, J. Chen, Enhancing the mechanical properties of casting eutectic high entropy alloys with Mo addition, *Appl. Phys. A* 125 (3) (2019), <https://doi.org/10.1007/s00339-019-2506-z>.
- [582] X. Jin, J. Bi, L. Zhang, Y. Zhou, X. Du, Y. Liang, B. Li, A new CrFeNi2Al eutectic high entropy alloy system with excellent mechanical properties, *J. Alloys Compd.* 770 (2019) 655–661, <https://doi.org/10.1016/j.jallcom.2018.08.176>.
- [583] R. Jain, M.R. Rahul, S. Samal, V. Kumar, G. Phanikumar, Hot workability of Co–FE–Mn–Ni–Ti eutectic high entropy alloy, *J. Alloys Compd.* 822 (2020) 153609, <https://doi.org/10.1016/j.jallcom.2019.153609>.
- [584] L. Han, X. Xu, Z. Li, B. Liu, C.T. Liu, Y. Liu, A novel equiaxed eutectic high-entropy alloy with excellent mechanical properties at elevated temperatures, *Mater. Res. Lett.* 8 (10) (2020) 373–382, <https://doi.org/10.1080/21663831.2020.1772395>.
- [585] H. Jiang, H. Zhang, T. Huang, Y. Lu, T. Wang, T. Li, Microstructures and mechanical properties of Co2MoxNi2VWx eutectic high entropy alloys, *Mater. Des.* 109 (2016) 539–546, <https://doi.org/10.1016/j.matdes.2016.07.113>.
- [586] S. Samal, M. Rahul, R.S. Kottada, G. Phanikumar, Hot deformation behaviour and processing map of Co–Cu–Fe–Ni–Ti eutectic high entropy alloy, *Mater. Sci. Eng. A* 664 (2016) 227–235, <https://doi.org/10.1016/j.msea.2016.04.006>.
- [587] X. Chen, Y. Sui, J. Qi, Y. He, F. Wei, Q. Meng, Z. Sun, Microstructure of Al<sub>1.3</sub>CrFeNi eutectic high entropy alloy and oxidation behavior at 1000 °C, *J. Mater. Res.* 32 (11) (2017) 2109–2116, <https://doi.org/10.1557/jmr.2017.10>.
- [588] X. Jin, Y. Zhou, L. Zhang, X. Du, B. Li, A novel FE 20 Co 20 Ni 41 al 19 eutectic high entropy alloy with excellent tensile properties, *Mater. Lett.* 216 (2018) 144–146, <https://doi.org/10.1016/j.matlet.2018.01.017>.
- [589] M. Braic, V. Braic, A. Vladescu, N. Zoița, C., & Balaceanu, M., Solid solution or amorphous phase formation in tizr-based ternary to quaternary multi-principal-element films, *Prog. Natl. Sci.: Mater. Int.* 24 (4) (2014) 305–312, <https://doi.org/10.1016/j.jpsc.2014.06.001>.
- [590] W. Shen, M. Tsai, J. Yeh, Machining performance of sputter-deposited (Al0.34Cr0.22Nb0.11Si0.11Ti0.22)50N50 high-entropy nitride coatings, *Coatings* 5 (3) (2015) 312–325, <https://doi.org/10.3390/coatings5030312>.
- [591] Z. An, H. Jia, Y. Wu, P.D. Rack, A.D. Patchen, Y. Liu, P.K. Liaw, Solid-solution CrCoCuFeNi high-entropy alloy thin films synthesized by sputter deposition, *Mater. Res. Lett.* 3 (4) (2015) 203–209, <https://doi.org/10.1080/21663831.2015.1048904>.
- [592] H. Zhang, W. Wu, Y. He, M. Li, S. Guo, Formation of core–shell structure in high entropy alloy coating by laser cladding, *Appl. Surf. Sci.* 363 (2016) 543–547, <https://doi.org/10.1016/j.apsusc.2015.12.059>.
- [593] T. Yue, H. Xie, X. Lin, H. Yang, G. Meng, Microstructure of laser re-melted AlCoCrCuFeNi high entropy alloy coatings produced by plasma spraying, *Entropy* 15 (12) (2013) 2833–2845, <https://doi.org/10.3390/e15072833>.
- [594] C. Yao, P. Zhang, M. Liu, G. Li, J. Ye, P. Liu, Y. Tong, Electrochemical preparation and magnetic study of Bi–FE–Co–Ni–Mn high entropy alloy, *Electrochim. Acta* 53 (28) (2008) 8359–8365, <https://doi.org/10.1016/j.electacta.2008.06.036>.
- [595] J.B. Cheng, X.B. Liang, Z.H. Wang, B.S. Xu, Formation and mechanical properties of CoNiCuFeCr high-entropy alloys coatings prepared by plasma transferred arc cladding process, *Plasma Chem. Plasma Process.* 33 (5) (2013) 979–992, <https://doi.org/10.1007/s11090-013-9469-1>.
- [596] K. Cheng, C. Lai, S. Lin, J. Yeh, Structural and mechanical properties of multi-element (AlCrMoTaTiZr)Nx coatings by reactive magnetron sputtering, *Thin Solid Films* 519 (10) (2011) 3185–3190, <https://doi.org/10.1016/j.tsf.2010.11.034>.
- [597] H. Zhang, Y. He, Y. Pan, S. Guo, Thermally stable laser cladded CoCrCuFeNi high-entropy alloy coating with low stacking fault energy, *J. Alloys Compd.* 600 (2014) 210–214, <https://doi.org/10.1016/j.jallcom.2014.02.121>.
- [598] S. Lin, S. Chang, C. Chang, Y. Huang, Nanomechanical properties and deformation behaviors of multi-component (AlCrTaTiZr)NxSi high-entropy coatings, *Entropy* 16 (1) (2013) 405–417, <https://doi.org/10.3390/e16010405>.
- [599] C. Huang, Y. Zhang, J. Shen, R. Vilar, Thermal stability and oxidation resistance of laser clad TiVCrAlSi high entropy alloy coatings on Ti–6Al–4V alloy, *Surf. Coat. Technol.* 206 (6) (2011) 1389–1395, <https://doi.org/10.1016/j.surfcoat.2011.08.063>.
- [600] P. Huang, J. Yeh, Effects of nitrogen content on structure and mechanical properties of multi-element (AlCrNbSiTiVN) coating, *Surf. Coat. Technol.* 203 (13) (2009) 1891–1896, <https://doi.org/10.1016/j.surfcoat.2009.01.016>.
- [601] W. Huo, H. Shi, X. Ren, J. Zhang, Microstructure and wear behavior of CoCrFeMnNbNi high-entropy alloy coating by TiG cladding, *Adv. Mater. Sci. Eng.* 2015 (2015) 1–5, <https://doi.org/10.1155/2015/647351>.
- [602] X. Ye, M. Ma, W. Liu, L. Li, M. Zhong, Y. Liu, Q. Wu, Synthesis and characterization of high-entropy alloy FeCoNiCuCr by laser cladding, *Adv. Mater. Sci. Eng.* 2011 (2011) 1–7, <https://doi.org/10.1155/2011/485942>.
- [603] Y. He, J. Zhang, H. Zhang, G. Song, Effects of different levels of boron on microstructure and hardness of CoCrFeNiAlxCu0.7Si0.1By high-entropy alloy coatings by laser cladding, *Coatings* 7 (1) (2017) 7, <https://doi.org/10.3390/coatings7010007>.
- [604] M. Zhang, X. Zhou, X. Yu, J. Li, Synthesis and characterization of refractory TiZrNbWMo high-entropy alloy coating by laser cladding, *Surf. Coat. Technol.* 311 (2017) 321–329, <https://doi.org/10.1016/j.surfcoat.2017.01.012>.
- [605] H. Zhang, Y. Pan, Y. He, Synthesis and characterization of FeCoNiCrCu high-entropy alloy coating by laser cladding, *Mater. Des.* 32 (4) (2011) 1910–1915, <https://doi.org/10.1016/j.matdes.2010.12.001>.
- [606] C. Zhang, G.J. Chen, P.Q. Dai, Evolution of the microstructure and properties of laser-clad FeCrNiCoB<sub>x</sub>-C<sub>x</sub> high-entropy alloy coatings, *Mater. Sci. Technol.* 32 (16) (2016) 1666–1672, <https://doi.org/10.1080/02670836.2015.1138035>.
- [607] H. Zhang, Y. Pan, Y. He, Synthesis and characterization of FeCoNiCrCu high-entropy alloy coating by laser cladding, *Mater. Des.* 32 (4) (2011) 1910–1915, <https://doi.org/10.1016/j.matdes.2010.12.001>.
- [608] D. Lin, N. Zhang, B. He, G. Zhang, Y. Zhang, D. Li, Tribological properties of FeCoCrNiAlBx high-entropy alloys coating prepared by laser cladding, *J. Iron Steel Res. Int.* 24 (2) (2017) 184–189, [https://doi.org/10.1016/s1006-706x\(17\)30026-2](https://doi.org/10.1016/s1006-706x(17)30026-2).
- [609] H. Zhang, Y. Pan, Y. He, Effects of annealing on the microstructure and properties of 6FeNiCoCrAlTiSi high-entropy alloy coating prepared by laser cladding, *J. Therm. Spray Technol.* 20 (5) (2011) 1049–1055, <https://doi.org/10.1007/s11666-011-9626-0>.
- [610] H. Hsueh, W. Shen, M. Tsai, J. Yeh, Effect of nitrogen content and substrate bias on mechanical and corrosion properties of high-entropy films (AlCrSiTiZr)100–xNx, *Surf. Coat. Technol.* 206 (19–20) (2012) 4106–4112, <https://doi.org/10.1016/j.surfcoat.2012.03.096>.
- [611] Z. Chang, S. Liang, S. Han, Y. Chen, F. Shieh, Characteristics of TiVCrAlZr multi-element nitride films prepared by reactive sputtering, *Nucl. Instrum. Methods Phys. Res., Sect. B* 268 (16) (2010) 2504–2509, <https://doi.org/10.1016/j.nimb.2010.05.039>.
- [612] H. Zhang, Y. Pan, Y. He, H. Jiao, Microstructure and properties of 6FeNiCoSiCrAlTi high-entropy alloy coating prepared by laser cladding, *Appl. Surf. Sci.* 257 (6) (2011) 2259–2263, <https://doi.org/10.1016/j.apsusc.2010.09.084>.
- [613] W. Wu, L. Jiang, H. Jiang, X. Pan, Z. Cao, D. Deng, T. Li, Phase evolution and properties of Al2CrFeNiMoX high-entropy alloys coatings by laser cladding, *J. Therm. Spray Technol.* 24 (7) (2015) 1333–1340, <https://doi.org/10.1007/s11666-015-0303-6>.
- [614] D. Liu, J. Zhao, Y. Li, W. Zhu, L. Lin, Effects of boron content on microstructure and wear properties of FeCoCrNiBx high-entropy alloy coating by laser cladding, *Appl. Sci.* 10 (1) (2019) 49, <https://doi.org/10.3390/app10010049>.
- [615] B. Ren, Z. Shen, Z. Liu, Structure and mechanical properties of multi-element (AlCrMnMoNiZr)Nx coatings by reactive magnetron sputtering, *J. Alloys Compd.* 560 (2013) 171–176, <https://doi.org/10.1016/j.jallcom.2013.01.148>.
- [616] L. Liu, J. Zhu, C. Hou, J. Li, Q. Jiang, Dense and smooth amorphous films of multicomponent FeCoNiCuVZrAl high-entropy alloy deposited by direct current magnetron sputtering, *Mater. Des.* 46 (2013) 675–679, <https://doi.org/10.1016/j.matdes.2012.11.001>.
- [617] W. Li, P. Liu, P.K. Liaw, Microstructures and properties of high-entropy alloy films and coatings: a review, *Mater. Res. Lett.* 6 (4) (2018) 199–229, <https://doi.org/10.1080/21663831.2018.1434248>.
- [618] P. Huang, J. Yeh, Effects of nitrogen content on structure and mechanical properties of multi-element (AlCrNbSiTiVN) coating, *Surf. Coat. Technol.* 203 (13) (2009) 1891–1896, <https://doi.org/10.1016/j.surfcoat.2009.01.016>.
- [619] W. Sheng, X. Yang, C. Wang, Y. Zhang, Nano-crystallization of high-entropy amorphous NbTiAlSiWxNy films prepared by magnetron sputtering, *Entropy* 18 (6) (2016) 226, <https://doi.org/10.3390/e18060226>.
- [620] C. Cheng, J. Yeh, High-entropy BNbTaTiZr thin film with excellent thermal stability of amorphous structure and its electrical properties, *Mater. Lett.* 185 (2016) 456–459, <https://doi.org/10.1016/j.matlet.2016.09.050>.
- [621] J. Cheng, X. Liang, B. Xu, Effect of NB addition on the structure and mechanical behaviors of CoCrFeNi high-entropy alloy coatings, *Surf. Coat. Technol.* 240 (2014) 184–190, <https://doi.org/10.1016/j.surfcoat.2013.12.053>.
- [622] H. Hsueh, W. Shen, M. Tsai, J. Yeh, Effect of nitrogen content and substrate bias on mechanical and corrosion properties of high-entropy films (AlCrSiTiZr)100–xNx, *Surf. Coat. Technol.* 206 (19–20) (2012) 4106–4112, <https://doi.org/10.1016/j.surfcoat.2012.03.096>.
- [623] P. Lin, C. Cheng, J. Yeh, T. Chin, Soft magnetic properties of high-entropy Fe–Co–Ni–Cr–Al–Si thin films, *Entropy* 18 (8) (2016) 308, <https://doi.org/10.3390/e18080308>.
- [624] S.Q. Xia, X. Yang, T.F. Yang, S. Liu, Y. Zhang, Irradiation resistance in al X CoCrFeNi high entropy alloys, *JOM* 67 (10) (2015) 2340–2344, <https://doi.org/10.1007/s11883-015-1568-4>.
- [625] S. Xia, Z. Wang, T. Yang, Y. Zhang, Irradiation behavior in high entropy alloys, *J. Iron Steel Res. Int.* 22 (10) (2015) 879–884, [https://doi.org/10.1016/s1006-706x\(15\)30084-4](https://doi.org/10.1016/s1006-706x(15)30084-4).
- [626] Y. Zhang, G.M. Stocks, K. Jin, C. Lu, H. Bei, B.C. Sales, W.J. Weber, Influence of chemical disorder on energy dissipation and defect evolution in concentrated solid solution alloys, *Nat. Commun.* 6 (1) (2015), <https://doi.org/10.1038/ncomms9736>.
- [627] F. Granberg, K. Nordlund, M.W. Ullah, K. Jin, C. Lu, H. Bei, Y. Zhang, Mechanism of radiation damage reduction in Equiatomic multicomponent single phase alloys, *Phys. Rev. Lett.* 116 (13) (2016), <https://doi.org/10.1103/physrevlett.116.135504>.
- [628] T. Zuo, M.C. Gao, L. Ouyang, X. Yang, Y. Cheng, R. Feng, Y. Zhang, Tailoring magnetic behavior of CoFeMnNiX (X = al, CR, Ga, and Sn) high entropy alloys by

- metal doping, *Acta Mater.* 130 (2017) 10–18, <https://doi.org/10.1016/j.actamat.2017.03.013>.
- [629] T. Zuo, X. Yang, P.K. Liaw, Y. Zhang, Influence of Bridgman solidification on microstructures and magnetic behaviors of a non-equiautomic FeCoNiAlSi high-entropy alloy, *Intermetallics* 67 (2015) 171–176, <https://doi.org/10.1016/j.intermet.2015.08.014>.
- [630] S. Huang, W. Li, X. Li, S. Schönecker, L. Bergqvist, E. Holmström, L. Vitos, Mechanism of magnetic transition in ferroni-based high entropy alloys, *Mater. Des.* 103 (2016) 71–74, <https://doi.org/10.1016/j.matedes.2016.04.053>.
- [631] M. Tsai, J. Yeh, J. Gan, Diffusion barrier properties of AlMoNbSiTaTiVZr high-entropy alloy layer between copper and silicon, *Thin Solid Films* 516 (16) (2008) 5527–5530, <https://doi.org/10.1016/j.tsf.2007.07.109>.
- [632] M. Tsai, J. Yeh, J. Gan, Diffusion barrier properties of AlMoNbSiTaTiVZr high-entropy alloy layer between copper and silicon, *Thin Solid Films* 516 (16) (2008) 5527–5530, <https://doi.org/10.1016/j.tsf.2007.07.109>.
- [633] S. Vrtnik, P. Koželj, A. Meden, S. Maiti, W. Steurer, M. Feuerbacher, J. Dolinšek, Superconductivity in thermally annealed Ta-Nb-Hf-Zr-Ti high-entropy alloys, *J. Alloys Compd.* 695 (2017) 3530–3540, <https://doi.org/10.1016/j.jallcom.2016.11.417>.
- [634] K. Stolze, J. Tao, F.O. von Rohr, T. Kong, R.J. Cava, Sc–Zr–Nb–Rh–Pd and Sc–Zr–Nb–Ta–Rh–Pd high-entropy alloy superconductors on a CsCl-type lattice, *Chem. Mater.* 30 (2018) 906–914, <https://doi.org/10.1021/acs.chemmater.7b04578>.
- [635] H. Guo, C. He, X. Qiu, Y. Shen, G. Liu, X. Gao, A novel multilayer high temperature colored solar absorber coating based on high-entropy alloy MoNbHfZrTi: optimized preparation and chromaticity investigation, *Sol. Energy Mater. Sol. Cells* 209 (2020) 110444, <https://doi.org/10.1016/j.solmat.2020.110444>.
- [636] Q. Xing, J. Ma, C. Wang, Y. Zhang, High-throughput screening solar-thermal conversion films in a Pseudobinary (CR, FE, v)–(ta, W) system, *ACS Comb. Sci.* 20 (11) (2018) 602–610, <https://doi.org/10.1021/acscombsci.8b00055>.
- [637] Y. Zhang, T.T. Zuo, Z. Tang, M.C. Gao, K.A. Dahmen, P.K. Liaw, Z.P. Lu, Microstructures and properties of high-entropy alloys, *Prog. Mater. Sci.* 61 (2014) 1–93, <https://doi.org/10.1016/j.pmatsci.2013.10.001>.
- [638] X. Yan, Y. Zhang, Functional properties and promising applications of high entropy alloys, *Scr. Mater.* 187 (2020) 188–193, <https://doi.org/10.1016/j.scriptamat.2020.06.017>.
- [639] Y. Shi, L. Collins, R. Feng, C. Zhang, N. Balke, P.K. Liaw, B. Yang, Homogenization of al CoCrFeNi high-entropy alloys with improved corrosion resistance, *Corros. Sci.* 133 (2018) 120–131, <https://doi.org/10.1016/j.corsci.2018.01.030>.
- [640] X. Liu, Z. Tian, X. Zhang, H. Chen, T. Liu, Y. Chen, L. Dai, “Self-sharpening” tungsten high-entropy alloy, *Acta Mater.* 186 (2020) 257–266, <https://doi.org/10.1016/j.actamat.2020.01.005>.
- [641] M. Tsai, J. Yeh, J. Gan, Diffusion barrier properties of AlMoNbSiTaTiVZr high-entropy alloy layer between copper and silicon, *Thin Solid Films* 516 (16) (2008) 5527–5530, <https://doi.org/10.1016/j.tsf.2007.07.109>.
- [642] P. Yang, Y. Liu, X. Zhao, J. Cheng, H. Li, Electromagnetic wave absorption properties of mechanically alloyed FeCoNiCrAl high entropy alloy powders, *Adv. Powder Technol.* 27 (4) (2016) 1128–1133, <https://doi.org/10.1016/j.ap.2016.03.023>.
- [643] J. Kong, C. Xu, J. Li, W. Chen, H. Hou, Evolution of fractal features of pores in compacting and sintering process, *Adv. Powder Technol.* 22 (3) (2011) 439–442, <https://doi.org/10.1016/j.ap.2010.06.012>.
- [644] S.F. Guo, J.L. Qiu, P. Yu, S.H. Xie, W. Chen, FE-based bulk metallic glasses: brittle or ductile? *Appl. Phys. Lett.* 105 (16) (2014) 161901 <https://doi.org/10.1063/1.4899124>.
- [645] W. Chen, K. Chan, S. Guo, P. Yu, Plasticity improvement of an FE-based bulk metallic glass by geometric confinement, *Mater. Lett.* 65 (8) (2011) 1172–1175, <https://doi.org/10.1016/j.matlet.2011.01.030>.
- [646] B. Zhao, B. Fan, G. Shao, B. Wang, X. Pian, W. Li, R. Zhang, Investigation on the electromagnetic wave absorption properties of Ni chains synthesized by a facile solvothermal method, *Appl. Surf. Sci.* 307 (2014) 293–300, <https://doi.org/10.1016/j.apsusc.2014.04.029>.
- [647] S. Wen, Y. Liu, X. Zhao, J. Cheng, H. Li, Facile synthesis of novel cobalt particles by reduction method and their microwave absorption properties, *Powder Technol.* 264 (2014) 128–132, <https://doi.org/10.1016/j.powtec.2014.05.030>.
- [648] S. Wen, X. Zhao, Y. Liu, J. Cheng, H. Li, Synthesis of hierarchical sword-like cobalt particles and their microwave absorption properties, *RSC Adv.* 4 (76) (2014) 40456, <https://doi.org/10.1039/c4ra05716c>.
- [649] S.L. Wen, Y. Liu, X.C. Zhao, J.W. Cheng, H. Li, Synthesis, dual-nonlinear magnetic resonance and microwave absorption properties of nanosheet hierarchical cobalt particles, *Phys. Chem. Chem. Phys.* 16 (34) (2014) 18333, <https://doi.org/10.1039/c4cp01468e>.
- [650] Y. Zhang, B. Zhang, K. Li, G. Zhao, S. Guo, Electromagnetic interference shielding effectiveness of high entropy AlCoCrFeNi alloy powder Laden composites, *J. Alloys Compd.* 734 (2018) 220–228, <https://doi.org/10.1016/j.jallcom.2017.11.044>.
- [651] W. Dong, Z. Zhou, L. Zhang, M. Zhang, P.K. Liaw, G. Li, R. Liu, Effects of Y, GdCu, and Al addition on the thermoelectric behavior of CoCrFeNi high entropy alloys, *Metals* 8 (2018) 781, <https://doi.org/10.3390/met8100781>.
- [652] Chaofei Zan, Jie Chen, Huihui Zhang, Juntao Yuan, Insights into the hot corrosion of CoCrFeNi high entropy alloy in molten Na<sub>2</sub>SO<sub>4</sub> + 25 %K<sub>2</sub>SO<sub>4</sub> at 900 °C, *Int. J. Electrochem. Sci.* 18 (7) (2023), <https://doi.org/10.1016/j.ijoes.2023.100192>, <https://www.hindawi.com/journals/amse.100192>.
- [653] M. He, M. Eizadjou, H. Chen, et al., Microstructure and properties of CoCrFeNi-based multi-principal element alloys containing C and Sc, *J. Mater. Sci.* 57 (2022) 9442–9453, <https://doi.org/10.1007/s10853-022-07227-3>.
- [654] Yu Yuan, Jun Wang, Jinshan Li, Hongchao Kou, Haitao Duan, Jian Li, Weimin Liu, Tribological behavior of AlCoCrCuFeNi and AlCoCrFeNiTi0.5 high entropy alloys under hydrogen peroxide solution against different counterpartners, *Tribol. Int.* 92 (2015) 203–210, <https://doi.org/10.1016/j.triboint.2015.06.013>.
- [655] P.M. Gopal, K. Sooraya Prakash, V. Kavimani, Gopal Rajendiran, Processing and properties of AlCoCrFeNi high entropy alloys: a review, *Adv. Mater. Sci. Eng.* (2022), <https://doi.org/10.1155/2022/119016>.
- [656] Modupeola Dada, Popoola Patricia, High entropy nanomaterials for energy storage and catalysis applications, *Front. Energy Res.* 11 (2023), <https://doi.org/10.3389/fenrg.2023.1149446>.
- [657] Surekha Yadav, Arvind Kumar, Krishanu Biswas, Wear behavior of high entropy alloys containing soft dispersoids (Pb, Bi), *Mater. Chem. Phys.* 210 (2018) 222–232, <https://doi.org/10.1016/j.matchemphys.2017.06.020>.
- [658] A. Dutta, T. Sivaji, M. Ghosh, R. Fernandes, P.S. De, D. Nayak, R. Sharma, Corrosion behavior of AlCuFeMn alloy in aqueous sodium chloride solution, *Mater. Chem. Phys.*, Volume 276, 2022, 125397, doi:10.1016/j.matchemphys.2021.125397.
- [659] Z. Lv, X. Liu, B. Jia, et al., Development of a novel high-entropy alloy with eminent efficiency of degrading azo dye solutions, *Sci. Rep.* 6 (2016) 34213, <https://doi.org/10.1038/srep34213>.
- [660] Z. Xu, Q.Y. Li, Wei Li, D.Y. Li, Microstructure, mechanical properties, and wear behavior of AlCoCrFeNi high-entropy alloy and AlCrFeNi medium-entropy alloy with WC addition, *Wear* 522 (2023) 204701, <https://doi.org/10.1016/j.wear.2023.204701>.
- [661] Baran Sarac, Vladislav Zadorozhnyy, et al., Hydrogen storage performance of the multi-principal-component CoFeMnTiVZr alloy in electrochemical and gas–solid reactions, (paper), *RSC Adv.* 2020 (10) (2020) 24613–24623, <https://doi.org/10.1039/DORA04089D>.
- [662] I. Kunc, M. Polanski, J. Bystrzycki, Structure and hydrogen storage properties of a high entropy ZrTiVCrFeNi alloy synthesized using Laser Engineered Net Shaping (LENS), *Int. J. Hydrog. Energy* 38 (27) (2013) 12180–12189, <https://doi.org/10.1016/j.ijhydene.2013.05.071>.
- [663] Yih-Farn Kao, Swe-Kai Chen, Jen-Haur Sheu, Jiun-Ting Lin, Wei-En Lin, Jien-Wei Yeh, Su-Jien Lin, Tzungs-Hsien Liou, Chia-Wen Wang, Hydrogen storage properties of multi-principal-component CoFeMnTiVYzr alloys, *Int. J. Hydrog. Energy* 35 (17) (2010) 9046–9059, <https://doi.org/10.1016/j.ijhydene.2010.06.012>.
- [664] T.P. Yadav, A. Kumar, S.K. Verma, et al., High-entropy alloys for solid hydrogen storage: potentials and prospects, *Trans Indian Natl. Acad. Eng.* 7 (2022) 147–156, <https://doi.org/10.1007/s41403-021-00316-w>.
- [665] Songqin Xia, X. Yang, T.F. Yang, S. Liu, Y.H. Zhang, Irradiation resistance in Al<sub>x</sub>CoCrFeNi high entropy alloys, *JOM* 67 (2015) 2340–2344.
- [666] T. Egami, W. Guo, P.D. Rack, et al., Irradiation resistance of multicomponent alloys, *Metall. Mater. Trans. A* 45 (2014) 180–183, <https://doi.org/10.1007/s11661-013-1994-2>.
- [667] Lu Yiping, Hefei Huang, Xuzhou Gao, Cuilan Ren, Jie Gao, Huanzhi Zhang, Shijian Zheng, Qianqian Jin, Yonghao Zhao, Lu Chenyang, Tongmin Wang, Tingyu Li, A promising new class of irradiation tolerant materials: Ti<sub>2</sub>ZrHF<sub>0.5</sub>Mo<sub>0.2</sub> high-entropy alloy, *J. Mater. Sci. Technol.* 35 (3) (2019) 369–373, <https://doi.org/10.1016/j.jmst.2018.09.034>.
- [668] Lin Luo, Hongxian Shen, Ying Bao, Hangbo Yin, Sida Jiang, Yongjiang Huang, Shu Guo, Shenyuan Gao, Dawei Xing, Ze Li, Jianfei Sun, Magnetocaloric effect of melt-extracted high-entropy Gd<sub>19</sub>Tb<sub>19</sub>Er<sub>18</sub>Fe<sub>19</sub>Al<sub>25</sub> amorphous microwires, *J. Magn. Magn. Mater.* 507 (2020) 166856, <https://doi.org/10.1016/j.jmmm.2020.166856>.
- [669] S. Dey, N.S. Mehta, Oxidation of carbon monoxide over various nickel oxide catalysts in different conditions: A review, *Chem. Eng. J. Adv.* 1 (2020) 100008, <https://doi.org/10.1016/j.cej.2020.100008>.
- [670] K. Sarlar, A. Tekgül, I. Kucuk, Magnetocaloric properties of rare-earth-free Mn<sub>2</sub>Cr<sub>7</sub>Ni<sub>3</sub>Ge<sub>2</sub>Si<sub>8</sub> high-entropy alloy, in: *IEEE Magnetics Letters* 10, 2019, pp. 1–5, <https://doi.org/10.1109/LMAG.2019.2955667>. Art no. 2109905.
- [671] Chih-Fang Tsai, Kung-Yu Yeh, Wu Pu-Wei, Yi-Fan Hsieh, Pang Lin, Effect of platinum present in multi-element nanoparticles on methanol oxidation, *J. Alloys Compd.* 478 (1–2) (2009) 868–871, <https://doi.org/10.1016/j.jallcom.2008.12.055>.
- [672] Sajjad Ur Rehman, Qingzheng Jiang, Qing Ge, Weikai Lei, Lili Zhang, Qingwen Zeng, A. Ul Haq, Renhui Liu, Zhenchen Zhong, Microstructure and magnetic properties of alnico permanent magnetic alloys with Zr-B additives, *J. Magn. Magn. Mater.* 451 (2018) 243–247, <https://doi.org/10.1016/j.jmmm.2017.11.043>.
- [673] Suok-Min Na, Jin-Hyeong Yoo, Paul K. Lambert, Nicholas J. Jones, Room-temperature ferromagnetic transitions and the temperature dependence of magnetic behaviors in FeCoNiCr-based high-entropy alloys, *MAGNETISM AND MAGNETIC MATERIALS*, *AIP Adv.* 8 (2018) 056412, <https://doi.org/10.1063/1.5007073>.
- [674] Bin Zhang, Yuping Duan, Xuan Yang, Guojia Ma, Tongmin Wang, Xinglong Dong, Yunsong Zeng, Tuning magnetic properties based on FeCoNiSiO<sub>4</sub>Al<sub>0.4</sub> with dual-phase nano-crystal and nano-amorphous microstructure, *Intermetallics* 117 (2020) 106678. ISSN 0966-9795, <https://doi.org/10.1016/j.intermet.2019.106678>.
- [675] Peipei Yang, Ying Liu, Xiuchen Zhao, Jingwei Cheng, Hong Li, Electromagnetic wave absorption properties of mechanically alloyed FeCoNiCrAl high entropy

- alloy powders, *Adv. Powder Technol.* 27 (4) (2016) 1128–1133. ISSN 0921-8831, <https://doi.org/10.1016/j.apert.2016.03.023>.
- [676] H. Jiang, K. Han, D. Li, Z. Cao, Microstructure and mechanical properties investigation of the CoCrFeNiNb<sub>x</sub> high entropy alloy coatings, *Crystals* 8 (2018) 409, <https://doi.org/10.3390/cryst8110409>.
- [677] G. Popescu, et al., IOP Conf. Ser.: Mater. Sci. Eng. 400 (2018) 022049DOI, <https://doi.org/10.1088/1757-899X/400/2/022049>.
- [678] Kshay Kumar, Alok Singh, Amit Suhane, Mechanically alloyed high entropy alloys: existing challenges and opportunities, *J. Mater. Res. Technol.* 17 (2022) 2431–2456, <https://doi.org/10.1016/j.jmrt.2022.01.141>.
- [679] Shan-Hsiu Chang, Wei-Pin Kao, Kai-Yuan Hsiao, Jien-Wei Yeh, Lu Ming-Yen, Che-Wei Tsai, High-temperature shape memory properties of Cu15Ni35Ti25Hf12.5Zr12.5 high-entropy alloy, *J. Mater. Res. Technol.* 14 (2021) 1235–1242. ISSN 2238-7854, <https://doi.org/10.1016/j.jmrt.2021.07.008>.
- [680] K. Jasiewicz, B. Wiendlocha, P. Korber, S. Kaprzyk, J. Tobola, Superconductivity of Ta34Nb33Hf8Zr14Ti11 high entropy alloy from first principles calculations, *Condensed Matter > Superconductivity* (2016), <https://doi.org/10.48550/arXiv.1603.07274>.
- [681] Naoki Ishizu, Jiro Kitagawa, New high-entropy alloy superconductor Hf21Nb25Ti15V15Zr24, *Results in Physics* 13 (2019) 102275, <https://doi.org/10.1016/j.rinp.2019.102275>.
- [682] Akshay Kumar, Alok Singh, Amit Suhane, Mechanically alloyed high entropy alloys: existing challenges and opportunities, *J. Mater. Res. Technol.* 17 (2022) 2431–2456, <https://doi.org/10.1016/j.jmrt.2022.01.141>.
- [683] T.D. Ngo, A. Kashani, G. Imbalzano, K.T. Nguyen, D. Hui, Additive manufacturing (3D printing): A review of materials, methods, applications and challenges, *Compos. Part B Eng.* 143 (2018) 172–196, <https://doi.org/10.1016/j.compositesb.2018.02.012>.
- [684] C. Han, Q. Fang, Y. Shi, S.B. Tor, C.K. Chua, K. Zhou, Recent advances on high-entropy alloys for 3D printing, *Adv. Mater.* 32 (26) (2020) 1903855, <https://doi.org/10.1002/adma.201903855>.
- [685] S.J. Wolff, S. Lin, E.J. Faierson, W.K. Liu, G.J. Wagner, J. Cao, A framework to link localized cooling and properties of directed energy deposition (ded)-processed ti-6al-4V, *Acta Mater.* 132 (2017) 106–117, <https://doi.org/10.1016/j.actamat.2017.04.027>.
- [686] R. Kumar, M. Kumar, J.S. Chohan, The role of additive manufacturing for biomedical applications: a critical review, *J. Manuf. Process.* 64 (2021) 828–850, <https://doi.org/10.1016/j.jmapro.2021.02.022>.
- [687] B.E. Carroll, T.A. Palmer, A.M. Beese, Anisotropic tensile behavior of ti-6al-4V components fabricated with directed energy deposition additive manufacturing, *Acta Mater.* 87 (2015) 309–320, <https://doi.org/10.1016/j.actamat.2014.12.054>.
- [688] N. Raghavan, S.S. Babu, R. Dehoff, S. Pannala, S. Simunovic, M. Kirka, N. Carlson, Corrigendum to “Numerical modeling of heat-transfer and the influence of process parameters on tailoring the grain morphology of IN718 in electron beam additive manufacturing” [ACTA mater. 112C (2016) 303–314], *Acta Mater.* 140 (2017) 472, <https://doi.org/10.1016/j.actamat.2017.08.067>.
- [689] T. Borkar, B. Gwalani, D. Choudhuri, C. Mikler, C. Yannetta, X. Chen, R. Banerjee, A combinatorial assessment of AlxCrCuFeNi2 (0 < X < 1.5) complex concentrated alloys: microstructure, microhardness, and magnetic properties, *Acta Mater.* 116 (2016) 63–76, <https://doi.org/10.1016/j.actamat.2016.06.025>.
- [690] T. Borkar, V. Chaudhary, B. Gwalani, D. Choudhuri, C.V. Mikler, V. Soni, R. Banerjee, A combinatorial approach for assessing the magnetic properties of high entropy alloys: role of Cr in AlCoxCr1-xFeNi<sub>j</sub>, *Adv. Eng. Mater.* 19 (8) (2017) 1700048 <https://doi.org/10.1002/adem.201700048>.
- [691] S. Saedi, N. Shayesteh Moghaddam, A. Amerinatanzi, M. Elahinia, H.E. Karaca, On the effects of selective laser melting process parameters on microstructure and thermomechanical response of Ni-rich NiTi, *Acta Mater.* 144 (2018) 552–560, <https://doi.org/10.1016/j.actamat.2017.10.072>.
- [692] C.N. Kuo, C.K. Chua, P. Peng, Y.W. Chen, S.L. Sing, S. Huang, Y.L. Su, Microstructure evolution and mechanical property response via 3D printing parameter development of Al-Sc alloy, *Virtual Phys. Prototyp.* 15 (1) (2019) 120–129, <https://doi.org/10.1080/17452759.2019.1698967>.
- [693] C. Han, Y. Li, Q. Wang, S. Wen, Q. Wei, C. Yan, Y. Shi, Continuous functionally graded porous titanium scaffolds manufactured by selective laser melting for bone implants, *J. Mech. Behav. Biomed. Mater.* 80 (2018) 119–127, <https://doi.org/10.1016/j.jmbbm.2018.01.013>.
- [694] Z. Sun, X. Tan, S.B. Tor, C.K. Chua, Simultaneously enhanced strength and ductility for 3D-printed stainless steel 316L by selective laser melting, *NPG Asia Mater.* 10 (4) (2018) 127–136, <https://doi.org/10.1038/s41427-018-0018-5>.
- [695] P. Tan, F. Shen, B. Li, K. Zhou, A thermo-metallurgical-mechanical model for selective laser melting of Ti6Al4V, *Mater. Des.* 168 (2019) 107642, <https://doi.org/10.1016/j.matdes.2019.107642>.
- [696] Y.M. Wang, T. Voisin, J.T. McKeown, J. Ye, N.P. Calta, Z. Li, T. Zhu, Additively manufactured hierarchical stainless steels with high strength and ductility, *Nat. Mater.* 17 (1) (2017) 63–71, <https://doi.org/10.1038/nmat5021>.
- [697] J.H. Martin, B.D. Yahata, J.M. Hundley, J.A. Mayer, T.A. Schaeder, T.M. Pollock, 3D printing of high-strength aluminium alloys, *Nature* 549 (7672) (2017) 365–369, <https://doi.org/10.1038/nature23894>.
- [698] Y. Brif, M. Thomas, I. Todd, The use of high-entropy alloys in additive manufacturing. *Scripta Materialia*, 99, 93–96. doi:10.1016/j.scriptamat.2014.11.037 [4] Yu, W., Sing, S. L., Chua, C. K., & Tian, X. (2019). Influence of re-melting on surface roughness and porosity of AlSi10Mg parts fabricated by selective laser melting, *J. Alloys Compd.* 792 (2015) 574–581, <https://doi.org/10.1016/j.jallcom.2019.04.017>.
- [699] Y. Li, K. Zhou, P. Tan, S.B. Tor, C.K. Chua, K.F. Leong, Modeling temperature and residual stress fields in selective laser melting, *Int. J. Mech. Sci.* 136 (2018) 24–35, <https://doi.org/10.1016/j.ijmechsci.2017.12.001>.
- [700] C. Han, C. Yan, S. Wen, T. Xu, S. Li, J. Liu, Y. Shi, Effects of the unit cell topology on the compression properties of porous co-CR scaffolds fabricated via selective laser melting, *Rapid Prototyp. J.* 23 (1) (2017) 16–27, <https://doi.org/10.1108/rpj-08-2015-0114>.
- [701] C. Han, Y. Yao, X. Cheng, J. Luo, P. Luo, Q. Wang, Z. Zhang, Electrophoretic deposition of gentamicin-loaded silk fibroin coatings on 3D-printed porous cobalt-chromium-molybdenum bone substitutes to prevent orthopedic implant infections, *Biomacromolecules* 18 (11) (2017) 3776–3787, <https://doi.org/10.1021/acs.biromac.7b01091>.
- [702] S. Rouf, A. Raina, M.I.U. Haq, N. Naveed, S. Jegannathan, A.F. Kichloo, 3D printed parts and mechanical properties: influencing parameters, sustainability aspects, global market scenario, challenges and applications, *Adv. Ind. Eng. Polym. Res.* (2022), <https://doi.org/10.1016/j.aierp.2022.02.001>.
- [703] A. Puglione, B. Dovgyy, C. Liu, C. Gourlay, P. Hooper, M. Pham, Printability and microstructure of the CoCrFeMnNi high-entropy alloy fabricated by laser powder bed fusion, *Mater. Lett.* 224 (2018) 22–25, <https://doi.org/10.1016/j.mlet.2018.04.052>.
- [704] T. Fujieda, H. Shiratori, K. Kuwabara, T. Kato, K. Yamanaka, Y. Koizumi, A. Chiba, First demonstration of promising selective electron beam melting method for utilizing high-entropy alloys as engineering materials, *Mater. Lett.* 159 (2015) 12–15, <https://doi.org/10.1016/j.matlet.2015.06.046>.
- [705] H. Shiratori, T. Fujieda, K. Yamanaka, Y. Koizumi, K. Kuwabara, T. Kato, A. Chiba, Relationship between the microstructure and mechanical properties of an equiatomic AlCoCrFeNi high-entropy alloy fabricated by selective electron beam melting, *Mater. Sci. Eng. A* 656 (2016) 39–46, <https://doi.org/10.1016/j.msea.2016.01.019>.
- [706] Y. Chew, G. Bi, Z. Zhu, F. Ng, F. Weng, S. Liu, B. Lee, Microstructure and enhanced strength of laser aided additive manufactured CoCrFeNiMn high entropy alloy, *Mater. Sci. Eng. A* 744 (2019) 137–144, <https://doi.org/10.1016/j.msea.2018.12.005>.
- [707] S. Guan, D. Wan, K. Solberg, F. Berto, T. Welo, T. Yue, K. Chan, Additive manufacturing of fine-grained and dislocation-populated CrMnFeCoNi high entropy alloy by laser engineered net shaping, *Mater. Sci. Eng. A* 761 (2019) 138056, <https://doi.org/10.1016/j.msea.2019.138056>.
- [708] M.A. Melia, J.D. Carroll, S.R. Whetten, S.N. Esmaely, J. Locke, E. White, A. B. Kustas, Mechanical and corrosion properties of additively manufactured CoCrFeMnNi high entropy alloy, *Addit. Manuf.* 29 (2019) 100833, <https://doi.org/10.1016/j.addma.2019.100833>.
- [709] S. Xiang, H. Luan, J. Wu, K. Yao, J. Li, X. Liu, Q. Li, Microstructures and mechanical properties of CrMnFeCoNi high entropy alloys fabricated using laser metal deposition technique, *J. Alloys Compd.* 773 (2019) 387–392, <https://doi.org/10.1016/j.jallcom.2018.09.235>.
- [710] Z. Sun, X. Tan, M. Descoings, D. Mangelinek, S. Tor, C. Lim, Revealing hot tearing mechanism for an additively manufactured high-entropy alloy via selective laser melting, *Scr. Mater.* 168 (2019) 129–133, <https://doi.org/10.1016/j.scriptamat.2019.04.036>.
- [711] R. Li, P. Niu, T. Yuan, P. Cao, C. Chen, K. Zhou, Selective laser melting of an equiatomic CoCrFeMnNi high-entropy alloy: Processability, non-equilibrium microstructure and mechanical property, *J. Alloys Compd.* 746 (2018) 125–134, <https://doi.org/10.1016/j.jallcom.2018.02.298>.
- [712] Z. Zhu, Q. Nguyen, F. Ng, X. An, X. Liao, P. Liaw, J. Wei, Hierarchical microstructure and strengthening mechanisms of a CoCrFeNiMn high entropy alloy additively manufactured by selective laser melting, *Scr. Mater.* 154 (2018) 20–24, <https://doi.org/10.1016/j.scriptamat.2018.05.015>.
- [713] T. Fujieda, M. Chen, H. Shiratori, K. Kuwabara, K. Yamanaka, Y. Koizumi, S. Watanabe, Mechanical and corrosion properties of co-crfe-ni-based high-entropy alloy additive manufactured using selective laser melting, *Addit. Manuf.* 25 (2019) 412–420, <https://doi.org/10.1016/j.addma.2018.10.023>.
- [714] X. Yang, Y. Zhou, S. Xi, Z. Chen, P. Wei, C. He, H. Wu, Additively manufactured fine grained Ni6Cr4WFe9Ti high entropy alloys with high strength and ductility, *Mater. Sci. Eng. A* 767 (2019) 138394, <https://doi.org/10.1016/j.msea.2019.138394>.
- [715] X. Yang, Y. Zhou, S. Xi, Z. Chen, P. Wei, C. He, H. Wu, Grain-anisotropied high-strength Ni6Cr4WFe9Ti high entropy alloys with outstanding tensile ductility, *Mater. Sci. Eng. A* 767 (2019) 138382, <https://doi.org/10.1016/j.msea.2019.138382>.
- [716] P. Wang, P. Huang, F.L. Ng, W.J. Sin, S. Lu, M.L. Nai, J. Wei, Additively manufactured CoCrFeNiMn high-entropy alloy via pre-alloyed powder, *Mater. Des.* 168 (2019) 107576, <https://doi.org/10.1016/j.matdes.2018.107576>.
- [717] J.H. Kim, K.R. Lim, J.W. Won, Y.S. Na, H. Kim, Mechanical properties and deformation twinning behavior of as-cast CoCrFeMnNi high-entropy alloy at low and high temperatures, *Mater. Sci. Eng. A* 712 (2018) 108–113, <https://doi.org/10.1016/j.msea.2017.11.081>.
- [718] C. Kenel, N.P. Casati, D.C. Dunand, 3D ink-extrusion additive manufacturing of CoCrFeNi high-entropy alloy micro-lattices, *Nature, Communications* 10 (1) (2019), <https://doi.org/10.1038/s41467-019-08763-4>.
- [719] Z. Wu, S. David, Z. Feng, H. Bei, Weldability of a high entropy CrMnFeCoNi alloy, *Scr. Mater.* 124 (2016) 81–85, <https://doi.org/10.1016/j.scriptamat.2016.06.046>.
- [720] Y. Fan, P. Li, K. Chen, L. Fu, A. Shan, Z. Chen, Effect of fiber laser welding on solute segregation and proprieties of CoCrCuFeNi high entropy alloy, *J. Laser Appl.* 32 (2) (2020) 022005, <https://doi.org/10.2351/1.5128535>.

- [721] B. Liu, J. Wang, Y. Liu, Q. Fang, Y. Wu, S. Chen, C. Liu, Microstructure and mechanical properties of equimolar FeCoCrNi high entropy alloy prepared via powder extrusion, *Intermetallics* 75 (2016) 25–30, <https://doi.org/10.1016/j.intermet.2016.05.006>.
- [722] E. George, W. Curtin, C. Tasan, High entropy alloys: a focused review of mechanical properties and deformation mechanisms, *Acta Mater.* 188 (2020) 435–474, <https://doi.org/10.1016/j.actamat.2019.12.015>.
- [723] A. Kumar, M. Gupta, An insight into evolution of light weight high entropy alloys: a review, *Metals* 6 (9) (2016) 199, <https://doi.org/10.3390/met6090199>.
- [724] S. Kumar, R. Kumar, Influence of processing conditions on the properties of thermal sprayed coating: a review, *Surf. Eng.* 37 (11) (2021) 1339–1372, <https://doi.org/10.1080/02670844.2021.1967024>.
- [725] S. Kumar, A. Handa, V. Chawla, N.K. Grover, R. Kumar, Performance of thermal-sprayed coatings to combat hot corrosion of coal-fired boiler tube and effect of process parameters and post-coating heat treatment on coating performance: a review, *Surf. Eng.* 37 (7) (2021) 833–860, <https://doi.org/10.1080/02670844.2021.1924506>.
- [726] S. Kumar, M. Kumar, A. Handa, Erosion corrosion behaviour and mechanical properties of wire arc sprayed Ni-CR and Ni-al coating on boiler steels in a real boiler environment, *Mater. High Temp.* 37 (6) (2020) 370–384, <https://doi.org/10.1080/09603409.2020.1810922>.
- [727] S. Kumar, M. Kumar, A. Handa, Comparative study of high temperature oxidation behavior and mechanical properties of wire arc sprayed Ni CR and Ni al coatings, *Eng. Fail. Anal.* 106 (2019) 104173, <https://doi.org/10.1016/j.engfailanal.2019.104173>.
- [728] M. Kumar, S. Kant, S. Kumar, Corrosion behavior of wire arc sprayed Ni-based coatings in extreme environment, *Mater. Res. Express* 6 (10) (2019) 106427, <https://doi.org/10.1088/2053-1591/ab3bd8>.
- [729] T.S. Bedi, S. Kumar, R. Kumar, Corrosion performance of hydroxyapatite and hydroxyapatite/Titania bond coating for biomedical applications, *Mater. Res. Express* 7 (1) (2019) 015402, <https://doi.org/10.1088/2053-1591/ab5cc5>.
- [730] S. Kumar, M. Kumar, A. Handa, Combating hot corrosion of boiler tubes – A study, *Eng. Fail. Anal.* 94 (2018) 379–395, <https://doi.org/10.1016/j.engfailanal.2018.08.004>.
- [731] S. Kumar, M. Kumar, N. Jindal, Overview of cold spray coatings applications and comparisons: A critical review, *World J. Eng.* 17 (1) (2020) 27–51, <https://doi.org/10.1108/wje-01-2019-0021>.
- [732] S. Kumar, R. Kumar, S. Singh, H. Singh, A. Handa, The role of thermal spray coating to combat hot corrosion of boiler tubes: a study, 2020, *J. Xidian Univ.* 14 (5) (2020), <https://doi.org/10.37896/jxu14.5/024>.
- [733] V. Sharma, S. Kumar, M. Kumar, D. Deepak, High temperature oxidation performance of Ni-CR-Ti and Ni-Sal coatings, *Mater. Today: Proc.* 26 (2020) 3397–3406, <https://doi.org/10.1016/j.matpr.2019.11.048>.
- [734] S. Harsimran, K. Santosh, K. Rakesh, Overview of corrosion and its control: a critical review, *Proc. Eng. Sci.* 3 (1) (2021) 13–24, <https://doi.org/10.24874/pes03.01.002>.
- [735] Y. Ye, Q. Wang, J. Lu, C. Liu, Y. Yang, High-entropy alloy: challenges and prospects, *Mater. Today* 19 (6) (2016) 349–362, <https://doi.org/10.1016/j.mattod.2015.11.026>.